Modeling and optimization of vacuumed regeneration process for liquid desiccant dehumidification system

Kulathunga S.M. Asiri Indrajith

2018

Kulathunga S.M. Asiri Indrajith. (2018). Modeling and optimization of vacuumed regeneration process for liquid desiccant dehumidification system. Doctoral thesis, Nanyang Technological University, Singapore.

http://hdl.handle.net/10356/73791

https://doi.org/10.32657/10356/73791

MODELING AND OPTIMIZATION OF VACUUMED REGENERATION PROCESS FOR LIQUID DESICCANT DEHUMIDIFICATION SYSTEM

KULATHUNGA S.M. ASIRI INDRAJITH

School of Electrical and Electronic Engineering

A thesis submitted to the Nanyang Technological University

in partial fulfillment of the requirement for the degree of

Doctor of Philosophy

2016

Acknowledgement

First and foremost, I would like to express my most sincere gratitude to my supervisor, Associate Professor Cai Wenjian, for his invaluable support, guidance and encouragement throughout my research work.

I would also like to express my appreciation to the staff and all the fellow research students specially Dr. Yan Jia, Dr. Ding Xudong and Dr. Xing Li of Process Instrumentation Laboratory for their support.

I would like to give my deepest gratitude to my dear parents for their continuous encouragement throughout my research career. Finally I would like to express my special appreciation to my lovely wife, Kasumi, for providing me encouragement, understanding and support during this journey.

Nanyang Technological University is gratefully acknowledged for the research scholarship granted.

Finally, I would like thank Namal, Kumudu, Prasad & Hasith for their comfort, friendship and support during hard times and for the enjoyable discussions held; to Neligama, Diluka, Mohasha and the Sri Lankan cluster in NTU, I extend my gratitude for their friendship and support.

Abstract

Since the last few decades the world has been facing global warming due to the increased percentage of atmospheric CO_2. Much attention is therefore devoted to building air conditioning and, mechanical ventilation (ACMV) systems to provide a comfortable environment to occupants of residential houses and buildings. Liquid Desiccant Dehumidification System (LDDS) has gained much attention due to the possibility of combining secondary level energy sources like renewable energy and waste heat as its main energy source. However, the regeneration process of LDDS absorbs a vast amount of heat to vaporize water from the weak desiccant solution. With proper study and investigation nevertheless, challenges such as the requirement of high temperature heat sources, inefficiency of the regeneration process, and the complexity of combining renewable energy sources with the regeneration system can be overcome.

Thus, a new vacuumed regenerator was designed to improve key performance indices of the regeneration process, while taking important parameters into consideration, such as; evaporator and condenser heat, mass transfer mechanism and driving force, solution flow method through the heat exchanger, condenser tube arrangement and liquid desiccant properties. Vacuumed condition of the regenerator increases the mass transfer driving force and reduces the evaporation temperature of the water; thus lowering the required heat source temperature. Carry over effect of the liquid desiccant is prevented, by making the regenerator a fully closed system where liquid desiccant circulates internally, with no direct contact with other fluids.

Data was collected by testing the system to study the regeneration performance, with respect to different parameter conditions like; hot water and chilled water temperatures and flow rates, solution flow rate, initial solution concentration and initial vacuum pressure. Mathematical models for the water vapour evaporation, and water vapour condensation processes of the regeneration system, were developed. Overall heat and mass transfer coefficients for evaporator were modeled, by considering external convection over a tube bank and internal convection of a cylindrical tube. Evaporator mass transfer Sherwood number was modeled as a function of two phases Reynolds number, Schmidt number, concentration gradient and heat flux. Both evaporator heat transfer and mass transfer models were validated within ±10% good agreement with actual results. Condensation process was modeled by considering external natural condensation over a tube bank and internal convection of a cylindrical tube. Heat transfer rate of the condensation process is a function of chilled water flow rate, mean temperature difference and the number of rows of tubes. The heat transfer and mass transfer models for the condensation process were validated within ±10% good agreement with actual values. This theoretical contribution can be equally applied to any kind of similar system by changing system dependent parameters.

Finally, optimization for the developed model was conducted to identify the best operating condition of the system. Minimizing total energy consumption and maximizing heat and mass transfer of evaporation and condensation processes were set as objectives of the multi objective genetic algorithm optimization. MATLAB's genetic algorithm tool was employed for the optimization calculation, and it was found that the optimum condition can be achieved by several combinations of constraint parameters. Hence, a suitable solution was selected from the optimum settings by considering the resource availability and

economic factors. It was found that the optimum output can be achieved from a low temperature heat source around 38 ^{0}C, chilled water temperature of 8 ^{0}C with a vacuum condition of 695 Pa.

Table of Contents

List of Figures

List of Tables

Chapter 1 Introduction

1.1 Background

The process of air conditioning is one of the most impacted inventions of modern times, for human comfort. Applications such as cooling houses, industrial buildings, food storages and office buildings are widely spread all over the world. According to the US energy information administration, figure 1-1 shows the percentage rise of the number of air conditioned homes in America, from 1980 to 2009. Since the mid-19th century different types of air conditioning systems have been introduced to the market like; vapor compression systems, vapor absorption systems, window type air cooling systems, etc.

As the world has become wary of traditional energy sources, the demand for alternative energy sources, and more efficient machinery to replace old energy wasting machinery, is on the rise. On the other hand, global warming has begun to effect human lives, creating great difficulty in dealing with the situation and an overwhelming threat to the environment. Therefore, it is essential to design more energy efficient machinery which can operate from alternative energy sources. This chapter describes the motivations which lead to a more energy efficient machine for heating ventilation and air conditioning (HVAC) application, a description of the proposed design, and the objective of this research.

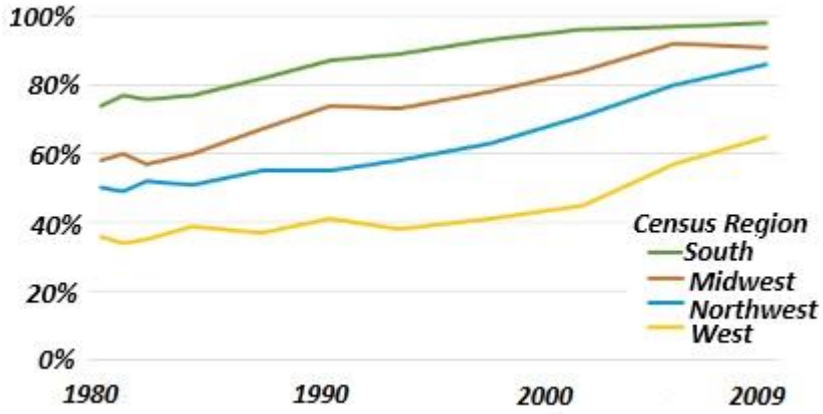

Figure 1-1. (Source: US energy information administration, 2009 Residential Energy Consumption survey) Percentage rise of air conditioning house in America

1.2 Motivation

After the industrial revolution in the 18th century, fossil fuel was used to power the economy, and became one of the energy providing mechanisms that were most utilized. It delivered unprecedented affluence to countries, which led to an exponential growth in the usage of fossil fuel around the world, during the last few decades. Due to the rising world population since 1960 and increased demands, along with the heavy usage of energy in different applications, natural energy resources are shrinking. Figure 1-2 shows the variation of the fuel usage from 1989 to 2014, and it shows that coal and oil, are major contenders in the present energy market [1]. Due to this uncontrolled usage of fossil fuels, the world is looking for alternative or renewable energy sources or energy efficient machinery.

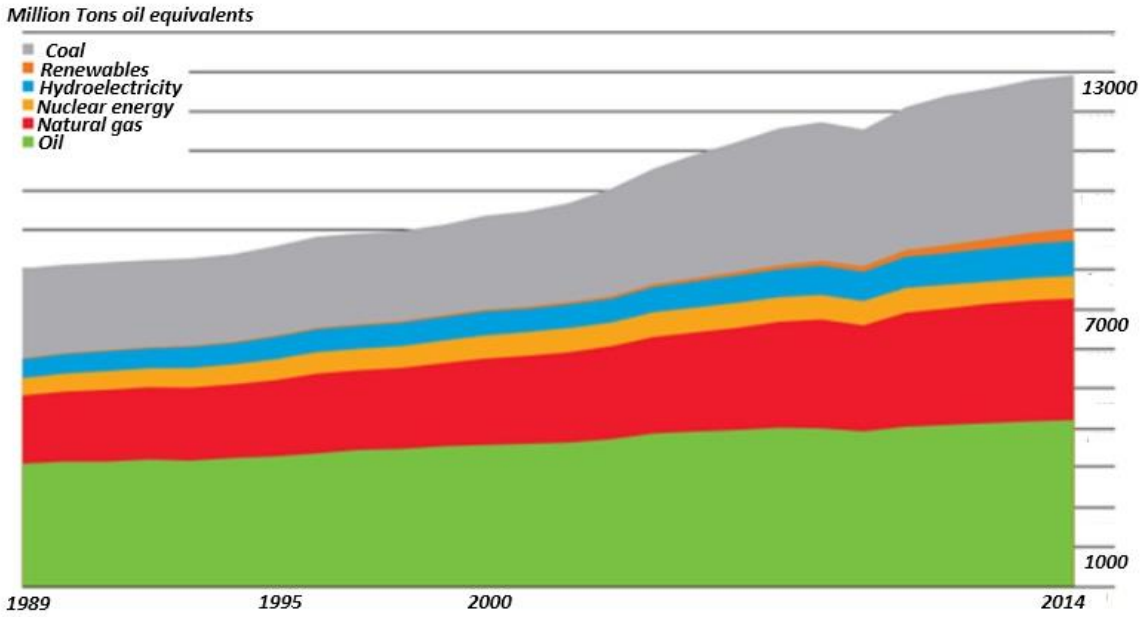

Figure 1-2.(Source: Statistical Review of World Energy 1,2015) Growth of Energy usage in the world with time in million tons of oil

Global warming is a rising issue, as people experience a warmer environment than in the past decade. Burning of fossil fuels like coal, crude oil, or any other form, emits Carbon Dioxide (CO_2) to the atmosphere and contributes to global warming. Figure 1-3 shows the emission of CO_2[2] in different countries, and figure 1-4 shows the rise of atmospheric temperature in the past few decades. Moreover, due to the vast amount of deforestation, purifying the air is an almost impossible task. This directly affects the temperature rise. According to figure 1-4 it is clear that the global temperature rises around 0.75 degrees every 50 years. Therefore more energy efficient machinery or machineries which can be powered by renewable energy will cause less fossil fuel reduction.

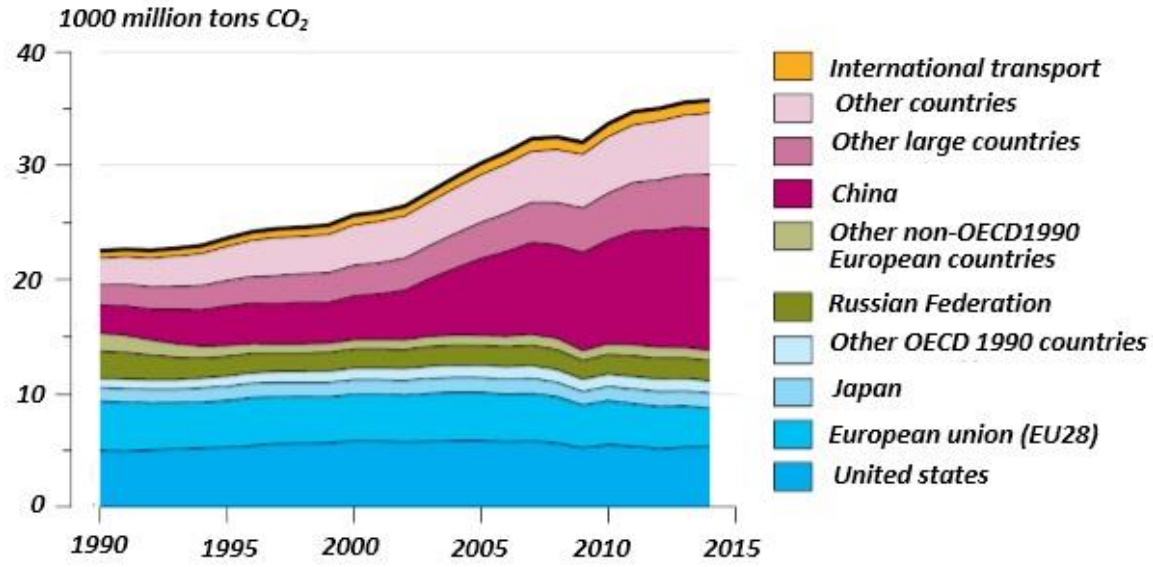

Figure 1-3. (Source: Trend in global CO_2 emissions) Carbon Dioxide emission all around the world

HVAC system has become a necessity in every building to provide ventilation,; either heating, or cooling, and, ventilation for a comfortable life. But to date, there has not been a system that fulfills this requirement efficiently. All over the world, buildings consume a huge amount of electrical energy every day. For example 40% of the global energy is consumed by buildings, and in Singapore, it is higher than 50%. In Singapore, buildings consume around 450kWh/m^2 a year, out of which, more than 50% is used for air conditioning. This is a vast amount of energy. Here, most required energy is produced, by burning fossil fuels. Therefore, designing buildings in a more energy efficient manner is a vital step to reduce energy consumption and CO_2 emission.

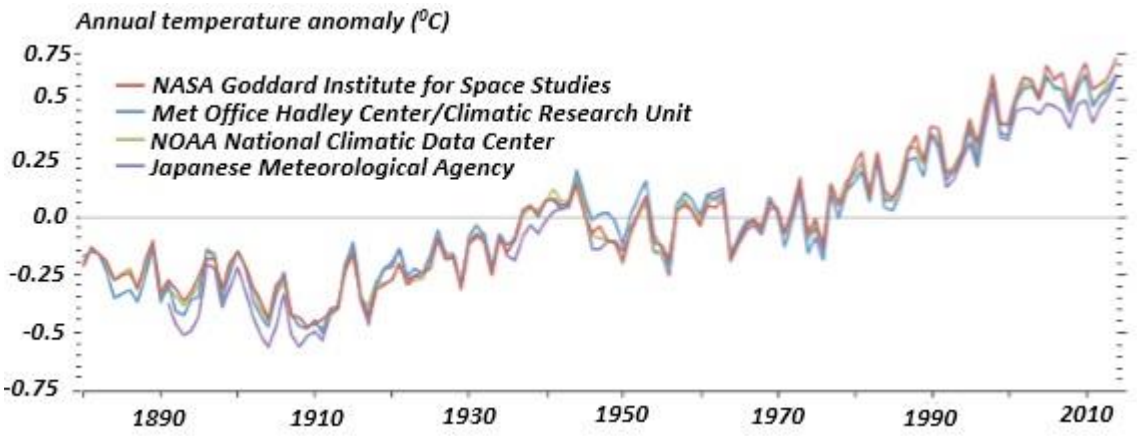

Figure 1-4.(Source: NASA Observatory) Rising of global temperature from different sources

Figure 1-5 shows the energy usage by buildings, for different applications. HVAC is the highest building energy consumption application, and it consumes more than the transportation industry all over the world. Therefore, a more efficient technology and design is needed in the HVAC process, in order to reduce the usage of energy. Efficient HVAC systems will address the issues of higher energy consumption, global warming effects, and heavy usage of natural resources.

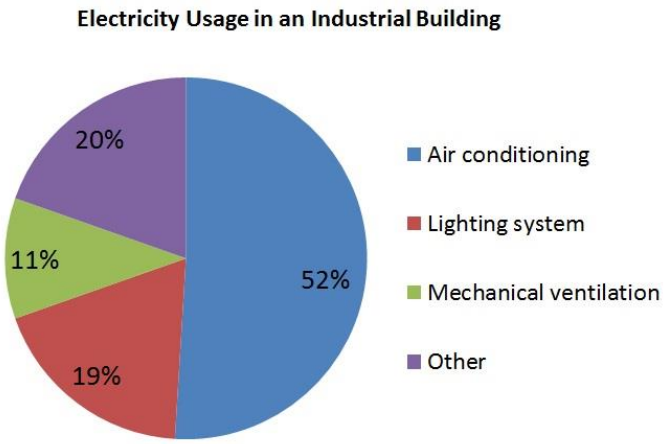

Figure 1-5. Energy usage of a building for different applications

In the pathway of finding alternative, efficient, HVAC systems to provide quality indoor environments with sufficient fresh air and accurate control of air temperature, the liquid desiccant dehumidification system comes into action. It uses desiccant solution to absorb water vapor from the conditioning air, and cools it down. The regenerator in the LDDS is the most critical component, as it absorbs large amounts of energy for the regeneration process, which brings the liquid desiccant to its initial concentration. The effectiveness of the process determines how efficiently, the dehumidification process occurs. However, most existing regenerators are neither efficient nor effective. Conventional type regenerators have several disadvantages like; carryover of desiccant solution with the air, taking a much longer time to regenerate, and very low in efficiency. Due to the carryover effect, the amount of liquid desiccant solution reduces with time. Therefore, a more efficient and effective regenerator needs to be designed which can address the above issues.

Vapor compression HVAC system is most popular all over the world, due to its simple cycle and easy implementation. But the system is not environmental efficient as it consumes a large amount of primary energy. If a system can be implemented successfully by

combining both primary and secondary level energy, it will reduce electricity consumption drastically.

Most industrial processes generate heat by burning fossil fuel, and then heat is released to the environment as waste. Large amounts of waste heat is being released into the environment; such as waste heat from power plants, exhaust gas from turbines and waste heat from industrial plants.

- Out of the total energy input for an industrial process waste heat could range from 20-50%. There is a 1.6 quadrillion Btu/year energy saving possibility from waste heat.

Solar energy can be utilized vastly in tropical climate countries and most other countries can receive a considerable amount of solar thermal energy. The capability of implementation of a solar thermal system or a waste heat recovery system in the regeneration process of the LDDS system is the main advantage which can save money and energy, as well is be one of the promising technologies of the future. However the issue is, that existing regenerators require higher heating temperature to achieve the vaporization temperature. In conventional LDDS, liquid desiccant solution sprays from the top of the chamber and flows downwards, whereas the hot air enters the chamber from the bottom and flows upwards. Desiccant mixes with hot air, and absorbs required amount of energy and water vapor evaporates. Therefore, a new regenerator design should be implemented to address: higher energy efficiency, with a low vaporization temperature to operate from solar thermal, geo thermal and waste heat, and to prevent the carry over effect of the desiccant.

1.3 Objective of the work

Liquid desiccant dehumidification technology is a promising replacement for the conventional inefficient vapor compression technology. The LDDS can be modified to make use of solar thermal energy, geo thermal energy or waste heat without depending on depleting fossil fuels. This would address many subjects like energy inefficient HVAC system, global warming effect, fossil fuel depletion, application of renewable energy sources and green building. However, there are some drawbacks of using renewable energy sources like solar thermal, because of their unpredictable nature and dependency on weather and climatic changes. LDDS has many areas that need to be improved to address current issues, and if there is a possibility to overcome above issues from a new design it will be a break though in HVAC industry. Therefore, the motivation for this project lies on the potential to save energy, possibility of combining renewable energy with the regenerator and reduction of greenhouse gas emission by lower fuel burning to generate primary energy. This study was conducted to achieve following five objectives.

Objective 1:

To conduct a literature review to identify influential regenerator design parameters for the performance of a regenerator, suitable heat transfer mechanism between the solution and the heating source, suitable environmental condition for the heat and mass transfer process using a low temperature heat source and suitable optimization algorithm to apply for the regenerator.

Objective 2:

To design a new regenerator which can fulfill objective one and address most of the prevailing issues related the regeneration cycle.

Objective 3:

To develop a mathematical model that would represent the real system with the highest agreement in order to get the performance for different parameter configuration.

Objective 4:

To conduct different types of testing by varying parameter values in order to examine the performance changes. Thereby, verify model with a fine tune using experimental data, to determine the best agreement.

Objective 5:

To optimize the system by using selected optimization algorithm for the new regenerator design and study the optimum operating condition of the parameters to achieve the highest heat and mass transfer for the lowest power consumption.

1.4 Novelty of the New Design

Dissolved water in the desiccant solution must be removed more efficiently with lower energy consumption within the regenerator. With the help of a new design by increase the efficiency of the regeneration process, energy consumption for the heating source can be reduced.

- New design provides more space for water vapor to release
    - When the evaporator is compact, if the released water vapor comes in contact with the solution again, it can get absorbed into the solution. Therefore, soon after water evaporates, it moves up in the chamber and due to pressure difference moves to another compartment, where the condensing process occurs.
- Vacuumed chamber for regeneration
    - Chamber is vacuumed and maintained the pressure around 1000 Pa. Vacuum chamber provides lower saturation temperature for water evaporation. Low saturation temperature provides opportunity to use a low temperature energy sources as the heating source.
- Lower temperature energy source
    - Lower temperature energy sources like solar thermal or waste heat can be implemented with the system as the saturation temperature is low.

1.5 Contribution

The main contributions of the thesis are summarized below:

- A newly designed vacuumed regenerator system, hybrid mathematical model for the parametric evaluation, and optimization of the system parameters for the maximum power efficiency, heat and mass transfer performance are investigated in this study. Vacuum pressure level, hot water flow rate and temperature, chilled water flow rate and chilled water temperature are identified as the key performance indices affect to the performance of the design. Formulas have been derived for heat and mass transfer coefficients for the evaporation and condensation process as a design guideline. The system is optimized by using multi objective genetic algorithm approach and the most efficient feasible and practical initial conditions are decided.

1.6 Thesis organization

The thesis is organized into seven chapters; Chapter 1 introduces the background, motivation for this research and novelty of the design. Current issues related to HVAC field and LDDS, environmental impact due to CO_2 emission and fossil fuel usage, factors which motivated to conduct the research and the novelty of the new design were discussed.

Chapter 2 provides a detailed literature review on the dehumidification system, including the regeneration process, available regenerator technologies and optimization techniques. Modeling of the regeneration process and condensation process are briefly explained. Advantages of different regenerator designs are discussed. Optimization of dehumidification systems, different approaches used, single objective and multi objective optimization with constraints are discussed.

Chapter 3 presents a detailed description of the newly designed vacuumed regenerator for LDDS. The arrangement, operation and specification of each component are described as well as the system operation procedure for better results.

Chapter 4 presents the modeling of the evaporation process considering heat and mass transfer. Overall heat transfer coefficient is modeled considering internal and external convective heat transfer coefficients and described here. Mass transfer coefficient for desorption process is also modeled described. In addition parametric analysis using experimental data is conducted and identified the effect to the heat and mass transfer.

Chapter 5 presents the modeling procedure of the vapor condensation process over external tube bank in condenser. Condensation on horizontal tube bank and the effect of water film generation over the tube, and its flow are investigated. Heat and mass transfer of the

condensation are modeled and presented. In addition parametric analysis is conducted and investigated the effect of operating parameters to the condensation process.

Chapter 6 explores the optimization procedure of the system for optimum heat and mass transfer and optimum power consumption. Procedure conducted for multi objective genetic algorithm to optimize five objective functions with constraints is presented. The achieved optimum condition and the application of that to the optimum operation are described.

Chapter 2 Literature Review

Heating ventilation and air conditioning (HVAC) industry faced huge problems in past few decades due to scarcity of energy resources, increase of energy demand for other applications due to population growth, greenhouse gas emission and other regulations to save environment [3]. To address these issues more energy efficient HVAC systems needed to be implemented. Eminent phase out of Chlorofluorocarbons (CFCs), eventual phase out of Hydro chlorofluorocarbons (HCFCs) and higher considerations for indoor air quality and occupant health, the increase of ventilation are some constraints needs to be faced during this implementation process.

2.1 Occupant Health and Indoor Air Quality

Air conditioning means conditioning of air, transports it, and introduces it to the conditioned space. It also controls and maintains the temperature, humidity, air cleanliness, air movement, and sound level for the comfort and health of the occupants. Temperature and humidity control within a control space for occupant health and comfort was studied by American society of heating refrigeration and air conditioning engineers (ASHRAE) and introduced health and comfort standards. ASHRAE standard 55 thermal comfort conditions for human occupancy [4] should have to follow for occupant health and indoor air quality during designing a conditioned space. Even though air conditioning systems like vapor compression and absorption systems capable of controlling temperature, they fail to provide required humidity level in humid climates.

2.2 Liquid Desiccant Dehumidification System

Air dehumidification system becomes a promising alternative to vapor compression and vapor absorption systems which overcomes issues and constraints related to latter systems. Dehumidification system was introduced more than 60 years ago for applications like product drying, corrosion prevention, clean rooms, hospitals, museums and other special cases that require highly controlled humidity levels. Since then the demand for dehumidification systems are increased substantially as shown in figure 2-1 [3].

Atmospheric temperature around 28^0C – 34^0C in tropical climatic countries and sometimes more than 40^0C during summer in other countries people suffer hugely from the heat. In the past few decades, the surface temperature of earth has rapidly increased due to global warming. Burning of fossil fuels releases CO_2 to the atmosphere and increases atmospheric temperature. To provide required thermal comfort, cooling load in high atmospheric temperature is higher. Increase of cooling load absorbs more primary energy from the grid for HVAC system, as a result more fossil fuel burns and releases more CO_2 to the atmosphere and the cycle continues again. Therefore, not only to control global warming but also to reduce fuel usage, energy efficient and alternative energy consuming machinery should be designed.

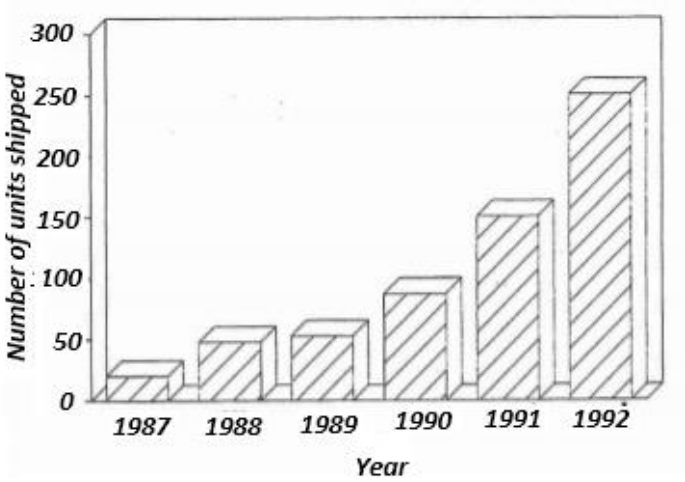

Figure 2-1.(Source: Review of Desiccant Dehumidification Technology. in Electric Dehumidification) Growth of Liquid Desiccant Dehumidification System Demand with time

Vapor compression system is an adaptive design for many applications to supply cooling to buildings. It has drawbacks such as, consuming huge amounts of electricity for the compression process and fails to provide required humidity in humid climates. Therefore, alternative solutions were studied. One such alternative solution is the evaporative cooling system that offers advantages like simplicity of operation, low initial and maintenance cost and requires much less primary energy. But this system does not perform well in humid climates and the moisture has to be removed from the air. Therefore, the liquid desiccant system comes into play to remove moisture or add moisture to the conditioning air. Newly designed hybrid dehumidification systems can effectively promote the single stage performance [5]. Following are main advantages of LDDS systems [6].

1. Can use renewable energy like solar or geo thermal energy and low grade waste heat instead of primary electrical energy.
2. Temperature and humidity can be controlled independently

3. Can use an environmentally friendly liquid that doesn't affect the ozone layer as working fluid of the system.

Air dehumidification can be achieved by two methods: cool down the air below its dew point and then moisture can be removed by condensation or by using a desiccant material to remove moisture by sorption [3]. Figure 2-2 shows the basic concept of desiccant dehumidification. The entering air must be cooled below its dew point to achieve the desired degree of dehumidification. Line 1 shows the conventional method of sensible cooling and reheating. Desiccant is used to reduce the humidity of the air stream in line 2, which is then sensibly cooled. Conditioning air achieved temperature above wet bulb temperature. As shown by line 2, dehumidification process is done adiabatically. Line 3 shows the simultaneous drying and sensible cooling known as isothermal drying [7]. For the desiccant dehumidification process both solid desiccant material and liquid desiccant material can be used. Even though the basic thermodynamic cycle is same in both approaches, the possibilities of improvements that can be done in the areas of system design, equipment and operation are different. Silica gel, molecular sieves, composite desiccants, nanoporous inorganic materials and polymetric desiccants can be used as solid desiccant materials and Lithium Chloride, Lithium Bromide and various glycols considers as liquid desiccants.

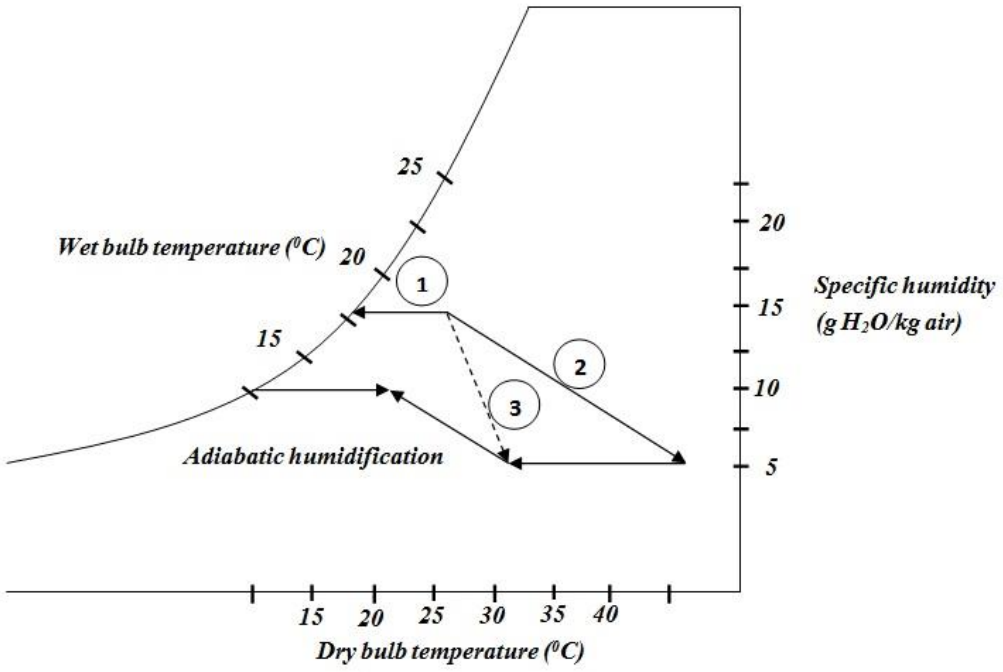

Figure 2-2. (Source: A packed bed dehumidifier/regenerator for solar air conditioning with liquid desiccant) Basic concept of desiccant air conditioning in the chart [7]

Triethylene glycol was used as the absorbent and solar heated air was used for the regeneration purpose in earliest liquid desiccant systems by Lof [8]. In this system, return air from a room was dehumidified and using an absorber it was cooled simultaneously and then evaporatively cooled [9]. Calcium Chloride and water mixture system has been suggested by Bolzan and Lazzarin. By using a huge amount of cold water, temperature around 17 ^{0}C, Robinson designed a LDDS system [9]. After Lof hundreds of people who had tried to improve the efficiency of the system design. Xing Li studied a packed column hybrid dehumidifier model and monitored the performance in real time and optimized the system using particle swarm optimization algorithm [6].

This conventional mechanical dehumidification system utilizes a huge amount of electrical energy to cool the conditioned air below the dew point temperature and reheats.

Hence the liquid desiccant dehumidification system which was more energy efficient was proposed and the conventional system was replaced. In this, moisture in the conditioned air is removed in the dehumidifier by the solution. Solution is regenerated and concentration is increased to reuse in the regenerator by outside air.

The most appropriate dehumidifier configuration for air conditioning application is the rotary wheel type as shown in figure 2-3. Processed air enters the system and comes into contact with the desiccant wheel and releases moisture to the desiccant and exits hot and dry. The Wheel is then rotates and the portion which absorbs moisture, removes moisture by using hot reactivation air. Since the air exit is hot because of the absorption heat it should be cooled down by using a sensible heat exchanger.

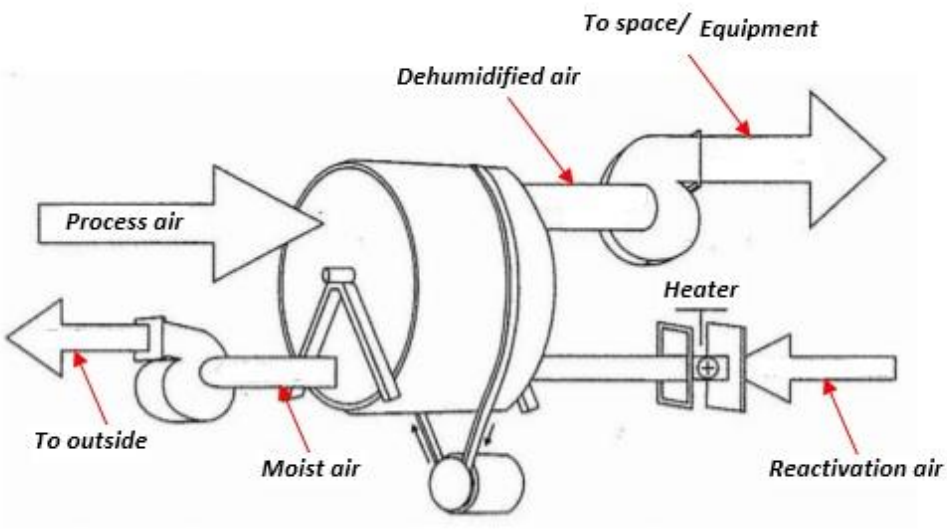

Figure 2-3 (Source: Review of Desiccant Dehumidification Technology. in Electric Dehumidification) Rotary wheel type dehumidifier configuration

Conventional liquid desiccant dehumidification system (LDDS) general structure is shown in figure 2-4. It consists of two packing beds: dehumidifier and regenerator. Moisture of the processed air is removed within the dehumidifier and the solution concentration is increased within the regenerator. Packing provides a good platform for the heat and mass transfer process. The working principle of the LDDS is as follows:

- Pre cooled liquid desiccant, by using the cooling heat exchanger, is sprayed on to the top of the packing bed of the dehumidifier. Process air blows from the bottom of the dehumidifier and makes contact with the sprayed desiccant solution and releases water vapor to the desiccant solution, thereby reduces the humidity.

- Desiccant solution gets collected to the bottom of the dehumidifier and it pumps back to the regenerator.

- In the regenerator, the pre-heated liquid desiccant is sprayed on to the top of the packing bed to make contact with the ambient air blowing from the bottom of the packing bed. Since the hot desiccant solution has a higher surface vapor pressure than that of the ambient air, heat and mass transfer takes place from the desiccant solution to the ambient air.

- Desiccant temperature difference between the dehumidifier and the regenerator is around $50^{o}C$. A heat exchanger is placed in between to recover heat from the hot desiccant to the cold desiccant.

- It is required to place a cooler and a heater at dehumidifier and regenerator side respectively, in order to meet their respective dehumidifying and regenerating temperatures.

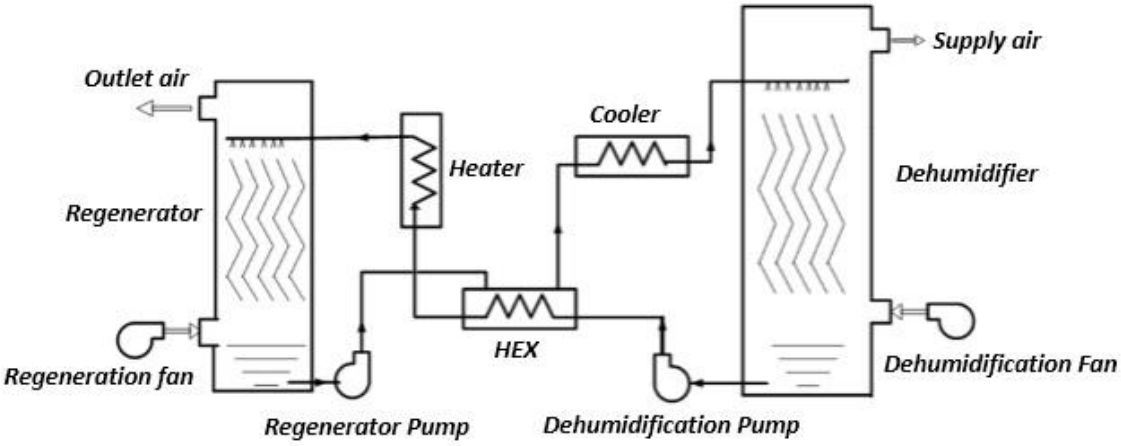

Figure 2-4. Conventional LDDS general structure

Regeneration Process:

Regeneration process is one of the most critical processes in LDDS system as the whole system performance depends on the effectiveness of this process. The liquid desiccant solution, after absorbing the water vapor from the air, it should be regenerated. The concentration of the liquid desiccant solution reduces after absorbing the water vapor. Therefore, it should be processed back to the original concentration. This process is called the regeneration process. Performance of a dehumidifier and regenerator was investigated, which ran on 60-80 ^{0}C with a mean mass transfer coefficient of around 4g/m^{2}s [10].

Low grade secondary energy like solar thermal or waste heat can be used in the regeneration process instead of primary energy [11]. Many researchers investigated the effect of parameters like air and desiccant flow rates, air temperature and humidity, desiccant temperature and concentration and the area available for heat and mass transfer.

A theoretical model was developed and investigated the heat and mass transfer process of a packed bed liquid desiccant regenerator and studied the effect of above mentioned parameters to the performance [11]. In the experiment system they used Triethylene glycol was the liquid desiccant and solar thermal collector was used to provide required heat for the regeneration process.

Regenerator Design:

In a dehumidifier, liquid desiccant sprays from the top and flows down as droplets while the process air flows from bottom to top. Liquid desiccant absorbs water vapor from the process air and reduces the humidity of the process air. The capability of this mass transfer process depends on the water vapor pressure difference between the liquid desiccant and air. When liquid desiccant absorbs more water vapor, the vapor pressure increases leading to a reduction in the vapor pressure difference, due to which the mass transfer driving force will reduce. Therefore, this liquid desiccant should remove its absorbed water vapor. The regenerator chamber is the place which is used to regenerate liquid desiccant to a higher concentration. Regeneration process is an evaporation process which involves phase change and breaking of chemical bonds. Therefore huge amount of energy is required. The performance of the regeneration process is studied as a function of desiccant flow rate, inlet desiccant condition and inlet air humidity by using a mixture of Calcium Chloride and Lithium Chloride as liquid desiccants [11]. Different types of liquid desiccant regenerators were studied by many researchers for effective regeneration process. The parallel flow regenerator has the best mass transfer performance than the counter flow regenerator, with hot air as the heat source. In the hot desiccant driven regenerator counter flow regenerator

has the better mass transfer performance than the parallel flow regenerator [12]. Table 2-1 discusses different types of regenerator designs and their drawbacks.

Table 2-1. Different regenerator designs and their drawbacks

Regenerator design	Description	Drawbacks
Vertical chamber regenerator	• Solution flows downward from the top of the chamber and dry air flows upward from the bottom of the chamber. • Solution sprays from top and touches with the dry air and water vapor releases to dry air.	• Two fluids touch each other • Carryover effect of desiccant • Mass transfer area is small
Packed bed regenerator	• Solution sprays from top and flows downwards and dry air flows upward from bottom of the chamber. • A packing material introduces inside the chamber to provide more time and space for the solution and air to contact each other. Packing comes with structured and unstructured packing methods. Small plastic balls, rectangular objects are used as packing material.	• Two fluids touch each other • Carryover effect of desiccant

	• Juan Yu studied the performance of packed bed regenerator using balls and packed them randomly inside the chamber [13].	
Submerged type regenerator	• Desiccant solution filled inside the chamber. • Heat exchanger submerged within the desiccant solution. • Hot water flows inside the tubes of the heat exchanger and supplies required amount of heat. • Desiccant absorbs heat and releases water vapor.	• Requires a high temperature heat source • Carryover effect of desiccant
Flat plate regenerator	• Solution flows from top to bottom through vertical flat plates. • Isothermal walls provide required amount of heat to the solution. • Solution collects at the bottom of the chamber and re-circulates for further desorption.	• Solution remain at the bottom causes to absorb water vapor again • Isothermal walls limits the upper temperature
Heat exchanger type regenerator	• Hot water flows through horizontal tubes lay inside the chamber. • Solution flows down from top to bottom and catches heat from heat exchanger tubes.	• Required heat source temperature is high.

	• Two types: solution flows on top of the tubes, solution sprays on top of tubes.	• Solution can absorb water vapor again.

Modeling of regenerator:

Many authors developed models to study the performance of the regeneration process of the LDDS. Considering the operating conditions following key components are modeled: heat and mass transfer coefficient, heat and mass transfer effectiveness, desorption rate, condensation rate and overall efficiency. Total heat transfer coefficient of the system defines how effectively the heat can be transferred to the solution from the heat source. Total heat transfer coefficient depends on many other parameters and the optimum values for those parameters can be identified by optimizing the derived equations.

Maximum efficiency of the LDDS can be achieved by the optimum operating condition of the regenerator. Desorption rate and condensation rate of the regeneration process should be equal in the new system. Therefore the effect of hot water circulation rate, chilled water circulation rate, solution circulation rate, hot water temperature, chilled water temperature and vacuum pressure level should be identified through the model to maintain the required condition.

Many researches were carried out for packed column regenerator with structured and unstructured packing. Researchers investigated the heat and mass transfer characteristics of the system to find out affecting parameters. M. Krause developed a model for absorber and

regenerator in liquid desiccant air conditioning unit and validated the model using experimental data [14].

Figure 2-5 shows the heat flow from one liquid to another through a solid wall. In an instant where fluid A is inside a tube and fluid B outside the tube, there will be three types of resistances acting on the heat flow. They are, resistance between fluid A and solid wall (R_A) on the heat flow, resistance of the solid wall (R_w) on the heat flow and resistance between fluid B and solid wall (R_B) on the heat flow. All three resistances can be represented from an electrical circuit as shown in figure 2-5. These resistances relate to the overall heat transfer coefficient, to calculate the overall resistance on the heat flow [17].

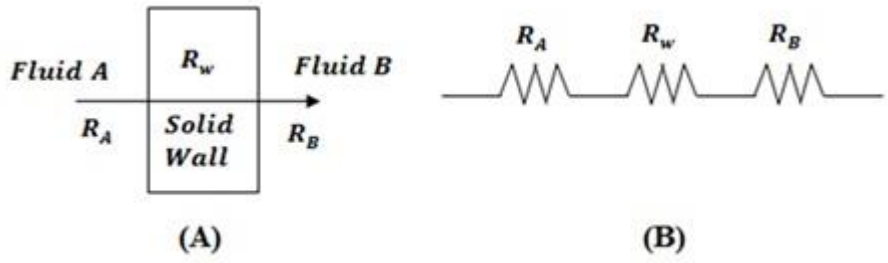

Figure 2-5. Thermal resistance for heat flow from one fluid to another

Heat transfer rate is related to overall heat transfer coefficient, heat transfer area and temperature difference as shown in the below equation [17].

$$Q = U\ A\ \Delta T$$

$U - Overall\ heat\ transfer\ coefficient$

$A - Heat\ transfer\ area$

$\Delta T - Temperature\ difference$

Resistances can be related to the overall heat transfer coefficient by using the heat transfer coefficient of both fluid sides and thermal conductance of the solid wall as below [6].

$$\frac{1}{UA} = \frac{1}{h_A A_A} + \frac{dx}{kA} + \frac{1}{h_B A_B}$$

$h_A - \ Fluid\ A\ side\ convective\ heat\ tranfer\ coefficient$

$h_B - \ Fluid\ B\ side\ convective\ heat\ tranfer\ coefficient$

2.3 Heat & Mass Transfer Model

An analytical model was developed and studied for a direct contact cooler condenser in a packed column [7]. Gas and liquid interface temperature was taken and applied the Olander's model to calculate the vapor pressure. Nusselt number definition can be used to calculate the convective heat transfer coefficient. Reynolds number and Prandlt number can be calculated from fluid properties and heat exchanger properties [15].

$$Nu_D = \frac{hD}{k} = C\ Re_D^e Pr^f = C\left(\frac{\rho\ u\ D}{\mu}\right)^e \left(\frac{C_p\ \mu}{k}\right)^f$$

Liquid desiccant based evaporative cooling for a tropical climate was tested, and a computer model was developed and simulated to study the performance [9]. Reynold's analogy was used to calculate the heat transfer coefficient and the Gnielinski correlation was used to calculate the Nusselt number [9]. Different operating conditions of the system were

obtained by varying the temperature ratio of the air, humidity ratio of the air and mass flow rate of solution, air and water, thereafter predictions were verified with a 30% error margin.

$$Nu_D = \frac{f \times \Pr\left(\frac{Re_a - 1000}{2}\right)}{1 + 12.7\sqrt{\frac{f}{2}}(Pr^{2/3} - 1)} \quad ; \quad \begin{matrix} 0.5 \leq \Pr \leq 200 \\ 2300 \leq Re \leq 5 \times 10^6 \end{matrix}$$

where,

$$\sqrt{f} = \frac{1}{(1.58\ln(Re_a - 3.28))}$$

A heat and mass transfer hybrid model for the dehumidifier of the LDDS was developed by considering the energy balance, heat transfer and the resistance to heat transfer. Following basic equations were used for the general calculation for the heat transfer and mass transfer [6].

$$Q = \frac{T_{a,in} - T_{s,in}}{R_h}$$

where,

$Q - Heat\ transfer\ rate$

$T_{a,in} - \ Inlet\ process\ air\ temperature$

$T_{s,in} - \ Inlet\ desiccant\ solution\ temperature$

$R_h - \ Thermal\ resistance\ to\ overall\ heat\ transfer$

$$h = C\left(\frac{4\,\dot{m}}{\pi\,\mu\,D}\right)^e \left(\frac{C_p\,\mu}{k}\right)^f \frac{k}{D} = b\,\dot{m}$$

Overall thermal resistance can be given by the following equation [6].

$$R_h = \frac{1}{h_s A_s} + \frac{1}{h_a A_a} = \frac{b_1 A_s \dot{m}_s^e + b_2 A_a \dot{m}_a^e}{b_1 A_s \dot{m}_s^e \; b_2 A_a \dot{m}_a^e}$$

A packed bed generator used in absorption refrigeration system has the same mechanism for liquid evaporation used by Balamurugan and Mani. Hot water enters the vertical plate heat exchanger from the bottom and flows out from the top. R134a/DMF solution enters from the top to the heat exchanger, absorbs heat and R134a releases as vapor. Log mean temperature difference method was used to calculate the overall heat transfer coefficient and two phase Reynolds number was calculated using the Lockart- Martinelli parameters. Nusselt number was calculated using the Reynolds number and Prandtl number. Sherwood number was calculated using Reynolds number, Schmidt number, concentration gradient and heat flux. Constants of both equations were calculated using MATLAB [16, 17].

$$Nu = 4.442 \times 10^{-7} \left(Re_{tp}\right)^{2.508} (Pr_l)^{-3.714}$$

$$Sh = 2.520 \times 10^{7} \left(Re_{tp}\right)^{-1.24} (Sc_l)^{-0.549} (X_{sw})^{-0.642} Q^{1.844}$$

Air to solution heat and mass transfer study can be shown as below figure 2-6 [8]. Basic Mass balance and energy balance equations were used for air side, solution side and for water flow to calculate unknown parameters. Equations were non-linear first order differential equations and numerical solutions were obtained by dividing the regenerator into a large number of pieces. Gnielinski correlation was used to calculate the Nusselt number [8].

$$Nu = \frac{f \times \Pr\left((Re_a - 1000)/2\right)}{1 + 12.7\sqrt{\frac{f}{2}}(Pr^{2/3} - 1)}$$

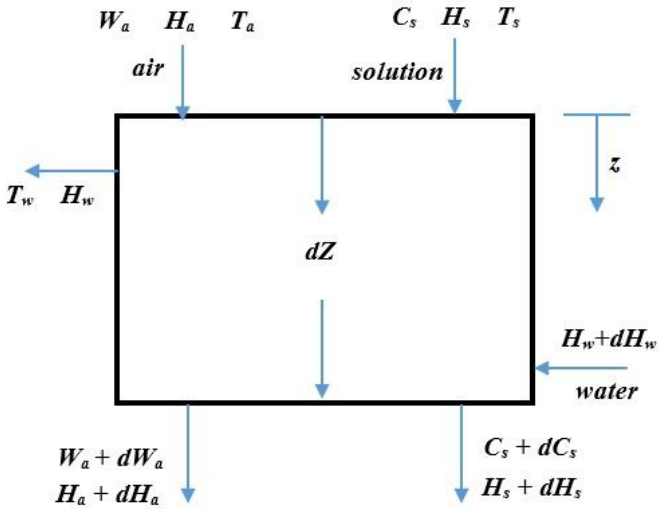

Figure 2-6. Air, solution and water flow through the selected area and their humidity and energy changes

Heat and mass transfer process in a packed bed liquid desiccant regenerator was studied. Higher mass transfer gradient on the interface was achieved by higher solution flow rate. Constant humidity ratio was assumed for the derivation of the analytical solution. The effect of, air and liquid desiccant flow rate, air temperature and humidity, desiccant temperature and concentration on the evaporation rate were studied. Here, Chung correlation for gas phase mass transfer coefficient for structured packing was used. It was found that the desiccant concentration has the highest effect to the evaporation rate, and desiccant temperature and air flow rate also has a significant effect [18].

The performance of a packed tower for liquid dehumidification and regeneration using lithium chloride desiccant was studied. Wetted surface area was calculated by using Ondas

correlation, where k type mass transfer coefficient proposed by Oberg and Goswami was used. Air flow rate, humidity ratio, desiccant temperature and desiccant concentration have the highest effect on the dehumidifier performance. Desiccant temperature, desiccant concentration and air flow rate have the most effect on the condensation performance and he found out that influence of those parameters is linear [19].

When there is a chamber or a system which contains two or more fluids whose concentration varies from one point to another there is a tendency for that component to move to the less concentrated area. This is called the mass transfer and it is a very important phenomenon that should be studied deeply for many industrial processes like, absorption, desorption and mixing. The mechanism of mass transfer involves both molecular diffusion and convection.

By considering the water vapor pressure between the process air and desiccant solution as the driving force for mass transfer, Henry's two film theory and Onda's proposed mass transfer correlations between air and desiccant solution can be used to calculate the overall mass transfer coefficient [6].

$$N = K_G\left(P_{a,in} - P_{s,in}\right)$$

where,

$N - Mass\ transfer\ rate$

$K_G - Overall\ mass\ transfer\ rate\ in\ the\ dehumidifer$

$P_{a,in} - Water\ vapor\ pressure\ in\ the\ inlet\ air$

$P_{s,in} - Equilibrium\ water\ vapor\ pressure\ of\ desiccant\ solution$

$$K_G = \frac{1}{\frac{1}{K_a} + \frac{1}{H\,K_s}}$$

where,

$K_a -$ *Convective mass transfer coefficient of gas phase*

$H -$ *Henry's law constant*

$K_s -$ *Convective mass transfer coefficient of liquid phase*

$$K_a = a_1 \left(\frac{4\dot{m}_a}{\alpha_t \mu_a \pi D^2}\right)^{e1} \left(\frac{\mu_a}{\rho_a D_a}\right)^{f1} (\alpha_t D_p)^{g1} \frac{\alpha_t D_a}{R\, T_a}$$

$$K_s = a_2 \left(\frac{4\dot{m}_s}{\alpha_w \mu_s \pi D^2}\right)^{e2} \left(\frac{\mu_s}{\rho_s D_s}\right)^{f2} (\alpha_t D_p)^{g2} \left(\frac{\rho_s}{\mu_s\, g}\right)^{j2}$$

where,

$\alpha_t -$ *specific surface area*

$\alpha_w -$ *wetted specific surface area*

$D_p -$ *nominal size of packing material*

D_a, ρ_a, μ_a *and* D_s, ρ_s, μ_s

$-$ *diffusivity, density, viscosity of process air & desiccant solution*

2.4 Water Vapor Condensation

Water vapor condensation is another important and critical phenomenon that needs to be modeled. Condensation is defined as the phase change from vapor state to liquid state. Pressure reduces due to condensation with a mass transfer takes place towards the area where condensation occurs. Surface condensation occurs when the vapor contacts a cold

surface which has the temperature below than its saturation temperature. Mostly heat exchangers are used for heat transfer purposes and depending on the type of heat exchanger, study of condensation differs.

Before analyzing a bundle of horizontal tubes, studying a single tube and modifying the equation for the bundle is easier. Condensed vapor flow of the external surface of the tube considers in laminar flow state, due to the length to travel is shorter as shown in figure 2-7.

The equation for the liquid heat absorbed, can be written as below.

$$h_{LG}\frac{d\tau}{dz} = \frac{k_L\left(T_{sat}\left(P_g\right) - T_w\right)}{\delta}$$

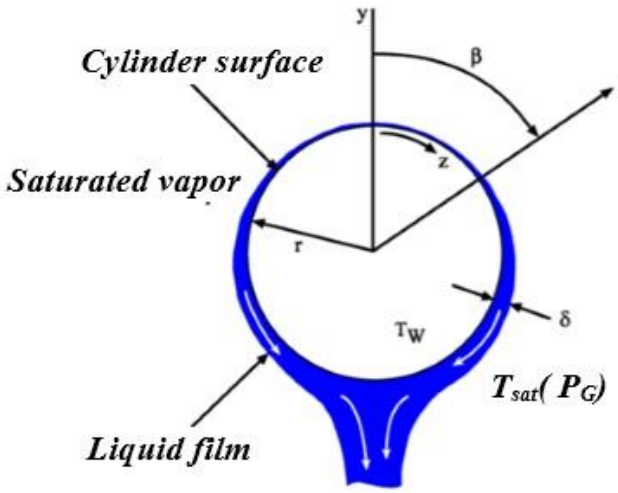

Figure 2-7. Water vapor condensation around the tube

The amount of vapor condensate (τ) per unit length can be calculated by developing the velocity profile to the liquid layer and integrating from the wall to the liquid layer surface. By integrating along the top of the tube $\tau = 0\ at\ \beta = 0$ to the bottom of the tube $\tau = \tau\ at\ \beta = \pi$, the total amount of condensation in half of the tube, can be calculated and the equation can be given as shown below [20].

$$\tau = 1.924 \left[\frac{r^3 k_L^3 (T_{sat} - T_w)^3 (\rho_L - \rho_G)\ g}{h_{LG}^3 v_L}\right]^{1/4}$$

By using the above mean heat transfer coefficient was developed as below.

$$\alpha_f = 0.728 \left[\frac{\rho_L (\rho_L - \rho_G)\ g\ h'_{LG} k_L^3}{D\ \mu_L (T_{sat} - T_w)}\right]^{1/4}$$

When there is a bundle of tubes, analysis depends on several factors. How the condensed liquid flows from top tubes to the bottom ones, whether the sub-cooling of the film is important or not, whether the effect of the vapor shear is significant or not and at which point the film turns from laminar to turbulent. There are different film flow modes from top to bottom such as droplet mode, column mode, sheet mode and spray mode.

Droplet Mode

Condensed liquid from the top tube to the bottom tube flows down as droplets. A droplet dropping frequency depends on the rate of condensation and the droplet size depends on fluid properties like density, viscosity and surface tension.

Column Mode

When the condensation rate is high droplets coalesce to form liquid columns and this can starts different locations of the tube as shown in figure 2-8-A. Liquid column reaches the top of the bottom tube and spreads over it as shown in figure 2-8-B.

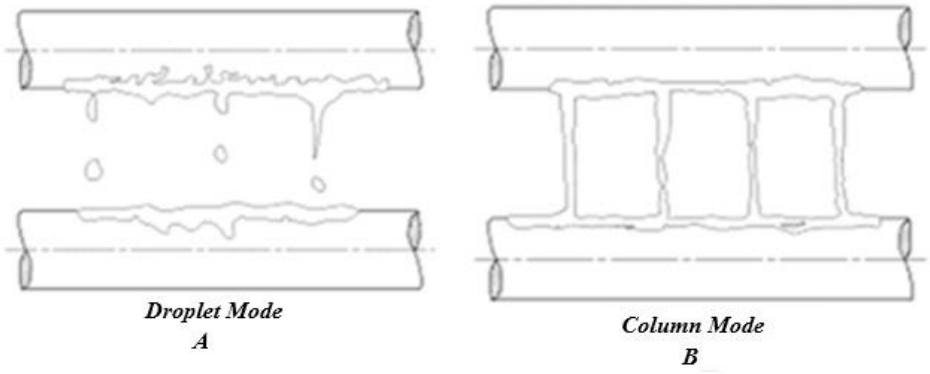

Figure 2-8. A- Droplet mode water film flow & B- Column mode water film flow

Sheet Mode

When the flow rate is very high the amount of film flow will not be enough and the columns become unstable. Thereafter a few columns combine and become sheets and later on all sheets become a single sheet as shown in the figure 2-9.

Spray Mode

When there is a force convection vapor flow, condensed liquid droplets are carried away by the vapor flow and carried to the tube below tube as spray of droplets in a chaotic manner.

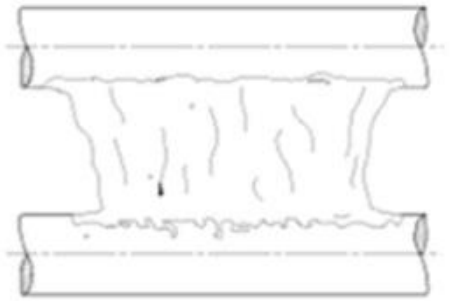

Figure 2-9. Sheet mode water film flow

In 1916 Nusselt studied the laminar flow of a condensing fluid on a vertical surface. He proposed a simple force balance, assuming the gravity and shear force to act on the fluid film layer, neglecting both energy convection and fluid acceleration. It was assumed that constant fluid properties and heat transfer process is due to condensation only. According to figure 2-11 balancing the forces of the liquid element gives the following equation subjected to that there isn't any acceleration or inertia effect [21].

$$(\delta - y)\, dz\, (\rho_L - \rho_G) g = \mu_L \frac{du_y}{dy}\, dz$$

Dimensionless Nusselt number was defined by the following equation [21].

$$Nu = \frac{h_m\, L}{k_l}$$

$h_m -$ *Global heat transfer coefficient*

$k_l -$ *Thermal conductivity of the condensate*

$L -$ *Total length of consideration*

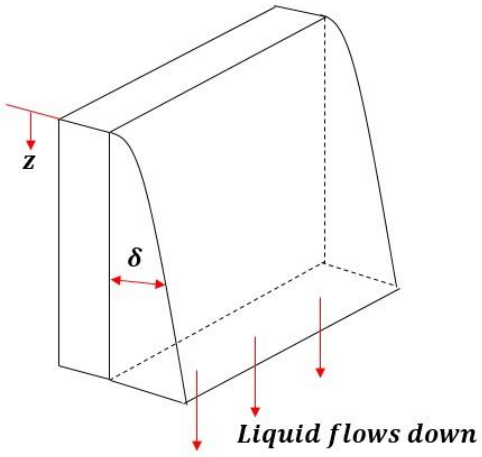

Figure 2-10. Liquid flow down on a vertical plate

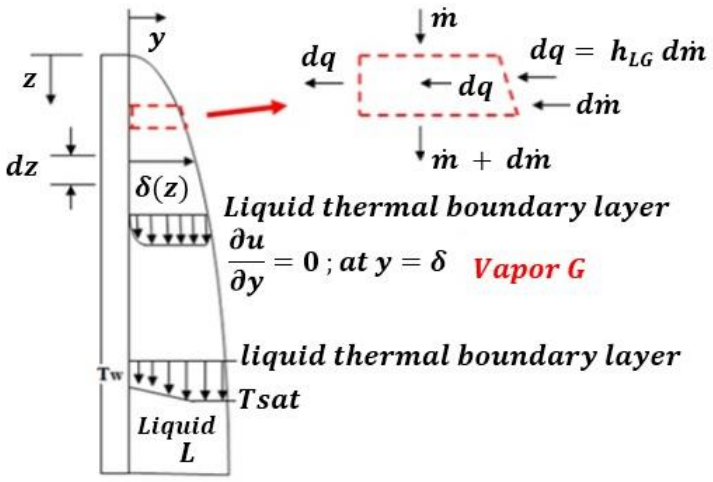

Figure 2-11. Velocity boundary layer and thermal boundary layer of a liquid flow down on a vertical plate

Boundary layer equations were solved by Ming Chen in his study for a single horizontal tube and vertical banks of horizontal tubes. The inertia effect was considered and assumed that vapor was stationary for a single tube case and found out that there was a larger effect from the inertia to heat transfer. The heat transfer effect for lower tubes which can be

calculated from the Nusselt theory was lower than the calculation results due to reasons being splashing and ripple [20, 22].

Water vapor condensation of a vertical plane which separate cold water and vapor air mixture was studied. A set of differential and algebraic equations were derived to represent the system and simultaneously solved them to find the water vapor flow, condensate and coolant flow [23]. Thermal resistance to water vapor condensation on horizontal tube bank was studied. The influence of vapor, cooling water and non-condensable gas properties were studied. Thereafter following equation with thermal resistances was presented. Different resistances were calculated separately and following parameters were checked for the performance: pipe material, cooling water velocity, cooling water inlet temperature, steam inlet velocity, tendency to fouling deposit formation and amount of non-condensable gases. After testing two types of condenser, it was seen that each parameter was affected in the same manner in both cases.

$$R = \frac{d_o}{d_i} R_w + R_d + R_p + R_a + R_v$$

$R_w -$ *water side thermal resistance*

$R_d -$ *Fouling thermal resistance*

$R_p -$ *wall resistance*

$R_a -$ *condensate thermal resistance*

$R_v -$ *non − condensible gases thermal resistance*

The condensation effect of steam and R113 on a horizontal tube bank in the presence of non-condensable gases was tested. There was a good agreement of a single tube theory on the top rows of tubes. Lower rows of tubes of the tube bank where air concentrations were higher and vapor velocities were lower, some discrepancies between the experimental results and theoretical results were occurred. To calculate the mass fraction of air in the vapor mixture he used Gibbs Dalton ideal gas mixture equation by assuming saturation conditions [24].

Performance Evaluation Parameters for the Regenerator

Effectiveness of the heat and mass transfer process in a packed bed LDDS dehumidifier and regenerator was studied by Viktoria. The effect of design variables like the difference between the vapor pressure of the desiccant, the partial pressure of the water vapor in the air, the area for heat transfer and some other design variables to the system performance were studied [25]. The desiccant solution vapor pressure was a function of its concentration and temperature. Following equations were used for the analysis.

$$Effectiveness; \quad \varepsilon_{HE} = \frac{Q_{actual}}{Q_{max}}$$

$$Humidity\ effectiveness; \quad \varepsilon_Y = \frac{Y_{IN} - Y_{OUT}}{Y_{IN} - Y_{EQU}}, \qquad Y\ is\ the\ humidity\ ratio$$

Martin and Goswami also used the above equation to calculate the humidity effectiveness but they also used the equation derived by Chung to calculate the humidity effectiveness based on air and solution flow rates, column and packing dimensions and equilibrium properties of the desiccant. For the theoretical modeling a finite difference model presented by Treybal for adiabatic gas absorption was used [11].

$$\varepsilon_Y = \frac{1 - \left\{\frac{0.205\left(\frac{G_{in}}{L_{in}}\right)^{0.174} exp\left[0.985\left(\frac{T_{a,in}}{T_{L,in}}\right)\right]}{(aZ)^{0.184}\pi^{0.168}}\right\}}{1 - \left\{\frac{0.152\ exp\left[-0.686\left(\frac{T_{a,in}}{T_{L,in}}\right)\right]}{\pi^{3.388}}\right\}}$$

Here the parameter π represents the equilibrium properties of the desiccant and it is defined as the ratio between the vapor pressure difference and the vapor pressure of the pure water.

$$\pi = \frac{P_w(T_{L,in}) - P_L(T_{L,in}, X_{in})}{P_w(T_{L,in})}$$

Evaluation of the performance of any newly designed system is the most prior target and there are several parameters that can be calculated to compare the performance of the regenerator. The objective of the regeneration process is to transfer water from the weak desiccant solution to the air. A novel liquid desiccant dehumification system utilizing LiCl with two columns, one for dehumidification of the process air and the other for regeneration was simulated [26]. COP of the system was calculated from the ratio between the cooling capacity of the system and regeneration load.

Desorption rate (e_d):

Desorption rate is the rate of water vaporizes from a solution per second. Desorption rate can be calculated using the heat transfer equation or by calculating the water concentration difference between the inlet solution and the outlet solution. The performance of structured packed bed liquid desiccant regenerator was studied and the evaporation rate of water vapor was calculated by the humidity difference between the inlet and outlet air streams [25].

$$e_d = \dot{m}_s(X_{xwi} - X_{swo})$$

Desorption ratio ($\boldsymbol{m_d}$):

Desorption ratio is the ratio between the amount of water evaporated from the solution, to the solution flow rate. This parameter indicates how the evaporation amount can change depending on the solution flow rate with time. This can be calculated using the following equation.

$$m_d = \frac{\dot{m}_d}{\dot{m}_s}$$

Concentration effectiveness ($\boldsymbol{\varepsilon_c}$)

Concentration effectiveness means how effectively the concentration of LiBr increases with respect to the maximum possible concentration increment. It can be calculated by taking the ratio between the actual concentration changes to the maximum possible concentration change [27].

$$\varepsilon_c = \frac{(X_i - X_f)}{(X_i - X_{f,max})}$$

Heat transfer effectiveness ($\boldsymbol{\varepsilon}$)

This is the ratio between the actual amounts of heat transfer to the maximum possible amount of heat transfer. It can be calculated using the following equation.

$$\varepsilon = \frac{\dot{Q}}{Q_{max}}$$

Condensation rate ($\boldsymbol{mc_c}$)

This is the amount of water vapor condenses per second and the value can be calculated using the rate of heat transfer within the condenser.

2.5 System Optimization

Performance evaluation parameters can be used to study and compare how effectively a system performs in different operating conditions. Outputs of different operating conditions of a system can be same or different and it depends on the effect of each parameter to the system performance. Therefore, conducting a proper study and finding out the best operating condition of the system to have the optimum output is known as optimization of the system.

General optimization function can be stated as below:

Optimize $G = g(x)$

x is subject to: $h(x) = 0$

$z(x) \leq 0$

The goal is to determine the decision variable x that optimize the subjective function G, while ensuring that the model operates within the constraints $h(x) = 0$, $(x) \leq 0$.

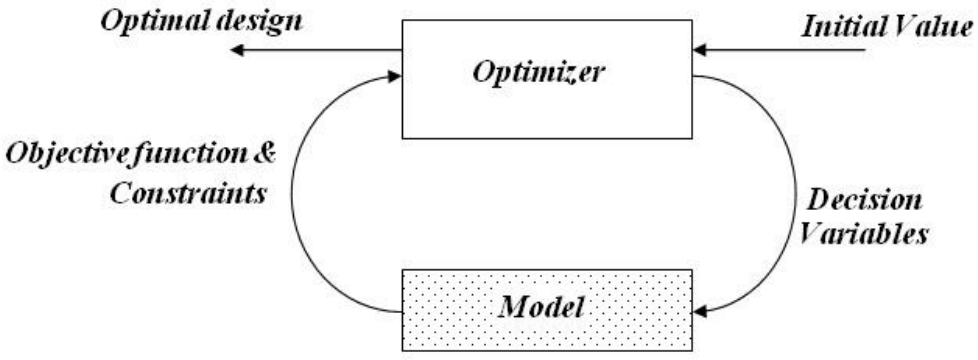

Figure 2-12. Simple schematic which explains how the optimization works

Particle swarm algorithm is a computer method of optimization which optimizes a problem iteratively. It uses the controlling parameter to improve the required solution with regard to a given measure of quality. It considers the search space as a space filled with particles and moves those particles around with simple mathematical formulae over the particle position and velocity, in search of the candidate solutions. Each particle moves with the influence of its 'local best known position' and also it is guided towards the search space 'best known position'. Each particle keeps track of its coordinates in the particle space which are associated with the best solution it has achieved so far. This best solution coordinates' value is known as the pbest. Another "best" value that is tracked by the particle swarm optimizer will become the best value and this location is called the Ibest. When particles take all the populations as its topological neighbors, the best value it obtains is the global best value called gbest.

Liquid desiccant regenerator was optimized by multi object particle swarm algorithm [28]. Energy usage was minimized by keeping, regeneration rate within an acceptable range, constraints of decision variables and component interactions. 8.85% energy is saved using the proposed method compared to the conventional optimization methods. Figure 2-13 illustrates the flowchart of the multi objective decreasing inertia weight particle warm optimization strategy used in [28] to optimize the LDDS.

LDDS was studied to improve the performance of the dehumidifier by considering the influences of parameters like desiccant temperature, desiccant concentration, desiccant flow rate, air flow rate and relative humidity on the effectiveness of the dehumidifier. Taguchi method has been used to find the optimum operation condition [60]. A data driven, dynamic neural network and strength multi-objective particle swarm algorithm was used to

optimize a heating ventilation and air conditioning system (HVAC) [29]. Data from a HVAC system was used and developed a dynamic model with the help of data mining algorithm. Particle swarm algorithm is suitable for solving complex non-linear, discrete and large scale systems. As shown in figure 2-14, a similar model has been studied in optimization of an HVAC system with a strength of multi objective particle swarm algorithm [30]. In the past several years many researchers followed the particle swarm algorithm and found out that this method gives better solutions in faster and cheaper ways compared to others.

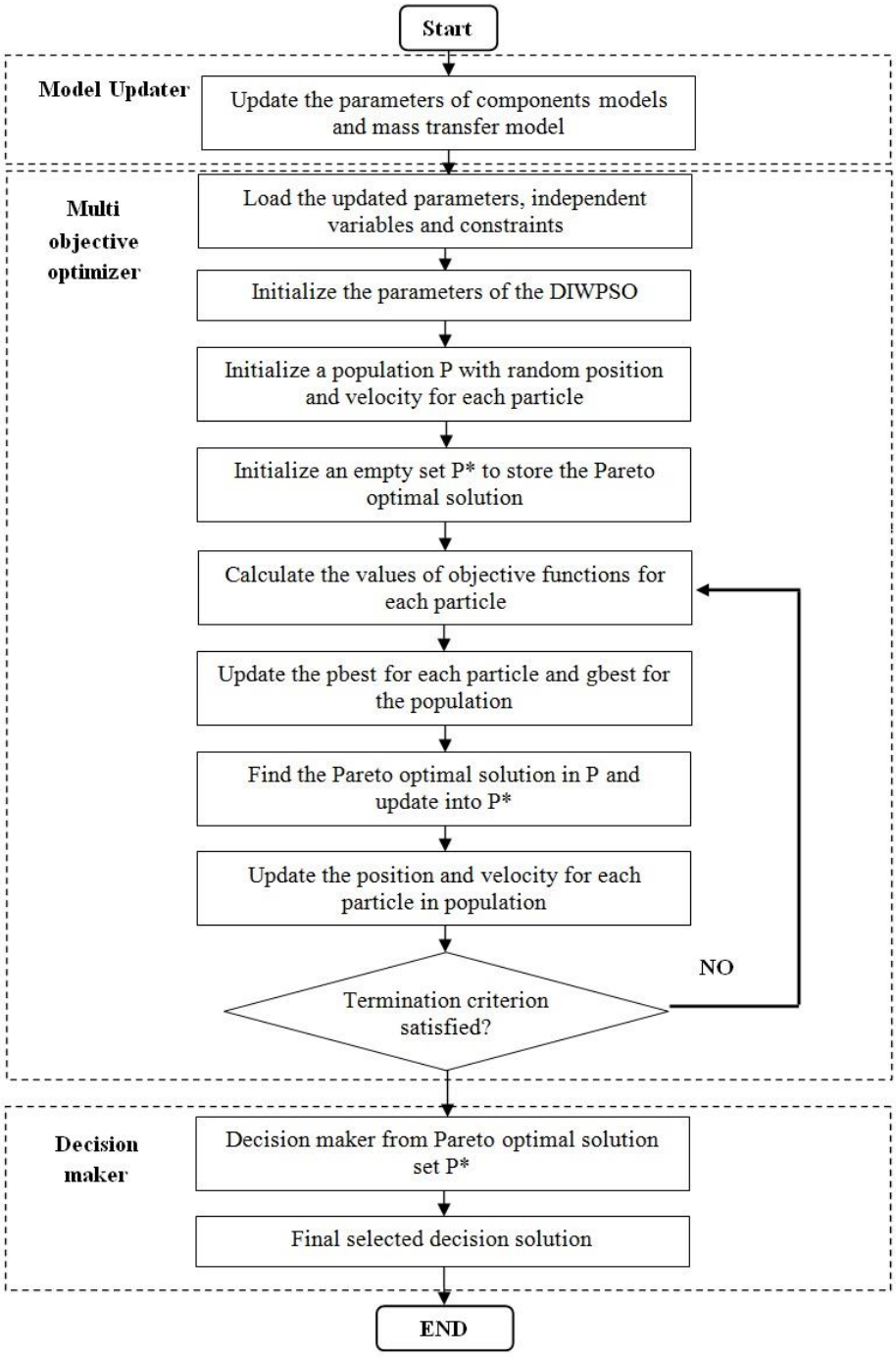

Figure 2-13. Multi objective decreasing inertia weight particle warm optimization strategy

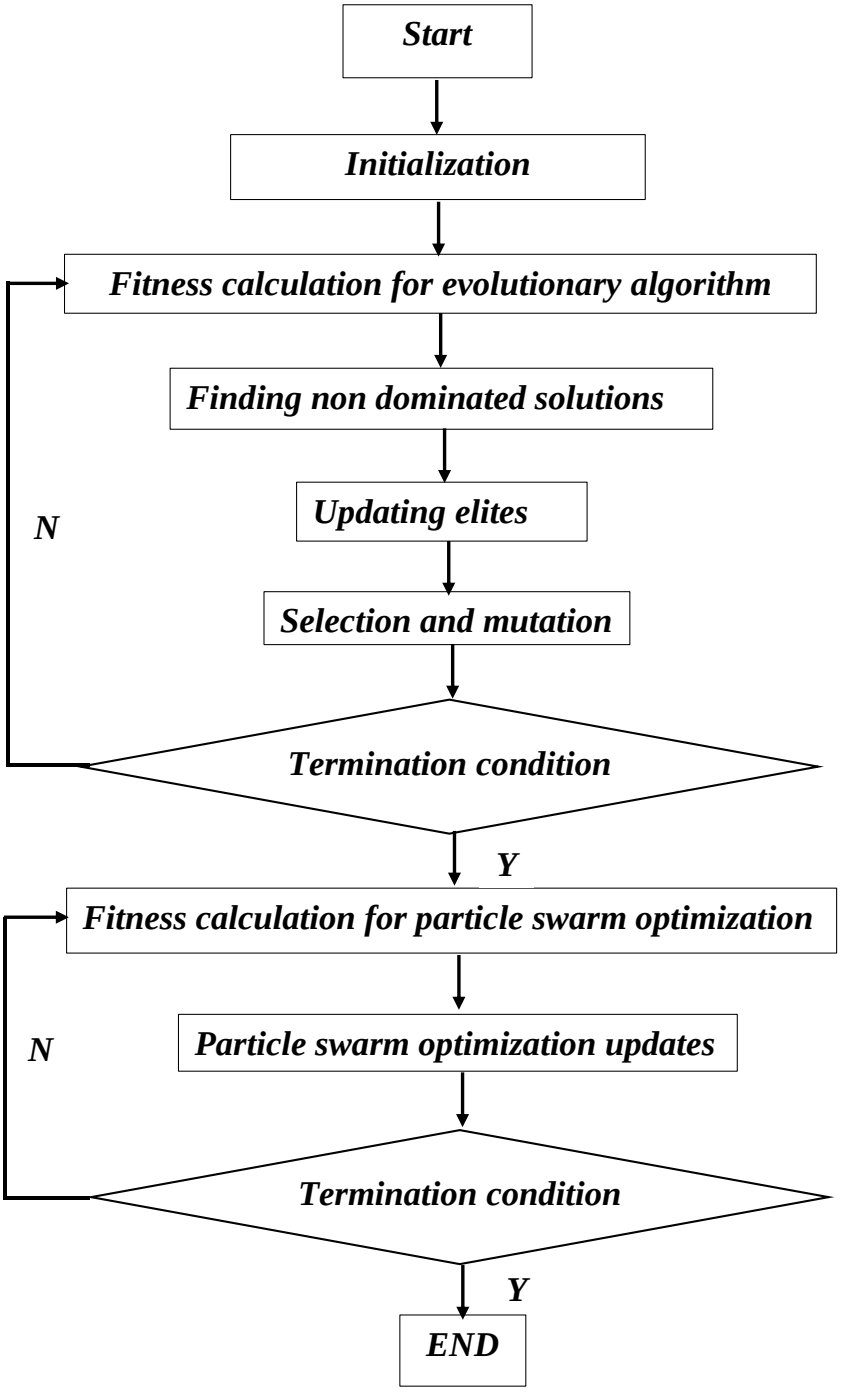

Figure 2-14. (Optimization of an HVAC system with a strength of multi-objective particle-swarm algorithm) Particle swarm optimization algorithm diagram

Neural networks are used to estimate or approximate functions, that can depend on a large number of inputs. In general a neural network can be assumed as a system of interconnected neurons which exchange data between each other. Unlike computationally complex analytical models with lots of assumptions, neural networks entirely depend on experimental data which make them, application relevant and easy to compute [31].

Kusiak developed a model to optimize a HVAC system using a dynamic neural network [31, 32]. In the Neural network approach, the predictive model with controllable and uncontrollable inputs and outputs were utilized. Optimization model was derived by using a dynamic neural network based on the concept of 'non-linear autoregressive with external inputs'. The model is solved by using multi-objective particle swarm optimization algorithm. Compared to the traditional control method, the method he developed saved up to 30% of energy.

Genetic algorithm

Genetic algorithm is a programming algorithm that imitates biological evolution as a problem solving technique. Genetic algorithm is an adaptive search technique based on the principles and mechanisms of natural selection and 'survival of the fittest' from natural evolution [33]. The input to the GA in a specific problem is set of potential solutions to that problem, encoded in some fashion. It is known as fitness function that allows each candidate to be quantitatively evaluated. Energy saving strategy in liquid desiccant dehumidification by using GA was studied [50]. Problem was solved as constrained nonlinear optimization problem to find the optimal control settings within the feasible range. Optimized strategy showed 12.2% energy saving potential.

Moisture condensation rate of liquid desiccant dehumidifier is optimized by GA [34]. Desiccant flow rate, desiccant concentration, desiccant inlet temperature, air humidity ratio and liquid to air flow rate ratio consider as model controlling parameters. Four different values for each parameter have been chosen and conducted the optimization for the LDDS by using GA [34]. Fuzzy based genetic algorithm was used to optimize the energy conservation potential for VAV air conditioning system keeping objective functions, as energy savings and thermal comfort [35].

GA operates as an iterative procedure on a fixed size population or pool of candidate solutions. Desiccant absorption system was studied using GA and system COP was maximized for different parameters like regenerator length, desiccant solution flow rate, desiccant concentration, and air flow rates. It was found that the maximum COP can be achieved for different combinations of regenerator length, desiccant solution flow rate and air flow rates [36]. Figure 2-15 illustrates the flow chart for the optimization tool. Even though GA provides the optimum parameter values, practical and economic factors should be taken into account for the final conclusion [36]. Exchanger size and solution flow rate were optimized in liquid desiccant run-around membrane energy exchanger [51]. Annual energy consumption rate was recovered up to 7% by using optimization control.

GA operates on a fixed size pool of candidate solutions in an iterative manner. “The candidate solutions represent an encoding of the problem into a form that is analogous to the chromosomes of biological systems. Each chromosome represents a possible solution for a given objective function. Associated with each chromosome is a fitness value, which is found by evaluating the chromosome with the objective function. It is the fitness of the chromosome, which determines its ability to survive and produce

offspring. Each chromosome is made up of a string of genes (whose values are called alleles). A chromosome is typically represented in the GA as a string of bits. GA begins by generating an initial population, P(t =0), and evaluating each of its members with the objective function. While the termination condition is not satisfied, a portion of the population is selected, somehow altered, evaluated, and placed back into the population. At each step in the iteration, chromosomes are probabilistically selected from the population for reproduction according to the principle of the 'survival of the fittest'. Offspring are generated through a process called crossover, which can be augmented by mutation. The offspring are then placed back in the pool, perhaps replacing other members of the pool. This process can be modeled using either a 'generational' or a 'steady state' genetic algorithm. The generational GA saves offspring in a temporary location until the end of the generation. At that time the offspring replace the entire current population. Conversely, the steady state GA immediately places offspring back into the current population " [33]. Probabilities of crossover and mutation greatly determine the degree of solution accuracy and the convergence speed [37].

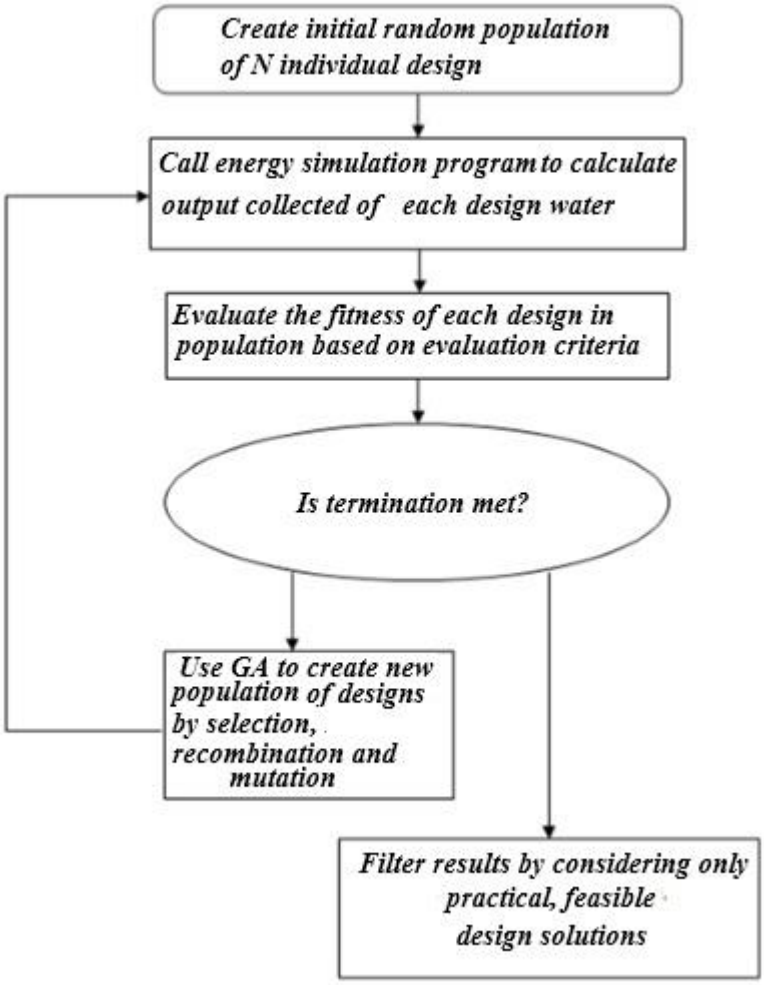

Figure 2-15. (Optimization of Desiccant Absorption System Using a Genetic Algorithm) Genetic algorithm diagram

Advantages of Genetic Algorithm

- Genetic algorithms are intrinsically parallel. Most other algorithms are serial and can only go for the solution in one direction at a time. If the solution discovers is suboptimal, nothing can be done other than abandoning all previous work and starting all over again. GA has multiple offspring, therefore there is a possibility of few to be suboptimal, and which can eliminate and continue with other promising paths.

- Due to that parallelism GA allows to evaluate many schemes at once and it is capable of handling problems with huge solution space or too much time consumed.
- Genetic algorithm performs well in complex fitness functions (discontinues, noisy, changes over time, has many local optima).
- Ability to manipulate many parameters simultaneously.

Limitations

- No guarantee of finding global maxima. If the fitness function was written poorly or defined imprecisely GA may be unable to find a solution for the function.
- Time taken for convergence: it requires a decent size population and a lot of generations to have good results and with heavy simulations it may take days for a solution.
- If the population size is too small the GA may not explore enough of the solution space to consistently find a good solution. If the rate or genetic change is too high or the selection scheme is chosen poorly, beneficial scheme may be disrupted and population may enter error region.
- Difficulty of dealing with the problems with defective fitness functions. Locations of the improved points give misleading information about where the global optimum is likely to be found.

Chapter 3 System design and experimental methodology

An experimental procedure was carried out to calculate the regeneration rate and investigate the effect of system parameters to the effectiveness of the regeneration process of the vacuumed liquid desiccant regenerator. In this chapter, description of the test facility, regenerator configuration and experimental procedure are explained.

3.1 Experimental setup description

Experiments were done on the vacuumed regeneration prototype installed in Process Instrumentation Laboratory, Nanyang Technological University. Prototype was built according to the conceptual design of Prof. Cai Wenjian and Dr. Xing Li [52]. Since most dehumidification systems related to building air conditioning system are based on conventional mechanical dehumidification, they are very inefficient, utilize higher amount of energy and have low regeneration effectiveness. The newly designed regeneration system shown in the schematic table 3-1, consist of main 9 components and table 3-2, 9 processes, which were shown in figure 3-1.

Table 3-1. Main components of the new system

Main components	
1-Solution Circulation pump	6-Condenser heat exchanger
2-Vacuum pump	7-Solution storage tank
3-Condensed water removal pump	8-Hot water circulation pump
4-Evaporator heat exchanger	9-Chilled water circulation pump

5-Control panel of the system	

Table 3-2. Main processes of the system

Processes involved in the system
A- Strong solution sprays from the top of the dehumidifier
B- Accumulated weak solution pumps back to the weak solution storage tank
C- Weak solution from the storage tank pumps to the regeneration chamber
D- Solution circulation
E- Strong solution from the Regeneration chamber pumps to the strong solution storage tank
F- Chilled water circulation
G- Hot water circulation
H- Vacuuming the regeneration chamber
I- Condensed water removes out from the regeneration chamber

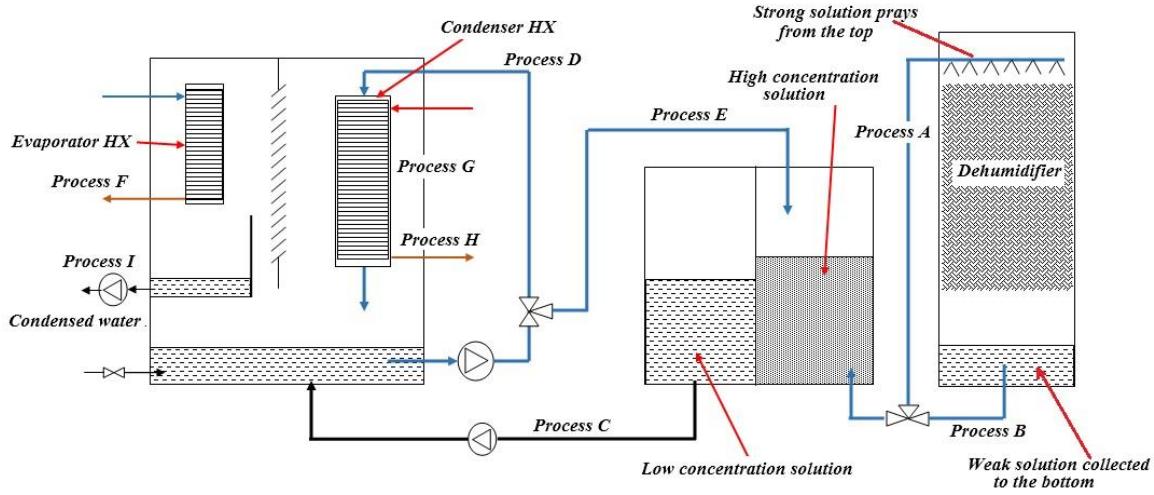

Figure 3-1. Schematic of the newly designed LDDS configuration

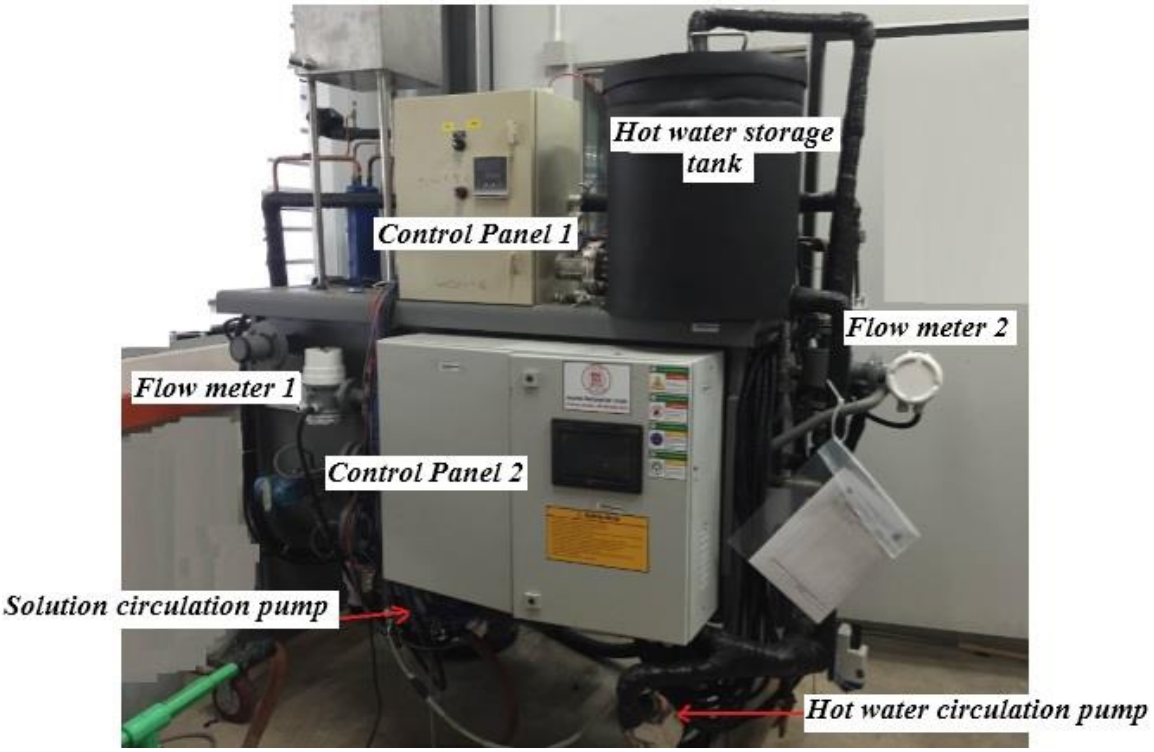

Figure 3-2. Actual system used for experiments

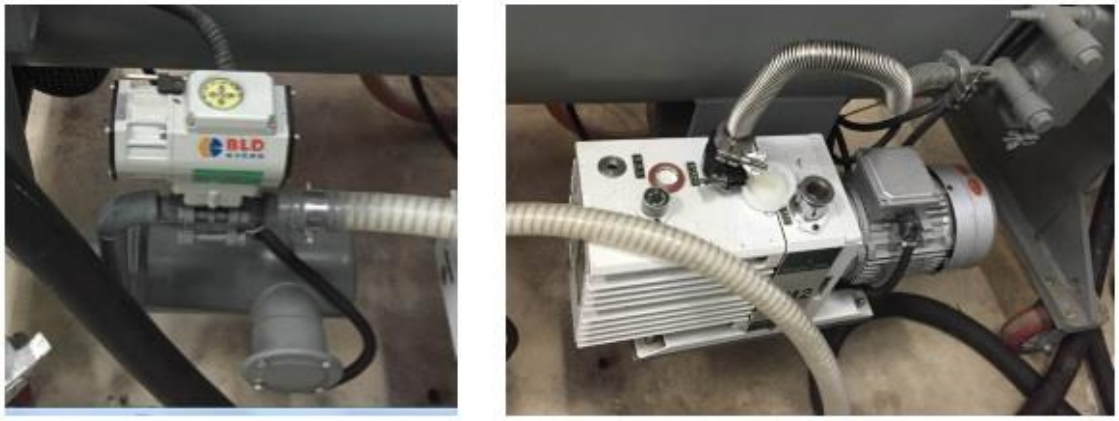

A B

Figure 3-3. A- Condensed water removing pump, B - Vacuum pump

Evaporator Heat Exchanger

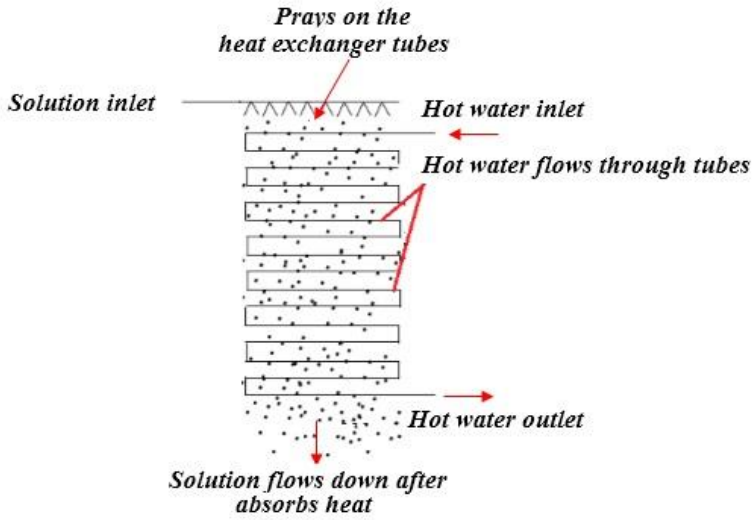

Figure 3-4. Evaporator arrangement

Solution sprays on top of the tube bank and flows downward as shown in the figure 3-4. By spraying solution, contact time and heat transfer area can be increased. High temperature

water flows in, from the top of the heat exchanger. The amount of heat supplied to the solution should not be higher than the water evaporation heat requirement, unless water vapor enters into the superheat region. This has two disadvantages, heat wastage for superheating and cooling load wastage for de-superheating.

Condenser Heat Exchanger

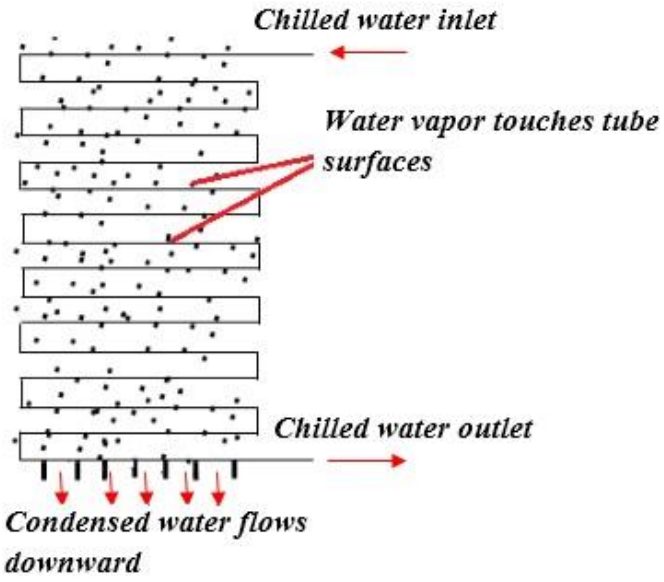

Figure 3-5. Condenser arrangement

The condenser heat exchanger is of a similar type to the evaporator as shown in figure 3-5. Condenser is located higher position than the evaporator and water vapor moves to the condenser side, contacts with the tube wall and releases latent heat. Therefore, heat transfer area should be enough to absorb latent heat of condensation. Condensed water flows down and gathers at the bottom of the chamber.

Water heater & Water chiller

A water heater with a reservoir of a capacity of 8 kW is used in the system to supply enough amount of heat to the hot water. A storage tank with a capacity of 20 l is being used to supply water as shown in figure 3-2. An 8 kW chiller with a 30 liters capacity reservoir is used to provide required cooling water.

3.2 Experimental setup control and measurement

Measurement apparatus

Accuracy of the measurement data is the most important factor during any testing. Therefore, pressure gauges, temperature sensors, flow meters and density gauges were used to measure the most important and required data for calculations. Figure 3-6 show the positioning of the above mentioned components in the real schematic. Purposes of sensors were given in the table 3-3.

Table 3-3. Description of the measurement apparatus used in the system

Sensor name and specification	Measuring quantity
T_1 – Pt 100 temperature sensor	Inside solution temperature before entering the desorption process
T_2 – Pt 100 temperature sensor	Inlet chilled water temperature to the condenser
T_3 - Pt 100 temperature sensor	Outlet chilled water temperature from the condenser
T_4 - Pt 100 temperature sensor	Inlet hot water temperature to the evaporator HX

T_5 - Pt 100 temperature sensor	Outlet hot water temperature from the evaporator HX
P_1 – Pressure gauge	Measuring the inside vacuum pressure
F_1 – EMFD HFD 3000	Hot water flow rate
F_2 – EMFD HFD 3000	Chilled water flow rate
F_3 – EMFD HFD 3000	Solution flow rate

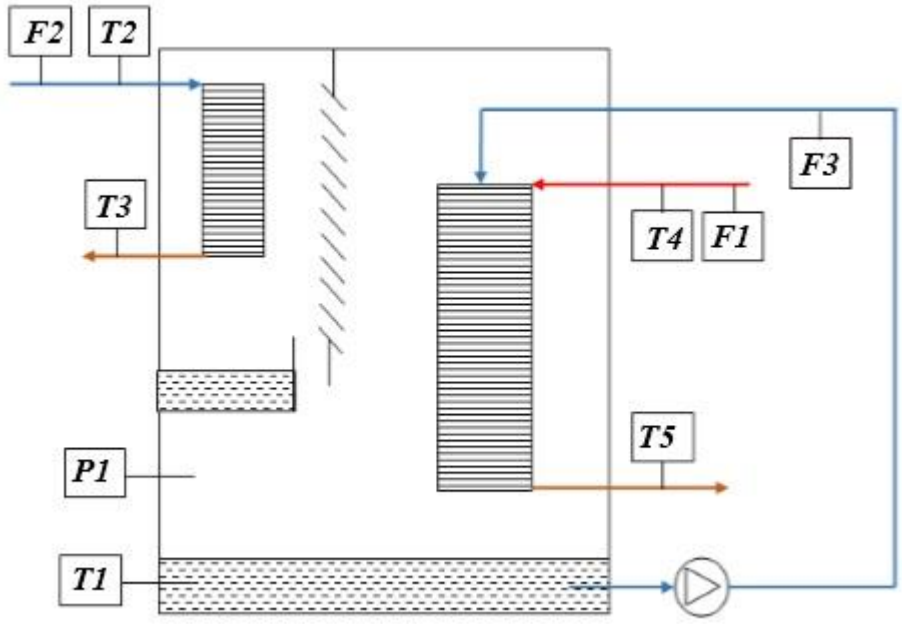

Figure 3-6. The arrangement of the measurement apparatus in the system

Controlling apparatus

System parameters needed to be changed for different sets of testing. The values of, flow rates of hot water, chilled water and solution, hot water temperature and chilled water temperature are the variable factors. Hot water circulation pump, chilled water circulation pump and solution circulation pump are variable speed drive pumps and by changing the frequency of the pump, flow rate can be changed. Table 3-4 shows the controlling components that were used in the system and the purpose of them.

Table 3-4. Controlling apparatus used in the system

Component	Purpose
Omron SYSDRIVE 3G3JZ Inverter	Frequency control of chilled water/ solution and hot water pump
Omron SYSMAC CP1H PLC	System safety control System fault check Control of other components
NI cRIO-9074 Data Acquisition system	Log temperature sensors and pressure sensor data Send signals to hot water pump inverter
Shimaden SR93 digital controller	Heater temperature controller

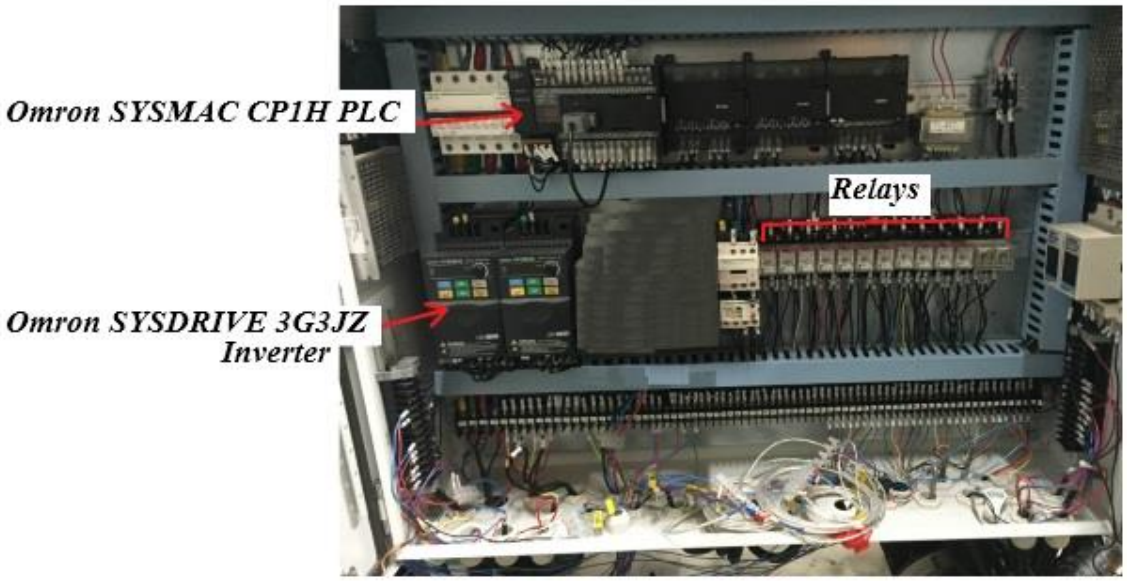

Figure 3-7. Panel board wiring arrangement for controlling components

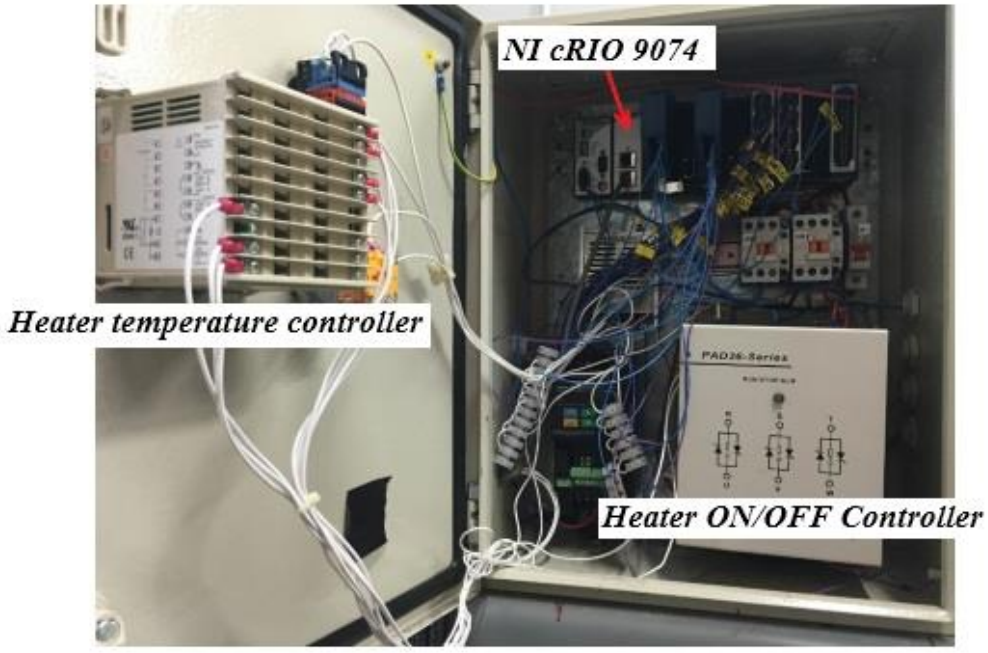

Figure 3-8. Sensor and water heater controller wiring arrangement

Figure 3-7 shows pictures of PLC controllers and inverters used in the system and figure 3-8 shows the inside arrangement of the NI cRIO 9074 controller, heater temperature controller and heater three phase on/off controller.

Figure 3-9 and figure 3-10 show the LabView program developed to capture data and control the hot water cycle. In real time, temperature, pressure and flow rate values can be seen from the graphical user interface. Computer is connected to the NI cRIO 9074 controller to send command or capture data. Temperature sensors, flow meters, pressure sensors and inverter are connected to the NI cRIO 9074.

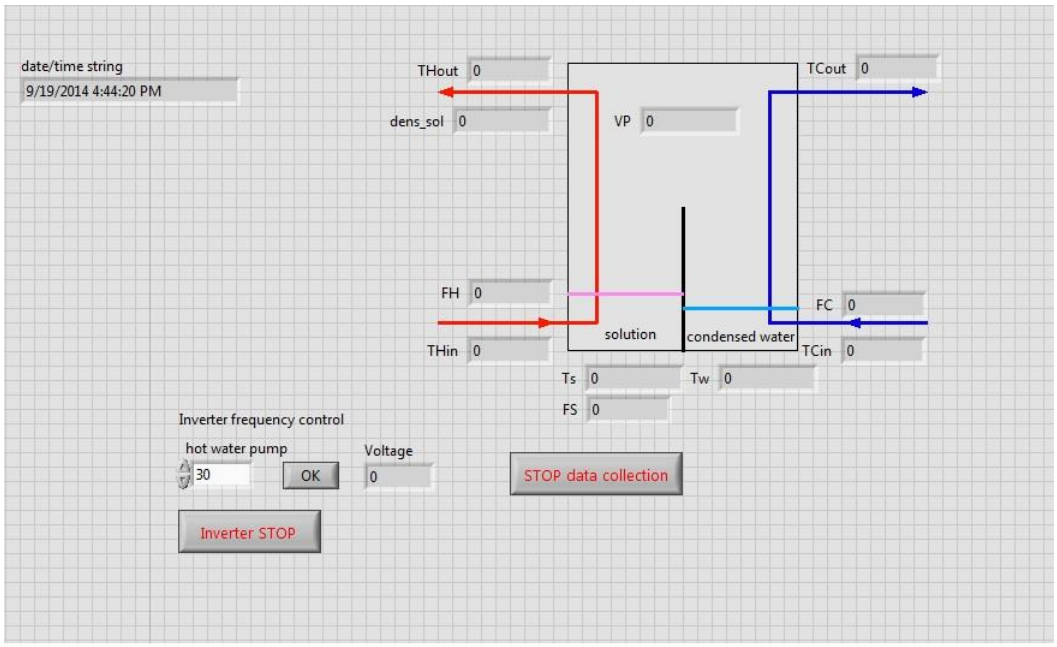

Figure 3-9. Simple LabVIEW program-1 for data capturing

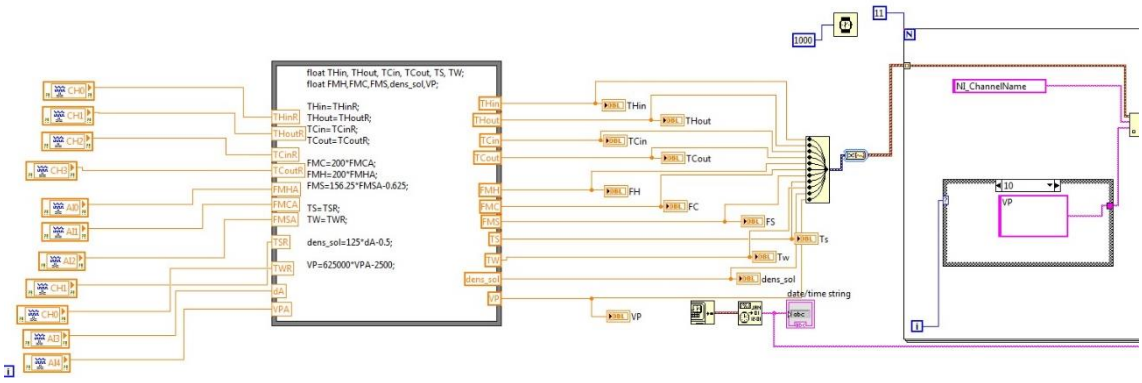

Figure 3-10. Simple LabVIEW program-2 for data capturing

Pump Details:

Table 3-5. Pump details used in the system

Pump	Specification
Vacuum pump	3 Phase 50 Hz/ 1.6-2.8A Power:- 550W Speed:-1400rpm Vacuum rate:- 2 l/s
Hot water circulation pump	3 Phase 50 Hz/ 2.5-4.8A Power:-1.15 kW Flow rate:- 0.6-3.6 m^3/hr
Chilled water circulation pump	3 Phase 50 Hz/1.8-3.2 A

	Power:-550 W Flow rate:- 0-6 m^3/hr
Condensed water removal pump	3 Phase 50Hz/2.3 A Power:-370 W Flow rate:-1.2 m^3/hr

3.3 Operation Procedure of the New System

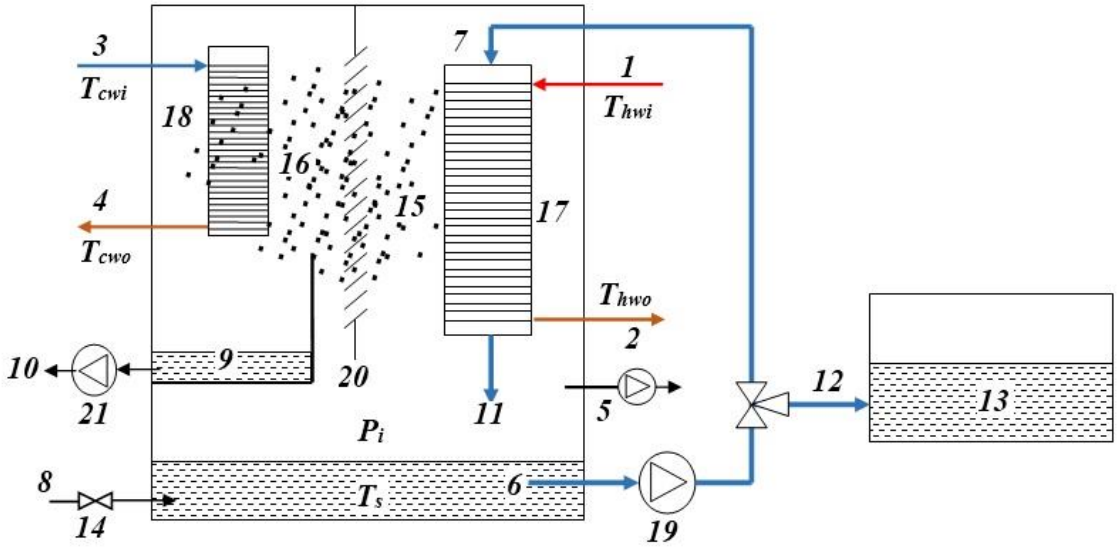

Figure 3-11.Detailed illustration of the system with process indication

- By opening the valve 14, allow the low concentration solution enter the chamber till the pre-determined level. This takes place due to the pressure difference between the inside and outside of the chamber.
- System can be vacuumed using the vacuum pump 5 to the required vacuum condition and pressure gauge is placed to measure the vacuum pressure level.
- Hot water circulates through the evaporator 17 from 1-2 and supplies required energy to the solution.
- Chilled water circulates through the condenser 18 from 3-4 and supplies required cooling load to condense the vaporized water.
- Solution which is in the bottom of the tank circulate using circulation pump 19 from 6-7 and spray on top of the evaporator heat exchanger filled with hot water and it absorb required latent heat. Thereafter, water vaporizes as shown from no 15 while the rest of the solution flows down 7-11 and gets collected to the bottom of the tank.
- Vaporized water vapor travels from the evaporator to the condenser 15-16 due to pressure difference and makes contact with the condenser which is filled with chilled water. There it releases latent heat and flows down as cool water. There is a separate collector 9 to collect the condensed water.
- Condensation rate of water vapor is important unless the pressure inside rises due to the accumulation of water vapor. Therefore, synchronization of vaporization and condensation is necessary to maintain a constant pressure level.
- There is a separation panel 20 to separate the evaporator section and the condenser section to reduce the radiation effect between two heat exchangers.

- When the condensed water level rises to the pre-determined level it is automatically removed 9-10 from the chamber using a pump 21.
- After the system run for a required time, the valve from 6-7 is closed and the valve from 6-12 is opened to charge the concentrated solution out to the tank 13.
- Temperature sensors are installed to measure real time temperature at inlets and outlets of hot water and chilled water circulation tubes T_{cwi} , T_{cwo} , T_{hwi} , T_{hwo} and to measure the solution temperatureT_s. Pressure sensor is installed to measure the real time pressure P_i .

3.4 Experimental procedure

System performance

The purpose of the regeneration is to increase the desiccant concentration to a higher concentration. Therefore, the process performance can be measured by the effective concentration increment within given time duration. System runs for a predetermined time duration for several configurations and check the final concentration increment.

$$system\ performance\ (After\ t\ time) = [Final\ concentration - Initial\ concentration]$$

To have correct set of data values, experiments should be carried out without any mistake. Different types of experiments were carried out by changing the controlling parameter value but the procedure remained same.

Following are the steps for experiments.

- First step is to fill the tank with solution of a required concentration level.
- Reduce the density (concentration) of outside LiBr solution by adding water.
- Charge the solution into the vacuumed chamber in a fairly higher quantity than the required level (when solution is charged out to check, required concentration level can be achieved).
- Circulate the solution inside by a solution pump and let the solution mix together to come to a stable concentration.
- Charge the solution out and measure the density of the solution inside (density value should be 1.35 for most cases except in cases where the changing parameter is the concentration)
- If the solution is higher than the required concentration, charge out some more solution, add some water and charge in the solution. Finally when the inside solution concentration comes to the required value, charge the solution out till the inside solution level comes to the required value.
- Vacuum the system to the required pressure level by using the vacuum pump (Around 1000 Pa – 2000 Pa depending on the experiment).
- Run the chilled water circulation in 50Hz and check the chilled water temperature and maintain it around 8 degrees.
- Run the hot water circulation in 42 Hz and check the hot water temperature and maintain the temperature around 38 degrees.
- When all parameters come to the required settings stop the vacuuming process.

- Run the LabView program and start the solution circulation while noting down the starting time of the testing, initial concentration, solution level, hot water temperature, chilled water temperature and vacuum pressure.
- Test runtime is 3 hours and during that time hot water temperature and chilled water temperature have to be monitored and maintained within the controlling limits.
- Stop the system after 3 hours, charge all the solution out, measure the concentration of the solution and save LabView data.
- After the system stops automatically, measure the solution level to make sure of the difference of the initial and the final solution levels.

3.5 Experiments conducted

Following are the key controlling parameters,

1. Hot water inlet temperature
2. Hot water flow rate
3. Chilled water inlet temperature
4. Chilled water flow rate
5. Initial vacuum pressure
6. Solution flow rate

Different types of experiments were carried out to investigate how above parameters affect the system performance. Table 3-6 illustrates the testing that was carried out.

Hot water is taken from the condenser, cooling water from another system. The temperature that it can provide is around 38 ^{0}C. Therefore, the system was tested for its performance

with a 35- 42 degree variation of hot water temperatures. The chilled water source can provide cool water of around 8 ^{0}C. Therefore, testing was carried out changing the value from 7-12 degree. Flow rates of hot water, chilled water and solution changes from the lowest to the highest of the pump capacities related to 30 Hz – 50 Hz. Vacuum condition of the tank was a critical component and it was very difficult and time consuming to achieve very low vacuum conditions around 500 Pa. Therefore, only two vacuum levels were tested being 1500 and 2000 Pa.

Table 3-6. Types of testing conducted to collect data

Parameter maintained	Tested parameter initial values			
Hot water inlet temperature	35 ^{0}C	36 ^{0}C	38 ^{0}C	40 ^{0}C
Hot water flow rate	1.14 m^3/hr	1.28 m^3/hr	1.58 m^3/hr	1.7 m^3/hr
Chilled water temperature	7 ^{0}C	8 ^{0}C	9 ^{0}C	10 ^{0}C
Chilled water flow rate	1.12 m^3/hr	1.3m^3/hr	1.64m^3/hr	1.99m^3/hr
Solution flow rate	1.68 m^3/hr	1.91 m^3/hr	2 m^3/hr	2.15 m^3/hr
Initial vacuum pressure	1500 Pa	2000Pa		
Initial solution density	1350m^3/kg	1370m^3/kg	1390m^3/kg	1410m^3/kg

Following settings were used for the testing and only one parameter changed according to the predetermined testing values.

Hot water inlet temperature = 38 ^{0}C

Hot water flow rate = 1.2 m^3/hr

Chilled water temperature = 8 ^{0}C

Chilled water flow rate = 1.2 m^3/hr

Solution flow rate = 1.6 m^3/hr

Initial vacuum pressure = 1000 Pa

Initial solution density = 1350 m^3/kg

For example when the changing parameter was the hot water inlet temperature; hot water flow rate 1.2 m^3/hr, chilled water temperature 8 ^{0}C, chilled water flow rate 1.2 m^3/hr, solution flow rate 1.6 m^3/hr, initial vacuum condition 1000 Pa and initial solution density 1350 m^3/kg were the maintained parameter values.

Important Considerations during the testing

Conducting a testing without any error is very important. If there is a single error, data has to remove and redo the testing. Therefore, following are the key important controlling steps.

1. Initial vacuum pressure should be maintained within control limits with $\pm 50Pa$.
2. Hot water temperature should be maintained within the control limits with $\pm 0.5^0C$.
3. Chilled water temperature should be maintained within the control limits with $\pm 0.5^0C$.

4. Initial concentration should be maintained within the control limits with $\pm$ 1%.

Even though, many testing data had to throw away due to few minutes' negligence and redid the same testing. System ran out from the controlling environment and lead to false values.

Testing results

Table 3-7. Testing results

Controlling parameter	Initial Concentration	Final concentration
Hot water temp (^{0}C)		
35	36.31%	44.75%
36	36.54%	46.98%
38	36.46%	45.64%
40	36.84%	49.85%
Hot water flow (m^3/hr)		
1.14	36.31%	45.81%
1.28	36.46%	45.98%
1.58	36.54%	47.07%
1.7	36.23%	52.69%
Chilled water temp(^{0}C)		

7	36.39%	48.40%
8	36.39%	45.56%
9	36.39%	47.62%
10	36.46%	46.39%
Chilled water flow(m^3/hr)		
1.12	36.77%	47.57%
1.3	36.62%	48.07%
1.64	36.39%	47.62%
1.99	36.46%	46.98%
Solution flow rate(m^3/hr)		
1.68	36.31%	43.27%
1.91	35.54%	45.80%
2	36.46%	47.17%
2.15	36.31%	45.71%
Initial Vacuum Pressure (Pa)		
1500	36.46%	49.41%
2000	36.31%	46.32%

Discussion

Testing were conducted in a controlled environment with minimum error. Accuracy of the gathered data were determined by how accurately controlling settings were maintained. It was found that controlling hot water temperature, chilled water temperature in a certain value were very difficult as the hot water and chilled water reservoirs were not large enough. Initial solution LiBr concentration had to maintain in a constant value throughout the testing. After each and every testing concentrated solution discharge from the regenerator but some amount of solution remains inside. Therefore, it was very difficult to bring the solution concentration to the same value. All other parameters were controlled and collected data without any difficulty.

Chapter 4 Heat and Mass Transfer of Evaporation process

This chapter presents a development of a mathematical model to study the heat and mass transfer of evaporator heat exchanger of the system. Developed model is validated using experimental data. The effect of controlling parameters on the performance of the evaporator is discussed.

Heat transfer method from inside hot water to the outside solution is symmetrical over the radial direction by looking at a cross section. Therefore, one dimensional heat and mass transfer study can accurately apply for the heat and mass transfer application of this study. Therefore, the propose model is considered as a one dimensional simultaneous heat and mass transfer model.

To develop the model following assumptions were made.

1. Desorption process is assumed to be in a steady state for the calculation time period.
    a. Data were collected for 1 second time interval and it is a valid assumption for a small time duration like 1 second, desorption process is assumed as constant.
2. There is no heat transfer to the outside environment from the hot water channel or the chilled water channel and if there is then that is negligible.
    a. Connecting tubes from the hot water and cold water reservoirs to the system were fully insulated. Therefore, heat waste to the environment was very small and it’s a valid assumption.
3. Evaporator heat exchanger tubes are completely wet with solution all the time.

a. The solution sprays on top of the evaporator tubes with a flow rate around 1.9 m^3/hr. There isn't a possibility that a single tube was not covered with solution. Even if there is, the space should be very small and therefore, the assumption is valid.

4. Lithium Bromide vaporization amount is negligible.
    a. LiBr evaporation temperature is higher than the heat source temperature. Therefore, there is a very slight chance for LiBr to evaporate.
5. Conduction heat transfer between the coolant tubes/heating tubes and the system frame is negligible.
    a. Coolant tubes and heating tubes touches the outer frame of the system only at the inlets and outlets. The amount of heat transfer through a small circumferential area was very small. Therefore, it's valid to have the above assumption.
6. Evaporation of the solution due to vacuum pressure is negligible. Evaporation of the solution before the testing is negligible.
    a. Vacuum pressure reduces the evaporation temperature of the solution. But, the amount of natural evaporation due to the pressure reduction was very small. Therefore, the above assumption is valid.
7. Axial heat conduction along the heat exchanger tube is insignificant
    a. Temperature gradient for the heat transfer is in radial direction both in evaporator and condenser. The amount of heat transfer in the axial direction is insignificant comparing to the radial direction.

Modeling the system

The objective of the regeneration process is to remove dissolved water from LiBr and increase the concentration. Figure 4-1 shows the simple schematic of the system, mathematical model is developed for each component separately. Loop A is the chilled water circulation and water vapor condensation loop. Chilled water generates in the chiller and then passes through the condenser heat exchanger and condenses the water vapor. Loop B is the hot water circulation-solution desorption loop. Hot water generates in the heater passes through the evaporator heat exchanger, solution absorbs required sensible load and the latent load, and then water vaporizes. The overall efficiency of the system depends on each operating parameter of both loops. Therefore, both loops are studied separately in following two chapters.

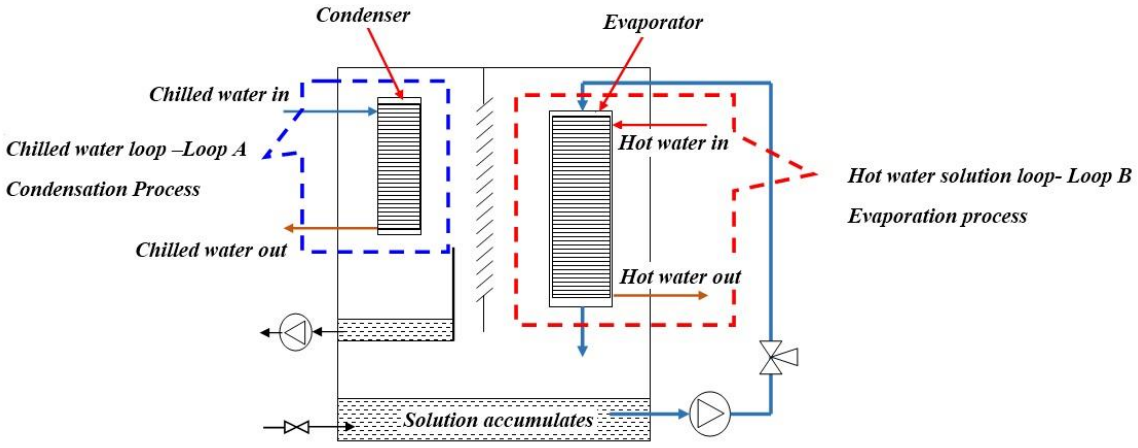

Figure 4-1.Loop A- Vapor condensation & Loop B- Solution desorption, study separately

Evaporator Heat transfer model

Lower concentration LiBr + water solution and hot water, flow direction is shown in figure 4-2. $\dot{m}_{wv}$ is the amount of water vapor released from the solution by absorbing the required amount of latent heat.

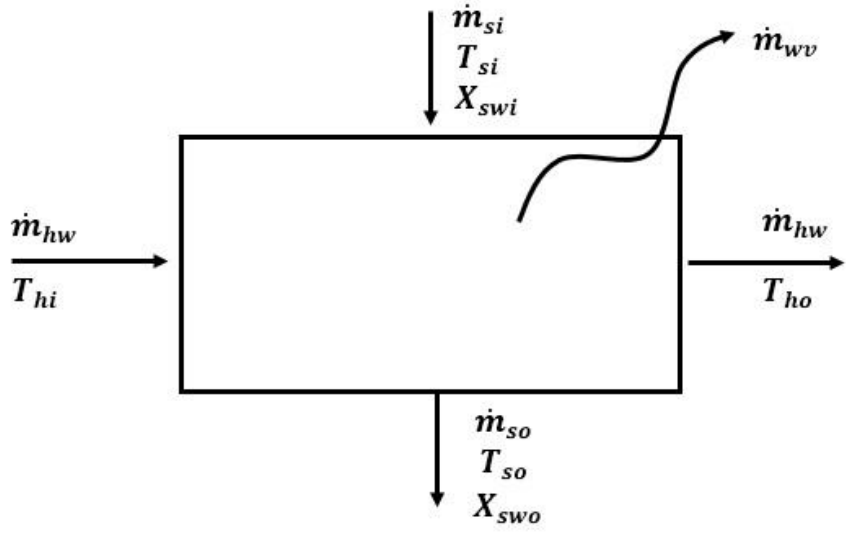

Figure 4-2.Evaporator heat exchanger considers as the whole control volume and input and output condition of the solution, hot water and water vapor is mentioned

Mass continuity equation for the solution side can be written as below:

Conservation of total solution mass flow:

$$\dot{m}_{si} = \dot{m}_{wv} + \dot{m}_{so} \quad -(4.1)$$

$\dot{m}_{si} - Solution\ flow\ rate\ inlet$

$\dot{m}_{wv} - Water\ vapor\ generation\ rate$

$\dot{m}_{so} - Solution\ flow\ rate\ outlet$

The amount of mass enters into the evaporator should leave according to the mass continuity. Conservation of water mass flow:

$$X_{swi}\dot{m}_{si} = \dot{m}_{wv} + X_{swo}\dot{m}_{so} \quad -(4.2)$$

Conservation of LiBr mass flow:

$$(1 - X_{swi})\,\dot{m}_{si} = (1 - X_{swo})\,\dot{m}_{so} \quad -(4.3)$$

Equation (4.1) can be solved to get the outlet solution mass flow rate as below.

$$\dot{m}_{so} = \dot{m}_{si} - \dot{m}_{wv} \quad -(4.4)$$

Equation (4.2) can be modified to get the outlet water mass concentration as below.

$$X_{swo} = \left(\frac{X_{swi}\dot{m}_{si} - \dot{m}_{wv}}{\dot{m}_{so}}\right)$$

$$X_{swo} = \left(\frac{X_{swi}\dot{m}_{si} - \dot{m}_{wv}}{\dot{m}_{si} - \dot{m}_{wv}}\right) \quad -(4.5)$$

Hot water enters the heat exchanger, releases energy to the solution and flows out with a lower temperature. By considering the water temperature difference, the rate of heat released can be calculated as below.

$$\dot{Q} = \dot{m}_{hw}C_{phw}(T_{hi} - T_{ho}) \quad -(4.6)$$

$\dot{Q} - The\ rate\ of\ heat\ release$

$C_{phw} - Hot\ water\ Specific\ heat\ capacity$

$T_{hi} - Hot\ water\ inlet\ temperature$

$T_{ho} - Hot\ water\ outlet\ temperature$

The saturation temperature of water depends on the pressure involved in the process. Part of the solution reaches saturation temperature and absorbs enough amount of latent heat and vaporizes. Following energy conservation equation can be written by considering solution side sensible and latent loads.

$$\dot{Q} = \dot{m}_{wv} L + \dot{m}_{wv} C_{pw}\left(T_{pwsat} - T_{si}\right) + \dot{m}_{so} C_{ps}(T_{so} - T_{si}) \quad -(4.7)$$

$$\dot{Q} = \dot{m}_{wv}\left[L + C_{pw}\left(T_{pwsat} - T_{si}\right)\right] + \dot{m}_{so} C_{ps}(T_{so} - T_{si}) \quad -(4.7)$$

By substituting from (4.4) and (4.5) into (4.7), the equation can be simplified as below:

$$\dot{Q} = \dot{m}_{wv}\left[L + C_{pw}\left(T_{pwsat} - T_{si}\right)\right] + (\dot{m}_{si} - \dot{m}_{wv}) C_{ps}(T_{so} - T_{si}) \quad -(4.8)$$

$$\dot{Q} = \dot{m}_{wv}\left[L + C_{pw}\left(T_{pwsat} - T_{si}\right)\right] + \dot{m}_{si} C_{ps}(T_{so} - T_{si}) - \dot{m}_{wv} C_{ps}(T_{so} - T_{si}) - (4.8)$$

(4.9) & (4.10) can be derived using (4.8),

$$\dot{Q} = \dot{m}_{wv}\left[L + C_{pw}\left(T_{pwsat} - T_{si}\right)\right] + (\dot{m}_{si} - \dot{m}_{wv}) C_{ps}(T_{so} - T_{si})$$

$$(T_{so} - T_{si}) = \frac{\left\{\dot{Q} - \dot{m}_{wv}\left[L + C_{pw}\left(T_{pwsat} - T_{si}\right)\right]\right\}}{\left\{(\dot{m}_{si} - \dot{m}_{wv}) C_{ps}\right\}}$$

$$T_{so} = T_{si} + \frac{\left\{\dot{Q} - \dot{m}_{wv}\left[L + C_{pw}\left(T_{pwsat} - T_{si}\right)\right]\right\}}{\left\{(\dot{m}_{si} - \dot{m}_{wv}) C_{ps}\right\}} \quad -(4.9)$$

and

$$\dot{Q} = \dot{m}_{wv}\left[L + C_{pw}\left(T_{pwsat} - T_{si}\right)\right] + \dot{m}_{si} C_{ps}(T_{so} - T_{si}) - \dot{m}_{wv} C_{ps}(T_{so} - T_{si})$$

$$\dot{m}_{wv}\left\{\left[L + C_{pw}\left(T_{pwsat} - T_{si}\right)\right] - C_{ps}(T_{so} - T_{si})\right\} = \dot{Q} - \dot{m}_{si} C_{ps}(T_{so} - T_{si})$$

$$m_{wv} = \frac{\left\{\dot{Q} - \left[\dot{m}_{si} C_{ps}(T_{so} - T_{si})\right]\right\}}{\left\{\left[L + C_{pw}\left(T_{pwsat} - T_{si}\right)\right] - C_{ps}(T_{so} - T_{si})\right\}} \quad -(4.10)$$

Many design variables affect the heat transfer effectiveness of the heat exchanger. For instance hot water inlet temperature, hot water flow rate, solution flow rate, solution inlet concentration, partial water pressure in the solution, area for the heat transfer, conductive and convective heat transfer co-efficient and heat exchanger materials act major roles in the process. The influence of above parameters should be studied and the model should be simulated in order to understand the effect of each parameter.

Overall Heat transfer coefficient

Two fluids are involved in heat exchanger, separated by a cylindrical wall and heat from the inside hot fluid to the outside cold fluid, through the tube wall. Heat transfers to the solid wall from hot fluid, through convection. By conduction, heat flows from hot wall surface to the cold wall surface and from the cold surface heat transfers to the cold fluid through convection. There are three processes involved in this heat transfer and therefore, three types of resistances can be identified. Below Figure 4-3 shows how the resistances act on the heat flow [38] and Figure 4-4 shows the resistance network.

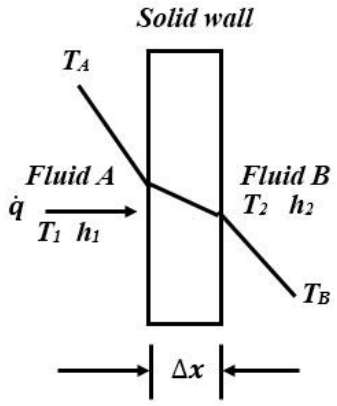

Figure 4-3. Heat transfer from Fluid A to Fluid B through a solid wall. h1 & h2 are convective heat transfer coefficients of two sides

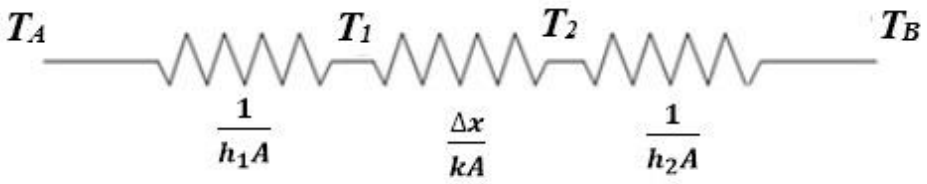

Figure 4-4. Representation of the thermal resistances of heat transfer from fluid A to fluid B though the wall

Heat transfer equation can be written as [6]:

$$\dot{q} = \frac{T_A - T_B}{\frac{1}{h_1 A} + \frac{\Delta x}{kA} + \frac{1}{h_2 A}}$$

By using the overall heat transfer coefficient the energy transfer equation can be written as [17]:

$$\dot{q} = U A \Delta T$$

Therefore =>

$$U A = \frac{1}{\frac{1}{h_1 A} + \frac{\Delta x}{kA} + \frac{1}{h_2 A}}$$

$$\frac{1}{U A} = R = \frac{1}{h_1 A} + \frac{\Delta x}{kA} + \frac{1}{h_2 A}$$

For the heat exchanger the equation can be modified as:

$$\frac{1}{U A} = R = \frac{1}{h_i A_i} + \frac{\Delta x}{kA} + \frac{1}{h_o A_o} \qquad -(4.11)$$

Heat exchanger was made of higher heat conductive material with a high heat transfer area and thin wall thickness tubes. Therefore the heat resistance through tubes can be neglected as $\frac{\Delta x}{kA}$ term has a very small heat resistance value. Therefore, (4.11) becomes,

$$\frac{1}{U\,A} = \frac{1}{h_i\,A_i} + \frac{1}{h_o\,A_o}$$

$h_i\,, h_o - Tube\ inner\ side\ and\ outer\ side\ convective\ heat\ trasnfer\ coefficients$

$A_i,\ A_o - Tube\ inside\ and\ outside\ heat\ transfer\ areas$

Since the heat exchanger has thin walls without any fins attached to the outside tubes to increase the heat transfer area, inner side heat transfer area and the outer side heat transfer area can be considered as equal. Therefore, the equation can be simplified as below:

$$\frac{1}{U} = \frac{1}{h_i} + \frac{1}{h_o} \qquad -(4.12)$$

Heat exchanger performance can be studied using Log Mean Temperature Difference (LMTD) method or Effectiveness NTU ($\varepsilon - NTU$) method. LMTD method can be used only when all the inlet and outlet conditions of fluids are known. It calculates the logarithmic average of the temperature difference between the hot and cold streams but $\varepsilon - NTU$ takes a different approach by using three dimensionless parameters, heat capacity ratio, effectiveness and number of transfer units, which don't require inlet and outlet conditions of fluids. Therefore, in this study $\varepsilon - NTU$ method which was introduced by Kays and London in 1955 is used for the calculations [39].

Heat transfer effectiveness can be calculated as:

$$\varepsilon = \frac{\dot{Q}}{\dot{Q}_{max}} = \frac{Actual\ Heat\ Transfer\ Rate}{Maximum\ possible\ heat\ trasnfer\ rate}$$

The actual heat transfer rate can be calculated using the temperature difference of hot water as in (4.6).

$$\dot{Q} = C_s(T_{so} - T_{si}) + m_{wv}L = C_{hw}(T_{hwi} - T_{hwo})$$

Where $C_s = \dot{m}_s C_{ps}$ and $C_{hw} = \dot{m}_{hw} C_{hw}$ are heat capacity rates of solution and hot water respectively, heat exchanger gives the maximum possible heat transfer rate when the hot water outlet temperature becomes solution inlet temperature. Therefore, the maximum possible heat transfer rate of the evaporator heat exchanger can be calculated as follows.

$$\dot{Q}_{max} = C_{min}(T_{hwi} - T_{si}) \qquad -(4.13)$$

where, C_{min} = The smaller heat capacity rate of hot water (C_{hw}) and solution (C_s).

If $C_{hw} < C_s\ , then\ C_{min} = C_{hw}$

If $C_s < C_{hw}\ , then\ C_{min} = C_s$

The effectiveness of the heat exchanger depends on the geometry of the heat exchanger and also the flow arrangement [39]. Evaporator heat exchanger in the application is a cross-flow, one fluid mixed and other unmixed type heat exchanger. Therefore, suitable effectiveness equation is as follows.

$$\varepsilon = \frac{1}{C}(1 - \exp\{1 - C[1 - exp\ (-NTU)]\})$$

$$\varepsilon = 1 - exp\left\{-\frac{1}{C}[1 - exp\,(-\,C\,NTU)]\right\} \quad -(4.14)$$

Where C is a dimensionless quantity, named as the capacity ratio, it can be given by the following equation.

$$C = \frac{C_{min}}{C_{max}} \quad -(4.15)$$

The dimensionless number of transfer units can be calculated using the following equation.

$$NTU = \frac{U\ A}{C_{min}} = \frac{U\ A}{(\dot{m}C_p)_{min}} \quad -(4.16)$$

$U -\ overall\ heat\ transfer\ coefficient$

$A - total\ heat\ transfer\ area$

As discussed above total heat transfer coefficient can be calculated using the (4.12) and total heat transfer area value of the heat exchanger is a constant to that heat exchanger.

Following steps are followed to calculate the actual heat transfer [38]:

- Calculate the capacity ratio $C = C_{min}/C_{max}$ and $NTU = UA/C_{min}$ for the data given
- For those values calculate the ε using the equation (4.14)
- By using the ε, actual heat transfer can be calculated using the below equation
    - $\dot{Q} = \varepsilon\, C_{min}(T_{hi} - T_{si})$
- Outlet temperature can be calculated using the equations below.
    - $T_{ho} = T_{hi} - \dot{Q}/C_h$
    - $T_{so} = T_{si} + \left(\dot{Q} - m_{wv}L\right)/C_s$

Once the actual heat transfer and hot water outlet temperature are known the results can be compared with the actual results.

4.1 Internal convective Heat transfer Model

Here, h_i is the internal convective heat transfer coefficient and h_o is the external heat transfer coefficient. Hot water flows inside and solution flows outside. Hot water flows due to the force applied by the hot water pump and solution flows due to the circulation pump. Therefore these two applications can be considered as force convection of internal cylinder and force convection of external cylinder bank.

Heat transfer between the interface and the surface wall depends on the following factors:

- Fluid properties (fluid density , fluid viscosity, fluid specific heat capacity)
- Interface geometry (in this case internal cylindrical tube and external cylindrical tube)
- Fluid velocity
- Thermal conductivities of surface walls

For the decided sets of experiments hot water flows through the pipe with higher flow rate more than 1 m^3/hr, in the system heat exchanger tube diameter is 0.01 m and the viscosity for water is 0.653 x 10^{-3} Ns/m^2. For the above values the Reynolds number can be calculated and it is higher than 10000, therefore the hot water flow is turbulent. Since the flow is turbulent the following study is carried out for a turbulent internal flow in tubes.

Heat transfer coefficient Nusselt number is a function of Prandle number, Reynolds number and friction factor and it can be written as below [39].

$$Nu = fun(\ Re\ , \mathrm{Pr}, f)$$

Above equation can be written with constants:

$$Nu = C\ Re^m Pr^n f^k \qquad -(4.17)$$

The values of C, m, n, k is needed to be determined for the application. Value for C depends on the geometry and the flow when m, n and k are constants.

Further Re can be written as below:

$$Re = \frac{Inertial\ force}{Viscous\ force} = \frac{\rho\ u\ D}{\mu}$$

$\rho = Density\ of\ the\ fluid$

$u = velocity\ of\ the\ fluid$

$D = Diameter\ of\ the\ tube$

$\mu = viscosity\ of\ the\ fluid$

Prandle number can be written as below:

$$\mathrm{Pr} = \frac{molecular\ diffusivity\ of\ momentum}{molecular\ diffusivity\ of\ heat} = \frac{\mu\ C_{pw}}{k}$$

$\mu = viscosity\ of\ the\ fluid$

$C_{pw} = Heat\ capacity\ of\ the\ fluid$

$k = thermal\ conductivity$

Explicit first Patukhov equation can be used to calculate the friction factor of turbulent flow in smooth tubes [39].

$$f = (0.79\, ln(Re) - 1.64)^{-2} \quad for \quad 10^4 < Re < 10^6$$

In the application, the flow is in a fully developed region. Therefore, the above equation can be modified as below.

$$f = 0.184\, Re^{-2}$$

By applying the values of Pr , Re and *f* to the Nu number equation:

$$Nu = C \left(\frac{\rho\, u\, D}{\mu}\right)^{m} \left(\frac{\mu\, C_{pw}}{k}\right)^{n} (0.184\, Re^{-2})^{k}$$

$$Nu = C \left(\frac{\rho\, u\, D}{\mu}\right)^{m} \left(\frac{\mu\, C_{pw}}{k}\right)^{n} Re^{-2k} (0.184\,)^{k}$$

$$Nu = C \left(\frac{\rho\, u\, D}{\mu}\right)^{m-2k} \left(\frac{\mu\, C_{pw}}{k}\right)^{n} (0.184\,)^{k}$$

$$m - 2k = m1$$

$$Nu = C \left(\frac{\rho\, u\, D}{\mu}\right)^{m1} \left(\frac{\mu\, C_{pw}}{k}\right)^{n} (0.184\,)^{k} \qquad -(4.18)$$

Heat transfer Nu number can be written as below by definition [6, 16]:

$$Nu = \frac{hD}{k} \qquad -(4.19)$$

h- Convective heat transfer coefficient

D- Diameter of the tube

k- Thermal conductivity of water

By substituting the (4.18) into (4.19) =>

$$Nu = \frac{hD}{k} = C \left(\frac{\rho\, u\, D}{\mu}\right)^{m1} \left(\frac{\mu\, C_{pw}}{k}\right)^{n} (0.184\,)^{k}$$

$$h = \frac{k}{D}\, C \left(\frac{\rho\, u\, D}{\mu}\right)^{m1} \left(\frac{\mu\, C_{pw}}{k}\right)^{n} (0.184\,)^{k} \qquad -(4.20)$$

If mass flow rate through the tube is $\dot{m}_{hw}$, it can be substituted in the equation as below.

$$\dot{m}_{hw} = \rho\, u\, A_{tube}$$

$$A_{tube} - Cross\ sectional\ area\ of\ the\ tube$$

$$\dot{m}_{hw} = \frac{\rho\, u\, \pi\, D^2}{4}$$

$$u = \frac{4\, \dot{m}_{hw}}{\rho \pi\, D^2}$$

$$h = \frac{k}{D}\, C \left(\frac{4\, \dot{m}_{hw}}{\mu\, \pi\, D}\right)^{m1} \left(\frac{\mu\, C_{pw}}{k}\right)^{n} (0.184\,)^{k}$$

For the tube inlet, convection heat transfer coefficient equation can be written as below.

$$h_i = \frac{k}{D}\, C \left(\frac{4\, \dot{m}_{hw}}{\mu\, \pi\, D}\right)^{m1} \left(\frac{\mu\, C_{pw}}{k}\right)^{n} (0.184\,)^{k}$$

One constant C' can be used for $(0.184\,)^{k}$ and C.

$$h_i = \frac{k}{D} C' \left(\frac{4\, \dot{m}_{hw}}{\mu\, \pi\, D}\right)^{m1} \left(\frac{\mu\, C_{pw}}{k}\right)^{n} \qquad -(4.21)$$

4.3 External convective heat transfer model

Outside solution flow can be considered as flow across tube bank. When there are a set of tubes instead of a single tube they can affect the flow pattern of the solution. In the desorption process, tubes are arranged an in-line manner and it is shown in Figure 4-5 [39, 40].

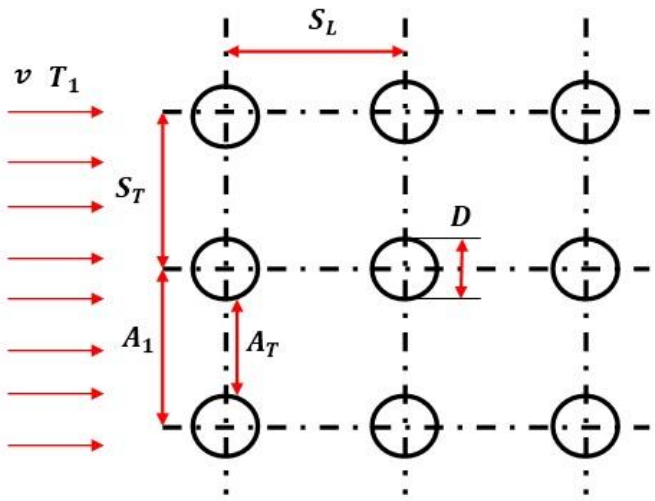

Figure 4-5. Tube bank geometry (aligned) of the evaporator heat exchanger and flow direction

$S_T = Transverse\ pitch$

$S_L = Longitudinal\ pitch$

$A_1 = Inlet\ area$

$A_T = Inside\ area$

A_1 reduces to A_T when the fluid enters into the tube bank.

$A_1 = S_T\, L$: L is the length of the heat exchanger

$A_T = (S_T - D)\, L$

Since the area available for the liquid to flow is low, fluid velocity within the tube bank is higher. Therefore, the Re for liquid flow, defines based on the maximum velocity within the tube bank.

$$Re_s = \frac{\rho_s v_{max}\, D}{\mu_s}$$

Maximum velocity can be calculated based on the mass continuity:

$\rho_s\, v\, A_1 = \rho_s v_{max} A_T$

$vS_T\, L = v_{max}(S_T - D)\, L$

$$v_{max} = \frac{vS_T}{(S_T - D)}$$

If v_1 takes as the velocity of the solution before entering into the heat exchanger, if the inner diameter of the tube is d_1, then the continuity equation for the solution inside the tube can be given as follows.

$\frac{1}{4}\, v_1\, \pi\, d_1^2\, \rho_s = \rho_s\, v\, A_1 n_g = \dot{m}_s$

$$v = \frac{v_1\, \pi\, d_1^2}{4\, A_1 n_g} \qquad -(4.22)$$

$A_1 -$ cross sectional area inside the tube

$n_g - number\ of\ gaps\ between\ tubes$

A suitable correlation for this kind of application proposed by Zukauskas is given below [39];

$$Nu_s = \frac{h_o D}{k} = C_1 Re_s^g Pr_s^{n2} \left(\frac{Pr_s}{Pr_{sw}}\right)^{0.25} \quad -(4.23)$$

All the parameter values in (4.23) except Pr_{sw} should be calculated based on the arithmetic mean temperature of the fluid. Values of the constants $C_1, g\ and\ n2$ depend on value Reynolds number. Since the operation involves vaporization process, there isn't much difference between the inlet and outlet solution temperatures. Therefore, in this study the usage of inlet solution temperature for calculations is a fair assumption. To calculate Pr_{sw} heat exchanger wall temperature should be used and it can be determined from the arithmetic mean of the hot water inlet and outlet temperature values. LiBr properties for the calculations can be found from the literature [41, 42].

Constants C_1, g, n_2 needs to be determined through experimental results.

By substituting the equations for *Re* and *Pr*, following equation can be proposed.

$$Nu_s = \frac{h_o D}{k} = C_1 \left(\frac{\rho_s v_{max}\, D}{\mu_s}\right)^g \left(\frac{\mu_s C_{ps}}{k_s}\right)^{n2} \left(\frac{\left(\frac{\mu_s C_{ps}}{k_s}\right)_s}{Pr_{sw}}\right)^{0.25}$$

$$Nu_s = \frac{h_o D}{k} = C_1 \left(\frac{\rho_s v S_T\, D}{\mu_s (S_T - D)}\right)^g \left(\frac{\mu_s C_{ps}}{k_s}\right)^{n2} \left(\frac{\left(\frac{\mu_s C_{ps}}{k_s}\right)_s}{Pr_{sw}}\right)^{0.25} \quad -(4.24)$$

By applying the solution mass flow rate to the equation:

$$Nu_s = \frac{h_o D}{k} = C_1 \left(\frac{\dot{m}_s S_T D}{\mu_s A_1 n_g (S_T - D)} \right)^g \left(\frac{\mu_s C_{ps}}{k_s} \right)^{n2} \left(\frac{\left(\frac{\mu_s C_{ps}}{k_s} \right)_s}{Pr_{sw}} \right)^{0.25} \quad -(4.25)$$

External convective heat transfer coefficient can be calculated using the following equation.

$$h_o = \frac{k}{D} C_1 \left(\frac{\dot{m}_s S_T D}{\mu_s A_1 n_g (S_T - D)} \right)^g \left(\frac{\mu_s C_{ps}}{k_s} \right)^{n2} \left(\frac{\left(\frac{\mu_s C_{ps}}{k_s} \right)_s}{Pr_{sw}} \right)^{0.25} \quad -(4.26)$$

By substituting the h_i and h_o into overall heat transfer coefficient equation,

$$\frac{1}{U} = \frac{1}{h_i} + \frac{1}{h_o}$$

$$\frac{1}{U} = \frac{1}{\left\{ \frac{k}{D} C' \left(\frac{4 \dot{m}_{hw}}{\mu \pi D} \right)^{m1} \left(\frac{\mu C_{pw}}{k} \right)^n \right\}} + \frac{1}{\left\{ \frac{k}{D} C_1 \left(\frac{\dot{m}_s S_T D}{\mu_s A_1 n_g (S_T - D)} \right)^g \left(\frac{\mu_s C_{ps}}{k_s} \right)^{n2} \left(\frac{Pr_s}{Pr_{sw}} \right)^{0.25} \right\}} \quad -(4.27)$$

When considering a small time period during a steady state there is a very small change in temperature of the fluid. Parameters like thermal conductivity of both water and solution, viscosity of both water and solution and thermal capacity of water can be considered as constants. Therefore, the above equations can be simplified as below.

$$\frac{1}{U} = \frac{1}{\left\{ C'' {\dot{m}_{hw}}^{m1} \right\}} + \frac{1}{\left\{ C''' {\dot{m}_s}^g {C_{ps}}^{n2} \right\}}$$

The above overall heat transfer coefficient model has 5 unknowns which should be determined. Non-linear least square algorithm widely known as Levenberg-Marquardt method is used for the calculation.

Above equation can be written as below:

$$\frac{1}{U} = \frac{1}{\{x_1 \dot{m}_{hw}{}^{x_2}\}} + \frac{1}{\{x_3 (\dot{m}_s)^{x_4} C_{ps}{}^{x_5}\}} \quad -(4.28)$$

By using the defined (4.14), (4.15), (4.16) and (4.28) following equation can be derived.

$$NTU = \frac{UA}{C_{min}} \quad , \quad C = \frac{C_{min}}{C_{max}}$$

$$\varepsilon = 1 - exp\left\{-\frac{1}{C}[1 - exp\,(-\,C\,NTU)]\right\}$$

$$\dot{Q} = \varepsilon\, C_{min}(T_{hi} - T_{si})$$

$$\dot{Q} = \left[1 - exp\left\{-\frac{1}{C}[1 - exp\,(-\,C\,NTU)]\right\}\right] C_{min}(T_{hi} - T_{si})$$

$$\dot{Q} = \left[1 - exp\left\{-\frac{1}{C}\left[1 - exp\left(-\,C\,\frac{UA}{C_{min}}\right)\right]\right\}\right] C_{min}(T_{hi} - T_{si})$$

$$\dot{Q} = \left[1 - exp\left\{-\frac{1}{C}\left[1 - exp\left(-\,\frac{UA}{C_{max}}\right)\right]\right\}\right] C_{min}(T_{hi} - T_{si})$$

$$\dot{Q} = \left[1 - exp\left\{-\frac{1}{C}\left[1 - exp\left(-\frac{\left[\frac{1}{\{x_1 \dot{m}_{hw}{}^{x_2}\}} + \frac{1}{\{x_3 m_s{}^{x_4} C_{ps}{}^{x_5}\}}\right]^{-1} A}{C_{max}}\right)\right]\right\}\right] C_{min}(T_{hi} - T_{si}) \quad -(4.29)$$

Equation (4.29) has 5 unknown constants, x_1, x_2, x_3, x_4 and x_5. By consider N number of testing data points under different operating conditions, by using the above 5 constants following function can be defined.

$$x_1, x_2, x_3, x_4, x_5: f(x) = f(x_1, x_2, x_3, x_4, x_5).$$

$$Q_i = f(x_1, x_2, x_3, x_4, x_5) + e_i$$

$e_i - Residue\ of\ the\ above\ calculation$

$Q_i - Calculated\ result\ from\ experimental\ data$

$$f(x_1, x_2, x_3, x_4, x_5) = \left[1 - exp\left\{-\frac{1}{C}\left[1 - exp\left(-\frac{\left[\frac{1}{\{x_1 \dot{m}_{hw}{}^{x_2}\}} + \frac{1}{\{x_3 (\dot{m}_s)^{x_4} C_{ps}{}^{x_5}\}}\right]^{-1} A}{C_{max}}\right)\right]\right\}\right] C_{min}(T_{hi} - T_{si})$$

Objective function can be defined as

$$f(X) = \sum_{i=1}^{N} e_i^2\,(x) = \sum_{i=1}^{N} [f(x_1, x_2, x_3, x_4, x_5) - Q_i]^2$$

Where:

$f(X)$ - Sum of squares of the errors or the residuals between the calculated and experimental data.

$x = [x_1, x_2, x_3, x_4, x_5]^T$ – Parameter vector to be calculated

Use the Taylor series expansion only with first order and use matrix algebra to calculate the error values or the deviations from the initial guesses [43].

$$f(x)_{i+1} = f(x)_i + \frac{\partial f(x)}{\partial x_1}\Delta x_1 + \frac{\partial f(x)}{\partial x_2}\Delta x_2 + \frac{\partial f(x)}{\partial x_3}\Delta x_3 + \frac{\partial f(x)}{\partial x_4}\Delta x_4 + \frac{\partial f(x)}{\partial x_5}\Delta x_5 + Higher\ orders\ omit$$

$\therefore$

$$Q_j - f(x)_j = \frac{\partial f(x)_j}{\partial x_1}\Delta x_1 + \frac{\partial f(x)_j}{\partial x_2}\Delta x_2 + \frac{\partial f(x)_j}{\partial x_3}\Delta x_3 + \frac{\partial f(x)_j}{\partial x_4}\Delta x_4 + \frac{\partial f(x)_j}{\partial x_5}\Delta x_5 + e_i$$

This can be written in matrix form:

$$[D] = [Z_j][\Delta x] + [E]$$

Where:

$$[D] = \begin{bmatrix} Q_1 - f(x)_1 \\ Q_2 - f(x)_2 \\ \vdots \\ Q_N - f(x)_N \end{bmatrix} [Z_j] = \begin{bmatrix} \frac{\partial f(x)_1}{\partial x_1} & \frac{\partial f(x)_1}{\partial x_2} & \frac{\partial f(x)_1}{\partial x_3} & \frac{\partial f(x)_1}{\partial x_4} & \frac{\partial f(x)_1}{\partial x_5} \\ \frac{\partial f(x)_2}{\partial x_1} & \frac{\partial f(x)_2}{\partial x_2} & \frac{\partial f(x)_2}{\partial x_3} & \frac{\partial f(x)_2}{\partial x_4} & \frac{\partial f(x)_2}{\partial x_5} \\ \vdots & \vdots & \vdots & \vdots & \vdots \\ \frac{\partial f(x)_N}{\partial x_1} & \frac{\partial f(x)_N}{\partial x_2} & \frac{\partial f(x)_N}{\partial x_3} & \frac{\partial f(x)_N}{\partial x_4} & \frac{\partial f(x)_N}{\partial x_5} \end{bmatrix}$$

$$[\Delta x] = \begin{bmatrix} \Delta x_1 \\ \Delta x_2 \\ \Delta x_3 \\ \Delta x_4 \\ \Delta x_5 \end{bmatrix}$$

This Z_j matrix is known as the Jacobian matrix and from the matrix algebra following equation can be written to calculate$[\Delta x]$ [15].

$$\left[Z_j{}^T Z_j\right][\Delta x] = \left[Z_j{}^T\right][D]$$

By starting with initial guesses, (j+1) point location value can be evaluated.

$$(x_1)_{j+1} = (x_1)_j + \Delta x_j$$

Above matrix equation is modified for easy convergence with respect to the initial guesses and the modified equation is known as Levenberg-Marquardt method.

$$\left[Z_j{}^T Z_j + \lambda I\right][\Delta x] = \left[Z_j{}^T\right][D]$$

Here *I* is the identity matrix of order 5, in this particular case, λ is a non-negative damping factor. Instead of using the identity matrix, Marquardt proposed following modification which is used in the calculation.

$$\left[Z_j{}^T Z_j + \lambda\, diag(Z_j{}^T Z_j)\right][\Delta x] = \left[Z_j{}^T\right][D] \qquad -(4.30)$$

λ is selected with higher positive values and checked whether the iteration is directed towards convergence or not. The iteration end criterion is selected for minimum error, for coefficient values.

$$|x_{k+1} - x_k| \leq 1 \times 10^{-5}$$

4.3 Evaporation Mass transfer model

When solution flows through the evaporator heat exchanger it absorbs enough amount of sensible energy to saturate, latent energy to vaporize. This vaporization process is a mass transfer process. Therefore, it is essential to study which parameters affect the mass transfer process and how to improve the performance. In this section mass transfer from the solution to the low pressure space is studied.

Dissolved water in aqueous Lithium Bromide solution has chemical bonds. Therefore, sufficient energy should be supplied to the solution to release water vapor. If there is more concentrated water vapor in the container space it creates another resistance. Therefore, partial pressure created by water vapor in the container is another type of resistance. Following equation can be used to calculate the rate of mass transfer based on the water vapor pressure difference as the driving force [6].

$$S = K_G\left(P_{s,sat} - P_{vacuum,w}\right)$$

$S = Mass\ transfer\ rate$

$K_G = Overall\ mass\ transfer\ coefficient$

$P_{s,sat} = Partial\ pressure\ of\ water\ vapor\ in\ the\ solution$

$P_{vacuum,w} = Partial\ water\ vapor\ pressure\ of\ vacuumed\ space$

Mass transfer process due to concentration gradient can be analogues to the heat transfer process. Hence, boundary layer for the heat transfer can be considered the same as for mass transfer.

Therefore, there is a similarity in equations are used for the mass transfer study. Nu number is used for heat transfer and Sherwood Number (Sh) is used for mass transfer study [17].

$$Sh = \frac{Convective\ mass\ transport}{Diffusive\ mass\ transport}$$

$$Sh = \frac{h_{mg}\ D}{D_{LiBrW}}$$

$Sh = Sherwood\ Number$

$h_{mg} = Convective\ mass\ trasnfer\ coefficient\ in\ liquid\ side$

$D = Tube\ diameter$

$D_{LiBrW} = Mass\ diffusivity\ between\ LiBr\ and\ water$

Molecular diffusivity D_{LiBrW} is a function of concentration and it can be calculated using the following equation [44][45].

$$D_{LiBrW} = (1.3378 - 0.2492\ X_{LiBr} + 0.3663\ X_{LiBr}^2 - 0.1163\ X_{LiBr}^3 + 0.0143\ X_{LiBr}^4) \times 10^{-9}\frac{m^2}{s} \quad -(4.31)$$

Nu number is a function of *Re* and *Pr*, likewise Sherwood number is a function of *Re* number and Schmidt number (*Sc*) [41].

$Sh = f(Re\ , Sc)$

In the study of compact generator for absorption refrigeration system, Sh number depends on the two phases Reynolds number, Schmidt number, concentration gradient and heat flux [16].

$$Sh = C_2\left(Re_{tp}\right)^{g2}(Sc_l)^{z1}(X_{io})^{z2}(q)^{r2} \quad -(4.32)$$

$Re_{tp} = two\ phase\ Reynolds\ number$

$Sc_l = Liquid\ side\ Schmidt\ number$

$X_{io} = concentration\ difference\ between\ inlet\ and\ outlet$

$X_{io} = X_i - X_o$

$q = Heat\ flux$

In the above equation C_2 , g_2 , z_1 , z_2 and r_2 are constant parameters that should be found from experimental results using non-linear least square method. Heat flux q can be calculated using the enthalpy difference of hot water.

Sc number is the ratio between the momentum diffusion and molecular diffusion. It can be given by the following equation.

$$Sc = \frac{Momentum\ Diffusion}{Molecular\ Diffusion}$$

$$Sc_l = \frac{\mu}{\rho\, D_{LiBrW}}$$

Two phase Reynolds number can be calculated using the liquid phase Reynolds number and Lockart-Martinelli (*F*) parameter [16]. The relationship between the Re_{tp} , *F* and Re_{sl} can be given by the following equation.

$$Re_{tp} = Re_{sl} F^{1.25}$$

$$Re_{sl} = \frac{\rho_s \dot{m}_s S_T D}{\mu_s A_1 (S_T - D)}$$

$$F = 2.35 \left(\frac{1}{X_{tt}} + 0.213\right)^{0.736}$$

$$\frac{1}{X_{tt}} = \text{Lockart} - \text{Martinelli parameter}$$

$$\frac{1}{X_{tt}} = \left(\frac{\rho_l}{\rho_v}\right)^{0.5} \left(\frac{\mu_v}{\mu_l}\right)^{0.1} \left(\frac{X_{gen,o}}{(1 - X_{gen,o})}\right)^{0.9}$$

$$Re_{tp} = \left(\frac{\rho_s \dot{m}_s S_T D}{\mu_s A_1 (S_T - D)}\right) \left\{ 2.35 \left(\left[\left(\frac{\rho_l}{\rho_v}\right)^{0.5} \left(\frac{\mu_v}{\mu_l}\right)^{0.1} \left(\frac{X_{gen,o}}{(1 - X_{gen,o})}\right)^{0.9} \right] + 0.213 \right)^{0.736} \right\}^{1.25} \quad -(4.33)$$

From the above equations Sh equation can be written as below:

$$Sh = \frac{h_{mg} D}{D_{LiBrW}} = C_2 (Re_{sl} F^{1.25})^{g2} \left(\frac{\mu}{\rho D_{LiBrW}}\right)^{z1} (X_i - X_o)^{z2} (q)^{r2}$$

$$h_{mg} = C_2 \frac{D_{LiBrW}}{D} (Re_{sl} F^{1.25})^{g2} \left(\frac{\mu}{\rho D_{LiBrW}}\right)^{z1} (X_i - X_o)^{z2} (q)^{r2}$$

$$K_G = h_{mg} = C_2 \frac{D_{LiBrW}}{D} (Re_{sl} F^{1.25})^{g2} \left(\frac{\mu}{\rho D_{LiBrW}}\right)^{z1} (X_i - X_o)^{z2} (q)^{r2} \quad -(4.34)$$

The above model requires thermodynamic and transport properties of the water, water + LiBr mixture for the calculation. Saturation vapor pressure is only affected by the temperature and it can be calculated for temperatures 15 ^{0}C to 35 ^{0} C as shown below [6, 45].

$$P_{s,sat} = \frac{2.718^{\left(77.345+0.0057\,T-\frac{7235}{T}\right)}}{T^{8.2}} \quad -(4.35)$$

$P_{s,sat} - \ Saturation\ water\ pressure\ (Pa)$

$T - Dry\ bulb\ temperature\ (K)$

Partial water pressure of the solution can be calculated based on the method below [52].

$$T_{DP,w} = \frac{T_s - A}{B}$$

$T_{DP,w} - Dew\ point\ temperature$

$T_s - Solution\ temperature$

A and B are functions of the solution concentration and mass fraction X_s and mole ratio M_s. They can be written as,

$$M_s = \frac{M_w}{M_s} \cdot \frac{X_s}{1 - X_s}$$

$$A = \sum_{i=0}^{4} A_i\, M_s^{i/2}$$

$$B = \sum_{i=0}^{4} B_i M_s^{i/2}$$

Values for A_i and B_i, when i=0 - 4 are given in the table below. Values are calculated based on the curve developed for Hoffmann and Florin vapor pressure equation [52].

Table 4-1. Ai & Bi Values for the A & B calculation

i	0	1	2	3	4
A	340.897	-2638.978	7262.473	-8119.078	3302.087
B	-0.0105	6.70042	-15.42090	16.42477	-6.34249

Vapor pressure can be calculated using the dew point temperature.

$$\theta = 1 - \frac{T_{DP,w}}{T_c}$$

$$ln\left(\frac{P}{P_c}\right) = \frac{T_c}{T_{DP,w}}(a_1\theta + a_2\theta^{1.5} + a_3\theta^3 + a_4\theta^{3.5} + a_5\theta^4 + a_6\theta^{7.5}) \quad -(4.36)$$

Table 4-2.Tc, Pc & a_i values for the calculation

a_1	a_2	a_3	a_4	a_5	a_6
-7.85951783	1.844408259	-11.7866497	22.6807411	-15.9618719	1.80122502
T_c	P_c				
647.096K	22.064MPa				

$$S = K_G\left(P_{sw,in} - P_{a,sat}\right)$$

$$= C_2\frac{D_{LiBrW}}{D}(Re_{sl}F^{1.25})^{g2}\left(\frac{\mu}{\rho\, D_{LiBrW}}\right)^{z1}(X_i - X_o)^{z2}(q)^{r2}\left(P_{sw,in} - P_{vacuum}\right) \quad -(4.37)$$

4.4 Results and Discussion

In order to use the developed general model for the heat and mass transfer of the evaporator heat exchanger with confidence, to predict the outlet condition and amount of heat transfer, verification is needed. The values of heat and mass transfer from the theoretical model must be in a fine agreement with the experimental values with minimum relative errors. Nonlinear least square method has been used with initial guesses to identify unknown parameter values using acquired experimental data.

4.4.1 Nonlinear least square model results

Nonlinear least square curve fitting using MATLAB has been used to identify the following parameters in the minimized model, shown below, using 288 data points in different operating conditions.

$$Q = \left[1 - exp\left\{-\frac{1}{C}\left[1 - exp\left(-\frac{\left[\frac{1}{\{x_1 \dot{m}_{hw}{}^{x_2}\}} + \frac{1}{\{x_3 m_s{}^{x_4} C_{ps}{}^{x_5}\}}\right]^{-1} A}{C_{max}}\right)\right]\right\}\right] C_{min}(T_{hi} - T_{si})$$

To evaluate the effectiveness of the developed model relative error (RE) and root mean square of relative error (RMSRE) have been calculated using the following equations [6].

$$RE = \frac{|\, Value_{real} - Value_{calculated} \,|}{Value_{real}} \times 100\% \qquad -(4.38)$$

$$RMSRE = \sqrt{\frac{\sum_{j=1}^{N}\left(\frac{Value_{real} - Value_{calculated}}{Value_{real}}\right)^2}{N}} \; ; N - Number\ of\ values \qquad -(4.39)$$

Table 4-3. Selected set of testing for the non-linear least square calculation

No	Hot water temp (^{0}C)	Hot water flow (m^3/hr)	Chilled water temp (^{0}C)	Chilled water flow (m^3/hr)	Solution flow (m^3/hr)	Pressure Pa
1	36	1.55	8	1.9	2	1500
2	40	1.55	8	1.9	2	1500
3	35	1.11	8	1.9	2	1500
4	35	1.62	8	1.9	2	1500
5	35	1.5	8	1.9	2	1500
6	35	1.5	12	1.9	2	1500
7	35	1.5	8	1.12	2	1500
8	35	1.5	8	2	2	1500
9	35	1.5	8	1.9	1.6	1500
10	35	1.5	8	1.9	2	1500
11	35	1.5	8	1.9	2	1000
12	35	1.5	8	1.9	2	2000

Table 4-3 shows the set of parameter values that have been used for calculation and verification purpose. For each testing, 24 sets of testing data were selected from different time intervals. Experimental heat transfer amount has been calculated based on hot water enthalpy difference. Theoretical heat transfer values have been calculated from the model. Calculated heat transfer rates have been compared for 288 data points. By using the following initial conditions [1775, 0.29, 800, 1.8, 0.6], values for the constant parameter x_1, x_2, x_3, x_4, x_5 of the equation (4.29), were calculated using MATLAB least square method.

$x_1 = 1775$

$x_2 = 2.1$

$x_3 = 800$

$x_4 = 1.8$

$x_5 = -0.1$

The comparison of experimental results and theoretical calculations of heat transfer rates within the evaporator heat exchanger is shown in figure 4-7. It can be seen that the theoretical calculation values are in ±10% good agreement with the experimental values. Figure 4-6 shows the RE of selected tests and 97.56% out of 288 values are within the RE of ± 10% and RMSRE is 0.0723. The experimental results show that the proposed model has good agreements with the experimental results.

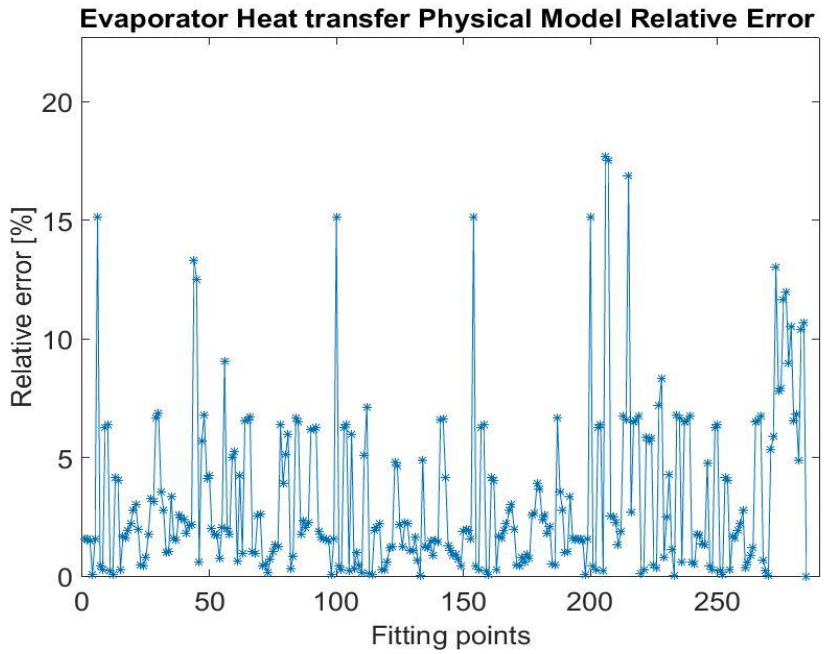

Figure 4-6.Evaporator heat transfer relative error between real value and theoretical calculated value

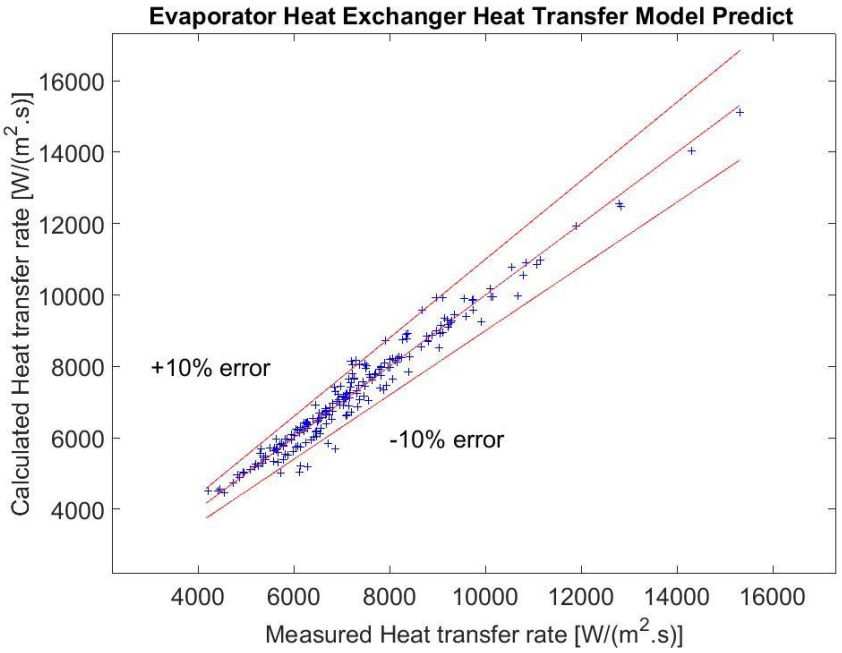

Figure 4-7. Comparison between model predication and actual values of heat transfer

Mass transfer rate for the evaporator heat exchanger have been calculated using the following equation. There were five constants needed to be identified by using the least square method. Different sets of test conditions were used for the following calculation and the calculated final concentrations and the actual final concentrations were compared.

$$S = x_{10}\frac{D_{LiBrW}}{D}(Re_{sl}F^{1.25})^{x_{11}}\left(\frac{\mu}{\rho\, D_{LiBrW}}\right)^{x_{12}}(X_i - X_o)^{x_{13}}(q)^{x_{14}}\left(P_{s,sat} - P_{vacuum}\right)$$

Keeping [0.01 -0.6 -0.14 -0.7 1.7] as initial conditions above five constant values, $(x_{10}, x_{12}, x_{13}, x_{14}, x_{15})$ were calculated using non-linear least square method and following results were obtained.

$x_{10} = 6.478 \times 10^{-8}$

$x_{11} = -0.6013$

$x_{12} = -0.1408$

$x_{13} = -.6994$

$x_{14} = 1.6991$

Comparison between the theoretical calculation mass transfer rates and experimental mass transfer rates are presented in figure 4-8. It can be seen that the RE for all the comparison values are within ± 10% good agreement and RMSRE value is 0.0351. Figure 4-9 illustrates the agreement between experimental and calculated values within ± 10% error band. Since the values fall within ± 10% confidence interval, within a minimum deviation from the equal line, the model can be used to represent the actual system. Above calculated constants is used for the below parameter analysis.

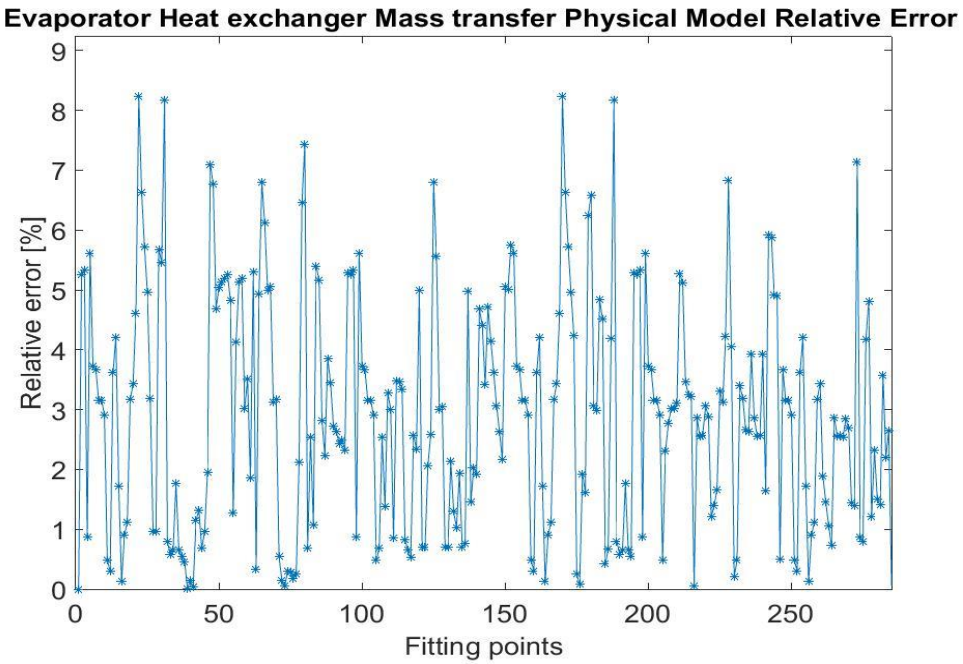

Figure 4-8. Evaporator mass transfer relative error between real value and theoretical calculated value

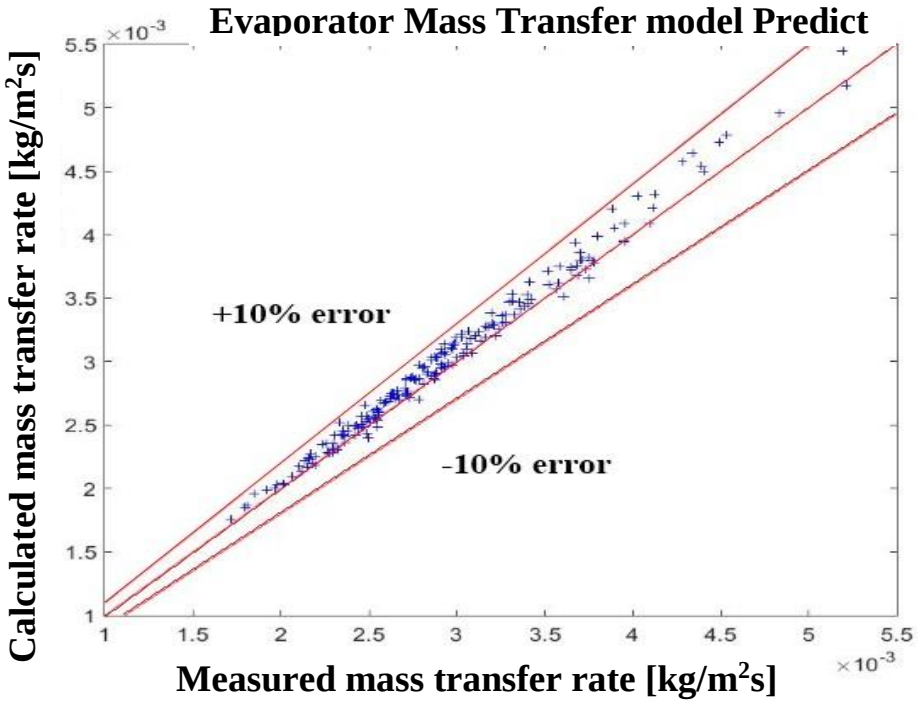

Figure 4-9. Comparison between model predication and actual values of mass transfer

4.4.2 Parametric analysis

Hot water flow rate, hot water temperature, chilled water flow rate, chilled water temperature, solution flow rate, initial vacuum pressure and initial solution concentration are design parameters focused in this study. Following set of testing were carried out and studied here.

Table 4-4. Changing parameter for experimental testing

Parameter maintained	Tested parameter initial values			
Hot water inlet temperature	35 ^{0}C	36 ^{0}C	38 ^{0}C	40 ^{0}C
Hot water flow rate	1.14 m^3/hr	1.28 m^3/hr	1.58 m^3/hr	1.7 m^3/hr
Chilled water temperature	7 ^{0}C	8 ^{0}C	9 ^{0}C	10 ^{0}C
Chilled water flow rate	1.12 m^3/hr	1.3m^3/hr	1.64m^3/hr	1.99m^3/hr
Solution flow rate	1.68 m^3/hr	1.91 m^3/hr	2 m^3/hr	2.15 m^3/hr
Initial vacuum pressure	1500 Pa	2000 Pa		
Initial solution density	1350m^3/kg	1370m^3/kg	1390m^3/kg	1410m^3/kg

The effect of hot water flow on the desorption performance

The effect of hot water flow rate was tested by changing the pump frequency by 30Hz-50Hz and it was seen that the flow rate changes from 1.14 m^3/hr-1.7 m^3/hr. Figure 4-10 shows the comparison between the actual and calculated desorption rates & figure 4-11 shows the actual and calculated condensation rates. Values are within ±10% agreement and there is a slight deviation of

desorption rate values when the flow rate is 1.7 m^3/hr. All the other values belong to other flow rates are within acceptable agreement, thereby the model can be used for the system representation.

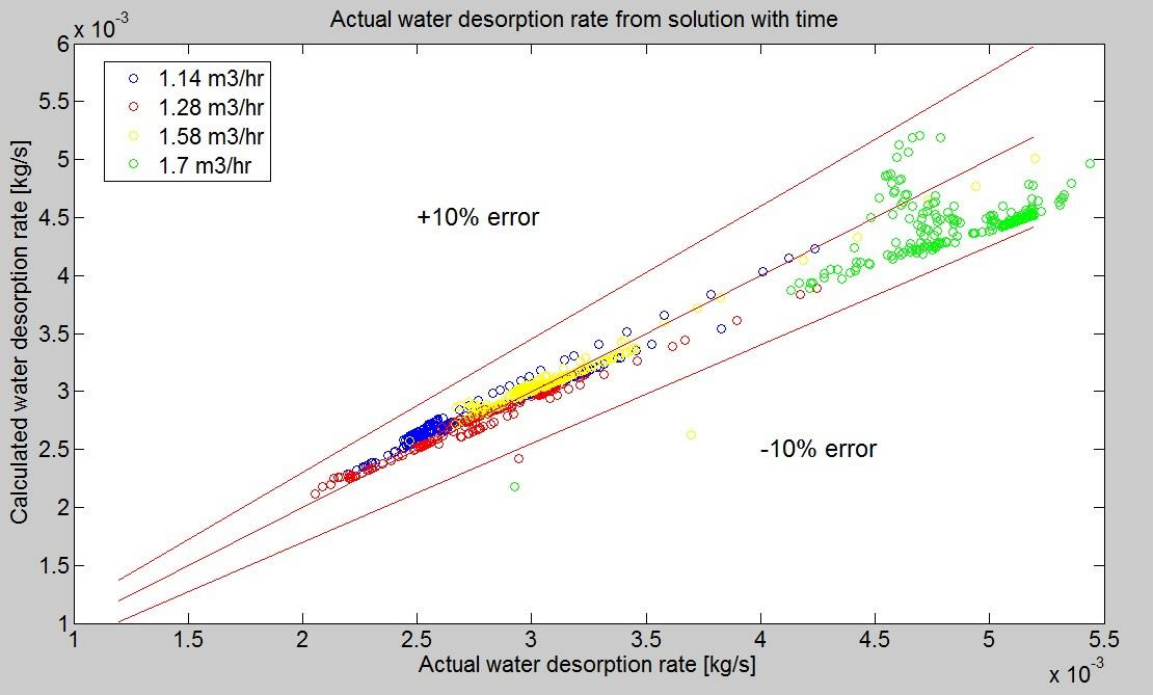

Figure 4-10. Comparison between calculated desorption rate Vs actual desorption rate

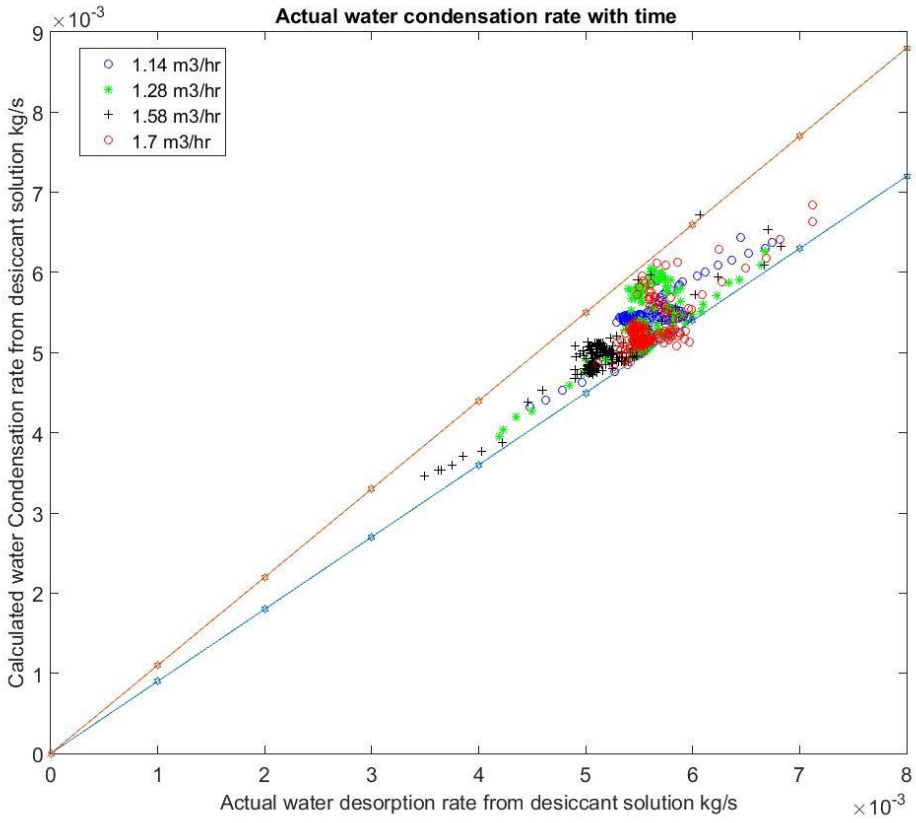

Figure 4-11.Comparison between calculated desorption rate Vs actual Condensation rate

Figure 4-12 shows the change of the hot water inlet temperature with respect to time for different hot water flow rates. Initially, when the flow rate increases, it provides a higher amount of heat for desorption process. When the amount of heat supply to hot water is not enough, hot water inlet temperature drops down to a very low value 31- 33 ^{0}C (as shown in Figure 4-12 with circle A). Initially, the amount of water vaporization is also high and later on with time, concentration of LiBr increases and desorption rate decreases. As a result heat requirement reduces, as a result temperature drop reduces, and therefore inlet temperature increases. When the flow rate is low, energy release becomes moderate and heater power becomes sufficient, therefore the temperature does not drop down to a very low value. Also desorption rate remains low resulting the concentration of LiBr to be low for about 20 minutes and as a result desorption capability remains same. Heat absorption

from hot water remains almost same and therefore, gradually inlet temperature increases. For the flow rate 1.58 m^3/hr heat supplies and releases are almost same for hot water (around 6kW) and it is difficult to increase temperature with time. Temperature varies hugely for each rates concern as shown by circle B in the figure 4-12 that affects the system performance.

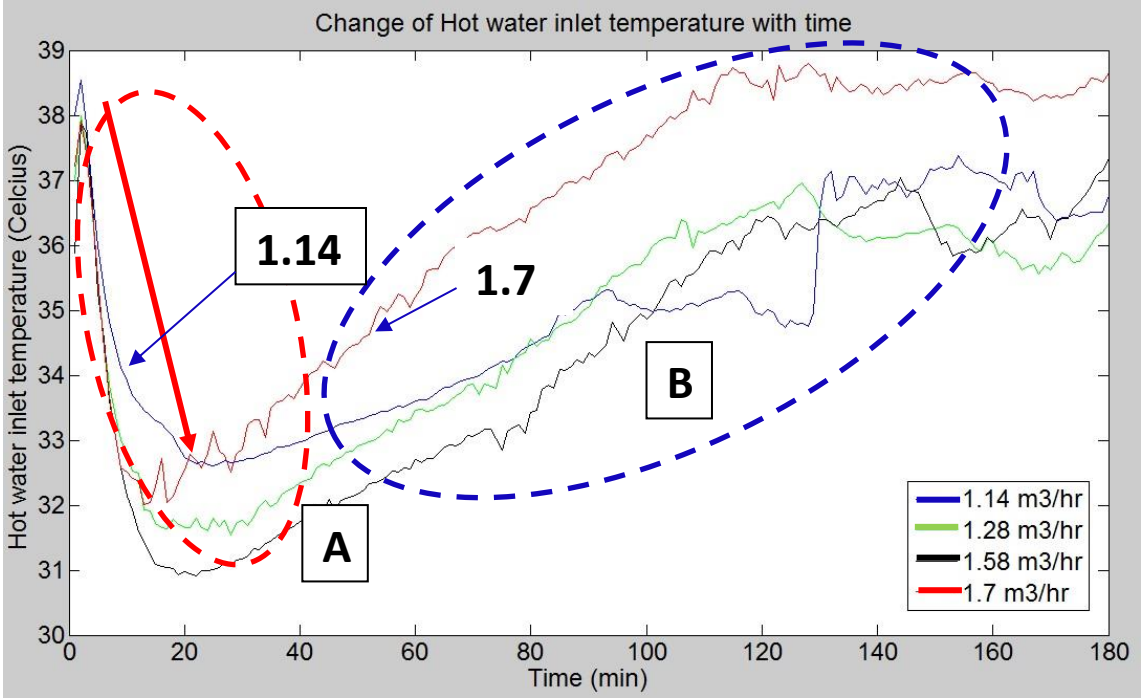

Figure 4-12.Change of Hot water temperature with time for different flow rates

Figure 4-13 shows the change of the hot water outlet temperature and it was seen that it has a similar behavior as the hot water inlet temperature. Since hot water inlet temperature of maximum flow rate drops to a very low value, outlet temperature also drops to a very lower value, from 34 ^{0}C to 26 ^{0}C, than other flow rates. At the end of the testing, the outlet temperature of all four flow rates reaches an almost similar value.

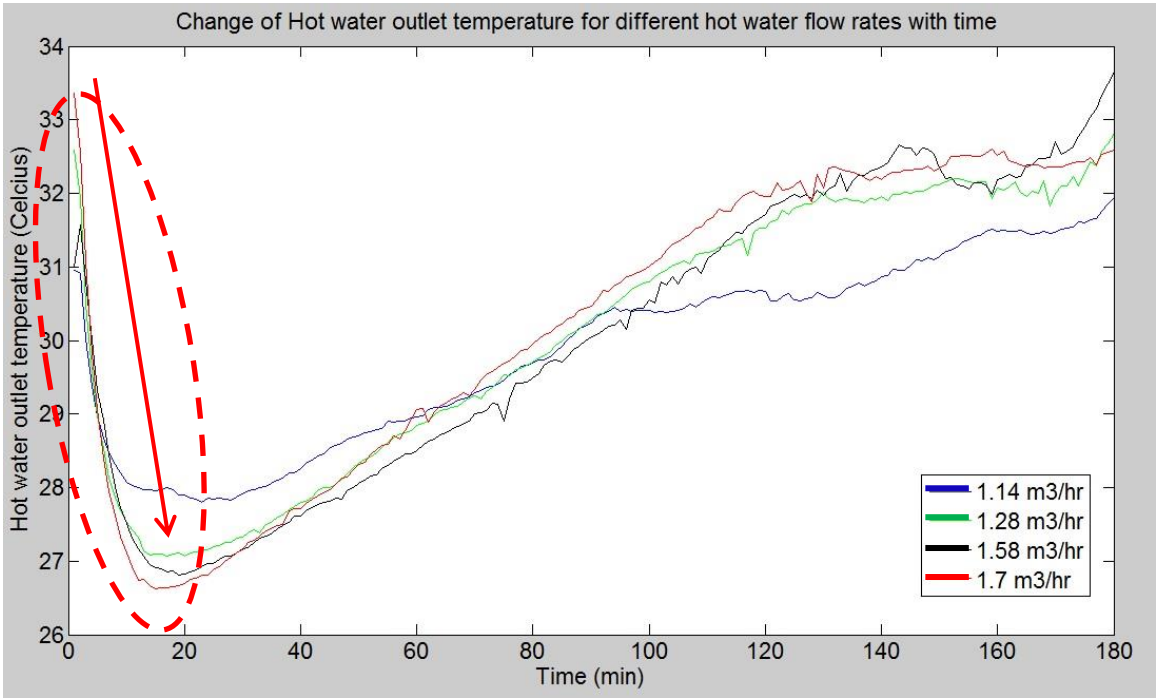

Figure 4-13. Change of hot water outlet temperature with time for different flow rates

Figure 4-14 illustrates the change of solution temperature with time for different hot water flow rates. Initial solution temperature of 1.7m^3/hr was around 21 ^{0}C which was lower than other tests. Initially, a considerably higher amount of heat was used as latent heat for vaporization and a small amount of heat was used as sensible heat to increase the temperature of the solution. It was seen that when the solution temperature rose, the sensible load reduced and when it reached to saturation temperature almost 100% heat was used as latent heat. The solution temperature of all four flow rates reached the range of 27-29^{0}C almost after the same time duration of 75min- 85min even though 1.7 m^3/hr flow rate temperature started from a lower solution temperature. It was identified that, the higher the hot water flow rate is higher the increasing rate of the solution temperature becomes, which allows better performance.

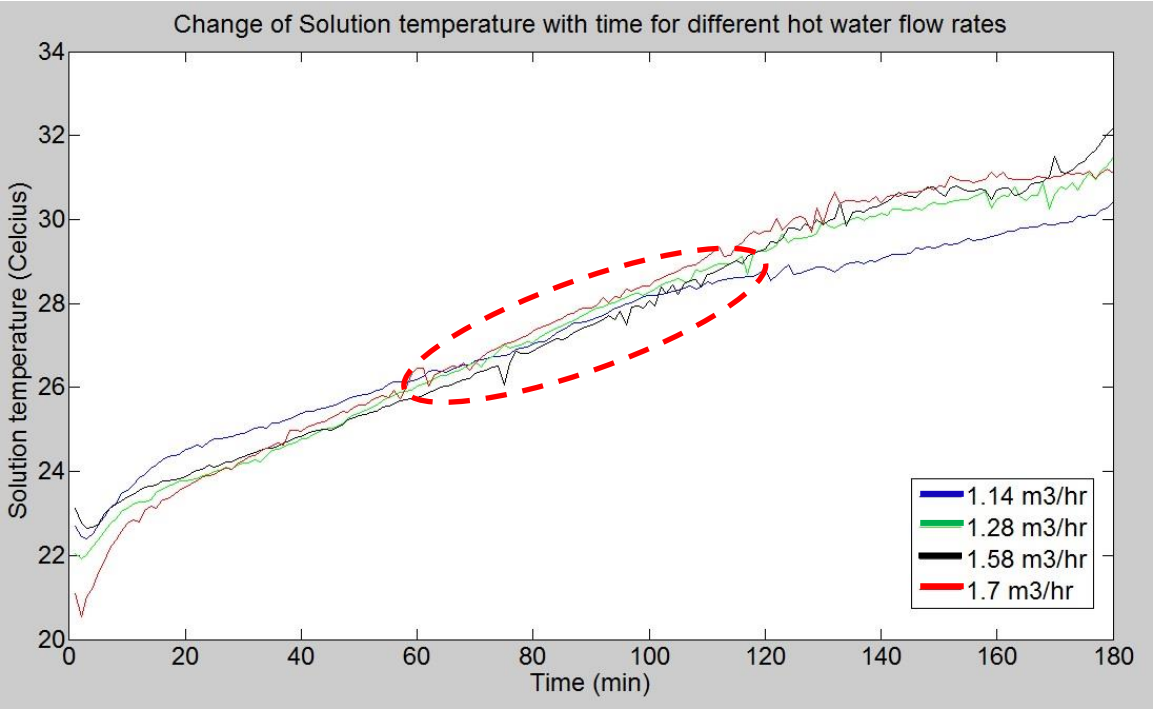

Figure 4-14. Change of solution temperature with time for different hot water flow rates

Figure 4-15 shows the increase of the Lithium Bromide mass ratio within the solution for different hot water flow rates with respect to time. The gradient of the mass ratio line increases, from a lower flow rate 1.14 m^3/hr to a higher flow rate 1.7m^3/hr as shown by the arrows in the figure 4-15. Figure 4-16 shows the decrease of the water mass ratio within the solution and it has (1- LiBr mass ratio) behavior. Water mass ratio reduces faster in higher flow rates than lower flow rates due to higher desorption rate. There is a considerable difference between final LiBr concentration values for different flow rates.

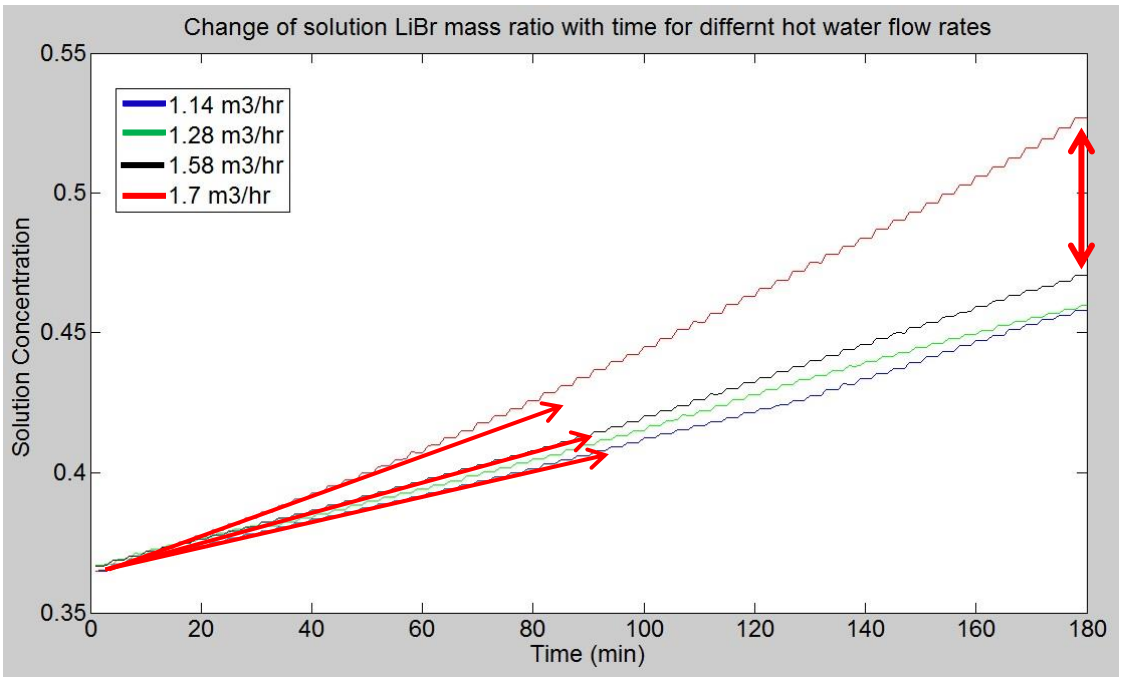

Figure 4-15. LiBr mass ratio change with time for different hot water flow rates

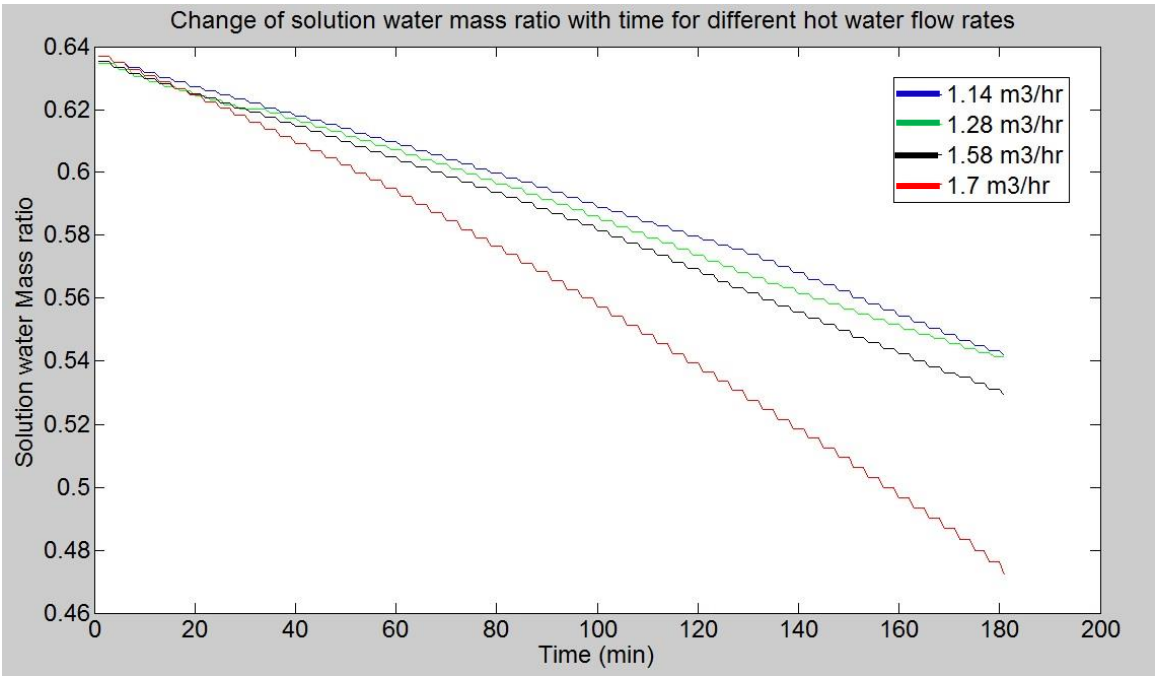

Figure 4-16. Water mass ratio change with time for different hot water flow rates

Figure 4-17 shows the final solution LiBr mass percentage for different hot water flow rates with respect to time. Initial mass ratio was same for all four instances and final mass ratio value was highest when the flow rate was highest 0.5269 at 1.7m^3/hr. The main objective of the system was to have a higher final LiBr mass ratio at the end of the process. Therefore, 1.7m^3/hr flow rate was found as best flow rate.

Table 4-5. Final LiBr mass percentage for different hot water flow rates

Test	1.14 m^3/hr	1.28 m^3/hr	1.58 m^3/hr	1.7 m^3/hr
Final LiBr mass ratio	45.81%	45.98%	47.07%	52.69%

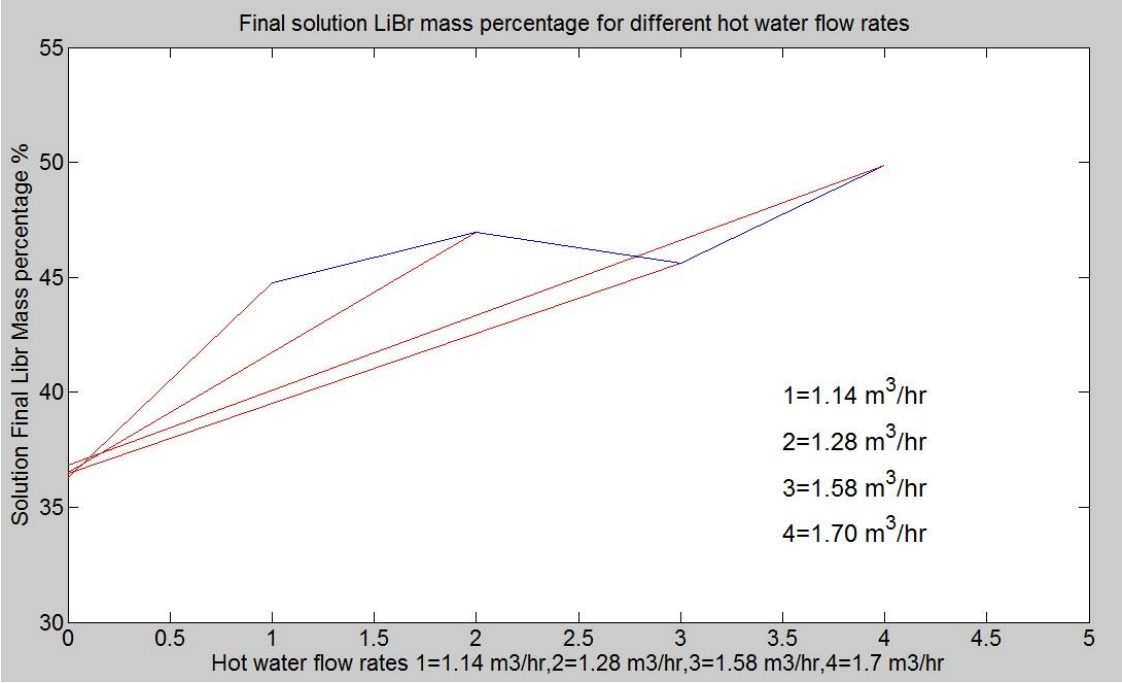

Figure 4-17.Final LiBr mass percentage for different hot water flow rates

Figure 4-18 illustrates the comparison and behavior of water desorption rate with time for different flow rates with respect to time. Highest flow rate 1.7 m^3/hr was found to have a considerably higher, 4-5 g/s desorption rate than lower flow rates. At the very initial stage there was a very low vacuum condition in the chamber and water vaporization was easier. Therefore, the amount of water vaporization was higher. To the flow rate 1.7m^3/hr, during the last 20 min of the test, solution almost reached to saturation temperature and most of its heat was for vaporization temperature.

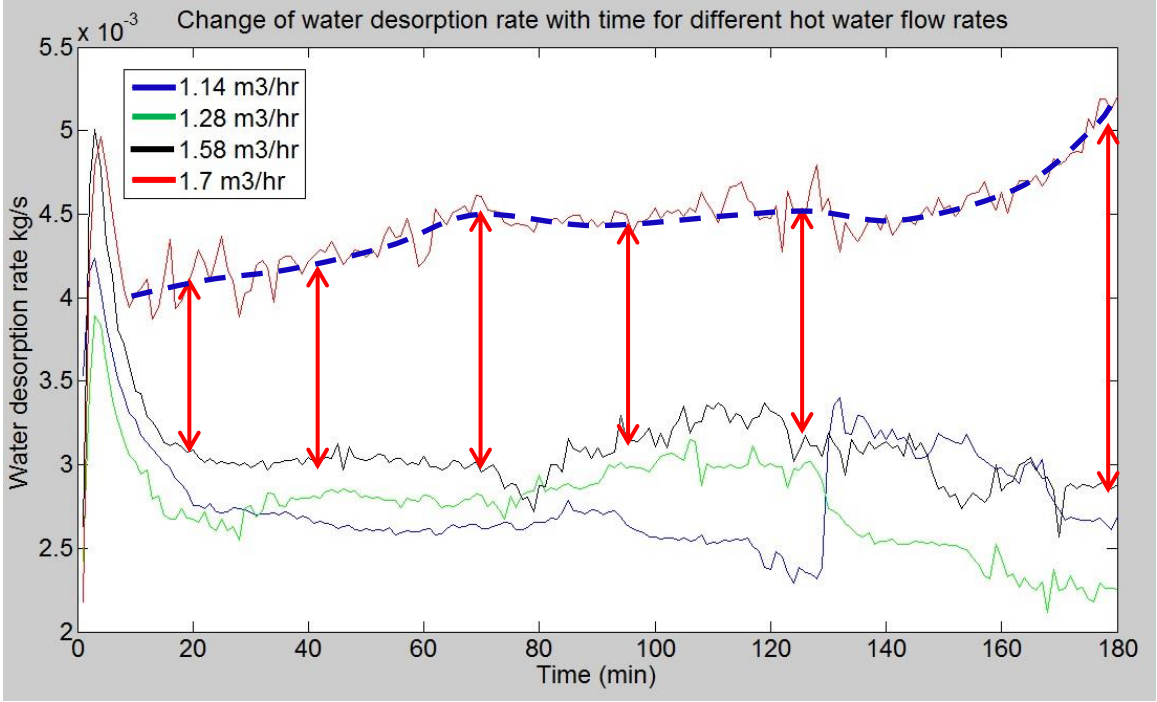

Figure 4-18. Change of water desorption rate for different hot water flow rates

Behavior of the heat transfer effectiveness with respect to different hot water flow rates is shown in figure 4-19. Heat transfer effectiveness is the ratio of actual heat transfers to the maximum possible heat transfer(Q_{real}/Q_{max}). Initial stage of the testing solution inlet temperature was very low around 22^0C and the maximum possible heat transfer rate was

high. Therefore, the heat transfer effectiveness was low. Same solution was made to circulate through the system, solution temperature increased with time and maximum possible heat transfer amount reduced and as a result heat transfer effectiveness increased. Heat transfer effectiveness of the higher flow rate was higher than the lower flow rates and it reached almost 90% at the end of the testing time for the flow rate 1.7m^3/hr.

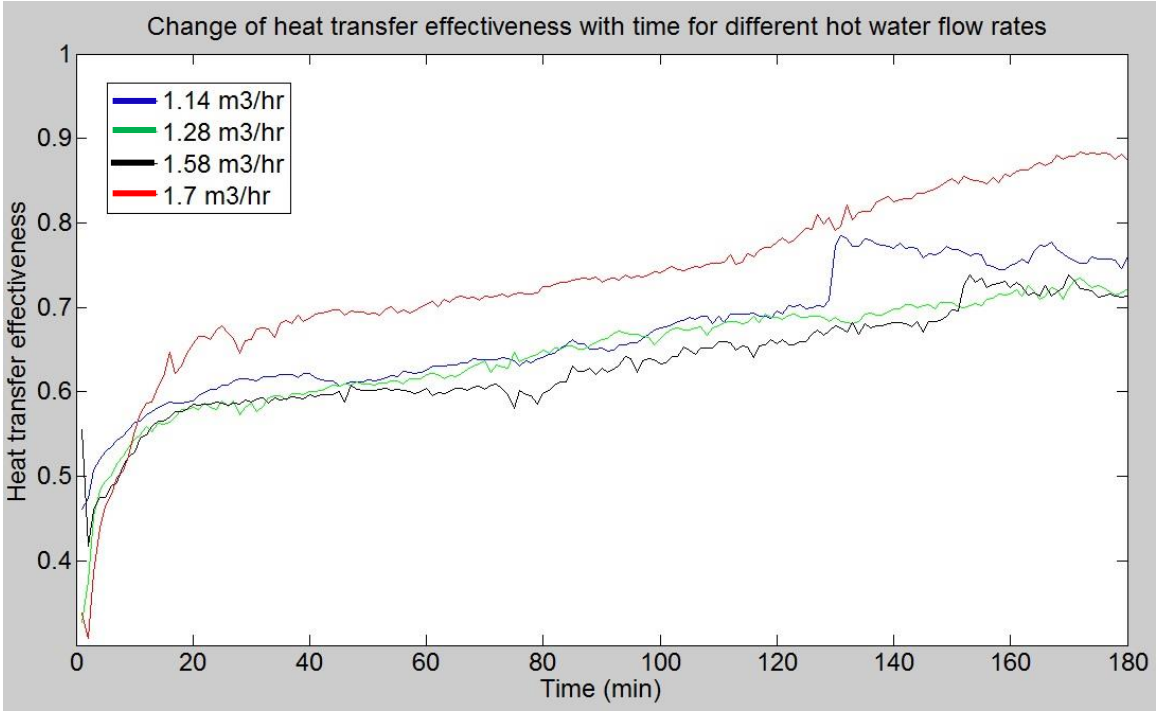

Figure 4-19. Behavior of heat transfer effectiveness for different hot water flow rates

Figure 4-20 shows the variation of the mass transfer effectiveness with time for different hot water flow rates. Mass transfer effectiveness is the ratio of the actual changes of solution water mass ratio to the maximum possible change of solution water mass ratio. Highest 1.7 m^3/hr hot water flow rate has the highest mass transfer effectiveness as it provides more energy to the solution. When it comes to lower flow rates according to figure 4-19,

1.14m^3/hr has a higher effectiveness than the 1.28 & 1.58 m^3/hr. Maximum possible heat transfer depends on the flow rates and heat capacities of two solutions, which flows through the heat exchanger. Heat transfer effectiveness and mass transfer effectiveness has the same behavioral graphs with they have slightly different individual values. In overall, higher hot water flow rate is favorable for higher heat transfer effectiveness.

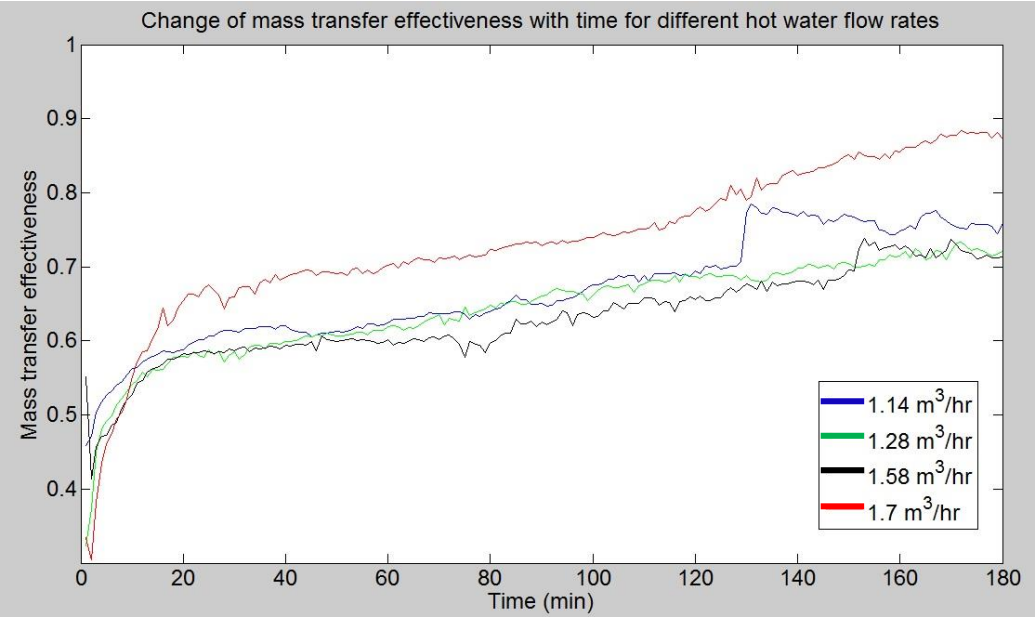

Figure 4-20. Change of mass transfer effectiveness for different hot water flow rates

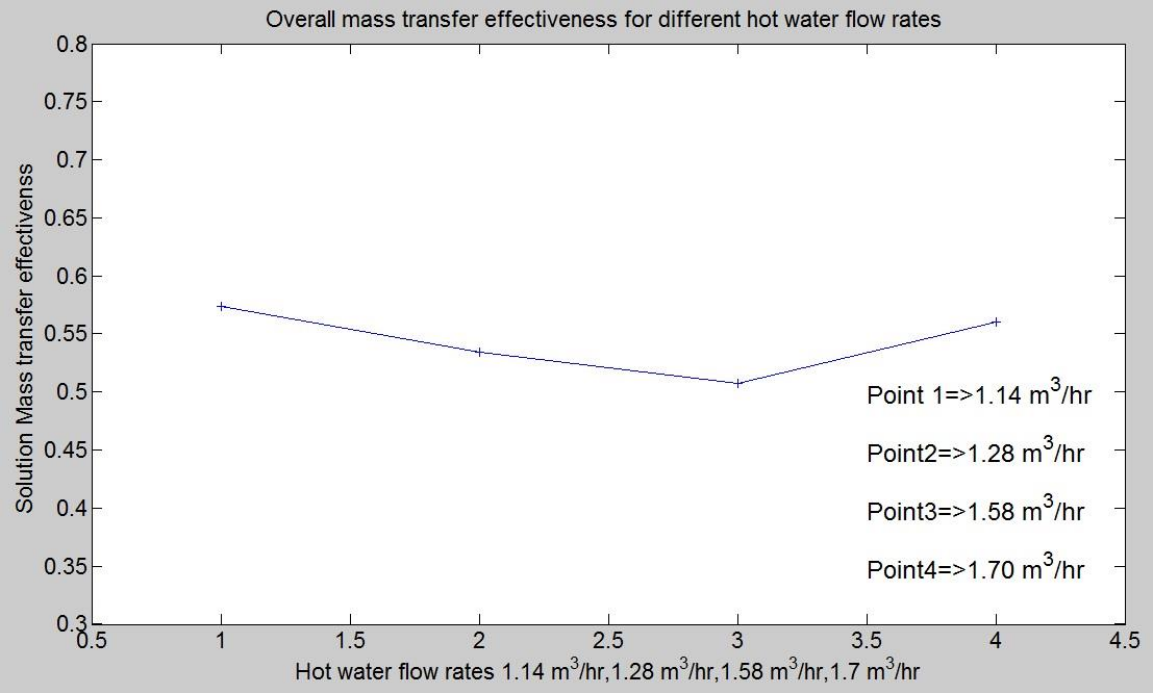

Figure 4-21. Overall mass transfer effectiveness value for four cases of hot water flow rate

Figure 4-21 shows the overall mass transfer effectiveness considering the initial and final LiBr concentrations of solutions. Overall mass transfer effectiveness of the system was highest when the flow rate was 1.14m^3/hr and it decreased when the flow rate was 1.28 & 1.58 m^3/hr further and increased again when the flow rate was 1.7m^3/hr. In overall, energy spent and mass transfer context for 1.14m^3/hr has a higher efficiency than others, except for the flow rate 1.7m^3/hr which has almost an equally higher value.

The effect of hot water temperature to the desorption performance

Hot water initial temperature was changed from 35, 36, 38, 40 Celsius to test the effect of the hot water temperature on the desorption performance. The hot water was made to circulate before the testing and when the hot water inlet temperature reached the above set

values, the pump was kept to run for a while to acquire steady state and then the solution pump was started to initiate the desorption process.

Table 4-6. Initial and final LiBr mass ratio for different hot water temperatures

Test	35 ^{0}C	36 ^{0}C	38 ^{0}C	40 ^{0}C
Initial LiBr mass ratio	36.31%	36.54%	36.46%	36.84%
Final LiBr mass ratio	44.75%	46.98%	45.64%	49.85%

Figure 4-22 shows the comparison between the actual desorption rates with the calculated desorption rates and figure 4-23 shows the actual and calculated condensation heat transfer rates for different hot water temperature testing. All values are within ±10% acceptable agreement and theoretical results successfully represent the actual values.

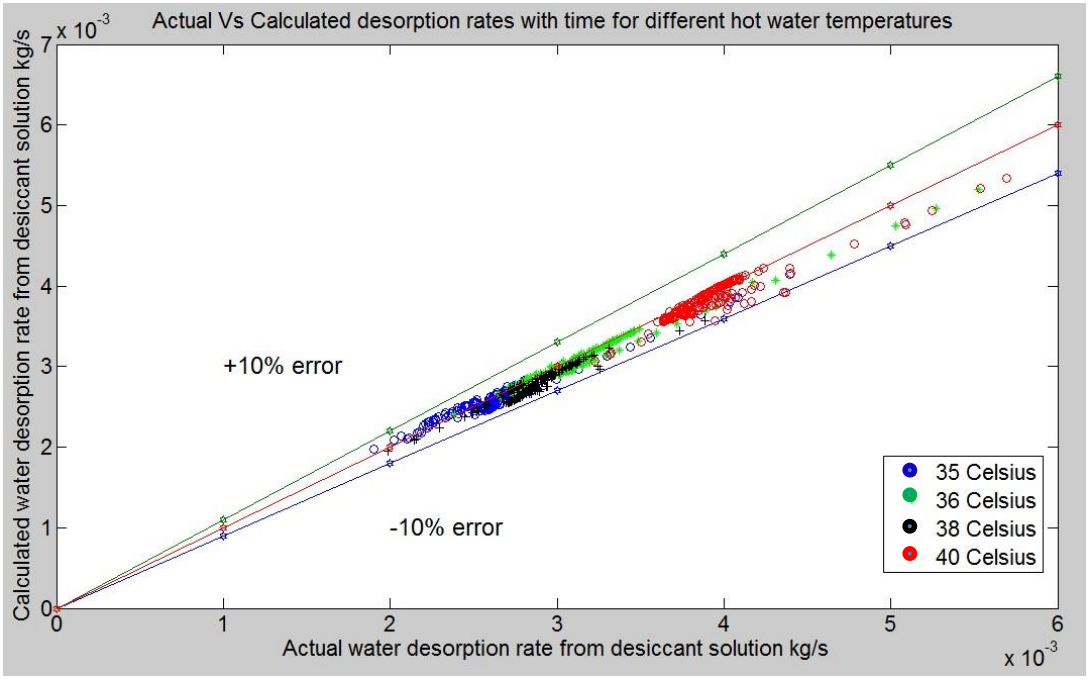

Figure 4-22. Actual desorption rate Vs calculated desorption rate

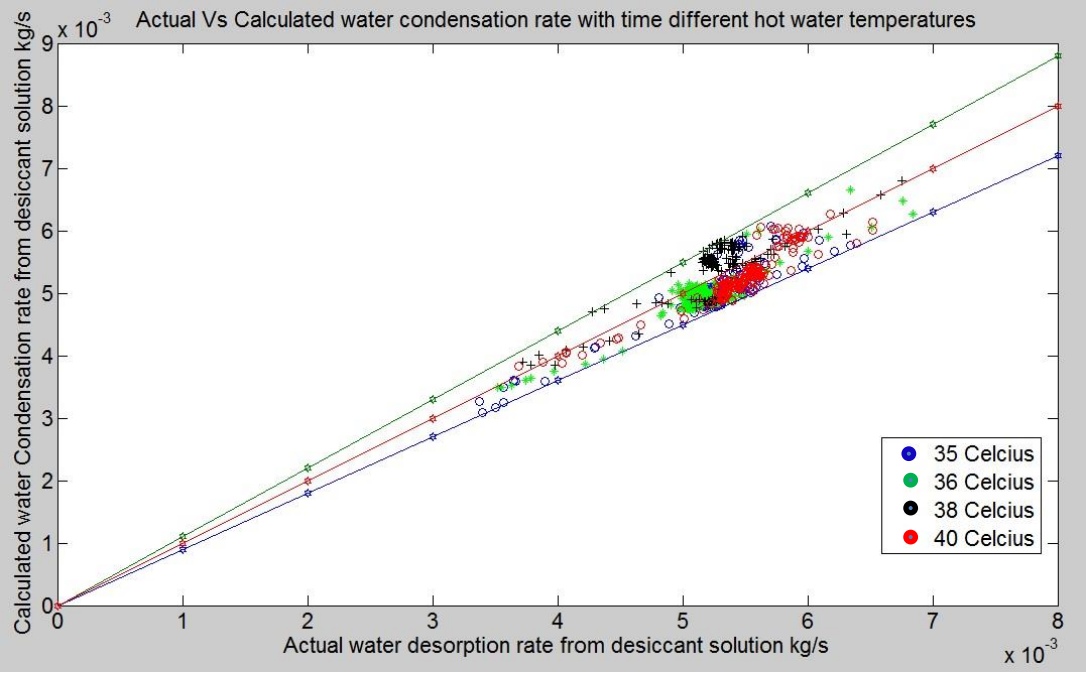

Figure 4-23. Actual Condensation heat transfer rate Vs Calculated condensation heat transfer rate

Figure 4-24 shows the variation of the hot water inlet and outlet temperature for different initial inlet temperatures with respect to time. The top four lines as shown in figure 4-24 depict inlet temperature changes and four lines below depict the outlet temperature changes. It can be seen that the inlet temperature reduces as soon as the system starts to run till 18 minutes and then starts to rise again till the end, to the temperature maintained. The reduction of temperature is due to the insufficient capacity of the heater that hinders the supply of required heat to the system. Outlet temperature also has a similar type of variation in temperature. Therefore, high capacity heater must be installed to provide required amount of heat to the hot water to maintain a constant temperature value.

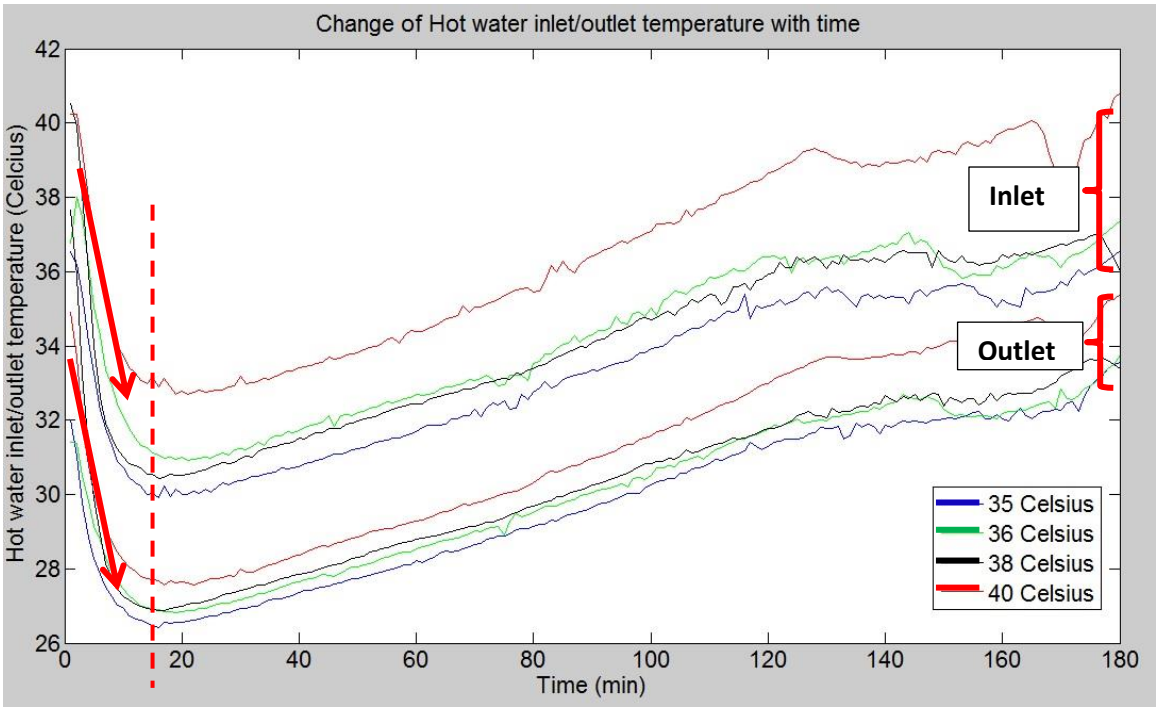

Figure 4-24. Change of hot water inlet/outlet temperature for different hot water inlet temperatures

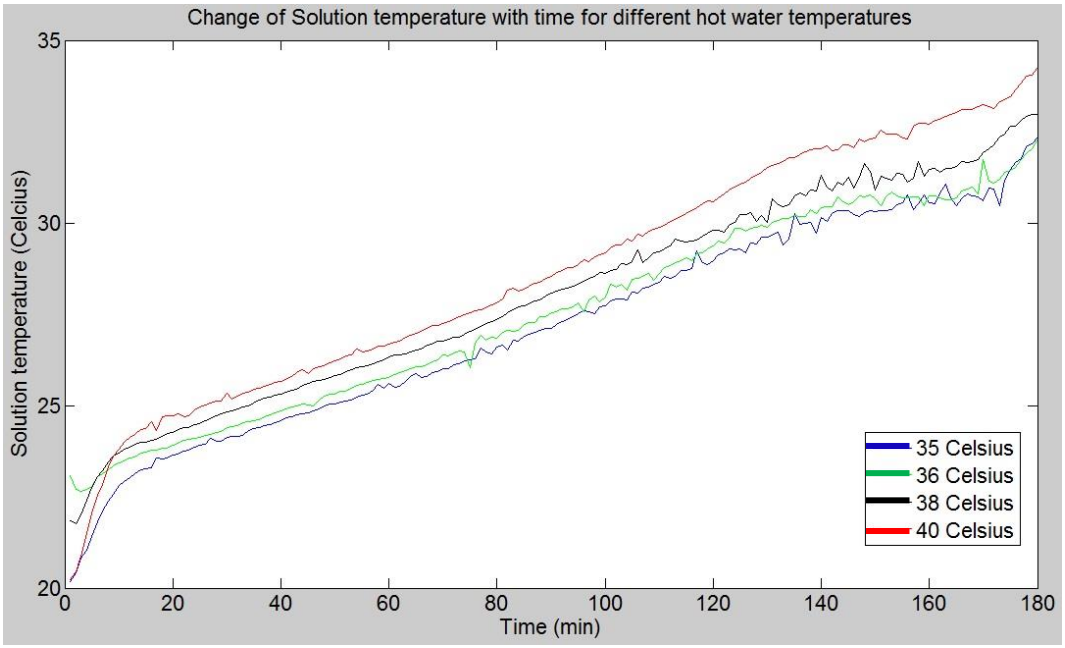

Figure 4-25. Change of solution temperature with time for different hot water temperature

Variation and change of the water mass ratio and the LiBr mass ratio with respect to time is shown in figure 4-26. Gradients of the water mass ratio reduction and LiBr mass ratio increment are highest when hot water temperature is at 40 ^{0}C. The temperature change of a single degree can cause a considerable change in the final concentration. When the temperature is at 35 ^{0}C final LiBr mass ratio is 45.75% and when it is at 40 ^{0}C it's 49.85%. Figure 4-27 shows the variation of the final LiBr mass ratio for four instances. Final LiBr mass ratio increases from 35^{0}C - 44.75% to 40^{0}C - 49.85%. However, there is a slight reduction when the temperature is at 38^{0}C-45.64% due to experimental conditions.

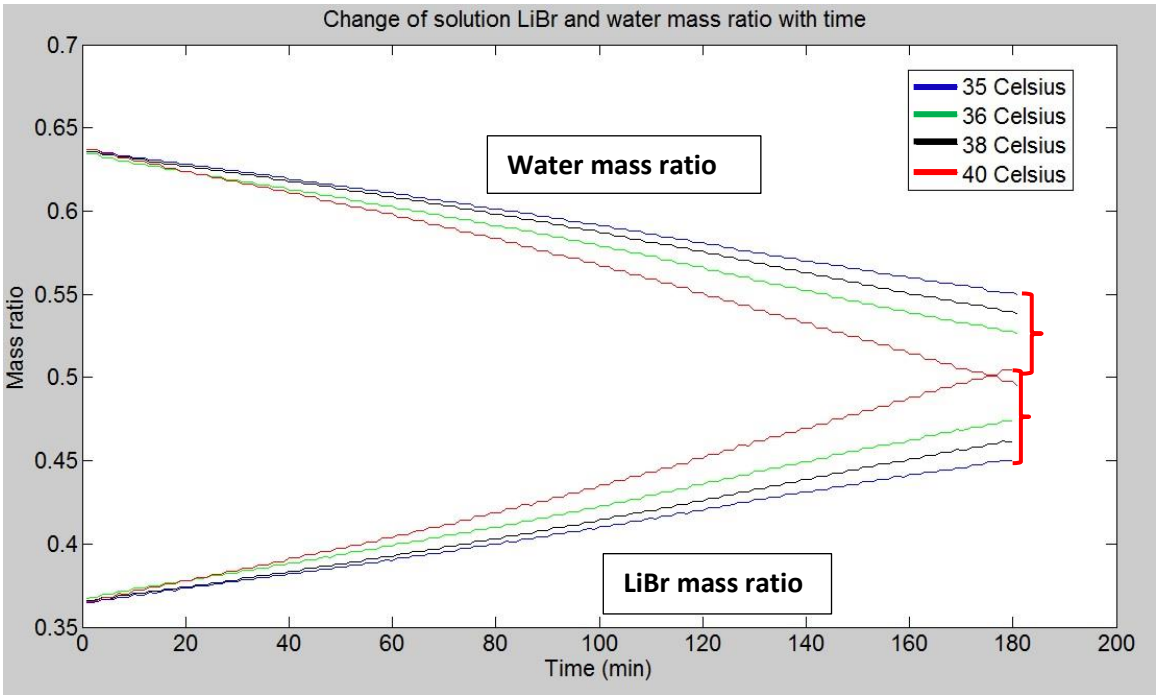

Figure 4-26. Change of LiBr mass ratio in the solution

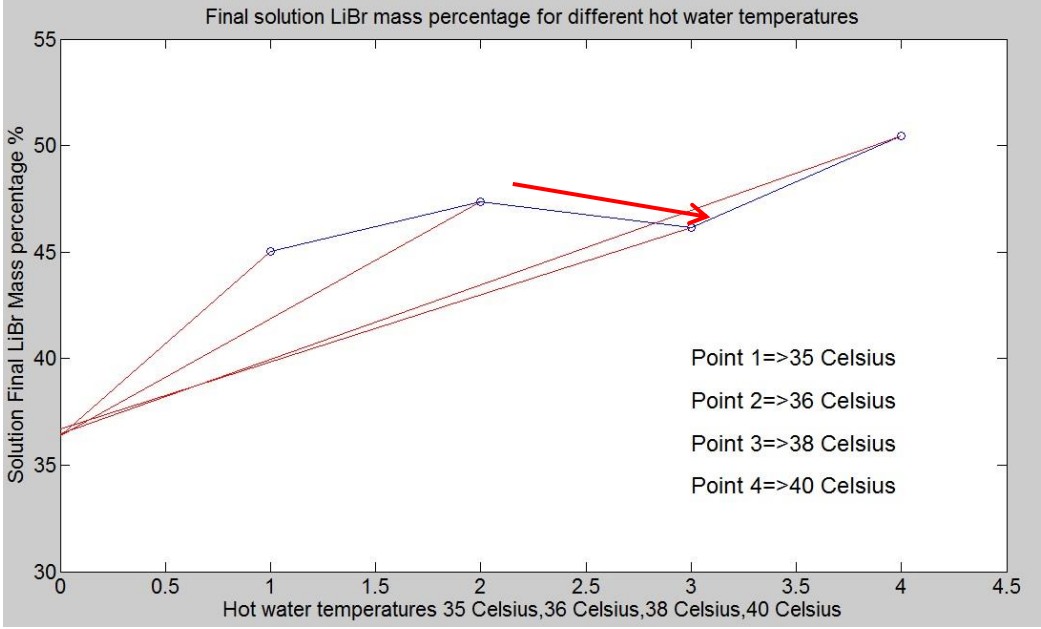

Figure 4-27. Final solution LiBr mass fraction variation

Figure 4-28 shows the change of the vacuum pressure with time. As soon as the solutions pump starts to run, vacuum pressure increases rapidly to a very higher value due to water vaporization. For example in this case initial pressure is around 1000 Pa and it raises up to 1900 Pa within seconds and most importantly all four tests it shows the same type of behavior. High temperature 40^0C causes to have highest vacuum pressure due to higher release of water vapor. However, after 3-5 minutes pressure started to reduce due to condensation. Initial vacuum pressure increment is uncontrollable. In order to reduce the pressure within few minutes' condensation process should be more efficient.

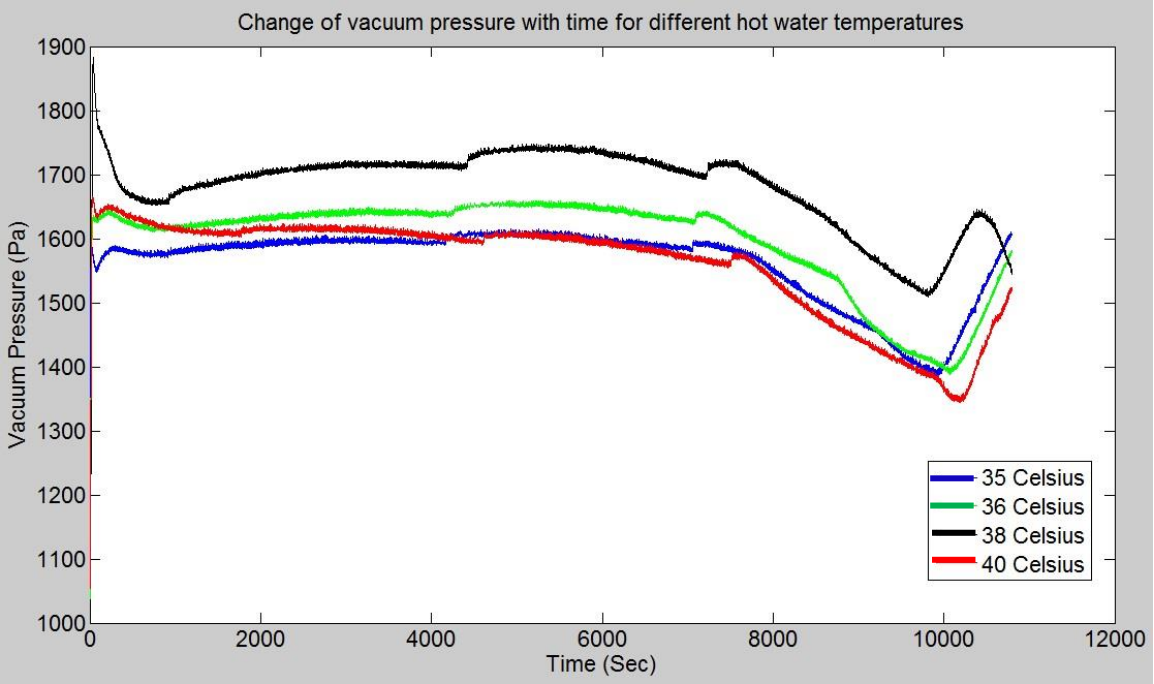

Figure 4-28. Change of vacuum pressure with time

Figure 4-29 illustrates the change of the desorption rate of the system with hot water temperature changes. At the beginning of the process water vapor pressure in the solution was very high and vacuum pressure was very low. High temperature hot water provided sufficient heat to achieve both sensible and latent load for the water within the solution. Initial desorption rate was high at around 5 g/s till 3-5 minutes in the instances with 36 and 40 degree hot water temperatures. But when the temperature was 38^0C the desorption rate was low because the sudden increase of the vacuum pressure to around 1900 Pa as shown in figure 28. Desorption rate for the 40^0C temperature testing maintained its value at around 3-4 g/s throughout the testing as shown in figure 29. High temperature provided a higher heat transfer driving force between hot water and solution $(T_h - T_s)$ and it increased the desorption capability. There is a slight variation of the desorption rate with time. Initially the variation was very low and it increased slightly in all four cases towards the end of the

testing. System control parameters were controlled manually and the system reaction time is slightly higher and the system parameters changed suddenly. The main parameter which affects to the desorption rate is the mass transfer driving force and water vapor partial pressure difference. Sudden variations of the vacuum pressure caused those effects. These are the reasons for these minor variations, but the percentage of variation is not quite high. Therefore, the effect for the final results on the testing of hot water temperature on the desorption rate was not significant. Therefore, it's important to design a control system to minimize these minor variations of the values to have the highest desorption rate.

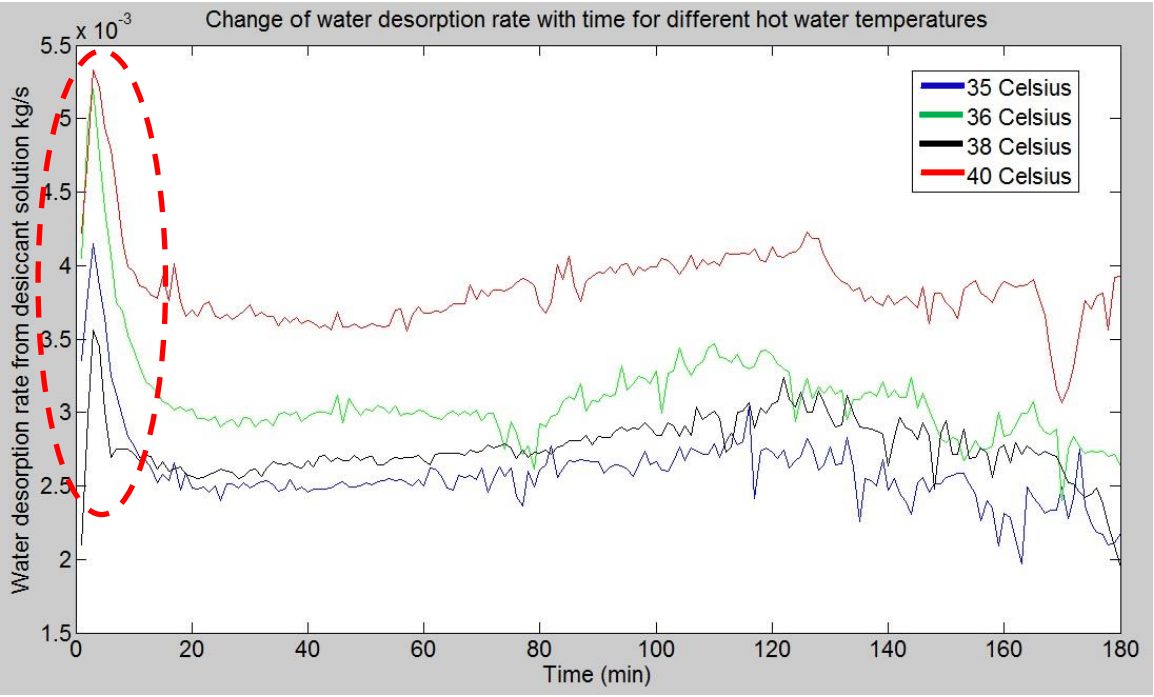

Figure 4-29. Change of water desorption rate with time for different hot water temperatures

Figure 4-30 illustrates the change of heat transfer effectiveness of the system with respect to time. System heat transfer effectiveness changes throughout the session with minor

variations and the heat transfer effectiveness value slightly increased with time. Initial sudden increment of heat transfer effectiveness was mainly due to the high temperature gradient and high actual heat release. It was seen, if the capacity of the heat source is high enough to maintain the hot water temperature, a constant higher temperature value and a high heat transfer effectiveness can be achieved. The heat transfer effectiveness variation slightly increased towards the end of the testing time period. This is due to the same reason discussed above, difficulty of manual control of controlling parameters and the sudden change of the system parameters towards the end of the testing time period. These effects can be overcome by implementing a control mechanism to the system which can minimize the variations. Figure 4-31 shows the behavior of mass transfer effectiveness with time. It has the similar behavior like heat transfer effectiveness.

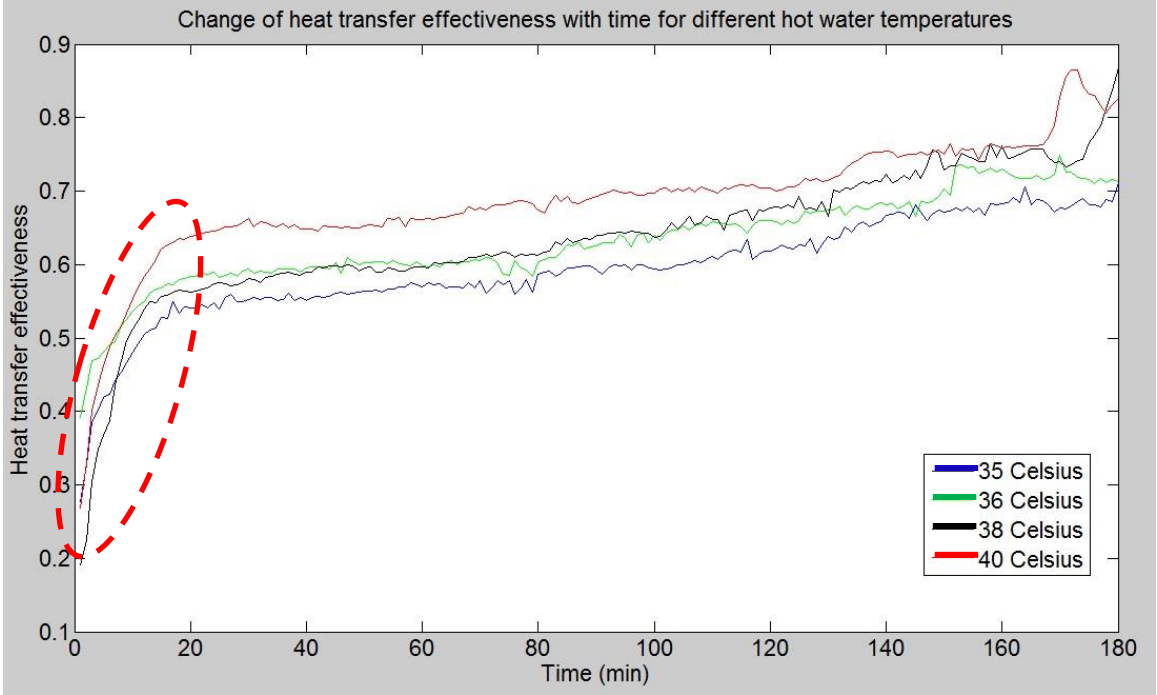

Figure 4-30. Variation of heat transfer effectiveness with time for different hot water temperatures

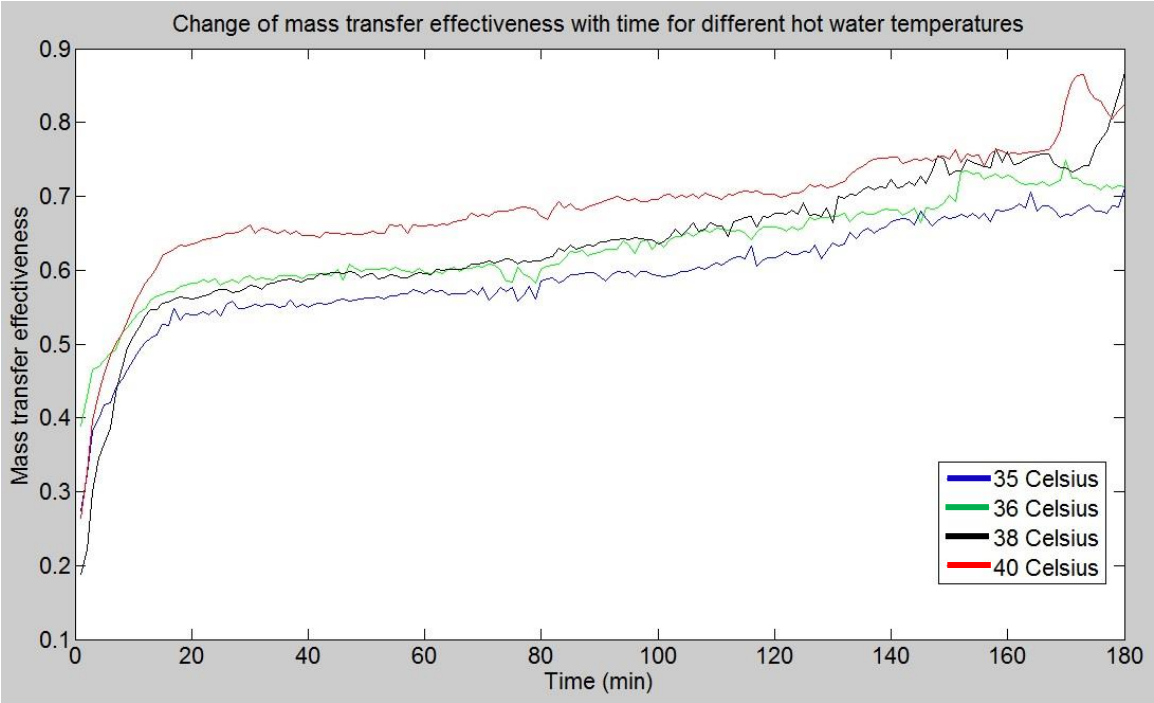

Figure 4-31. Variation of mass transfer effectiveness with time for different hot water temperatures

Figure 4-32 shows the overall mass transfer effectiveness and it was highest when the temperature was at 40 ^{0}C and lowest when the temperature was at 35 ^{0}C case. It was found that, although the final concentration was lower at 38 ^{0}C than at 36^{0}C, the mass transfer effectiveness was higher. Therefore, it is understood that a higher hot water temperature leads to a higher desorption rate resulting a higher final LiBr concentration.

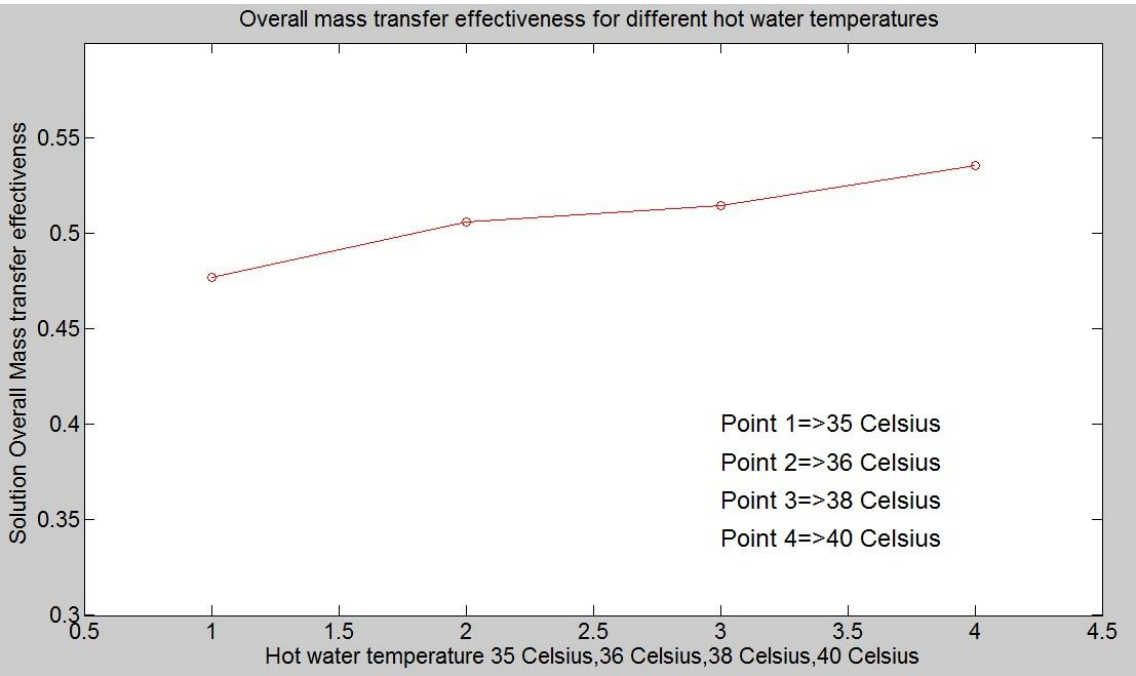

Figure 4-32.Overall mass transfer effectiveness for different temperature

Effect of solution flow rate to the evaporator performance

Solution flow rate is another important parameter which affects to the evaporator performance. Four testings' were conducted for the flow rates; 1.68m^3/hr , 1.91m^3/hr , 2m^3/hr , 2.15m^3/hr. Figure 4-33 shows the comparison between the actual desorption rate values and the theoretical values during the change of solution flow rate with time. It's clear that values are within $\pm$10% good agreement.

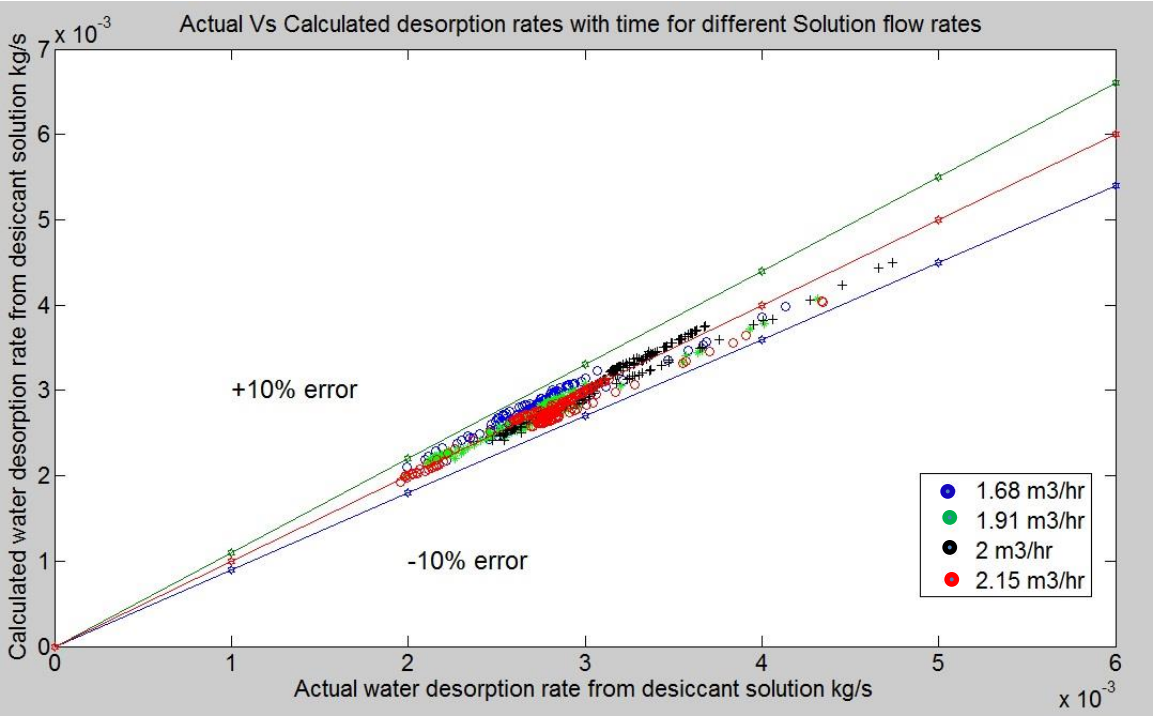

Figure 4-33. Theoretical desorption rate values vs actual desorption rate values

Figure 4-34 illustrates how the solution temperature changes for different solution flow rates. A higher solution flow rate achieves higher temperature and lower solution flow rate achieves lower temperature. Higher flow rate increases the number of circulations through the evaporator heat exchanger, thereby, increases the amount of heat absorbed by the solution. As a result higher solution flow rate brings the solution to its saturation temperature faster and reduces the sensible load requirement. But there isn't a considerable difference between gradients of temperature graphs except for 1.91m^3/hr.

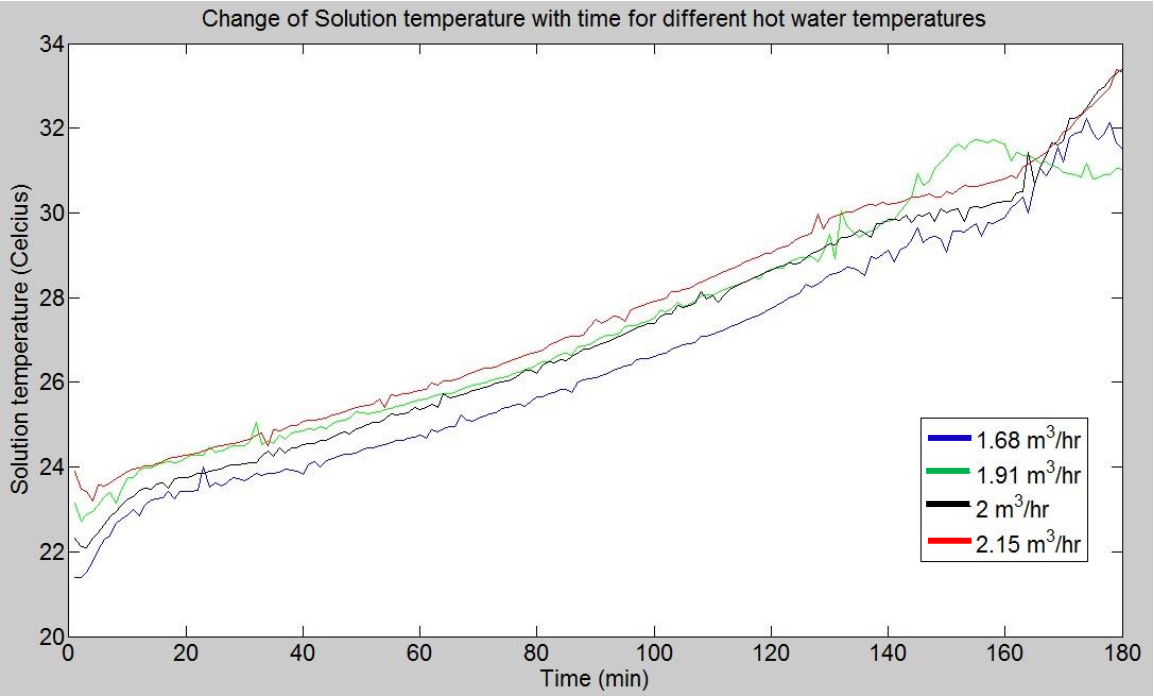

Figure 4-34. Change of solution temperature with time for different solution flow

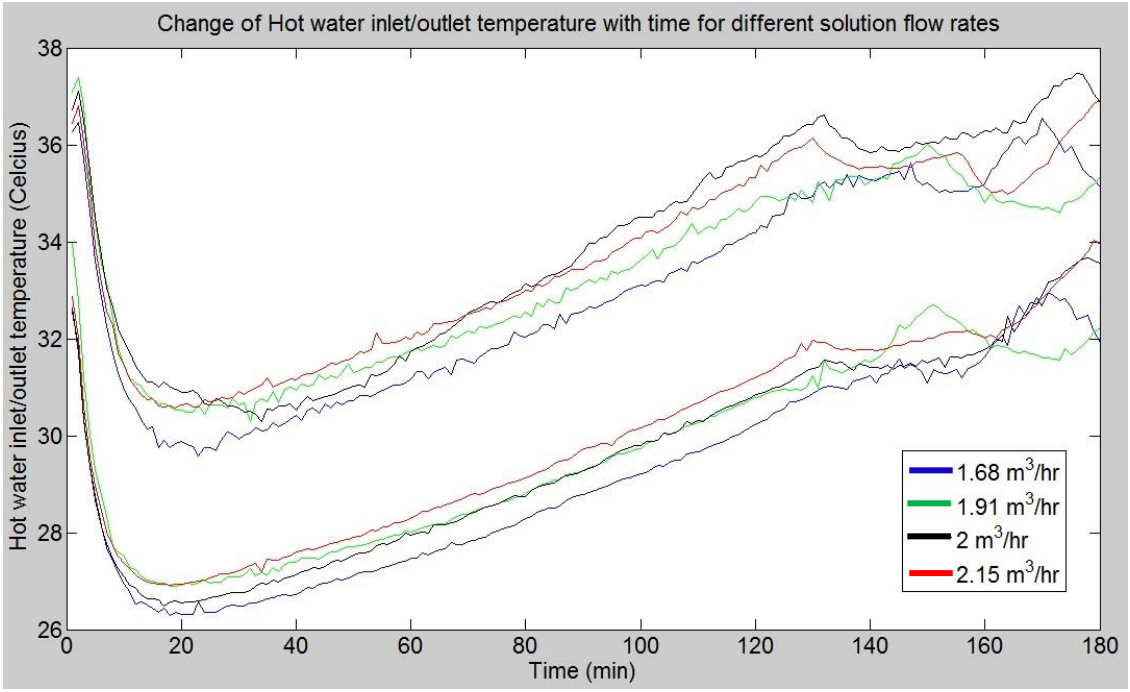

Figure 4-35. Change of hot water inlet-outlet temperature with time different solution flow

Hot water inlet and outlet temperature variation is shown in Figure 4-35. It can be seen that there was a slight difference in the variation of hot water inlet temperatures and outlet temperatures due to solution flow rate change. But initially, within 20 minutes, when the solution flow rate is 1.68m^3/hr, hot water inlet temperature drops around 7 degrees and when the solution flow rates are 1.91m^3/hr, 2 m^3/hr and 2.15m^3/hr hot water inlet temperature drops around 5.5 degrees. Later on the process hot water inlet temperature gradually increased to the temperature which was maintained. It is clear that the initial stage of the process, hot water provides higher amount of heat to the solution, therefore temperature reduces.

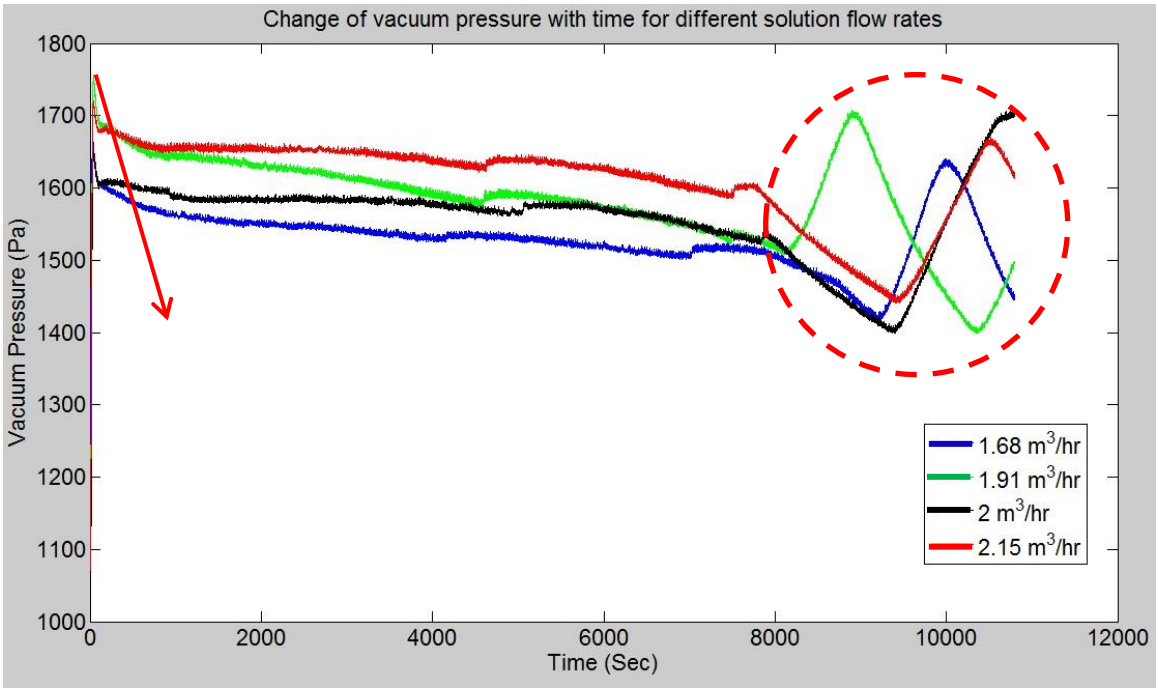

Figure 4-36. Change of vacuum pressure with time

Figure 4-36 shows the change of vacuum pressure with time for different solution flow rates. It is clear that when the solution flow rate was 2.15m^3/hr, vacuum pressure was high

and it remains above 1600 Pa for about 2 hours. When the solution flow rate is highest, it causes the generation of more water vapor at the very initial stage of the test. There is a huge variation of the vacuum pressure at the end of the testing, as shown by circling, which continuous to 45 minutes time duration. The desorption amount is directly proportional to the water vapor pressure difference between the solution and vacuum space $S \propto (P_{w,S} - P_{w,V})$. Therefore, when the vacuum pressure is high mass transfer driving force reduces. It was found that it's better to maintain a solution flow rate which causes the desorption rate equal to condensation rate, to maintain the inside pressure in a lower value. It's inevitable that the pressure at the first few minutes rise to a higher value. Actions should be taken to bring the pressure down to a lower value, less than 1500 Pa as shown by the arrow in Figure 4-37 to achieve higher desorption rate, thus higher LiBr mass ratio at the end.

Table 4-7. Initial and final LiBr mass fraction for different solution flow rates

Solution flow rate	1.68 m^3/hr	1.91 m^3/hr	2 m^3/hr	2.15 m^3/hr
Initial LiBr mass ratio	0.3631	0.3654	0.3646	0.3631
Final LiBr mass ratio	0.4327	0.4580	0.4717	0.4571

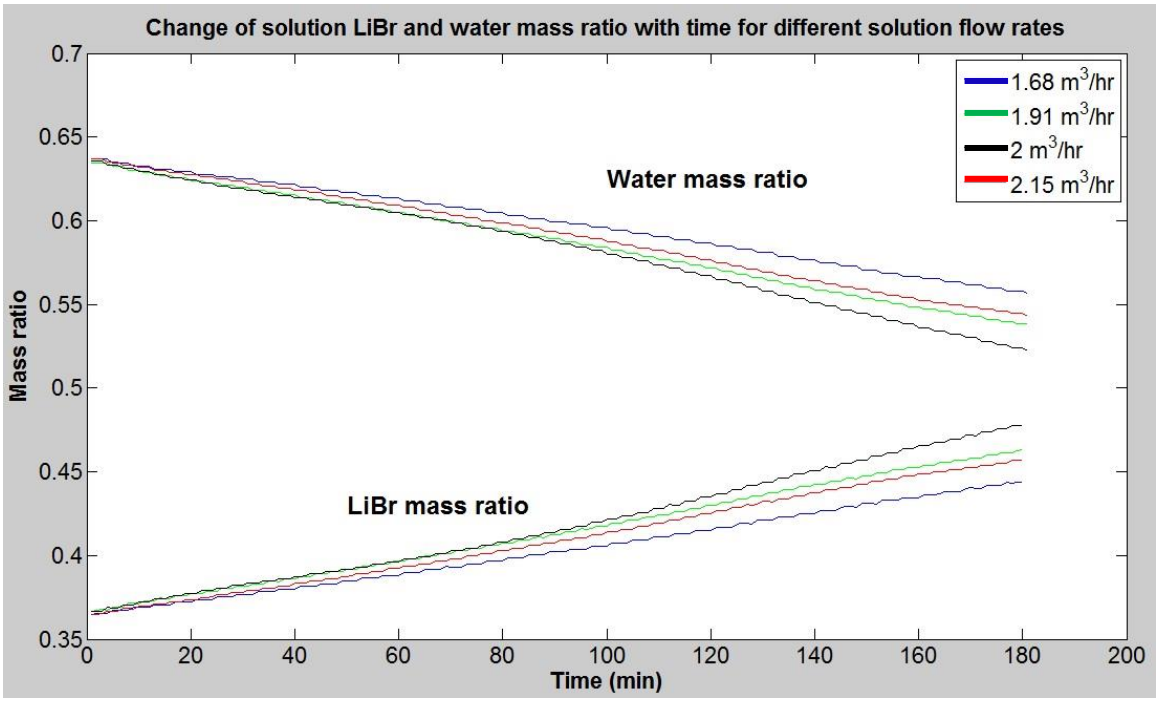

Figure 4-37. Change of LiBr and water mass fraction with time for different solution flow rates

Comparison of the mass transfer effectiveness for different solution flow rates is shown in Figure 4-38. Accordingly, the mass transfer effectiveness for all four flow rates are almost equal while the highest mass transfer effectiveness values belong to the lowest flow rate 1.68m^3/hr.

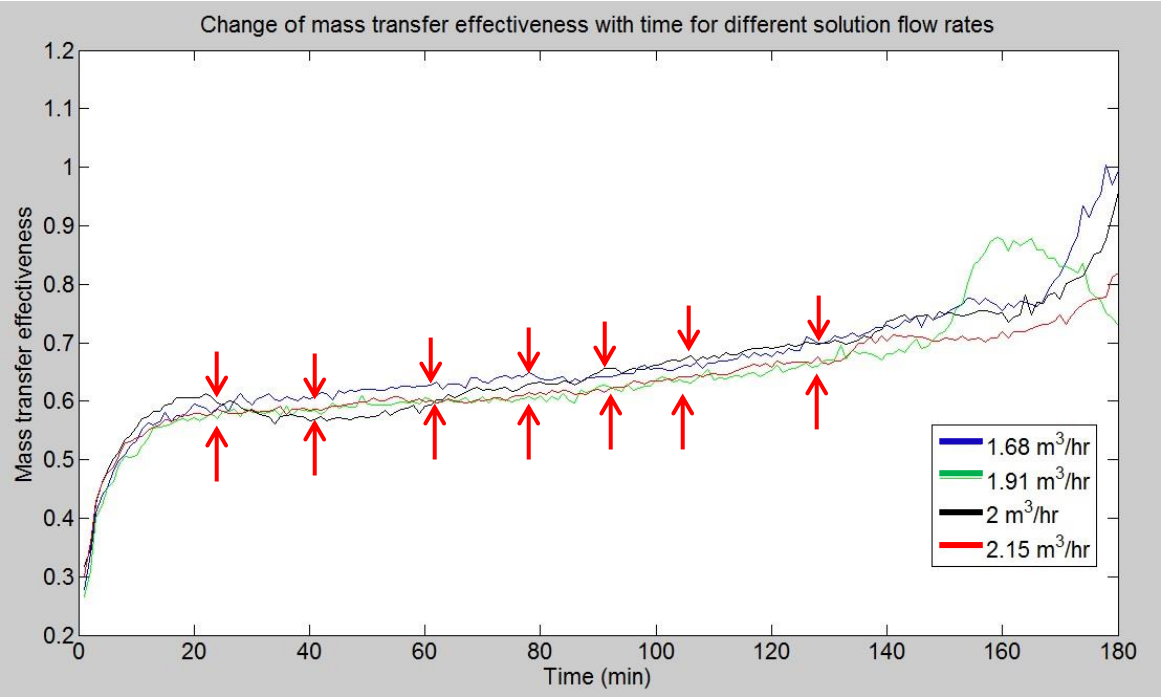

Figure 4-38.Change of mass transfer effectiveness with time for different solution flow rates

Figure 4-39 clearly shows the difference of final LiBr mass fraction of the solution. When the solution flow rate was higher, desorption rate was higher than condensation rate. Thereby, chamber inside pressure was risen and reduced the final LiBr mass fraction. Moderate flow rates created similar desorption and condensation rates and maintained the chamber pressure in a lower value. Therefore, it is clear that instead of using very high solution flow rates, moderate flow rates can achieve higher final LiBr mass fractions.

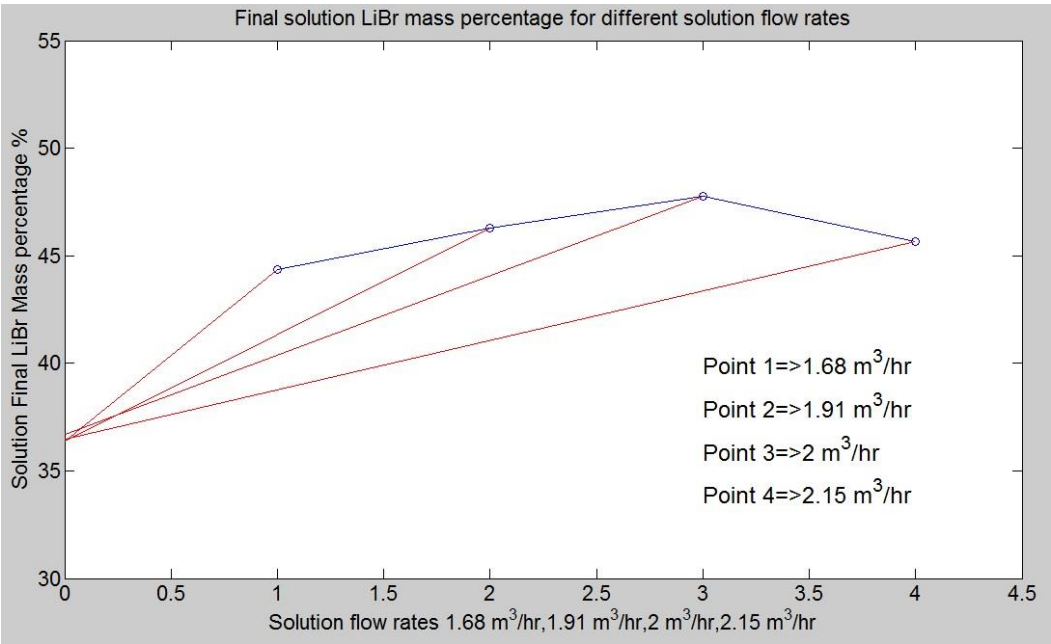

Figure 4-39. Final solution LiBr mass fraction for different solution flow rates

Effect of vacuum pressure to the desorption performance

System initial vacuum pressure was kept as 1500 Pa, 2000 Pa and was checked how the vacuum pressure and other parameters change with time. Figure 4-40 shows how the system vacuum presure behaves with time. The inside vacuum condition is an uncontrollable parameter and as shown in the figure, the initial vacuum pressure of 1500 Pa rises upto 2200 Pa within the first minute and the initial vacuum pressure of 2000 Pa rises upto 2500 Pa. It is clear that a higher initial vacuum condition creates a very high pressure level at the initial stage and reduce the performance of the system. Therfore, better performance can be achieved by initial lower vacuum pressure.

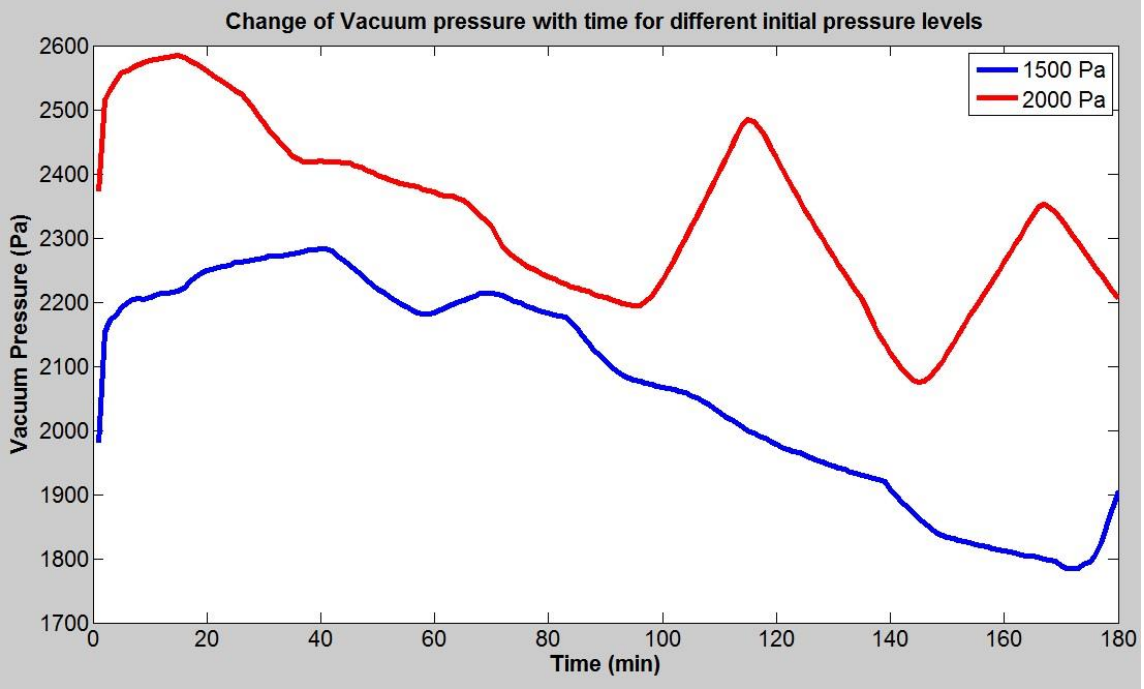

Figure 4-40. Change of vacuum pressure condition for different initial vacuum pressure levels

LiBr mass ratio and water mass ratio change with time is shown in Figure 4-41. It's clear that higher LiBr mass ratio can be achieved when the initial vacuum pressure is low as it provides a lower saturation temperature and a higher mass transfer driving force. Figure 4-42 shows the final LiBr concentration difference between two initial pressure levels, in which the difference is 2.82%. If the system vacuumed further, the result for 500Pa would be of a much higher value, but there are difficulties to face. Reduce the chamber pressure to a very lower value around 500 Pa is a time consuming process and it takes around 12 hours. Also, solution is inside the tank before vacuum starts for the new testing and when the pressure reaches a very low value, the solution automatically vaporizes and fills the gap. Therefore, evaporation slows down the vacuum process and also solution losses due to charge out by the vacuum pump.

Table 4-8. Solution final LiBr mass ratio

Initial Vacuum pressure	1500 Pa	2000 Pa
Final LiBr mass ratio	49.41%	46.32%

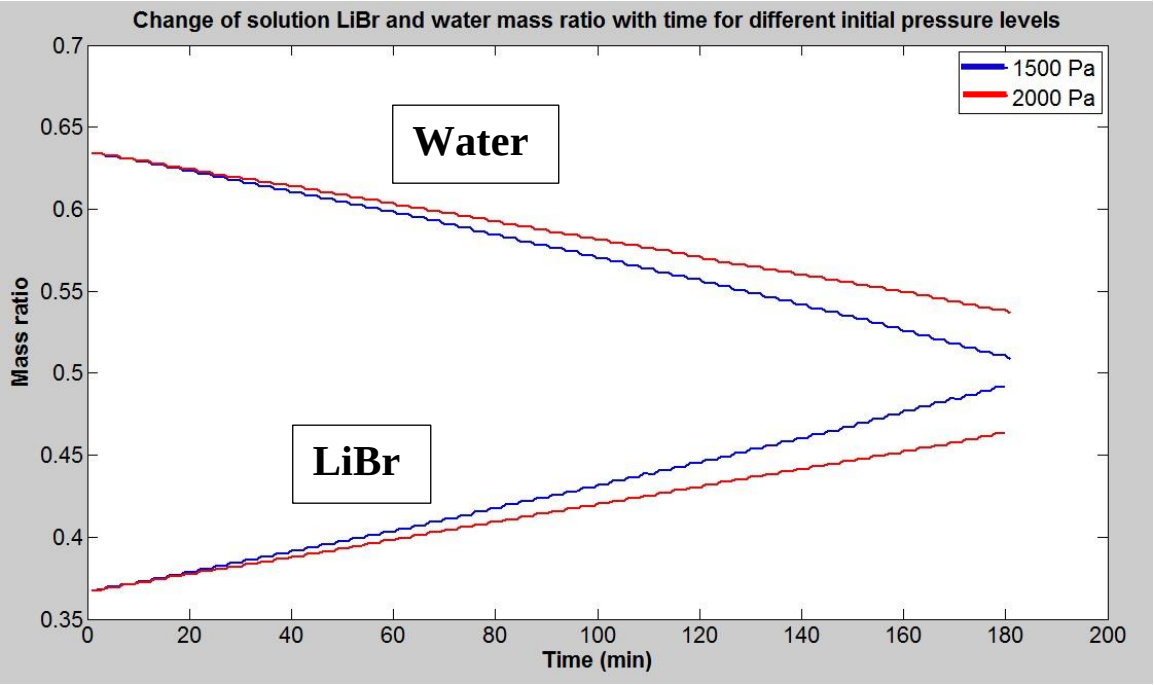

Figure 4-41. Solution LiBr & water mass ration change with time

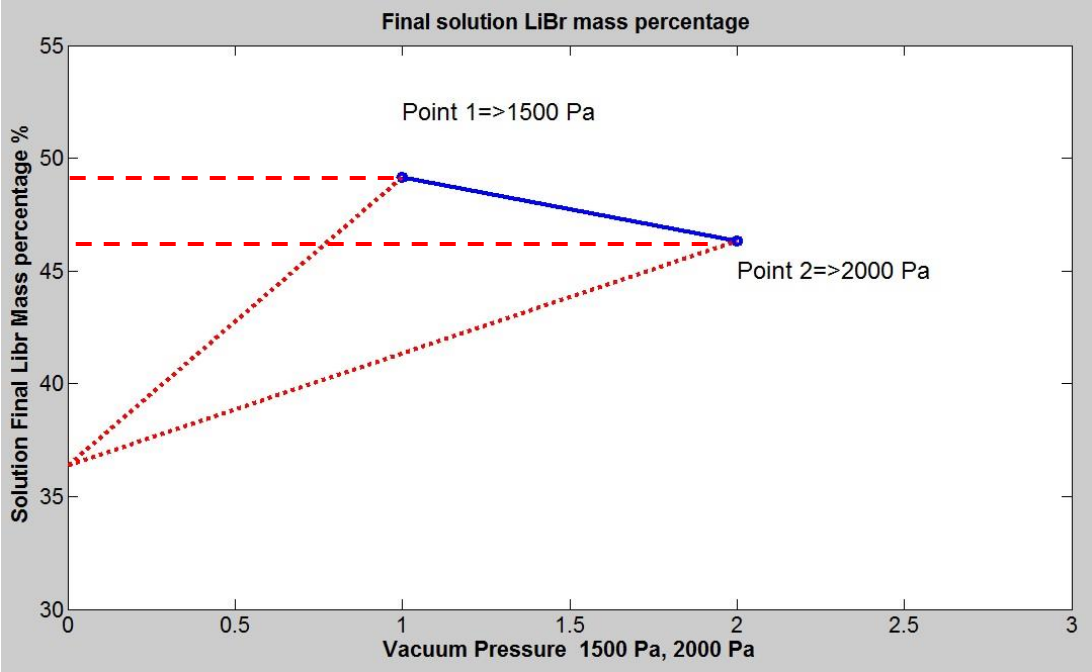

Figure 4-42. Final LiBr mass ratio for two pressure levels

Figure 4-43 shows the change of water desorption rate with time for the two initial pressure levels. There is a considerable difference throughout the time duration between the two desorption rate values around 0.8 g/s. This is mainly due to two factors; the rising of the saturation temperature due to higher vacuum pressure, and the reduction of the mass transfer driving force due to the higher vacuum pressure. Therefore, it's an important parameter needed to be controlled in a very low value for a better performance.

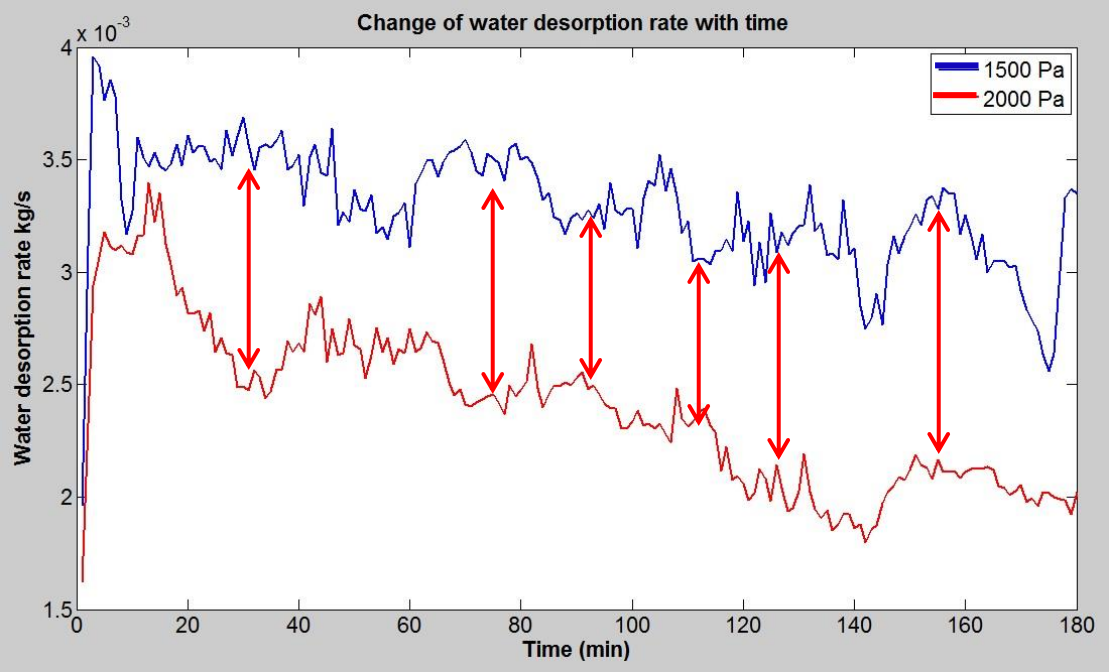

Figure 4-43. Change of water desorption rate with time for different initial pressure levels

Effect of initial concentration on the final mass fraction

Depending on the initial concentration, changes of the desorption rate and final concentration which can be achieved was studied here. Figure 4-44 shows the change of vacuum pressure for four initial LiBr mass fractions 36.54 %, 37.84%, 39.46% and 40.97%. LiBr mass fraction was set at a higher value and the effect of the final result was studied. It was seen that when the LiBr mass fraction is higher, water mass fraction and initial release of water vapor is less. Therefore, initial increase of pressure is low. Lower initial concentration rises to a higher pressure and higher initial concentration stops from a lower pressure. For the initial concentration 39.46% and 40.97% test there is an oscillation of vacuum pressure within 100-150 minutes time interval. This is due to an error, fails to control chilled water temperature for condensation.

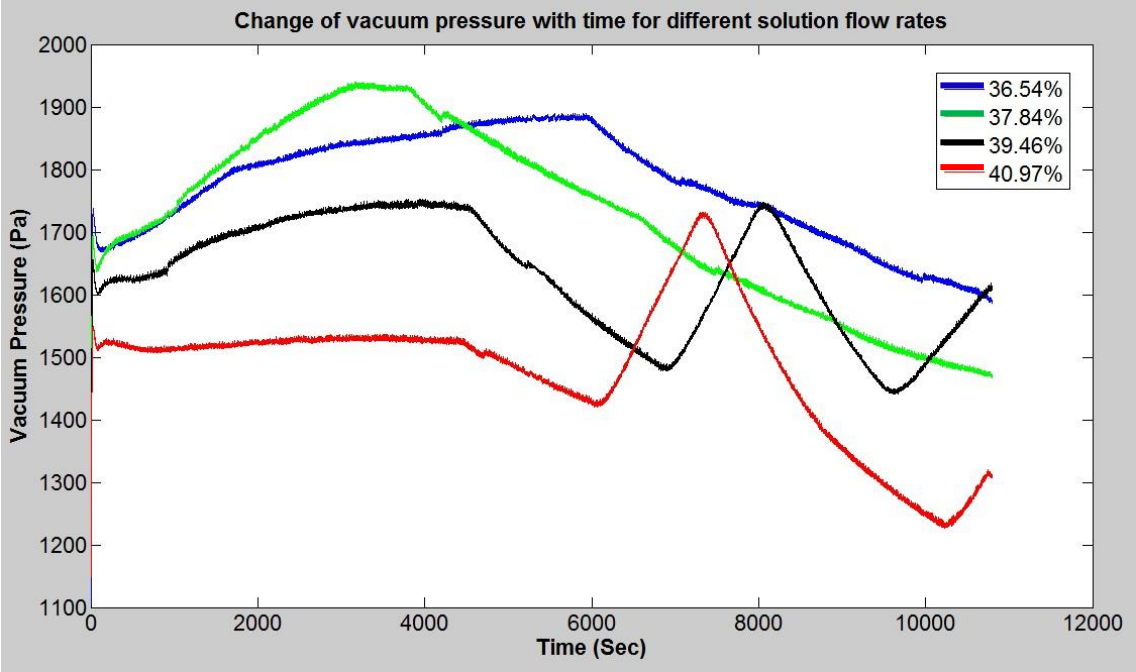

Figure 4-44. Change of vacuum pressure with time for different initial concentrations

Figure 4-44 clearly shows that the vacuum pressure for 40.97% is very low and this leads to a higher desorption rate and higher LiBr mass fraction. Figure 4-45 illustrates the variation of the desorption rate for the four different initial mass fractions. Initially desorption rate increases with the highest desorption rate belonging to the highest LiBr mass ratio test, as it has a low vacuum pressure increment. Other mass desorption ratio values vary between 3-3.75 g/s throughout the test. Figure 4-46 shows the change of LiBr mass fraction values whereas table 4-9 shows the initial and the final LiBr mass percentages. The gradient of the mass fraction curves within first 60 minutes are almost same. Therefore, four lines are almost parallel to each other till 60 minutes and then the gradient increases for 40.97% initial concentration incident than other incidents. It is clear from the table 4-9 that the incident of 36.54% initial mass fraction reaches to 46.66% final mass fraction and 40.97% initial mass fraction reaches to 51.8% final mass fraction. In these four testing, it is

clear that when the LiBr mass fraction is higher, the better the dehumidification performance. The figure 4-47 shows the change of final LiBr mass fraction percentage values and the mass fraction percentage difference. Highest LiBr mass percentage difference was achieved when the initial concentration was 40.97% and lowest when the initial mass fraction percentage was 37.84%. In overall, almost 10% LiBr mass fraction percentage increment was achieved for all four testing.

Table 4-9. Initial, Final and difference of LiBr mass fraction values

Initial LiBr mass fraction	36.54 %	37.84%	39.46%	40.97%
Final LiBr mass fraction	46.66%	47.6%	49.3%	51.8%
The amount change	10.12%	9.76%	9.84%	10.83%

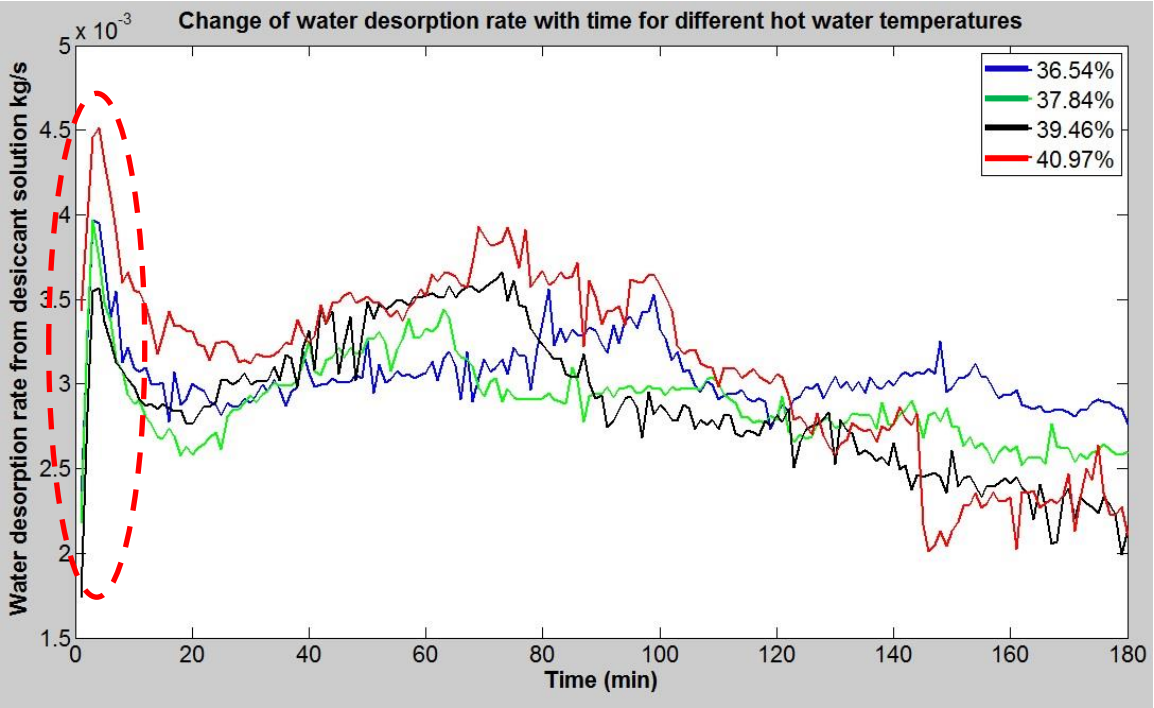

Figure 4-45. Mass desorption rate for different initial concentrations

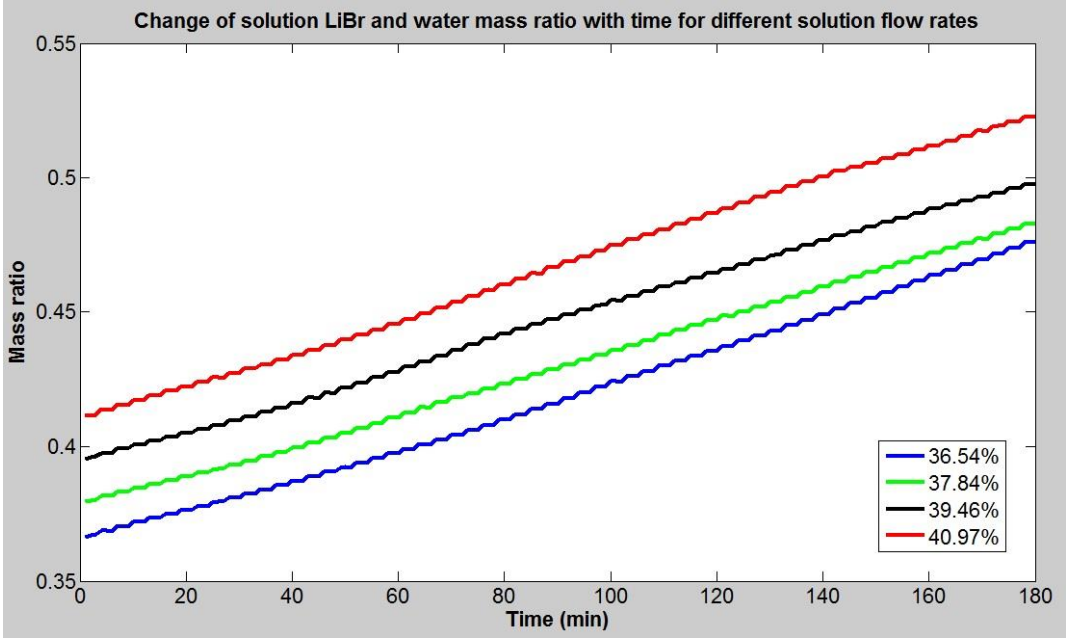

Figure 4-46. Change on LiBr mass ratio with time for different initial LiBr mass concentration

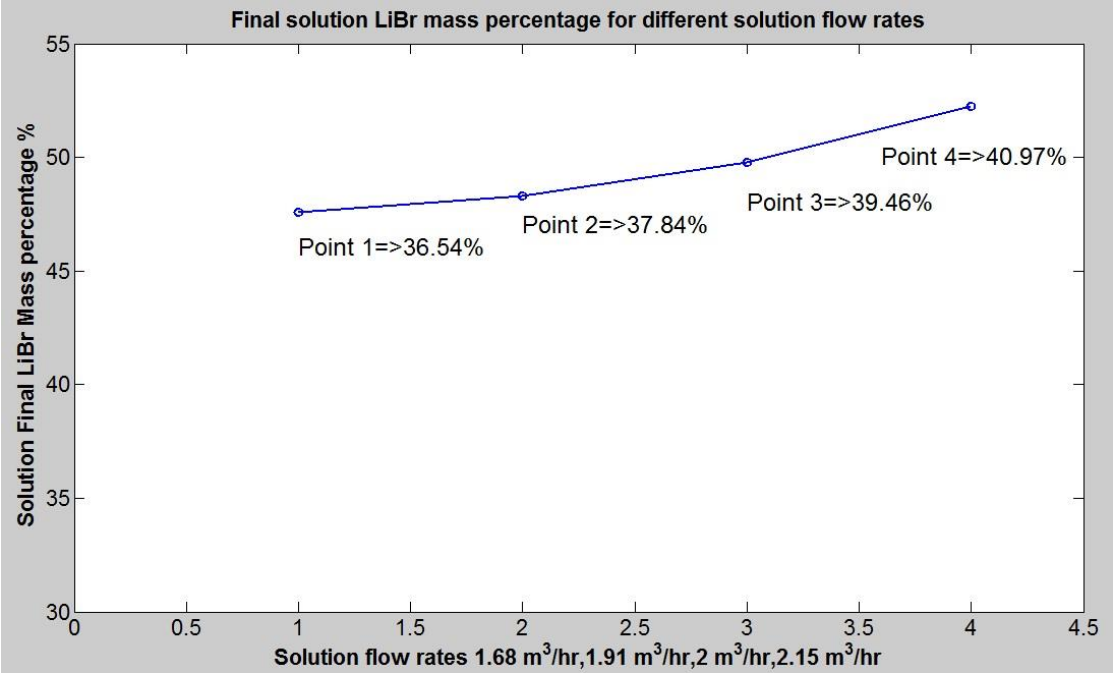

Figure 4-47. Final solution LiBr mass percentage for different initial LiBr mass concentrations

4.5 Summery

This chapter presented a mathematical model for the heat and mass transfer studies for the evaporation process of the evaporator heat exchanger of the vacuumed regenerator system. A numerical analysis was conducted using non-linear least square method to evaluate unknown parameters of the model. Developed heat transfer model and mass transfer model were validated within ± 10% agreement.

Efficiency measurement indices against design and control parameters such as, hot water temperature (T_{hw}), hot water flow rate (m_{hw}), solution flow rate (m_s), solution initial concentration (X_{swi}) and initial vacuum pressure (P_{vacuum}) were presented. Hot water temperature was maintained at 35, 36, 38 and 40 degrees and it was found higher the temperature, the better the performance of desorption process. Also, 10% Concentration increment could be achieved for temperatures higher than 36 ^{0}C. Hot water flow rates were changed as 1.14m^3/hr, 1.28m^3/hr, 1.58m^3/hr and 1.7m^3/hr and observed the system performance. Hot water flow rate had a considerable effect because at maximum flow rate, LiBr concentration was increased by 15%. Efficiency enhancement were studied by keeping the solution flow rates at 1.68 m^3/hr, 1.91 m^3/hr, 2 m^3/hr, 2.15 m^3/hr. It was identified that the highest LiBr mass percentage difference of 10% was achieved when the flow rate was 2m^3/hr.

Solution initial LiBr mass percentages depend on at what point the weak solution send back from the dehumidifier to the regeneration process. Four LiBr mass percentage levels; 36.54 %, 37.84%, 39.46% and 40.97% were studied. Highest LiBr mass percentage difference at the end of the testing for all four instances was 10.83%, which was achieved when the initial LiBr mass percentage was 40.97%. Since starting LiBr mass percentage was different in four instances, highest final LiBr mass percentage of 51.8% was achieved for LiBr mass percentage of 40.97%.

Initial vacuum pressure had a considerable influence on the system performance. Initial pressure of 1500 Pa, 2000 Pa were taken into account and more than 13% concentration increment was achieved for 1500 Pa and 10% was achieved for 2000 Pa. Proposed model successfully predicted the performance of the system within am acceptable error band. Higher performance of the evaporation process can be achieved by maintaining the system operating settings at higher hot water temperature, higher hot water flow rate, lower vacuum pressure, lower LiBr concentration. In comparison to other systems, this vacuumed regeneration system can achieve more than a 10% concentration increment within a short time period, such as 3 hours with a low hot water temperature source.

Chapter 5 Heat and Mass Transfer of Condenser

This chapter presents a development of a mathematical model to study the heat and mass transfer of condenser heat exchanger of the system. Developed model is validated by using experimental data. The effect of system controlling parameters to the condenser performance is discussed.

5.1 Condenser general model

Chilled water flow direction through the condenser is indicated by $\dot{m}_{cw}$ in Figure 5-1. Due to the lower temperature of the chilled water, water vapor which is in the chamber releases its heat and condenses on the heat exchanger tube surface, thereby drops down and gathers to the bottom of the chamber.

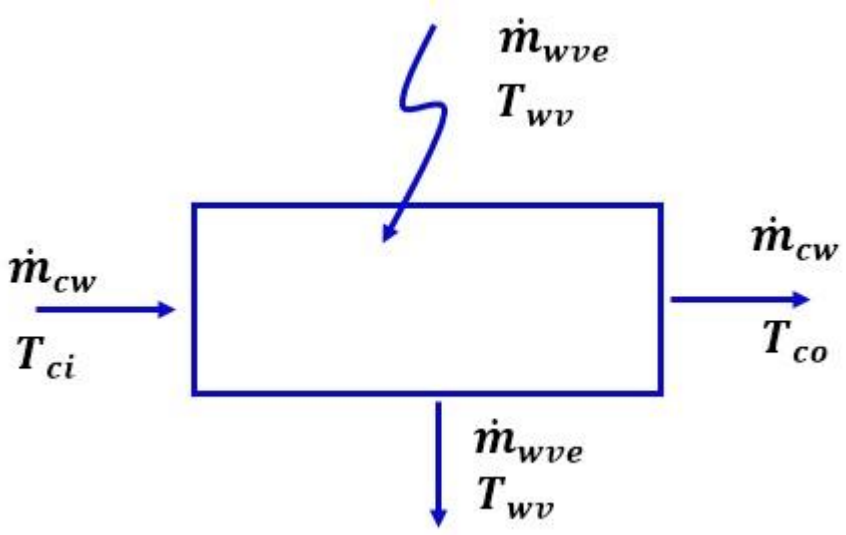

Figure 5-1. Input and output condition of the chilled water and water vapor to the condenser

Chilled water which enters the condenser absorbs heat from the water vapor and increases its temperature. The amount of heat absorbed can be calculated as below:

$$Q_c = \dot{m}_{cw} C_{pcw} (T_{co} - T_{ci}) \quad -(5.1)$$

The above heat is released by the water vapor and this water condenses on the external surface of the heat exchanger. Therefore the following equation can be written for the sensible load and latent load that is released.

$$\dot{Q}_{Tot} = \dot{Q}_{s1} + \dot{Q}_L + \dot{Q}_{s2}$$

$$\dot{Q}_{Tot} = m_{wvc}(T_{wv} - T_{sat}) + m_{wvc} L_p + m_{wvc}(T_{sat} - T_{mwc})$$

$\dot{Q}_{s1} - Water\ vapor\ sensible\ load\ until\ reduced\ to\ the\ saturation\ temperature$

$\dot{Q}_L - Latent\ load\ of\ condensation$

$\dot{Q}_{s2} - Sensible\ load\ of\ subcooling$

$m_{wvc} - water\ vapor\ condensation\ rate$

$T_{wv} - water\ vapor\ temperature$

$T_{mwc} - subcooled\ temperature$

Assuming that the water vapor does not increase in temperature within the superheat region after the vaporization process that it does not decrease in temperature within the sub-cooled region after the condensation process, then comparing with the latent heat of condensation,

those sensible loads considered negligible. Therefore, the above $\dot{Q}_{Tot}$ Equation can minimize to calculate the amount of condensation by using the absorbed heat.

$$Q_{Tot} = \ m_{wvc}L_p = \ Q_c = \ m_{cw}C_{pcw}(T_{co} - \ T_{ci})$$

$$m_{wvc}L_p = \ m_{cw}C_{pcw}(T_{co} - \ T_{ci}) \qquad -(5.2)$$

Heat transfer model for the vapor condensation process

Following assumptions are made:

- Steady state operation
- The vapor temperature is uniform and is very near to its saturation temperature
- There isn't any other external force except gravity acting on the fluid film
- The sensible cooling of the fluid is negligible compared to the latent heat
- Heat exchanger is well insulated and only heat transfer takes place between water vapor and chilled water
- Changes in kinetic and potential energy of fluid streams are negligible
- There is no fouling
- Temperature variation is negligible and fluid properties are remained as constants

The schematic of the condenser is given in figure 5-1. Condenser can be treated as a counter-flow type heat exchanger since the temperature of one of the fluids (water vapor) remains constant due to the condensation.

Temperature difference between the steam and chilled water at the two ends of the condenser can be written down as below:

$$\Delta T_1 = T_{wv} - T_{ci}$$

$$\Delta T_2 = T_{wv} - T_{co}$$

ΔT_1 is the temperature difference between the chilled water and water vapor at the inlet and ΔT_2 is the temperature difference between the water vapor and chilled water at the outlet.

When studying the performance of the heat exchanger Log Mean Temperature Difference LMTD method can be used. LMTD method uses Log Mean temperature difference of the two fluids flow through the heat exchanger to calculate the heat transfer amount. Log mean temperature difference value can be calculated as:

$$\Delta T_{lm} = \frac{\Delta T_1 - \Delta T_2}{ln\left(\frac{\Delta T_1}{\Delta T_2}\right)}$$

$$\Delta T_{lm} = \frac{(T_{wv} - T_{ci}) - (T_{wv} - T_{co})}{ln\left(\frac{T_{wv} - T_{ci}}{T_{wv} - T_{co}}\right)}$$

$\Delta T_{lm} - Log\ Mean\ Temperature\ difference$

Heat transfer can be written as:

$$\dot{Q}_c = U\ A_c\ \Delta T_{lm}$$

$$\dot{Q}_c = U\ A_c \frac{(T_{wv} - T_{ci}) - (T_{wv} - T_{co})}{ln\left(\frac{T_{wv} - T_{ci}}{T_{wv} - T_{co}}\right)} \quad - (5.3)$$

$\dot{Q}_c - Heat\ transfer\ rate\ of\ the\ condensation\ process$

Heat transfer from outside to the inside chilled water can be modeled using the same theories for modeling the evaporator heat exchanger.

Heat transfer equation can be written as:

$$\dot{q}_c = \frac{T_A - T_B}{\frac{1}{h_1 A} + \frac{\Delta x}{kA} + \frac{1}{h_2 A}}$$

By using the overall heat transfer coefficient, the equation can be written as:

$$\dot{q}_c = U\ A\ \Delta T$$

By having the same type of heat exchanger, overall heat transfer coefficient can be written down with same assumptions which was used for evaporator heat exchanger,

- Heat exchanger was made of a higher heat conductive material
- Heat exchanger wall thickness is very small
- Heat resistance through the tubes can be neglected as $\frac{\Delta x}{kA}$ term has a negligible resistance

$$\frac{1}{U_c} = \frac{1}{h_i} + \frac{1}{h_o}$$

$h_i - Tube\ inside\ convective\ heat\ transfer\ coefficient$

$h_o - Tube\ outside\ convective\ heat\ transfer\ coefficient$

Chilled water flows through tubes using a pump, therefore the flow inside can be considered as force convection, outside water vapor touches tubes external surface due to natural force and therefore, the outside can be considered as free convection.

5.2 Tube internal convective heat transfer model

Heat transfer between the interface and the surface wall depends on the following factors:

- Fluid properties (fluid density , fluid viscosity, fluid specific heat capacity)
- Interface geometry (in this case internal cylindrical tube and external cylindrical tube)
- Fluid velocity
- Thermal conductivity of surface wall

Chilled water flows through the pipe with a higher flow rate, higher than 0.5m^3/hr and the tube diameter is 0.01 m with a viscosity around 1.39 x 10^{-3} Ns/m^2. For the above values the Re is higher than 10000 and the flow is turbulent with the smooth surface of the tube. Turbulent flow is more advantageous to have a higher heat transfer coefficient. Therefore, the following study was carried on the turbulent internal flow of tubes.

Study for the internal chilled water flow is same as for the evaporator heat exchanger, therefore, the Nusselt number for the internal flow can be written as below.

$$Nu = C_c Re^q Pr^r f^s$$

The values for C_c, q, r, s are needed to be determined for the application where, C_c depends on the geometry and the flow when q, r and s are constants. Re number and Pr number can be written as below.

$$Re = \frac{Inertial\ force}{Viscous\ force} = \frac{\rho_c\ v\ D_c}{\mu_c}$$

$$\Pr = \frac{molecular\ diffusivity\ of\ momentum}{molecular\ diffusivity\ of\ heat} = \frac{\mu_c C_{pw}}{k_c}$$

Explicit first Patukhov equation with a simple modification was used to calculate the friction factor of turbulent flow in smooth tubes [39].

$$f = 0.184\, Re^{-2}$$

Nu number was modified with *f* as below.

$$Nu = C_c \left(\frac{\rho_c\ v\ D_c}{\mu_c}\right)^{q-2s} \left(\frac{\mu_c C_{pw}}{k}\right)^{r} (0.184)^{s}$$

Assumptions for the calculation:

- Steady flow
- Water density is constant throughout the process since there is a small change in temperature
- Water viscosity is constant throughout the process since there is a small change in temperature
- Heat exchanger material properties like heat conductivity remain unchanged

Heat transfer Nu number can be written as below by definition:

$$Nu = \frac{h_c D_c}{k_c}$$

$$h_{ci} = \frac{k_c}{D_c} C_c \left(\frac{\rho_c\ v\ D_c}{\mu_c}\right)^{q-2s} \left(\frac{\mu_c C_{pw}}{k_c}\right)^{r} (0.184)^{s}$$

If mass flow rate through the tube is $\dot{m}_{cw}$, it can be substituted in the equation as below

$$\dot{m}_{cw} = \rho_c\ v\ A_c$$

$$h_{ci} = \frac{k_c}{D_c} C_c \left(\frac{4\ \dot{m}_{cw}}{\mu_c\ \pi\ D_c}\right)^{q-2s} \left(\frac{\mu\ C_{pw}}{k_c}\right)^{r} (0.184)^{s} \qquad -(5.4)$$

5.3 Tube External Condensation model

The study carried out to calculate the external water vapor condensation convective heat transfer coefficient is slightly different from the previous study. This process is considered as a free convection condensation on external surface.

Mass transfer from water vapor phase to the liquid phase occurs in this condensation process. Inside the vacuum chamber water vapor as well as a cold source (chilled water condenser) are available. Water vapor moves towards the condenser due to the pressure difference since the water vapor closer to the condenser condenses by releasing latent load. This condensed water vapor accumulates as a liquid layer on the tube wall. Condensation is not high enough to form a sheet, therefore, it drops down in the form of drops. Theoretical approach to film condensation is involved with conservation of mass and momentum. Figure 5-2 shows the formation of the liquid film and the parameters considered for the study [46].

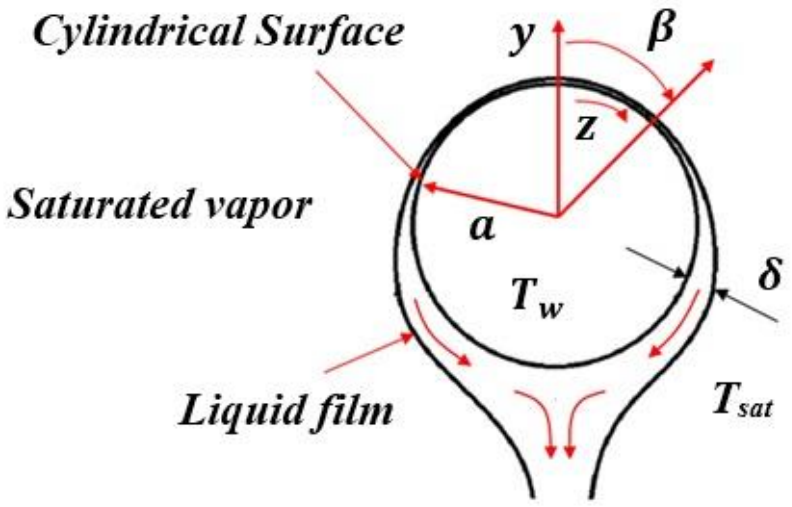

Figure 5-2. Condensed water flow around a single tube and measured parameters

Following assumptions are made for the analysis [22].

- Constant fluid properties due to small temperature change
- Fluid is laminar throughout the falling
- Heat transfer from vapor to liquid is only due to condensation
- $\frac{\partial u}{\partial y} = 0 \; at \; y = \delta$, shear stress at the interface is negligible
- Film is very thin, therefore, heat transfer occurs only due to conduction

By considering the energy balance for one dimensional heat conduction across the liquid film with thickness δ, the following equation can be written for the latent heat.

$$h_{fg} \frac{d\Gamma}{dz} = \frac{k_L\left(T_{sat}\left(P_g\right) - T_w\right)}{\delta}$$

$h_{fg} - \; latent \; heat$

$\Gamma - water \; condensed \; amount$

$\delta - liquid \; film \; thickness$

$k_L - \; water \; thermal \; conductivity$

$T_{sat}\left(P_g\right) - \; saturation \; temperature \; of \; water \; at \; Pg$

$T_w - \; tube \; wall \; temperature$

The amount of $(g \; sin\beta)$ gravitation is applied around the circumference of the tube and by using the momentum balance and by integrating with the vertical boundary condition u=0 at y=0, following equation can be written.

$$u_y = \frac{(\rho_{wl} - \rho_{wv})\, g \sin\beta}{\mu_L}\left[y\delta - \frac{y^2}{2}\right]$$

$\mu_L - water\ liquid\ viscosity$

$\rho_{wl}\,, \rho_{wv} - water\ liquid\ and\ gas\ density$

$g - gravitational\ acceleration$

Velocity profile integrates from the tube wall to the film surface. The relationship between the angle β and the circumferential length from top z can be given as below.

$\beta = \frac{z}{r} \quad r - the\ radius$

The amount of condensate mass flow rate per unit length of the tube (Γ) can be calculated as below.

$$\Gamma^{1/3}\, d\tau = \frac{r k_L (T_{sat} - T_w)}{h_{fg}}\left[\frac{(\rho_{wl} - \rho_{wv})g}{3v_L}\right]^{1/3} sin^{1/3}\beta\, d\beta$$

$h_{fg} - Latent\ heat\ of\ condensation$

$v_L - Fluid\ flow\ velocity$

By integrating along the top of the tube, where $\Gamma = 0\ at\ \beta = 0$ to the bottom of the tube, where $\Gamma = \Gamma\ at\ \beta = \pi$, the total amount of condensation for half of the tube can be calculated with the equation as given below.

$$\Gamma = 1.924\left[\frac{r^3 k_L^3 (T_{sat} - T_w)^3 (\rho_{wl} - \rho_{wv})\, g}{h_{fg}^3 v_L}\right]^{\frac{1}{4}} \quad -(5.5)$$

Energy balance along the circumference of the tube gives the mean heat transfer coefficient for the tube.

$$2\ h_{fg}\Gamma = 2\pi r h_{tube}(T_{sat} - T_w)$$

$$h_{tube} - Tube\ mean\ heat\ transfer\ coefficient$$

The average heat transfer coefficient for film condensation on the outer surface of a horizontal tube can be given by the following equation studied by Nusselt.

$$h_{tube} = 0.729\left[\frac{g\ \rho_{wl}(\rho_{wl} - \rho_{wv})h_{fg}k^3}{\mu_{wl}(T_{sat} - T_w)\ D}\right]^{\frac{1}{4}}$$

$$D - outside\ diameter\ of\ one\ tube$$

When horizontal tubes are stacked on top of each other as shown in the following figure 5-3 the average thickness of the water film at the lower tubes are much greater than the ones above. Water vapor which condenses on the top tubes, flow to the bottom tubes and thickens the liquid layer.

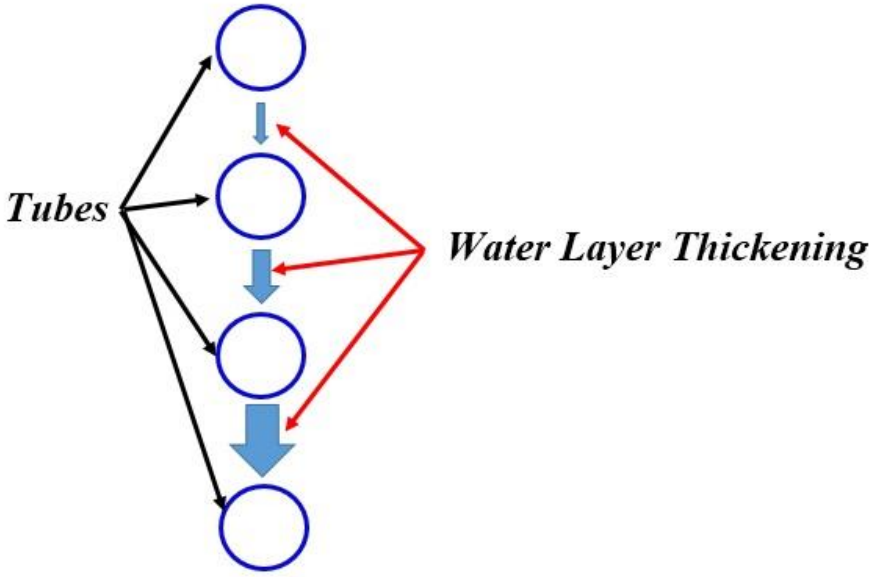

Figure 5-3. Condensed water flows from top tube to the bottom tube and the flow amount increases at the bottom

Therefore, average heat transfer area of the lower tubes reduces due to being covered by water. Assumptions for the analysis are as below [47].

- Zero shear stress at the liquid vapor interface
- In the integral equation analysis is done with stagnant vapor
- The condensing liquid always flows from the top tube tot the next tube below it and so on.

Therefore the following equation can be used to calculate the average heat transfer coefficient for the tube bank.

$$h_{wvo} = 0.729 \left[\frac{g\ \rho_{wl}(\rho_{wl} - \rho_{wv}) h_{fg} k^3}{\mu_{wl}(T_{sat} - T_w)\ ND} \right]^{\frac{1}{4}}$$

Where,

$N - number\ of\ rows\ of\ tubes$

$D - Outside\ diameter\ of\ one\ tube$

The condensing rate of the horizontal tubes reduces from upper half of the tube to the lower half by 46 percent.

There is a possibility that the condensed liquid film can cause some sort of additional condensation. Therefore, the following equation for the heat transfer coefficient can be used to calculate the total effect [47].

$$h_{wvo}^{1} = 0.729\left[1 + 0.2\ \frac{C_{pw}\,(T_{sat} - T_w)}{h_{fg}}(N-1)\right]\left[\frac{g\ \rho_{wl}(\rho_{wl} - \rho_{wv})h_{fg}k^3}{\mu_{wl}(T_{sat} - T_w)\ ND}\right]^{\frac{1}{4}} \quad -(5.6)$$

Applying a fine-tuning constant to the equation,

$$h_{wvo}^{1} = 0.729K_2\left[1 + 0.2\ \frac{C_{w\,(T_{sat} - T_w)}}{h_{fg}}(N-1)\right]\left[\frac{g\ \rho_{wl}(\rho_{wl} - \rho_{wv})h_{fg}k^3}{\mu_{wl}(T_{sat} - T_w)\ ND}\right]^{\frac{1}{4}} \quad -(5.7)$$

By substituting the h_{ci} and h_{wvo}^{1} into overall heat transfer coefficient equation,

$$\frac{1}{U_c} = \frac{1}{h_i} + \frac{1}{h_o}$$

$$\frac{1}{U_c} = \frac{1}{\left\{\frac{k_c}{D_c} C_c \left(\frac{4\,\dot{m}_{cw}}{\mu_c\,\pi\,D_c}\right)^{q-2s} \left(\frac{\mu\,C_{pw}}{k_c}\right)^{r} (0.184)^{s}\right\}} + \frac{1}{\left\{0.729K_2\left[1 + 0.2\,\frac{C_w\,(T_{sat} - T_w)}{h_{fg}}(N-1)\right]\left[\frac{g\,\rho_{wl}(\rho_{wl} - \rho_{wv})h_{fg}k^3}{\mu_{wl}(T_{sat} - T_w)\,ND}\right]^{\frac{1}{4}}\right\}}$$

By using the overall heat transfer coefficient heat released equation can be written as below.

$$\dot{Q}_c = A_c\left[\frac{1}{\left\{\frac{k_c}{D_c} C_c \left(\frac{4\,\dot{m}_{cw}}{\mu_c\,\pi\,D_c}\right)^{q-2s} \left(\frac{\mu\,C_{pw}}{k_c}\right)^{r} (0.184)^{s}\right\}} + \frac{1}{\left\{0.729K_2\left[1 + 0.2\,\frac{C_w\,(T_{sat} - T_w)}{h_{fg}}(N-1)\right]\left[\frac{g\,\rho_{wl}(\rho_{wl} - \rho_{wv})h_{fg}k^3}{\mu_{wl}(T_{sat} - T_w)\,ND}\right]^{\frac{1}{4}}\right\}}\right]^{-1}$$

$$\left[\frac{(T_{wv} - T_{ci}) - (T_{wv} - T_{co})}{ln\left(\frac{T_{wv} - T_{ci}}{T_{wv} - T_{co}}\right)}\right] \qquad -(5.8)$$

The summation of condensation flow from the above tubes on to the top of the N[th] tube. Applying energy balance to the entire surface area of the arrays of tubes yields,

$$2\,h_{fg}[\Gamma_{bottom}(N)] = 2\pi r h_{tube}\,N(T_{sat} - T_w)$$

$\Gamma_{bottom}(N) - Total\ condensed\ water\ flow\ from\ the\ bottom\ tube$

$h_{LG} - mean\ condensation\ heat\ transfer\ coefficient\ for\ all\ tubes$

Flow rate of condensed water draining from one side of the Nth tube is

$$\Gamma(\mathrm{N}) = \frac{N\pi D h_{tube}(T_{sat} - T_w)}{h_{fg}} \qquad -(5.9)$$

5.4 Results and Discussion

Coefficients of general model for the heat and mass transfer study of the condenser heat exchanger was calculated and the model was validated within an acceptable confidence interval. The values of heat and mass transfer from the theoretical model tallied with the experimental values with minimum relative error. Nonlinear least square method was used with initial guesses to identify unknown parameter values using acquired experimental data.

Nonlinear least square model result

Same test results used in chapter 4, (the least square method calculation to find out evaporator model parameters), was used here for the constants calculation purpose. Constants for the condenser heat transfer model were solved by using the non-linear least square method. Experimental heat transfer amount by the chilled water was calculated from the enthalpy difference of the chilled water. Following simplified equation for the heat transfer rate was used to calculate the theoretical heat transfer for condensation.

$$\dot{Q}_c = \boldsymbol{x_{10}} A_c \left[\frac{\boldsymbol{x_6}}{\{(\dot{m}_{cw})^{x_7}\}} + \frac{\boldsymbol{x_8}}{\left\{0.729\left[1 + 0.2\,\frac{C_w\,(T_{sat} - T_w)}{h_{fg}}(N-1)\right]\left[\frac{g\,\rho_{wl}(\rho_{wl} - \rho_{wv})h_{fg}k^3}{\mu_{wl}(T_{sat} - T_w)\,ND}\right]^{\boldsymbol{x_9}}\right\}} \right]^{-1} [(T_{sat} - T_w)] - (5.10)$$

By using the initial approximations as [100, 0.2, 100, 0.15, 56000], constant parameters of the equation (5.10), $x_6, x_7, x_8, x_9 \; and \; x_{10}$, final values were calculated using the non-linear least square method.

$x_6 = 100$

$x_7 = 0.3$

$x_8 = 100$

$x_9 = 0.1$

$x_9 = 56000$

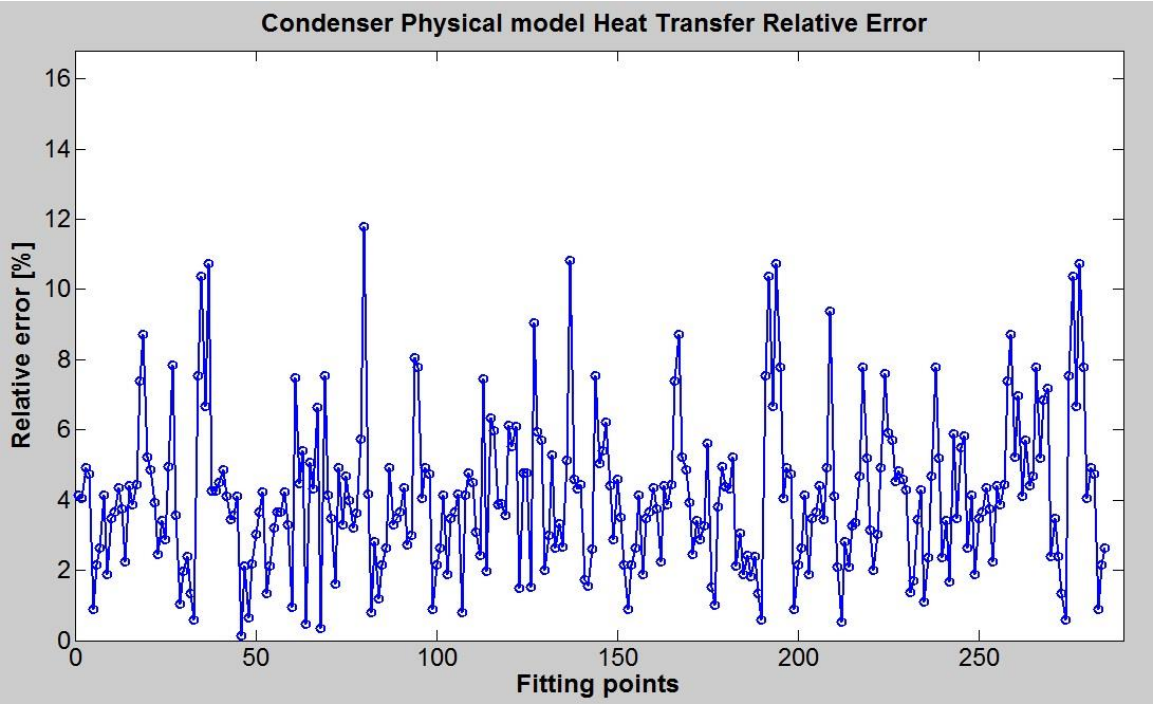

Figure 5-4. Condenser heat transfer relative error of theoretical result and experimental results

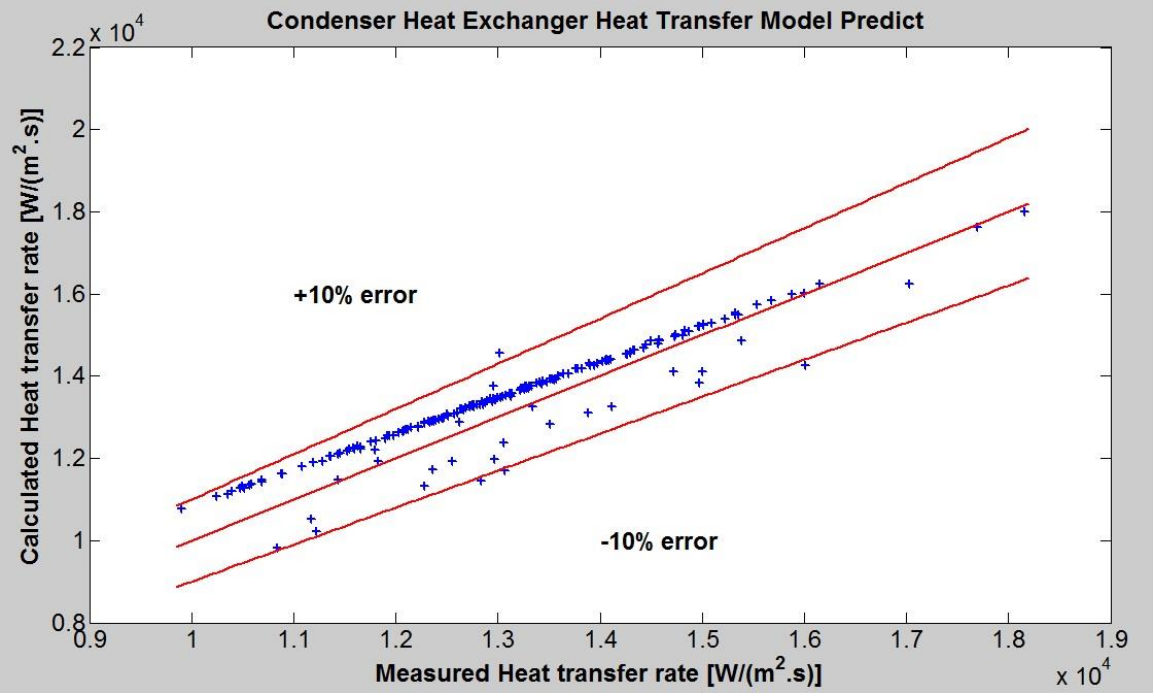

Figure 5-5. Comparison between Condenser experimental heat transfer rate and calculated heat transfer rate

Figure 5-5 shows the comparison between the experimental heat transfer rate and theoretical heat transfer calculation results for the water vapor condensation process. It can be seen that the theoretical calculation values are in ±10% good agreement with the experimental results. Figure 5-4 shows the RE of selected tests where, 97.22% out of 288 values are within the RE of ± 10% and RMSRE is 0.046.

Next, mass condensation rate of the condenser heat exchanger was theoretically calculated using the following equation, where h_{tube} is the mean convective heat transfer coefficient calculated in the heat transfer study.

$$\Gamma(\mathrm{N}) = \frac{N\pi D h_{tube}(T_{sat} - T_w)}{h_{fg}}$$

Comparison between the theoretical condensation rates and the actual condensation rates are shown in Figure 5-7. Relative error between the theoretical and experimental condensation rates are shown in Figure 5-6 and they are within ±10% good agreement. The experimental results show that the proposed model has a very good agreement with the experimental testing having RE < ± 10%. By using the developed model, parametric analysis is carried out as discussed in the next section.

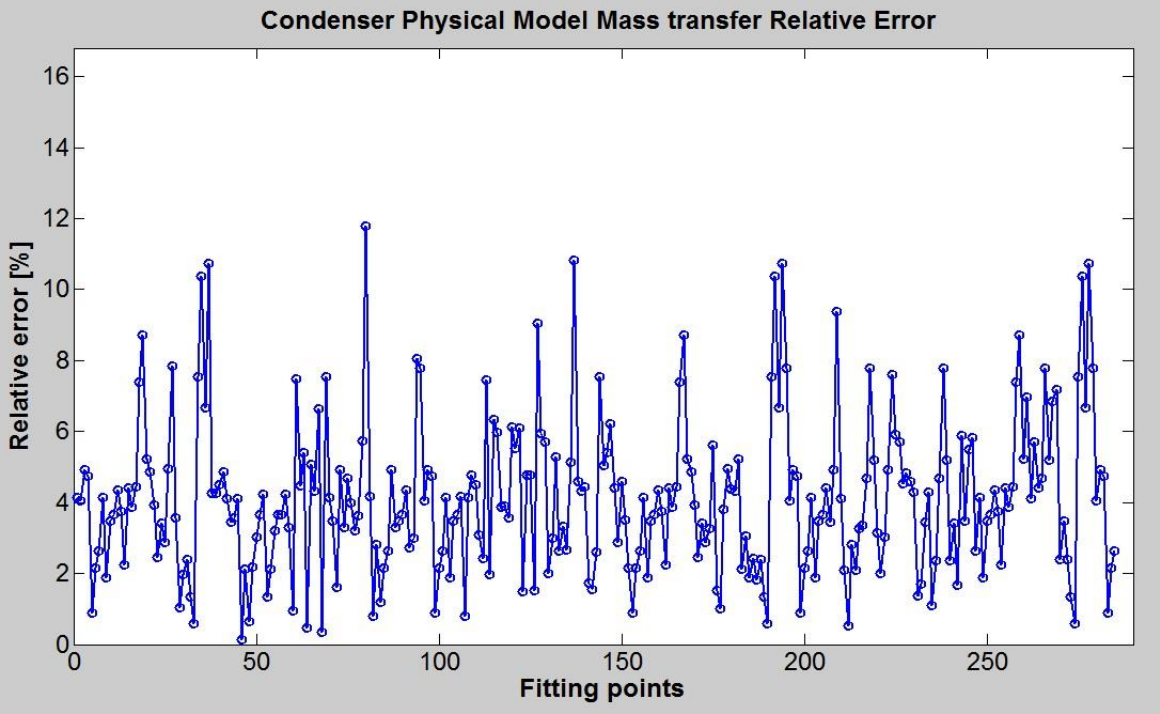

Figure 5-6. Condenser mass transfer relative error of theoretical result and experimental results

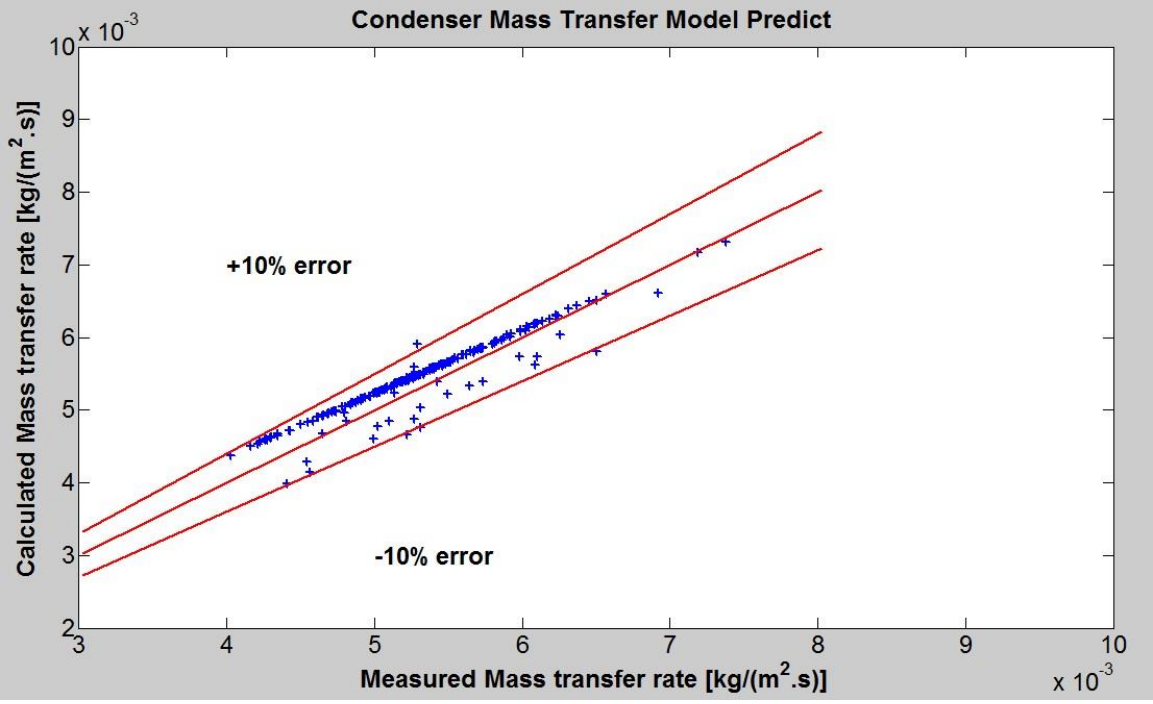

Figure 5-7. Comparison between Condenser experimental mass transfer rate and calculated mass transfer rate

Parametric Analysis

Effect of the chilled water temperature on the condensation process

Chilled water was used as the cooling source of the regenerator which has a considerable impact on the system performance. Therefore, chilled water condition was studied for the condensation performance. Temperature was varied from 7^0C, 8^0C, 9^0C, 10^0C and the system performance was checked. Figure 5-8 shows the comparison between the actual and calculated condensation rates & figure 5-9 shows the actual and calculated desorption rate, when the chilled water temperature is changing. It is evident that the calculated values in all 4 testing follow the actual values within ±10% good agreement.

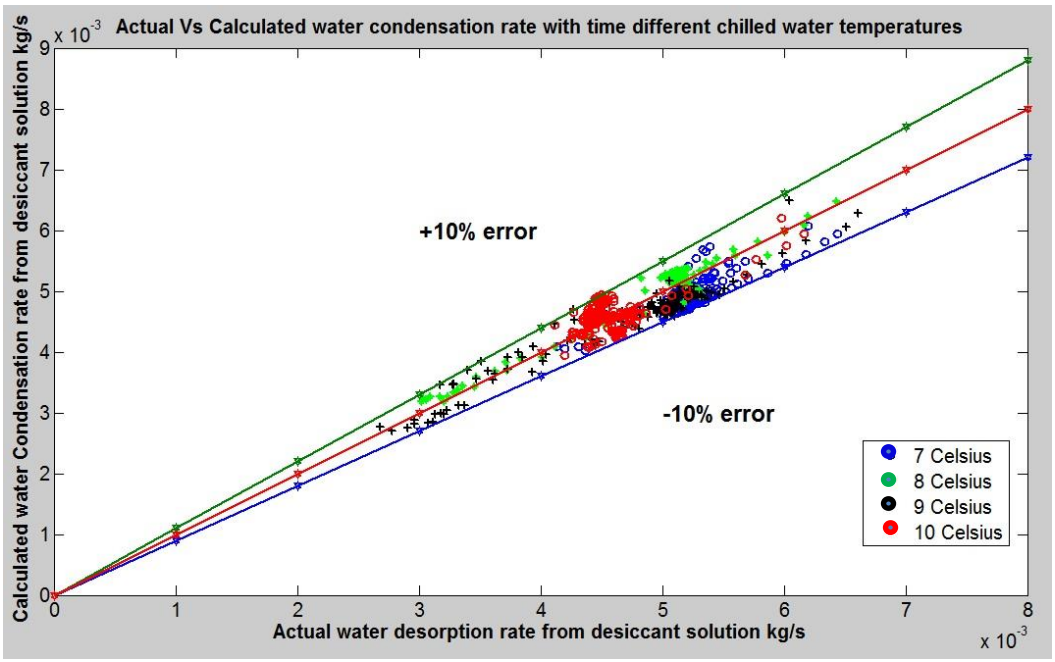

Figure 5-8. Actual condensation rate VS calculated condensation rate

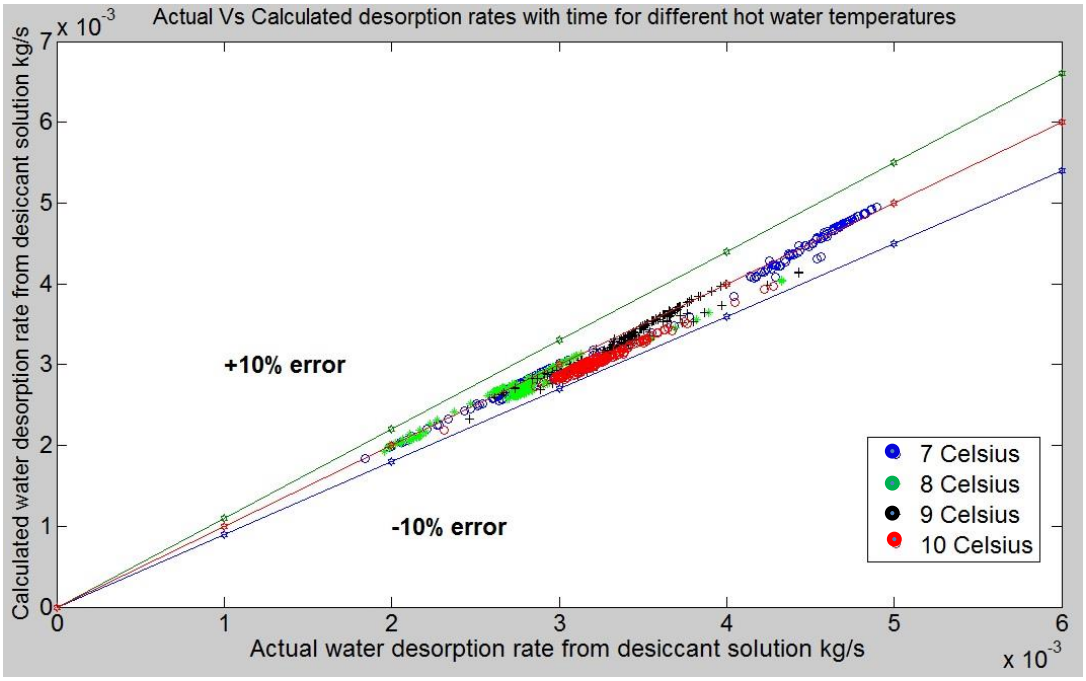

Figure 5-9. Actual desorption rate VS calculated desorption rate

Table 5-1. Initial and final values of LiBr mass ratio for different chilled water temperatures

	Test 1	Test 2	Test 3	Test 4
Chilled water temperature	7 ^{0}C	8 ^{0}C	9 ^{0}C	10 ^{0}C
Initial LiBr mass ratio	36.39	36.39	36.69	36.46
Final LiBr mass ratio	48.40	45.56	47.62	46.39

Figure 5-10 illustrates the change of chilled water temperature with respect to the process time for different initial chilled water temperatures. At the starting point, chilled water temperature was slightly lower than the temperatures 7 , 8, 9, 10 ^{0}C, which need to be maintained. During the condensation process, it was identified that the chilled water absorbs energy from water vapor which increases its temperature. Due to the high amount of latent heat released to the chilled water, it becomes difficult to maintain the temperature in a constant value. That was the reason to have slight variations of the temperature values throughout the testing time period. Towards the end of the testing period there are little higher variations of the temperatures of 8 & 9 degree cases. This is due to the sudden increment of the desorption rate and due to that effect all the other parameter settings changed. Increment of the desorption rate demanded for higher condensation load and it increased the chiller load. Since the chiller cannot provide enough amount of load, chilled water inlet temperature increased. If a proper control system can be implemented with the system these types of higher variations can be removed and also by having a large reservoir or a high capacity chiller. However, with time, when the condensation rate decreased due

to the decrease of the desorption process, temperature of chilled water gradually decreases.

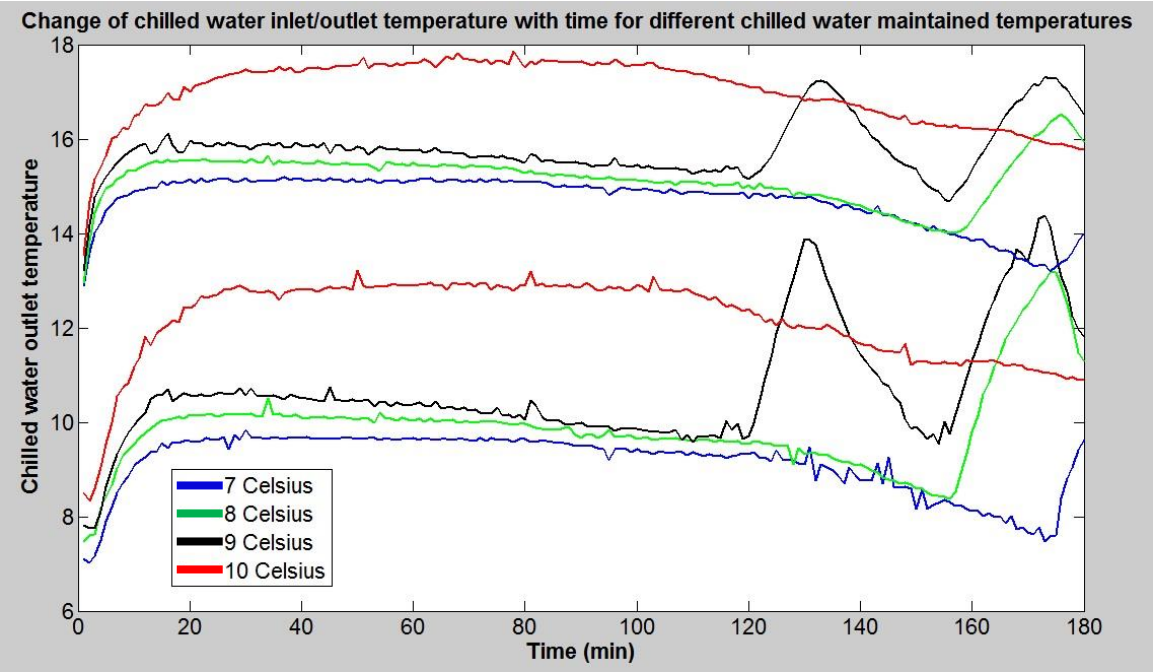

Figure 5-10. Change of chilled water inlet/outlet temperature for different initial chilled water temperatures

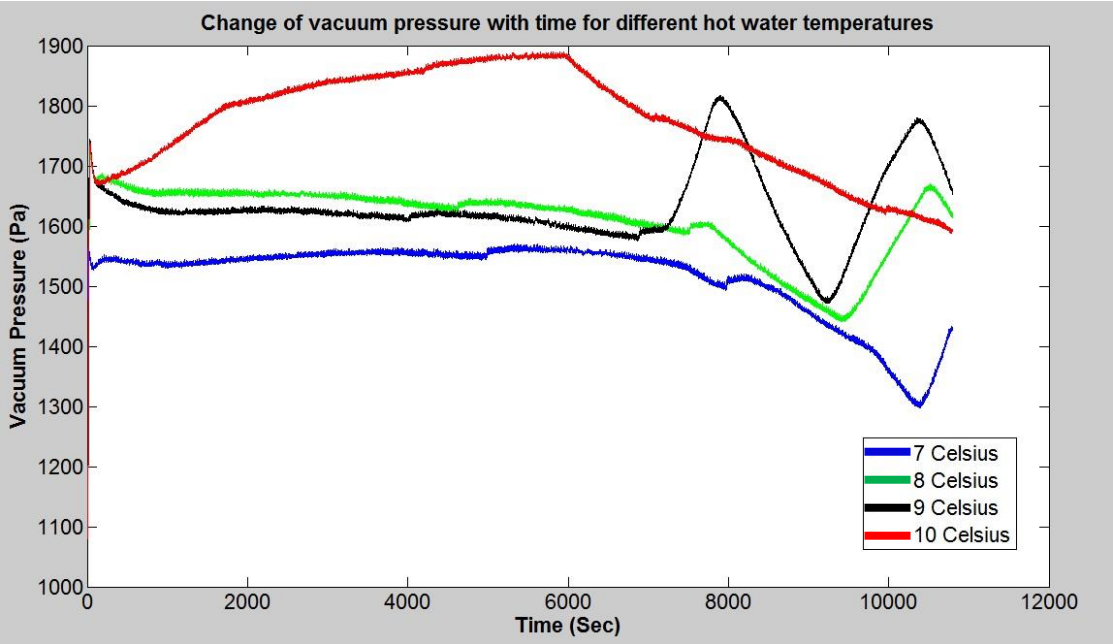

Figure 5-11. Change of vacuum pressure condition for different initial chilled water temperature

Change of vacuum pressure inside the chamber for different chilled water temperatures is shown in Figure 5-11. When the chilled water temperature is high, the condensation heat transfer is substantially lower than the chilled water temperature in low condition. Therefore, an excess amount of water vapor remains inside the chamber. In order to maintain a constant lower vacuum pressure there should be an equilibrium rate between desorption and condensation process rates. In figure 5-11 towards the end of the testing period there is a pressure variation due to the rise of the chilled water temperature. Higher chilled water temperature resulted in lower condensation rate. Hence higher vacuum pressure resulted in higher condensation temperature. Therefore, if there is a control system to see the direction of the chilled water temperature and react to that to reduce the hot water flow rate, there won't be excess water vapor to increase vacuum pressure.

Figure 5-12 shows the change of water vapor condensation rate with respect to time. It was seen that at the first few minutes condensation rate rose to a very high value. When the temperature was at 7^0C, condensation rate rose up to 6.5g/s whereas for the other entire instances condensation rate remained around 5-5.5 g/s. This was due to the sudden water desorption as well as the increment in the chilled water temperature. As a result, condensation rate also reduced to around 5 g/s when the temperature were at 7, 8, 9 ^{0}C, and around 4-4.5 g/s for 10 ^{0}C instance. There are variations of the condensation rate throughout the testing time period. Those variations were due to the sudden change of the uncontrollable parameter values of the system, since most of the parameters were controlled manually. But those minor variations can be reduced and omitted if a proper controlling method is introduced. It's clear from the graph that the highest condensation rate can be achieved when the chilled water temperature was lowest and so on.

The chilled water temperature variation effect on desorption process is shown in the figure 5-13. Desorption rate has a similar condensation rate behavior during the first few minutes. Initially, the rate rose to more than 4 g/s and dropped down to around 3 g/s within 20 min time. When figure 5-12 & figure 5-13 are compared, it is evident that the condensation rate is slightly higher than the water desorption rate, which is favorable for the maintenance of a constant pressure inside. As soon as the system started, vacuum pressure increased due to the rising of water vapor and since the condensation rate is almost same as desorption rate, this aids to maintain a high pressure until 5-10 minutes, then, gradually reduced as shown in pressure plot figure 5-11. There are variations of desorption rate during all four testing, especially for the 7 ^{0}C case and towards the end of the test all four cases indicates slight variation. At 7 ^{0}C case between 40 min to 120 min desorption

rate rose up to 4-5 g/s suddenly and dropped down again. These variations are caused due to the variations of the vacuum pressure inside. Higher vacuum pressure during the testing indicates more water vapor inside and it increases the condensation rate, but decreases the desorption rate. Due to the sudden increase of the initial desorption rate vacuum pressure increased which reduced the desorption rate and at the same time condensation rate increased and maintained the vacuum pressure. It's clear from the figure 5-11 that the variation of the vacuum pressure clearly caused this effect. By implementing a proper control method these variations can be removed from the system operation.

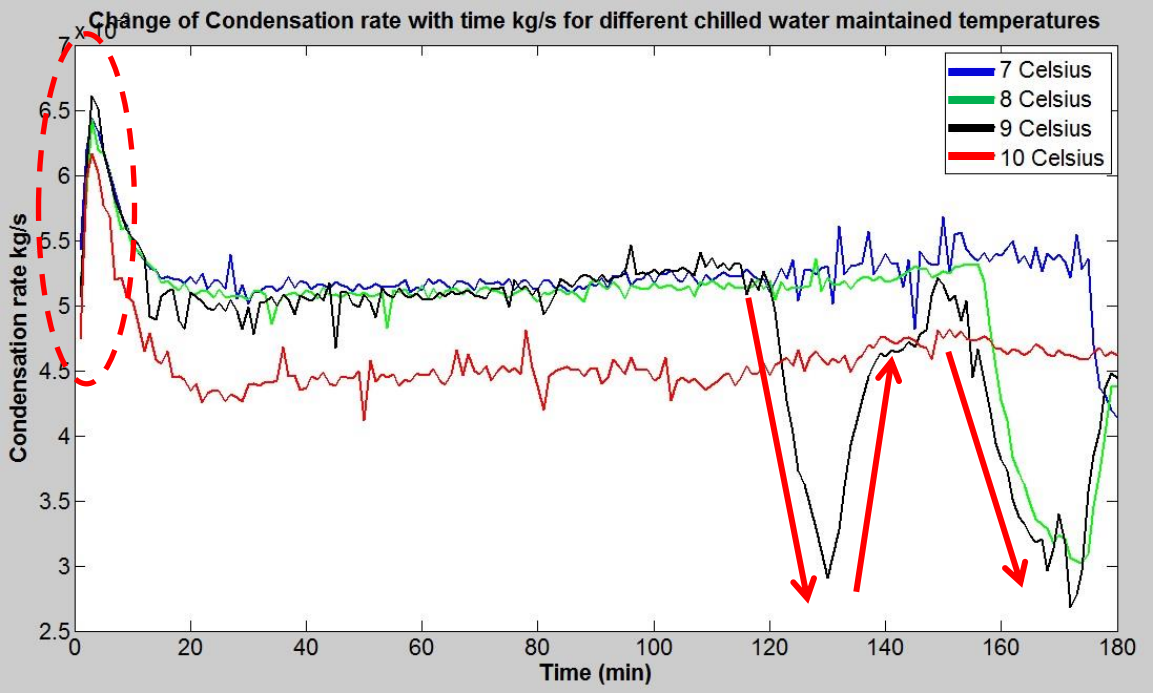

Figure 5-12. Change of water condensation rate for different chilled water temperatures

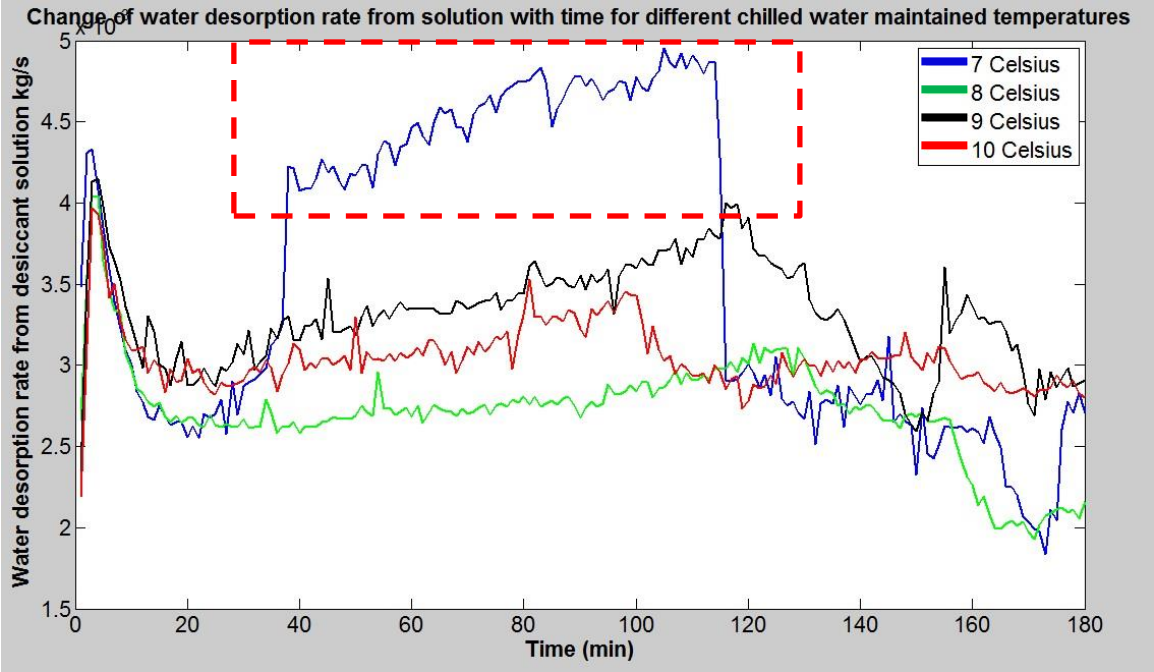

Figure 5-13. Change of desorption rate for different chilled water temperature

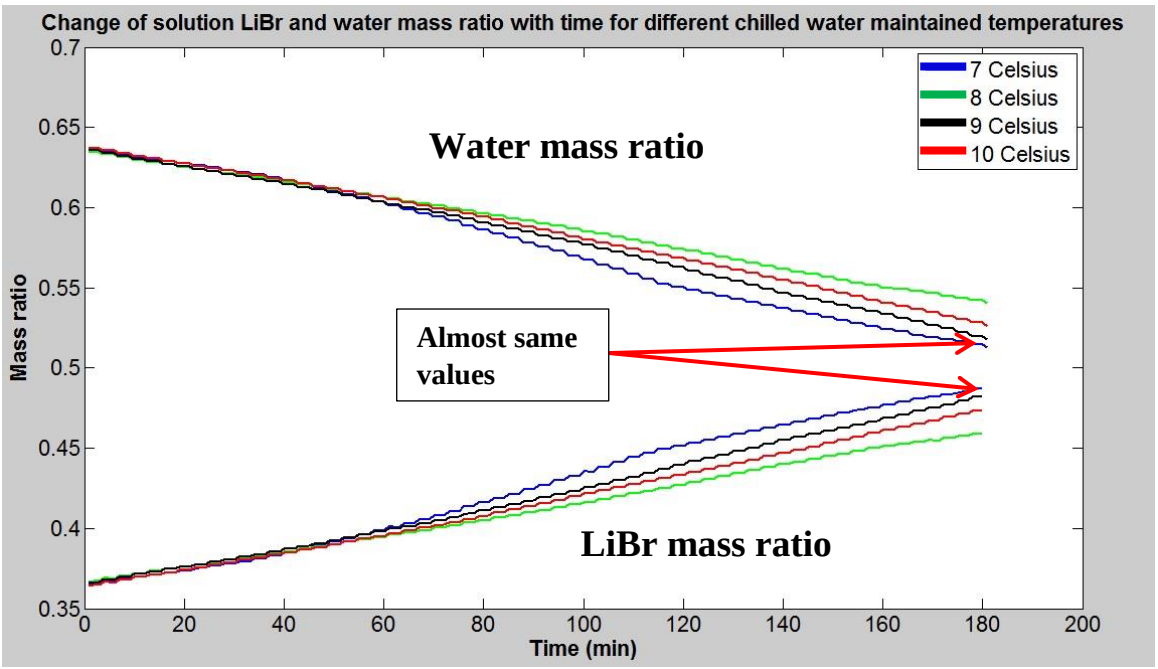

Figure 5-14. Change of LiBr & water mass ratio with time

Figure 5-14 shows the reduction of the water mass ratio and increase of the LiBr mass fraction with time for four chilled water temperature levels. Highest LiBr mass fraction value can be achieved when the chilled water is at its lowest temperature. Final LiBr mass fraction values for 7^0C & 9^0C were almost the same even though there was a difference in desorption rates. Figure 5-15 illustrates the change of mass transfer effectiveness of the system during the testing time duration. According to figure 5-15 the highest mass transfer effectiveness was achieved when the chilled water temperature was at 8 degrees. Thus the system operated to 60% of its maximum effectiveness in 8^0C temperature and 56%-60% effectiveness in other instances. There are slight variations of the mass transfer effectiveness value and towards the end of the testing time period this variation is slightly high. These are due to the sudden change of uncontrollable system parameters and by implementing a proper control strategy these can be overcome and can have more favorable results than this.

Figure 5-16 shows the variation of the final LiBr mass ratio percentage. It is evident that the highest final LiBr concentration can be achieved when the chilled water temperature at its lowest. Therefore, for an improved performance of the system all the other control parameters must be controlled with the lowest chilled water temperature. In addition to the temperature, chilled water flow rate is another factor that determines the amount of heat absorbed from the condensation process. In the next section the study on the effect of chilled water flow rate on the final LiBr concentration is discussed.

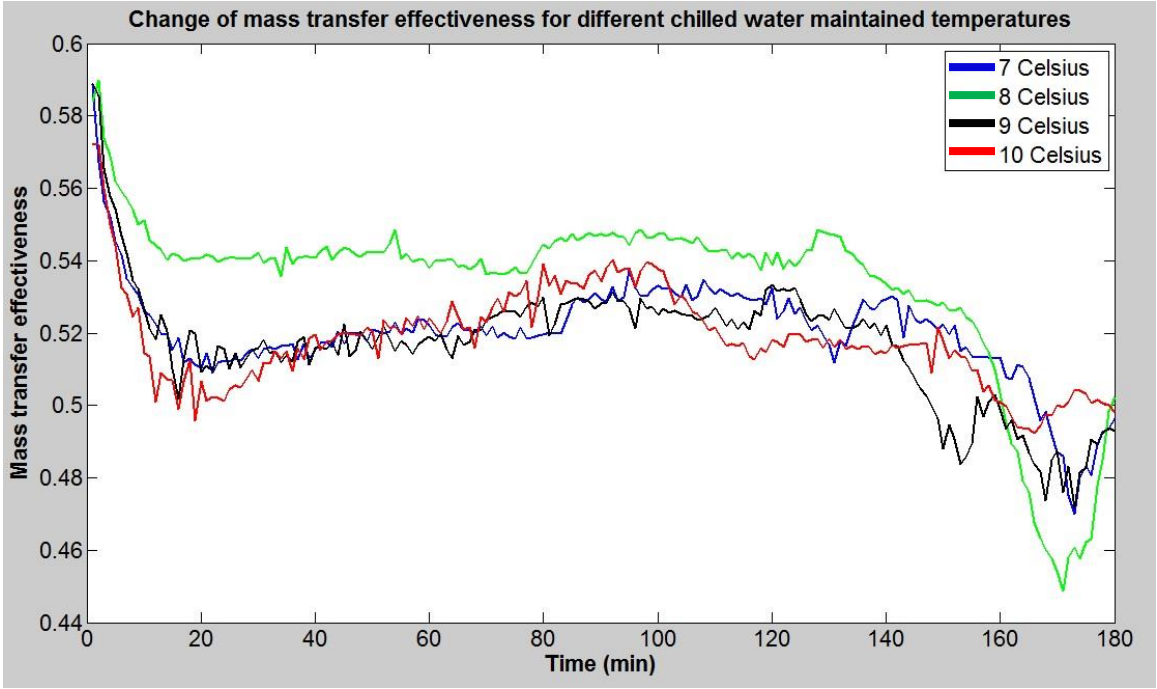

Figure 5-15. Change of mass transfer effectiveness with time for different initial chilled water temperatures

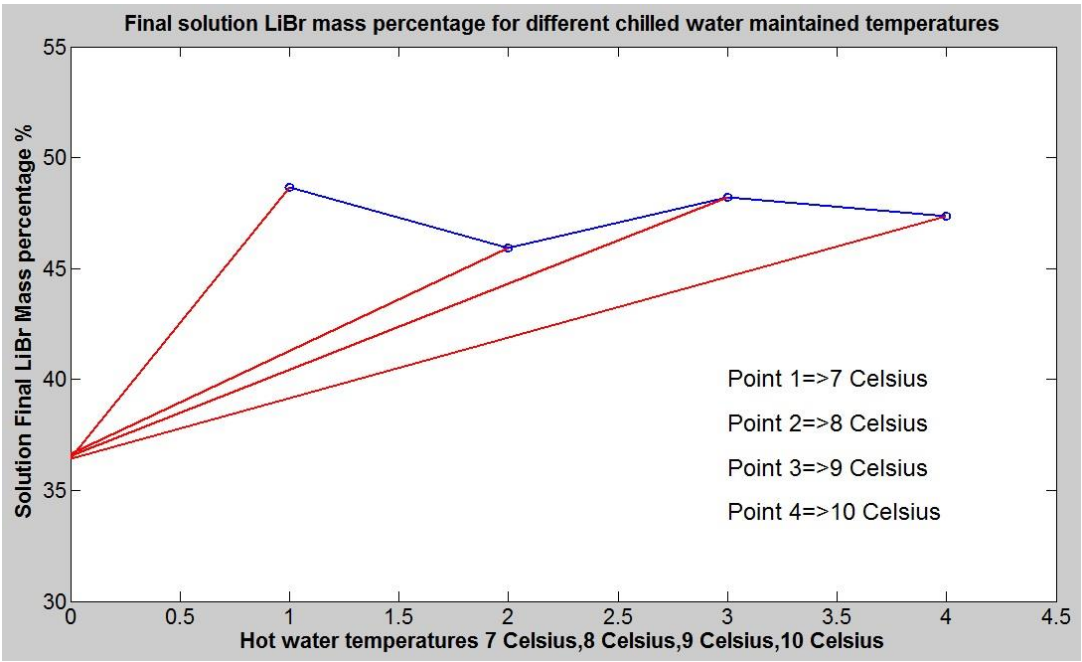

Figure 5-16. Final LiBr mass percentage for different initial chilled water temperatures

Effect of chilled water flow rate on the condensation process

Table 5-2. Initial and final values of LiBr concentration for different chilled water flow rate values

	Test 1	Test 2	Test 3	Test 4
Chilled water flow rate	1.12m^3/hr	1.3m^3/hr	1.64m^3/hr	1.99m^3/hr
Initial LiBr mass ratio	36.77%	36.62%	36.39%	36.46%
Final LiBr mass ratio	48.40%	45.56%	47.62%	46.39%

Since the heat capacity rate is decided by the chilled water flow rate and water heat capacity, the system characteristics against chilled water flow rate were analyzed here. Figure 5-17 illustrates the change of actual water condensation heat transfer rate with respect to calculated condensation heat transfer rate in which, the values are within ±10% good agreement level.

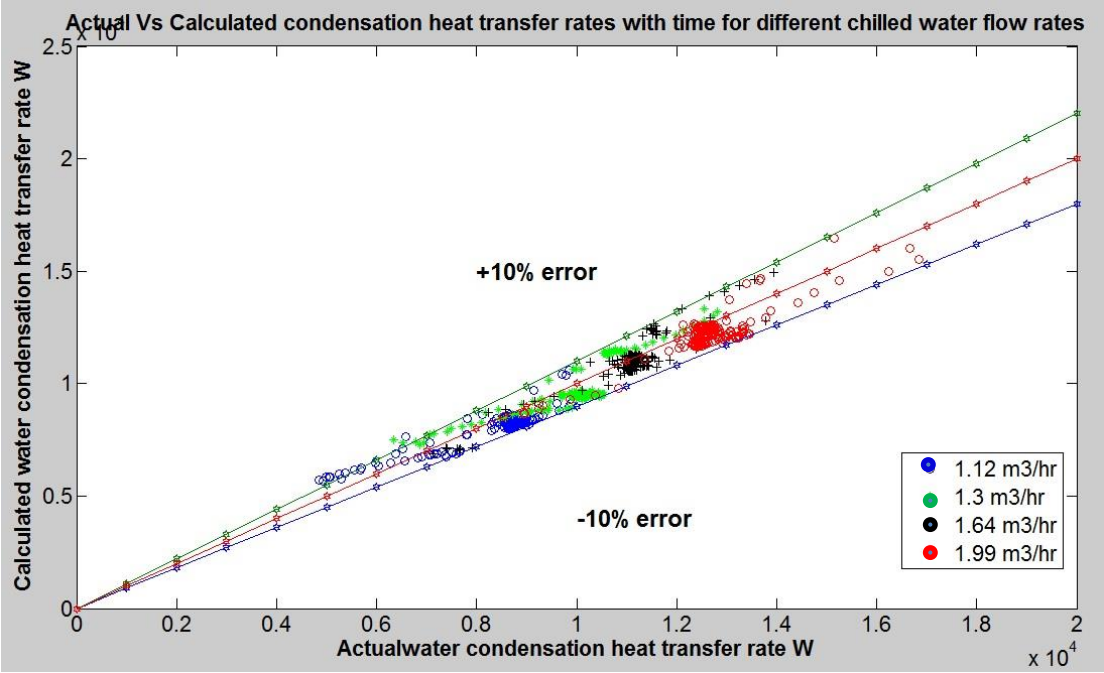

Figure 5-17. Calculated condensation heat transfer rate Vs actual condensation heat transfer rate

Figure 5-18 illustrates the chilled water inlet and outlet temperature variation within the testing time for different flow rates. When the flow rate was lowest at 1.12m^3/hr, the amount of energy absorbed by the water was higher. The low flow rate leads the chilled water to remain within the heat absorbing area of the heat exchanger for longer time duration. Therefore, the temperature difference between the inlet and outlet of chilled water increases. On the other hand the energy released to the chilled water within the heat exchanger decreases. Thereby, the chiller can maintain the chilled water temperature at a lower value. Nevertheless, when the flow rate increases, heat release to the chiller increases and due to that, chilled water temperature rises. If the chiller capacity is sufficient to provide a higher cooling load and a higher flow rate it would enable a higher performance. Towards the end of the testing chilled water inlet temperature variation is quite high. This is due to a different

reason than the earlier chilled water temperature situation. Slight increment of the chilled water temperature led to decrease of the condensation rate and due to that vacuum pressure increased and led to increment of the condensation temperature. One reaction led to another and when the corrective actions were taken it took quite time to react. That is the main reason that this system required a proper control system to react soon with corrective actions.

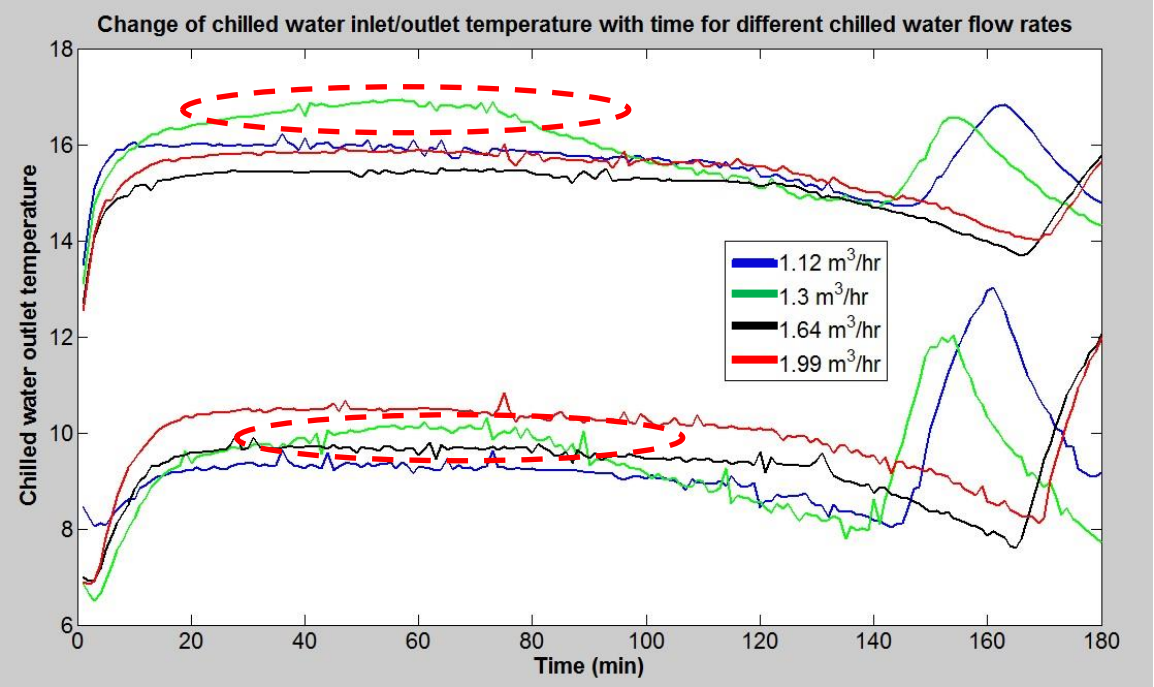

Figure 5-18.Change of chilled water in/out temperature for different chill water flow rates

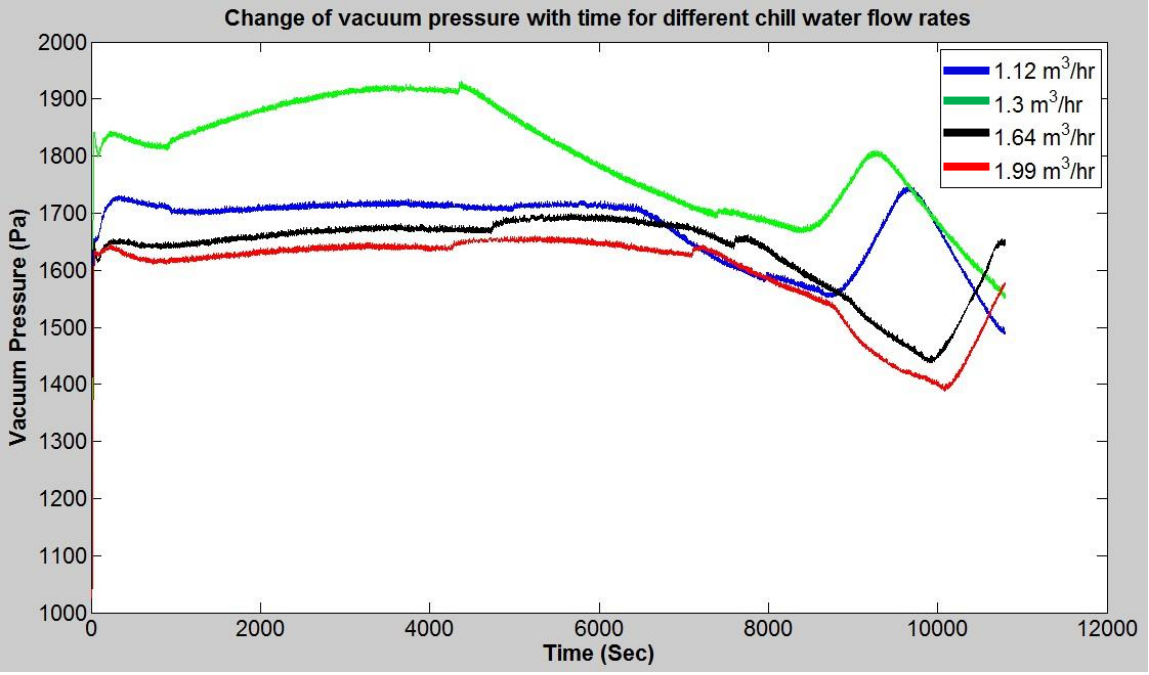

Figure 5-19. Change of vacuum pressure with time for different chill water flow rates

Figure 5-19 shows the change of vacuum pressure for different flow rates of chilled water. When the flow rate was 1.99m^3/hr, vacuum pressure was remained lowest as the condensation rate was higher. Therefore, it was understood that maintaining a lower vacuum pressure improves the performance of the desorption process. There are slight variations of the vacuum pressure through time. Mismatch of the desorption and condensation rate led to the increment of the vacuum pressure and then it led to change of several other parameter values as shown in previous figures. Figure 5-20 illustrates the change of desorption rate with time for the same testing. According to figure 5-20, flow rate of 1.3m^3/hr shows the highest desorption rate (as circled in the figure). The causes for the result of these misleading values were due to the considerably higher initial hot water temperature compared to the other testing. Here, more water vapor within the chamber increased provoking more condensation, which in turn increased the chilled water

temperature. In the other three scenarios, highest flow rate of 1.99m^3/hr corresponded to the highest desorption rate whereas flow rate of 1.12m^3/hr corresponded to the lowest desorption rate. Hence, higher condensation rate provides a good platform for the desorption process, therefore for better performance chilled water flow rate must be maintained a higher value not only to maintain the vacuum pressure a lower value but also to increase the condensation rate.

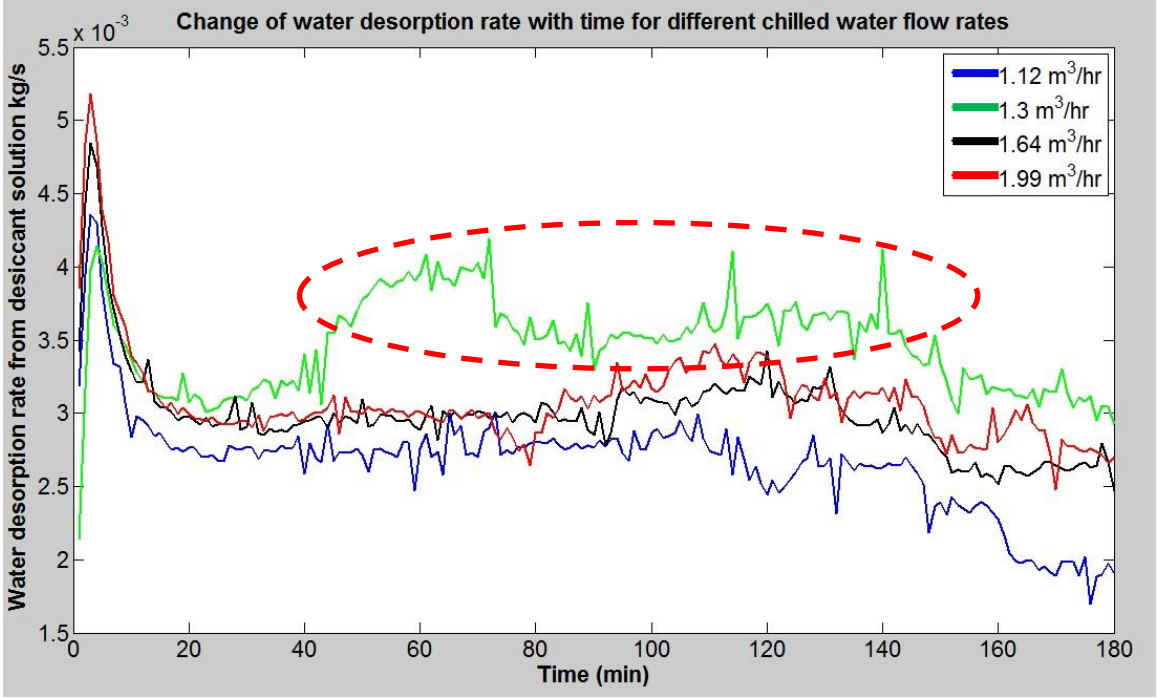

Figure 5-20. Change of water desorption rate with time for different chilled water flow rates

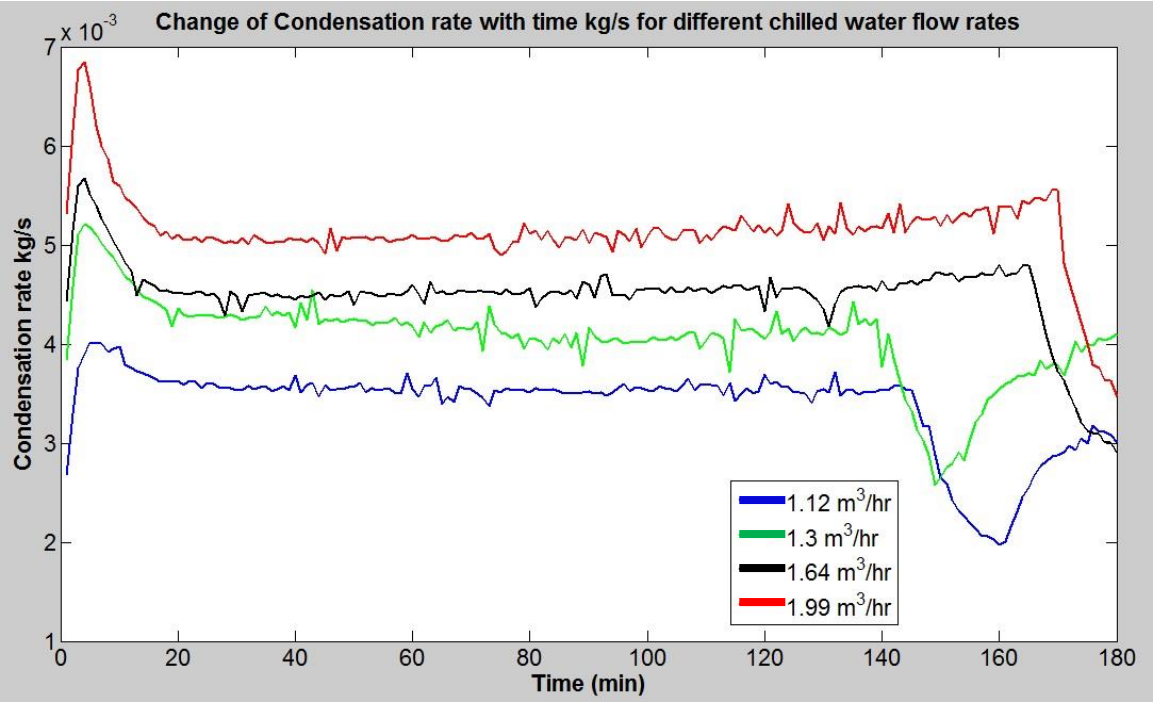

Figure 5-21. Change of condensation rate with time for different chilled water flow rates

Figure 5-21 shows the condensation rate variation against process time for four flow rates in consideration. It clearly illustrates that there is an increase of condensation rate when the flow rate is highest at 1.99m^3/hr. Initially, condensation rate rose up to 6.8 g/s and then dropped down to around 5 g/s. When the flow rate was 1.64m^3/hr condensation rate was around 4.7 g/s. there wasn't a considerable difference between the condensation rates for flow rates of 1.99m^3/hr and 1.64m^3/hr. It is clear that chilled water with low temperature and high flow rate can provide a better condensation rate to by avoiding a high vacuum pressure situation. In here there is a slight variation of the condensation value towards the end of the testing. This is due to increase of the chilled water temperature of this testing and it led to reduction of the desorption rate. Corrective actions can be taken by implementing a control system for the system. Figure 5-22 shows the change of the mass ratios for LiBr

and water within the solution with respect to time. Flow rates 1.99m^3/hr and 1.64m^3/hr had almost the same final LiBr mass ratios of 46.42% and 46.72% respectively.

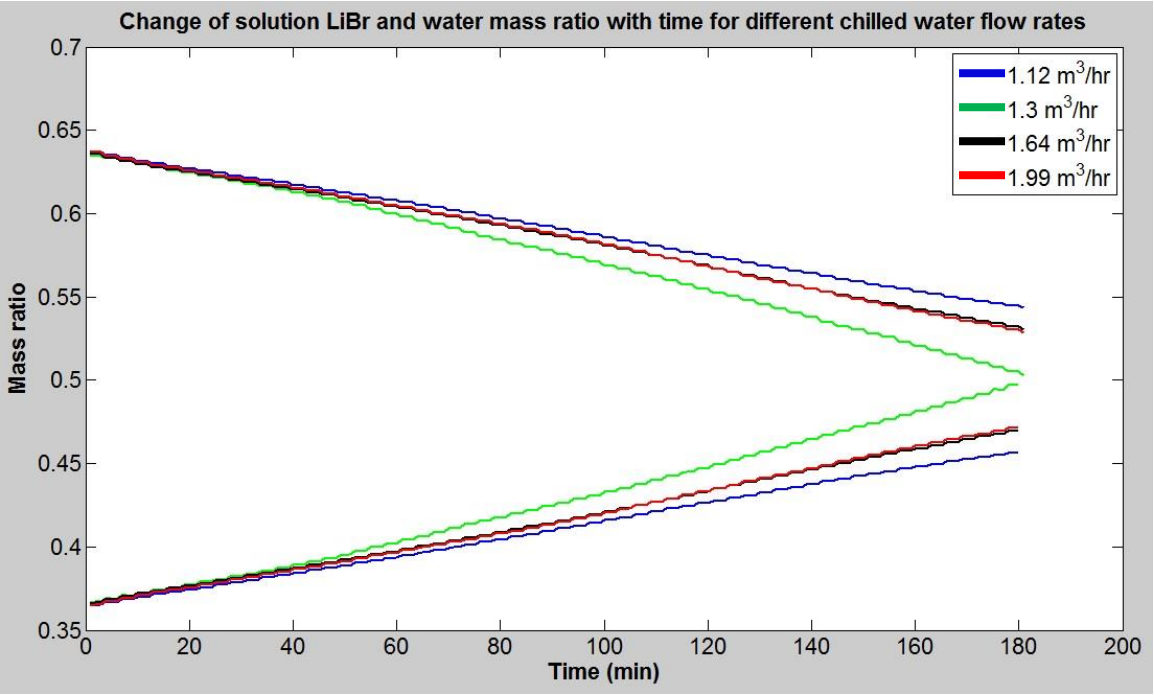

Figure 5-22. Change of LiBr/water mass ration with time for different flow rates

Effect of the vacuum pressure on the condensation process

Figure 5-23 shows the change of vacuum pressure with respect to time. The area shown as X in figure 5-23 is caused by the increase of chilled water inlet temperature due to an experimental error. Figure 5-24 -A shows the change of condensation rate accordingly with pressure change and figure 5-24-B shows the change of chilled water temperature with respect to time. It caused a reduction of the condensation rate 5.5 g/s to 3 g/s where, more water vapor got collected inside and increased the vacuum pressure as shown in figure 5-23. Until that point, condensation rate in the test where the initial pressure is 2000 Pa was

comparatively higher. Later on in the testing, due to the high pressure inside the chamber which is caused by more water vapor, the natural convection to the condenser surface increases, which in turn can cause a higher condensation rate.

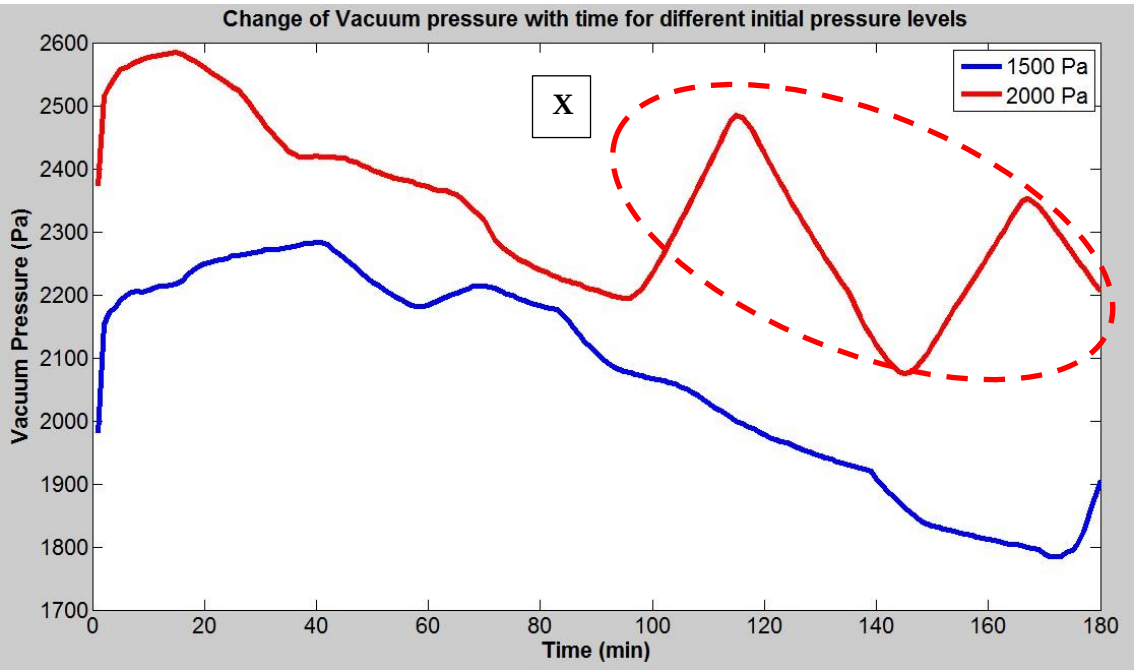

Figure 5-23. Change of vacuum pressure with time for two initial vacuum pressure conditions

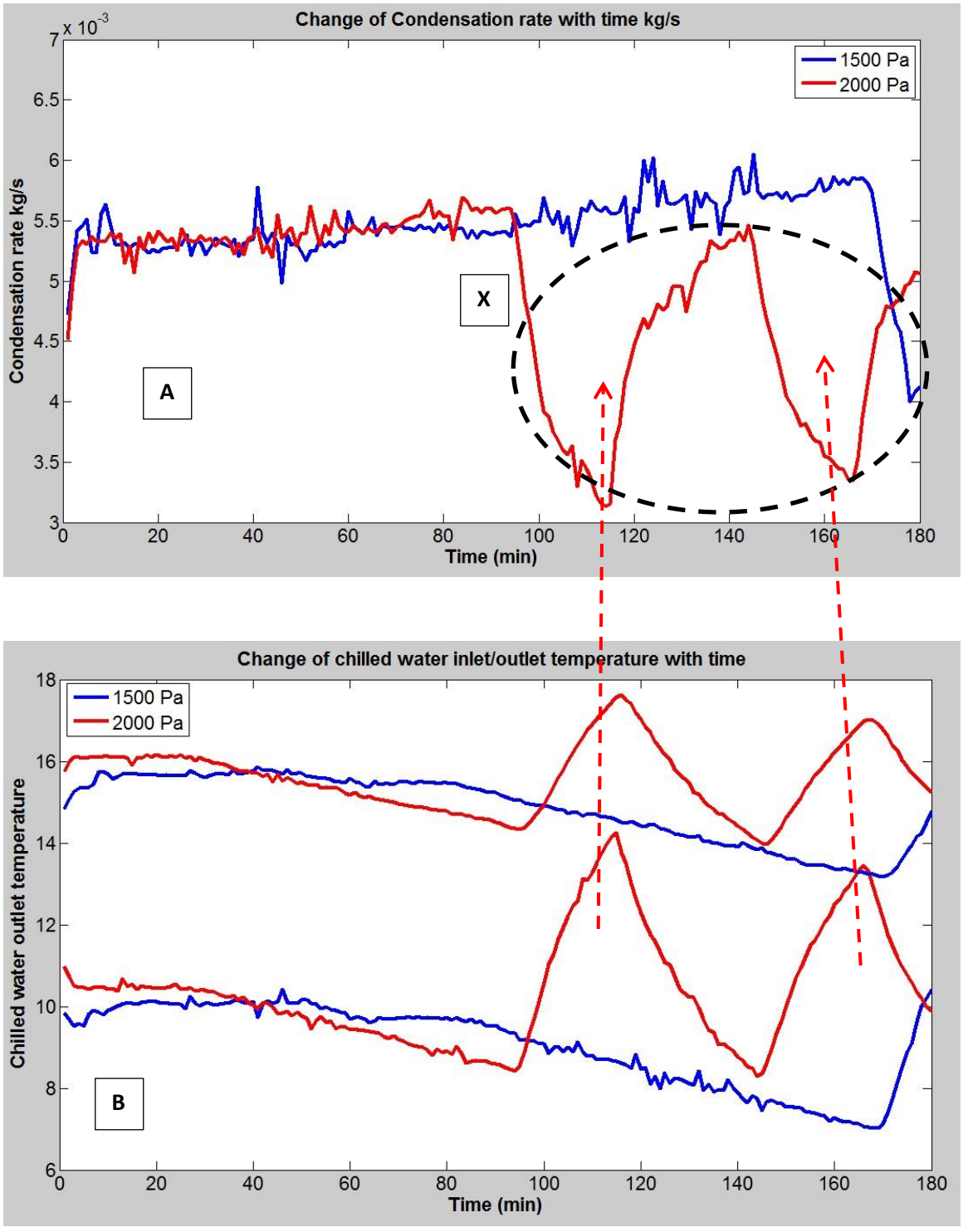

Figure 5-24. A- Change of condensation rate with time, B- Change of chilled water inlet-outlet temperature with time with respect to two pressure levels

Figure 5-25 shows the mass transfer effectiveness for two pressure levels. It clearly shows that when the vacuum pressure is higher mass transfer effectiveness is higher. High vacuum pressure is an indication of more water vapor inside the chamber. On the other hand higher saturation temperature reduces the maximum possible mass transfer. Even though the mass transfer effectiveness is higher in higher vacuum pressure condition, it is not suitable for the evaporation process.

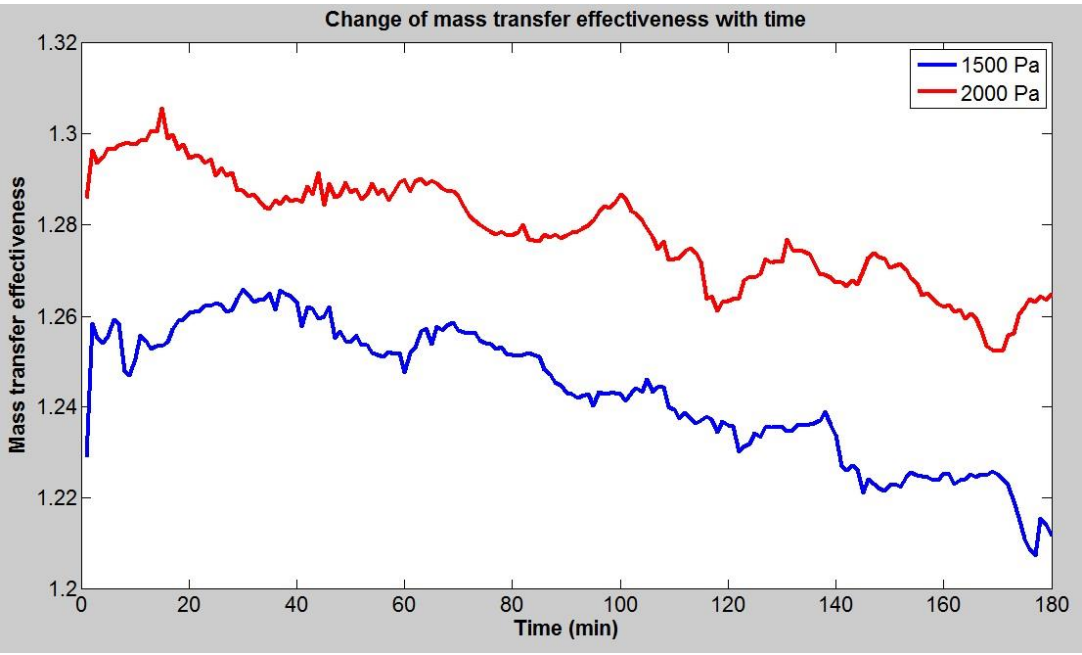

Figure 5-25. Change of mass transfer effectiveness with time for two pressure levels

The effect of higher hot water and cycle run time

A study was carried out to check how the system performs for a higher hot water temperature and longer regeneration time.

Table 5-3. Results of the effect of the high temperature and longer time duration testing

Testing	Initial LiBr mass percentage	Final LiBr mass percentage
Normal condition 3 hours	36.31%	45.61%
Normal condition 6 hours	36.62%	52.83%
Normal condition 7 hours	36.16%	54.41%
Normal condition Hot water temperature 45 Celsius	36.62%	50.88%
Normal condition Hot water temperature 55 Celsius	36.62%	55.48%

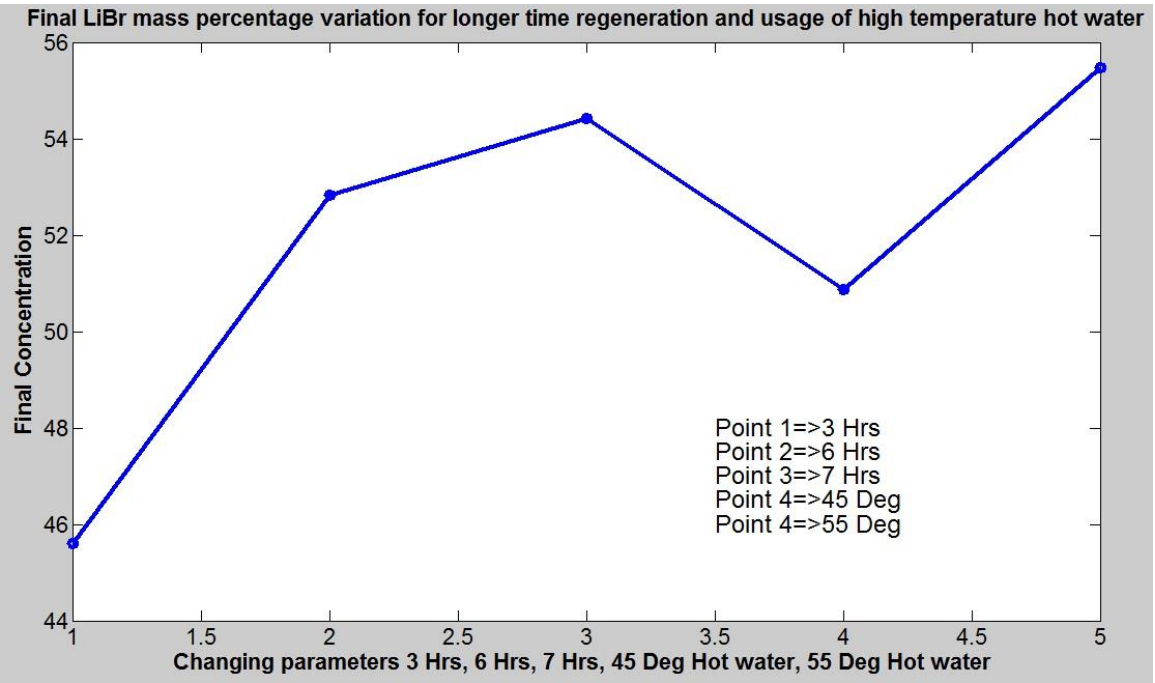

Figure 5-26. Final LiBr mass percentage variation for longer time regeneration and usage of high temperature hot water

From the table 5-3 & figure 5-26 it's clear that when the system runs around 6-7 hours, a higher LiBr mass ratio can be achieved. Likewise, if the hot water temperature is around 55 degrees, substantially a higher LiBr mass ratio can be achieved. Those are almost 20% increment of the mass ratio with respect to the initial conditions. However, to achieve both the above conditions (longer running time and high hot water temperature) a considerable amount of energy is required. Therefore, it was necessary to study whether it is profitable to spend a higher amount of energy to achieve this higher concentration or to spend a lower energy and achieve lower concentration.

5.5 Summary

This chapter presented a mathematical model for heat and mass transfer study of the condensation process of the condenser heat exchanger in the vacuumed regenerator. Numerical analysis using non-linear least square method was carried out to evaluate the mathematical model constant parameters. Heat transfer model and mass transfer model for the vapor condensation process was validated within ± 10% good agreement.

The effect of chilled water temperature (T_{cw}), chilled water flow rate (m_{cw}), vacuum pressure (P_{vacuum}) for the condensation performance was studied. Changes of condensation rates with respect to variables of chilled water temperatures were studied at 7^0C, 8^0C, 9^0C, 10^0C. When the chilled water temperature was at 7^0C, mean condensation rate was around 3.1g/s throughout the time. When the chilled water temperatures were at 8^0C, 9^0C, 10^0C, slightly lower condensations were achieved respectively, 3.0g/s, 2.9g/s, 2.7g/s. Highest vacuum pressure belongs to chilled water temperature 10^0C and lowest belongs to 7^0C.

The effect of chilled water flow rate on the condensation rate was studied. Chilled water flow rates were maintained at 1.12m^3/hr, 1.3m^3/hr, 1.64m^3/hr and 1.99m^3/hr, mean condensation rates 3.4 g/s, 4.1 g/s, 4.5 g/s, 5.1 g/s were achieved respectively. In a higher chilled water flow rate situation it absorbs a higher amount of heating load. Therefore, the chiller capacity should be sufficient enough to provide the required cooling load. The effect of two initial pressure states: 1500Pa and 2000Pa, of vacuum conditions for the condensation process were studied, in which the mean condensation rates were 5.4 g/s and 4.9 g/s. Therefore, by maintaining the chilled water temperature and the vacuum pressure

at a lowest possible value along with a chilled water flow rate at the highest possible value, a better performance of the condensation process can be achieved.

The effect of regeneration time duration and a higher hot water temperature on the regeneration performance was discussed. Analysis was conducted for the testing time duration of 3 hours, 6 hours and 7 hours. While maintaining the same initial LiBr mass percentage at 36.31%, following final mass percentages were achieved respectively, 45.61%, 52.83%, 54.41%. But the rate of increment was declined when the LiBr mass ratio was increased. Two states of hot water temperature of 45^0C and 55^0C were studied where the final LiBr mass percentage increased to 50.88% and 55.48%. Therefore, it can be concluded that developed heat and mass transfer model is with acceptable agreement with the system, where a lower chilled water temperature of 7^0C causes higher condensation rate of 3.1g/s, while a higher chilled water flow rate of 1.99m^3/hr causes a higher condensation rate of 5.1g/s, and finally, the pressure inside increases the condensation due to the high amount of water vapor. Therefore, optimization is required to find out the best operating condition of the system to have highest performance.

Chapter 6 Optimization of the Regeneration system

Liquid desiccant regeneration cycle plays an important role in liquid desiccant dehumidification system. This is the process which purifies or increases the concentration of liquid desiccant Lithium Bromide. There are some sub processes in the regeneration cycle that consume higher amount of energy. Primary electrical energy or renewable energy can be directly consumed for these processes and optimization of the system properties is a must for a better performance of the system. At the same time optimization provides the best operating conditions of the system to get higher efficiency of the regeneration process to get the best COP of the LDDS system.

In the liquid desiccant dehumidification system solution absorbs water vapor and reduces its concentration thereby needs to be regenerated to the required level of concentration. This regeneration process involves following sub processes.

- Heating of the solution in the evaporator heat exchanger by hot water
- Cooling down the water vapor in the condenser heat exchanger by chilled water

Solution inside the chamber circulates through the evaporator heat exchanger and absorbs required latent heat and water vaporizes. This vaporized water increases the inside pressure. The difference between the surface water vapor pressure of the solution and partial vapor pressure inside vacuumed space acts as the driving force for regeneration mass transfer. Hot water flow rate and temperature decides the amount of energy transfer to the solution and solution flow rate decides the amount of water to be vaporized. Water vapor inside releases latent heat of condensation to the chilled water and decreases the inside pressure. Chilled water temperature and flow rate decide the capacity of heat that can be absorbed.

Considering the above following parameters will be set for the optimization to understand the best operating condition [28, 48].

- Hot water temperature (T_{hwi})
- Hot water flow rate ($\dot{m}_{hw}$)
- Chilled water temperature (T_{cwi})
- Chilled water flow rate ($\dot{m}_{cw}$)
- Solution flow rate ($\dot{m}_{s}$)
- Vacuum pressure (P_{v})

6.1 Optimization model

The objective of optimization of the model is to get the highest heat and mass transfer rates with a minimum energy consumption. Models developed in the previous sections for heat and mass transfer are used for the optimization. Main objective of the regeneration system is to maximize the solution regeneration rate, maximize the water vapor condensation rate and minimize the energy consumption of the water heater, solution pump, hot water circulation pump and chilled water circulation pump. To maximize the regeneration rate both heat transfer and mass transfer maximization in the evaporator and the condenser are necessary. Considering the issues as minimization problems, the first four objectives of maximization can be considered as minimization the inverse function. Therefore, objective function can be written for the minimization problem as below. Total energy consumption is the summation of heater energy, chiller load and three pump power consumptions.

$$f_1 = \frac{1}{S_1}$$

$$f_2 = \frac{1}{S_2}$$

$$f_3 = \frac{1}{Q_1}$$

$$f_4 = \frac{1}{Q_2}$$

$$f_5 = Q_h + Q_c + W_{hw} + W_{cw} + W_s$$

S_1 - Regeneration rate

S_2 - Water vapor condensation rate

Q_1 - Evaporator heat transfer rate

Q_2 - Condenser heat transfer rate

Q_h - Heater energy

Q_c - Chiller load

W_{hw} - Hot water pump power input

W_{cw}- Chilled water pump power input

W_s - Solution pump power input

f_1, f_2 , f_3, f_4 and f_5 are five objective functions in the genetic algorithm that are to be minimized. Heat and mass transfer models for the above mentioned objectives were developed in the previous section can be used for the optimization calculations.

Physical limitations of the components

Constraints of this optimization model are the limitations that each parameter can reach. Some are based on physical and practical limitations of equipment's and others are component capacities. Decision parameters for this study are hot water temperature (T_{hwi}) , hot water flow rate ($\dot{m}_{hw}$) , chilled water temperature (T_{cwi}) , chilled water flow rate ($\dot{m}_{cw}$) , solution flow rate ($\dot{m}_s$) and vacuum pressure (P_v) , which are restricted to their upper and lower limits. Here the vacuum pressure is the initial vacuum pressure condition which later on becomes an independent variable that cannot be controlled and it should be preset before the optimization.

Following limiting constraints and upper bound and lower bound constraints were set for chromosome to not deviate from them.

- $Q_h \leq Q_{h,design}$
- $Q_c \leq Q_{c,design}$
- $T_{hwi,min} \leq T_{hwi} \leq T_{hwi,max}$
- $\dot{m}_{hw,min} \leq \dot{m}_{hw} \leq \dot{m}_{hw,max}$
- $T_{cwi,min} \leq T_{cwi} \leq T_{cwi,max}$
- $\dot{m}_{cw,min} \leq \dot{m}_{cw} \leq \dot{m}_{cw,max}$
- $\dot{m}_{s,min} \leq \dot{m}_s \leq \dot{m}_{s,max}$
- $P_{v,min} \leq P_v \leq P_{v,max}$

Hot water temperature upper limit is decided by the heat source maximum temperature. Hot water, chilled water and solution flow rates were limited to respective pump specifications. Chilled water temperature depends on the limitations of the chilled water generator.

Optimum values are going to search between 500 Pa and 1000 Pa of vacuum pressure due higher pressure creates lower efficiency as discussed in previous chapters and very lower pressure around 100Pa was very difficult to achieve.

Evaporator Heat transfer model:

Heat is transferred from hot water that flows inside the tubes of the heat exchanger to desiccant solution which flows outside the tubes. Following relationship was developed and was used in the optimization study. The temperature difference between hot water and desiccant solution provides the driving force for the heat to transfer.

$$Q_1 = \left[1 - exp\left\{-\frac{1}{C}\left[1 - exp\left(-\frac{\left[\frac{1}{\{x_1 \dot{m}_{hw}{}^{x_2}\}} + \frac{1}{\{x_3(\rho_s \dot{m}_s)^{x_4} C_{ps}{}^{x_5}\}}\right]^{-1} A}{C_{max}}\right)\right]\right\}\right] C_{min}(T_{hi} - T_{si})$$

Evaporator Mass transfer model

The difference of water vapor pressure between the solution and the vacuumed space acts as the driving force for desiccant solution desorption. The following equation was developed.

$$S_1 = C_2 \frac{D_{LiBrW}}{D} (Re_{sl} F^{1.25})^{g2} \left(\frac{\mu}{\rho\, D_{LiBrW}}\right)^{z1} (X_i - X_o)^{z2} (q)^{r2} \left(P_{s,sat} - P_{vacuum}\right)$$

Condenser heat transfer model

Water vapor in the vacuumed chamber releases its energy to the chilled water causing it to condense on the heat exchanger outer surface. Following equation was developed to calculate the heat transfer rate.

$$Q_2 = A_c \left[\frac{1}{\left\{ \frac{k_c}{D_c} C_c \left(\frac{4\,\dot{m}_{cw}}{\mu_c\,\pi\,D_c} \right)^{q-2s} \left(\frac{\mu_c C_{pw}}{k_c} \right)^{r} (0.184)^{s} \right\}} + \frac{1}{\left\{ 0.729 \left[1 + 0.2\, \frac{C_w\,(T_{pwsat} - T_{wall})}{h_{fg}} (N-1) \right] \left[\frac{g\,\rho_{wl}(\rho_{wl} - \rho_{wv}) h_{fg} k^3}{\mu_{wl}(T_{pwsat} - T_{wall})\,ND} \right]^{\frac{1}{4}} \right\}} \right]^{-1} \left[\frac{(T_{wv} - T_{ci}) - (T_{wv} - T_{co})}{ln\left(\frac{T_{wv} - T_{ci}}{T_{wv} - T_{co}} \right)} \right]$$

Condenser mass transfer model

The flow rate of condensed water from the N[th] tube is the condensation rate of the condenser and it can be given by the following equation.

$$S_2 = \frac{N\pi D(T_{pwsat} - T_{wall})}{h_{fg}}\, 0.729 \left[1 + 0.2\, \frac{C_{w\,(T_{pwsat} - T_{wall})}}{h_{fg}} (N-1) \right] \left[\frac{g\,\rho_{wl}(\rho_{wl} - \rho_{wv}) h_{fg} k^3}{\mu_{wl}(T_{pwsat} - T_{wall})\,ND} \right]^{\frac{1}{4}}$$

Water heater model

Water flows through the evaporator heat exchanger and releases heat to solution, then again returns to the heater chamber. Since, sufficient energy has to be provided to the hot water by the heater, a water heater was used in the system.

Water heater power input can be calculated based on the heat absorption within the evaporator heat exchanger by using the following equation. Here the amount of heat released by the heater is equal to the enthalpy change of the hot water.

$$Q_h = m_{hw} C_{phw} (T_{hi} - T_{ho})$$

Chiller model

Chiller provides enough amount of cooling load to the condenser to condense water vapor. The amount of cooling load can be calculated using the chilled water temperature difference between the inlet and the outlet.

$$Q_c = m_{cw} C_{pcw} (T_{co} - T_{ci})$$

Pump model

Hot water pump, chilled water pump and solution pump are equipped with variable speed drive (VSD), therefore their models can be identified by this equation.

$$W = Q \rho H g$$

$W - power\ consumption\ of\ the\ pump\ at\ actual\ flow\ rate$

$Q - Flow\ rate\ of\ the\ fluid\ (m^3/s)$

H – Head provided

Main objective of the system was to improve the regeneration rate. Therefore, it was of great interest to maximize the regeneration rate with different operating conditions with low computational cost in real time optimization.

6.2 Genetic algorithm for multi objective optimization

Five objectives f_1, f_2, f_3, f_4 and f_5 were set as multiple objectives as in fitness function and the final target was to minimize without chromosomes violating upper, lower bounds and constraints. Following steps were followed for the optimization.

Step 1: Set t = 0. Randomly generate *N* solutions to form the first population, P_0.

Step 2: Apply crossover and mutation to P_0 to create offspring population Q_0 of size N.

Step 3: If the stopping criteria was satisfied, stop and return to P_t.

Step 4: Set $R_t = P_t \cup Q_t$.

Step 5: Using fast non-dominated sorting algorithm, identify the non-dominated fronts F_1, F_2, F_3, F_4….F_N *in* R_t.

Step 6: for i= 1…..k do the following steps.

Step 6.1: calculate the crowding distance as below

Step 6.11: Rank the population and identify non-dominated front F_2, F_3, F_4….F_N *in* R_t, . For each front j=1..N repeat step 6.12 and 6.13

Step 6.12: For each objective function k, solutions of F_j must sort according to ascending order.

Let, Z = $|F_j|$ and $x_{[i,k]}$ represent the i^{th} solution of the sorted list with respect to the objective function k.

Assign: $cd_k(x_{[1,k]}) = \infty$ and $cd_k(x_{[Z,k]}) = \infty$, for i=1,2…..Z-1

$$cd_k(x_{[i,k]}) = \frac{f_k(x_{[i+1,k]}) - f_k(x^k_{[i-1,k]})}{f_k^{max} - f_k^{min}}$$

Step 6.13: to find the total crowding distance cd(x) of a solution x, sum the solution crowding distances with respect to each objective.

$$cd(x) = \sum_{r=1}^{k} cd_r\,(x)$$

Step 6.2: Create P_{t+1} as follows:

Case 1: If $|P_{t+1}| + |F_i| \leq N$, then

$$P_{t+1} = P_{t+1} \cup F_i$$

Case 2: If $|P_{t+1}| + |F_i| > N$,then add the least crowded N- $|P_{t+1}|$ solution from F_i to P_{t+1}

Step 7: Use binary tournament selection based on the crowding distance to select parents from P_{t+1}. Apply crossover and mutation to P_{t+1} to create offspring population Q_{t+1} of population N.

Step 8: Set t = t+1 and go to step 3

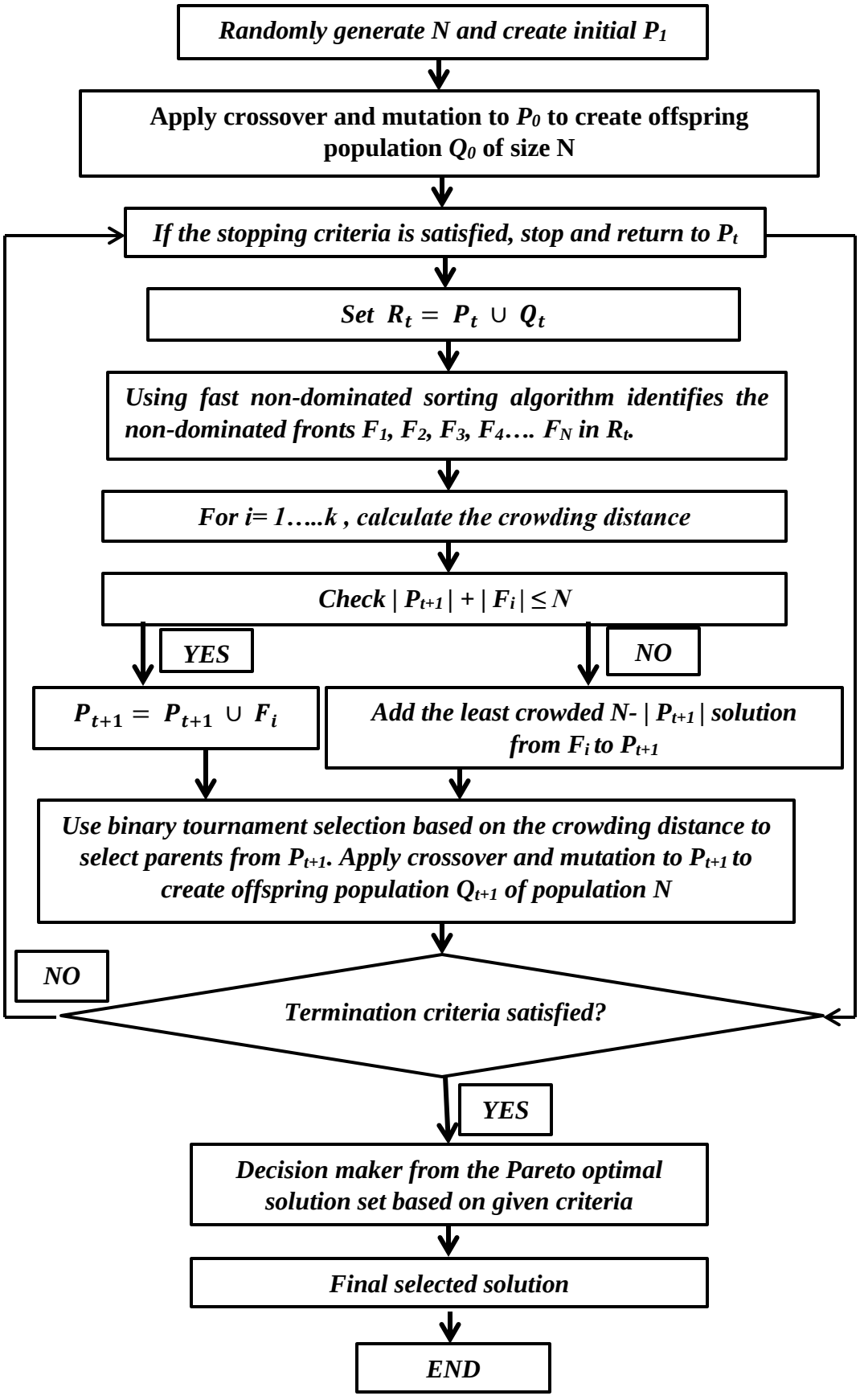
Randomly generate N and create initial P_1
Apply crossover and mutation to P_0 to create offspring population Q_0 of size N
If the stopping criteria is satisfied, stop and return to P_t
Set $R_t = P_t \cup Q_t$
Using fast non-dominated sorting algorithm identifies the non-dominated fronts $F_1, F_2, F_3, F_4 \ldots F_N$ in R_t.
For i= 1…..k , calculate the crowding distance
Check $|P_{t+1}| + |F_i| \leq N$
YES
NO
$P_{t+1} = P_{t+1} \cup F_i$
Add the least crowded N- $|P_{t+1}|$ solution from F_i to P_{t+1}
Use binary tournament selection based on the crowding distance to select parents from P_{t+1}. Apply crossover and mutation to P_{t+1} to create offspring population Q_{t+1} of population N
NO
Termination criteria satisfied?
YES
Decision maker from the Pareto optimal solution set based on given criteria
Final selected solution
END

6.3 Results and Discussion

Proposed multi objective genetic algorithm performance is studied here by using vacuumed regenerator design. Influential parameters; hot water temperature, hot water flow rate, chilled water temperature, chilled water flow rate, solution flow rate and initial vacuum pressure are optimized using multi objective genetic algorithm. MATLAB code is developed for the calculation with tuning parameters given in table 6-1.

Table 6-1.Parameter setting for MOGA

Parameter	Value
Population size	200
Maximum number of generations	700
Pareto front population fraction	0.2
Number of variables	7
Lower bounds	[0.3140,0.3135,36,8,0.66,500,29]
Upper bounds	[0.4554,0.557,42,12,0.815,1000,33]
Constraints	Q_{heater}-x(1)*4187*(x(3)-x(7)) $C_{chiller}$-x(2)*4187*(15-x(4))
Mutation	Adaptive feasibility

Heat transfer and mass transfer models developed in previous sections and total power consumption of the system are used as fitness functions to the minimization problem. Following constraints are used for the minimization problem.

- $Q_h \leq 14000$
- $Q_c \leq 16000$

Following lower and upper bounds are used as limiting values for parameters.

- $36^0C \leq T_{hwi} \leq 42^0C$
- $0.6\, m^3/h \leq \dot{m}_{hw} \leq 1.9\, m^3/h$
- $8^0C \leq T_{cwi} \leq 12^0C$
- $0.6\, m^3/h \leq \dot{m}_{cw} \leq 1.9\, m^3/h$
- $0.6\, m^3/h \leq \dot{m}_s \leq 1.4\, m^3/h$
- $500\, Pa \leq P_v \leq 1000\, Pa$

Since the testing was conducted for 3 hours, time interval is taken as 15min and optimization problem presented above was solved by multi objective genetic algorithm. Table 6-2 shows a resulted example data set for one operating condition. Most suitable solution was selected considering the feasibility of the solution and results obtained from heat and mass transfer study of evaporator and condenser.

Table 6-2. Optimization solution for one initial condition with 40 solutions

T_{hwi}(^{0}C)	$\dot{m}_{hw}$(kg/s)	T_{cwi}(^{0}C)	$\dot{m}_{cw}$(kg/s)	$\dot{m}_s$(kg/s)	P_v(Pa)
37.4956	0.371984	8.786933	0.4614	0.671058	820.9419
41.99999	0.455399	8.476863	0.557	0.719648	644.0748
41.99986	0.4554	8.534987	0.555822	0.660215	634.4785
41.61293	0.367499	8.188569	0.421926	0.722681	708.2801
42	0.4554	8.927045	0.556999	0.664723	634.3571
37.13171	0.317427	8.773318	0.550227	0.812086	850.9692
37.03912	0.353526	8.817418	0.513787	0.709481	834.9343
39.91558	0.372357	8.7846	0.503152	0.711469	662.2703
38.30923	0.414153	8.530193	0.532413	0.759117	828.7992
41.21969	0.441234	8.617731	0.55091	0.670828	661.1989
40.85386	0.442786	8.72239	0.539972	0.702676	780.7628
40.84824	0.428018	8.565759	0.55579	0.6861	696.0056
40.18742	0.382865	8.392729	0.551594	0.685852	725.2731
41.92669	0.451843	8.420063	0.517334	0.702357	715.2567
38.94164	0.395433	8.71482	0.463365	0.70249	810.8963
40.44536	0.444897	9.150451	0.521906	0.799073	755.169
41.97043	0.442006	8.85954	0.554408	0.712687	663.6427
38.22536	0.39528	8.805159	0.532058	0.665468	695.4604
41.99966	0.4554	8.159623	0.555859	0.660346	634.5695
36.8425	0.33014	9.181989	0.526735	0.806946	894.6616
37.74411	0.404994	8.735078	0.551589	0.711962	771.9862
41.98051	0.450751	8.834391	0.554819	0.676967	684.0411
41.99939	0.4554	8.366053	0.555844	0.660184	634.5804
40.13504	0.425999	8.687426	0.524415	0.695845	716.4513
41.1298	0.433582	8.491783	0.555862	0.676965	794.4864
37.37509	0.370377	8.775247	0.461641	0.687053	827.2396
40.12174	0.406832	9.082176	0.53719	0.780904	695.4533
41.53432	0.448015	8.602145	0.515774	0.731669	731.795
38.74943	0.372077	8.724704	0.471802	0.707971	768.2625
40.8672	0.424518	8.630898	0.535652	0.684942	663.3284
41.58804	0.447966	8.892043	0.530729	0.711727	642.5976
41.35065	0.420486	8.659797	0.552872	0.705931	689.2357
36.97222	0.451051	8.765496	0.54339	0.69988	720.9782
39.56673	0.449461	8.883789	0.51892	0.669004	755.6802
41.99956	0.4554	8.700682	0.556204	0.662966	634.5653
38.07724	0.412183	8.661605	0.519247	0.678236	674.8787
36.882	0.352261	8.819431	0.524886	0.739518	775.6209
37.76885	0.364253	8.67599	0.516277	0.704892	763.441
41.28985	0.43573	8.277459	0.556329	0.711934	652.6506
37.13805	0.332076	8.788699	0.546321	0.788648	850.9772

Even though the hot water temperature range was selected as 36-42 degrees, the solutions selected in red were taken as the most feasible solution in this case due to following reasons. Solutions which are not marked in blue have slight changes to the ones marked in blue.

1. Considerably higher condensation rate of 6.7 g/s and, considerably higher desorption rate of 3.1 g/s can be achieved.
2. Hot water inlet temperature is 38.22^0C in a feasible region to achieve from the heating source.
3. Chilled water inlet temperature of 8.8^0C that can be achieved from the chiller. It was identified from the heat and mass transfer that lower chilled water temperature increases condensation rate.
4. Initial vacuum pressure is a very critical component. It was found that lower initial pressure is better for the final performance.

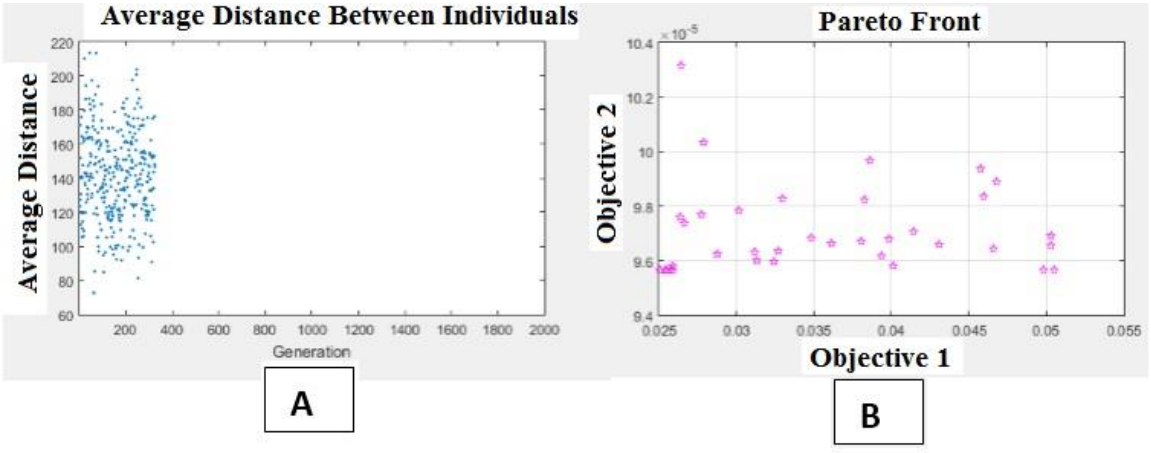

Figure 6-1. A- Average distance between individuals, B- Pareto Front

In the Pareto front, each point indicates optimum solution for fitness functions. Following study was carried out to compare the optimized results with actual results.

Figure 6-2 illustrates the comparison between the actual heat transfer and optimized heat transfer from the evaporator heat exchanger for selected operating conditions. It's clear that using the optimum conditions, heat is transferred to the solution as a moderate value throughout the process. Optimization enhances the effectiveness of the process and reduces the heat consumption.

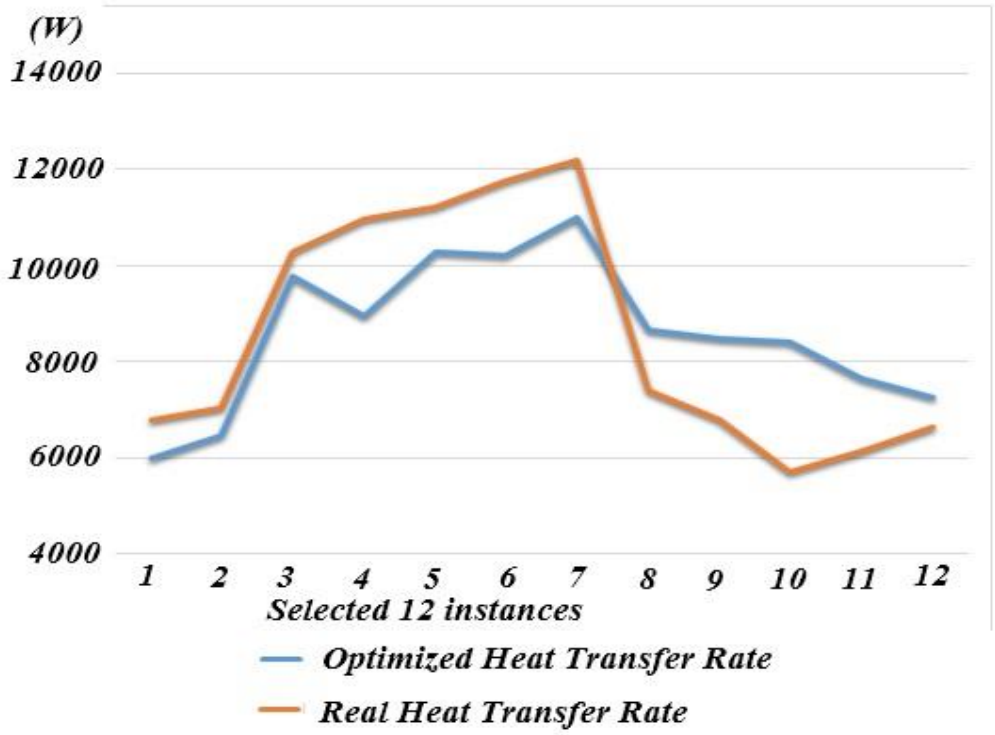

Figure 6-2. Comparison of Evaporator optimized heat transfer rate vs real heat transfer rate

Comparison between actual and optimized condensation heat transfer is shown in the figure 6-2. In optimum condition cooling load is much higher than actual condition and vacuum pressure inside can be reduced easily and the pressure can be maintained in a low value.

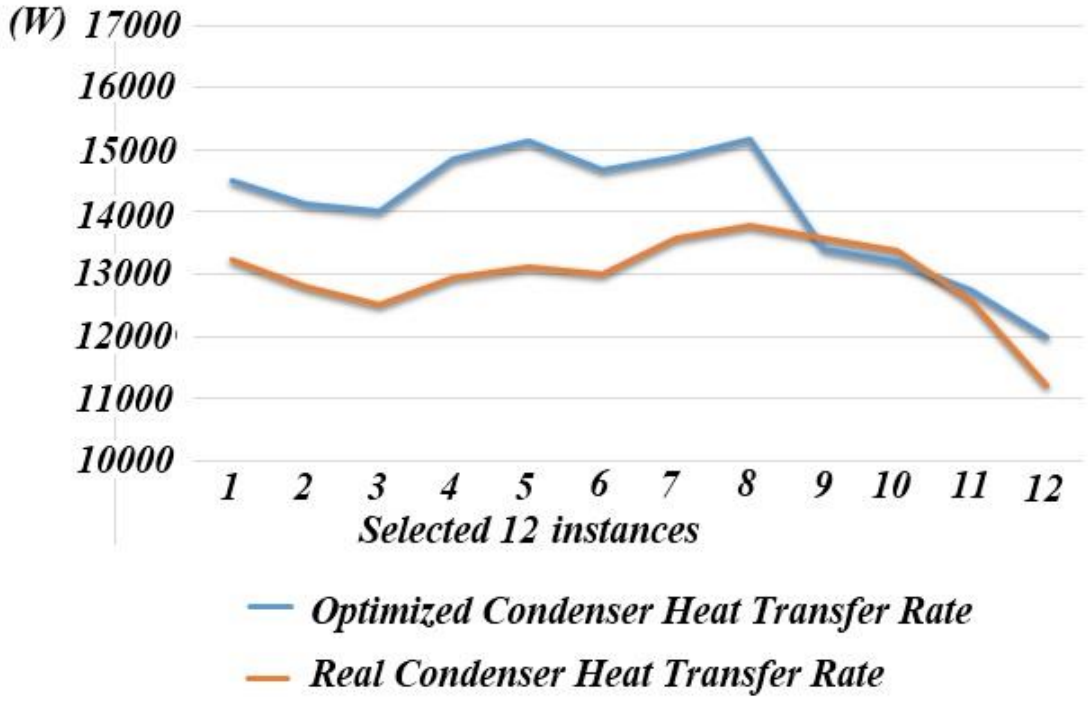

Figure 6-3. Optimized and real condenser heat transfer rate

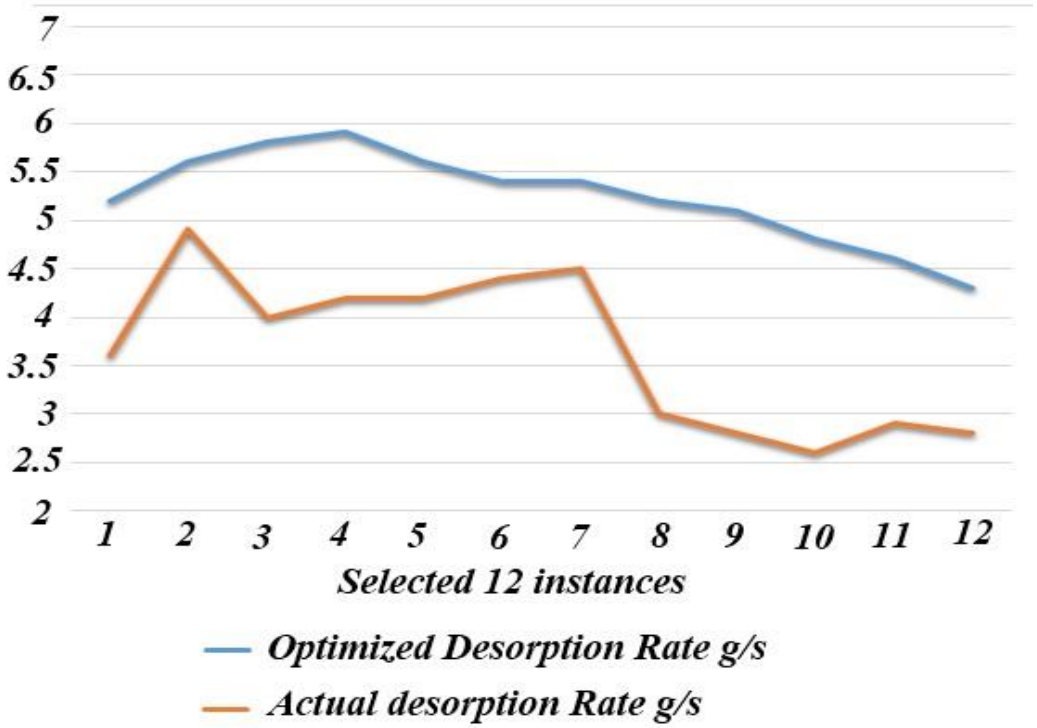

Figure 6-4. Optimized Vs real desorption rate (g/s)

Figure 6-4 illustrates the difference between the actual and optimized desorption rate of the system. By controlling temperature and mass flow rate of hot water, solution and chilled water, higher desorption rate can be achieved.

Actual condensation rate and optimized condensation rate was shown in figure 6-5. At the initial stage of the testing, higher condensation rate is a very important factor. It's clear from the optimum condition that condensation almost doubled in this scenario and reduced the inside pressure. Figure 6-6 shows the change of solution flow rate in optimum condition and real condition. According to the optimum condition solution flow rate should reduce after the first few minutes to reduce water vapor generation to maintain the inside pressure a lower value and at the end stage of the testing it should increase

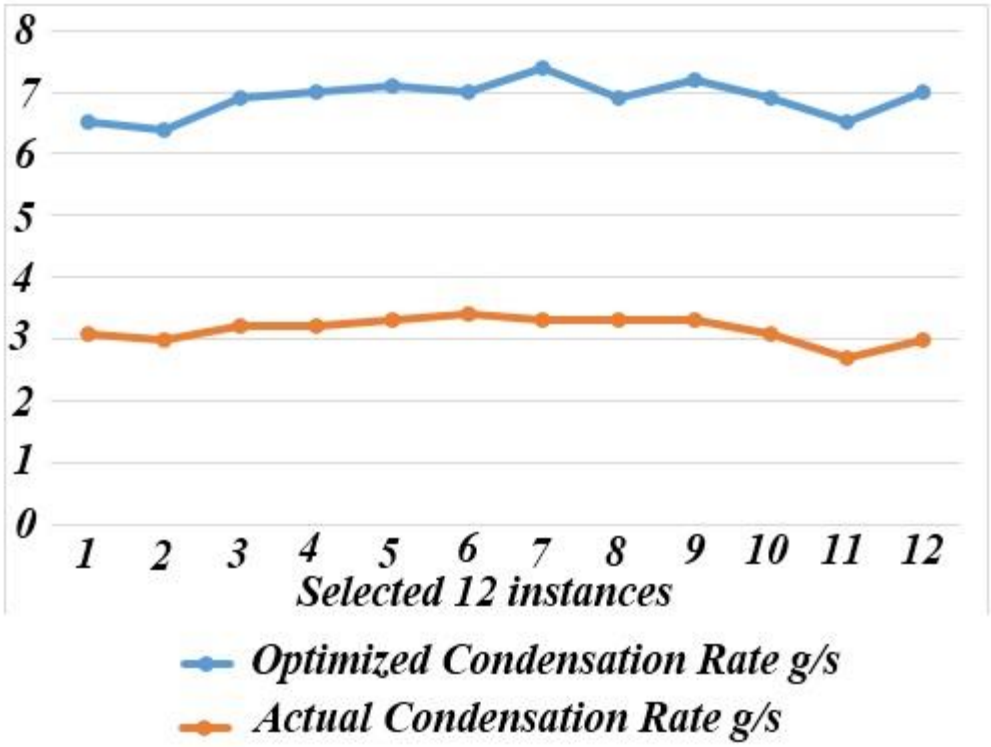

Figure 6-5. Optimized Vs Real condensation rate (g/s)

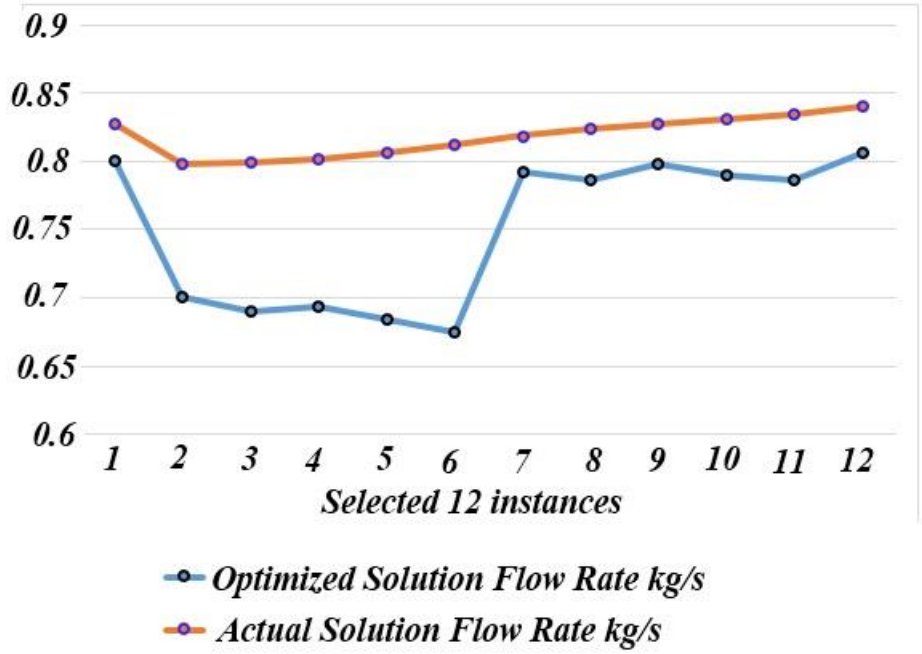

Figure 6-6. Optimized Vs real solution flow rate settings kg/s

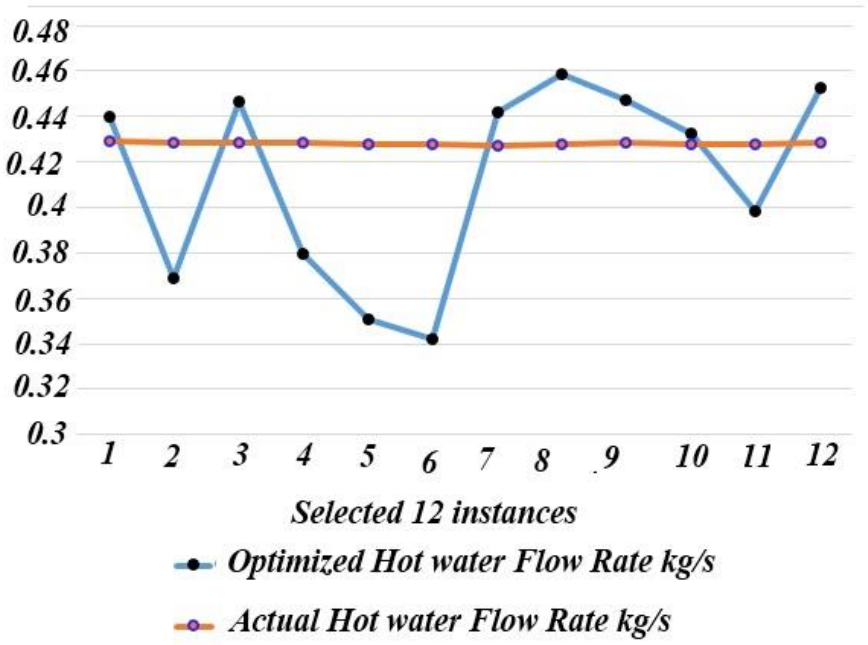

Figure 6-7. Optimized Vs real hot water flow rate settings kg/s

Figure 6-7 shows the change of hot water flow rate in optimum condition and in real condition. Hot water flow rate in real situation was almost constant, but in optimum condition it should change according to the system condition. The flow rate was initially higher than actual and then became lower, then again rose without allowing generating a subsequent amount of water vapor inside. Chilled water flow rate was almost constant in real situation but in optimum condition it varies up and down as shown in Figure 6-8.

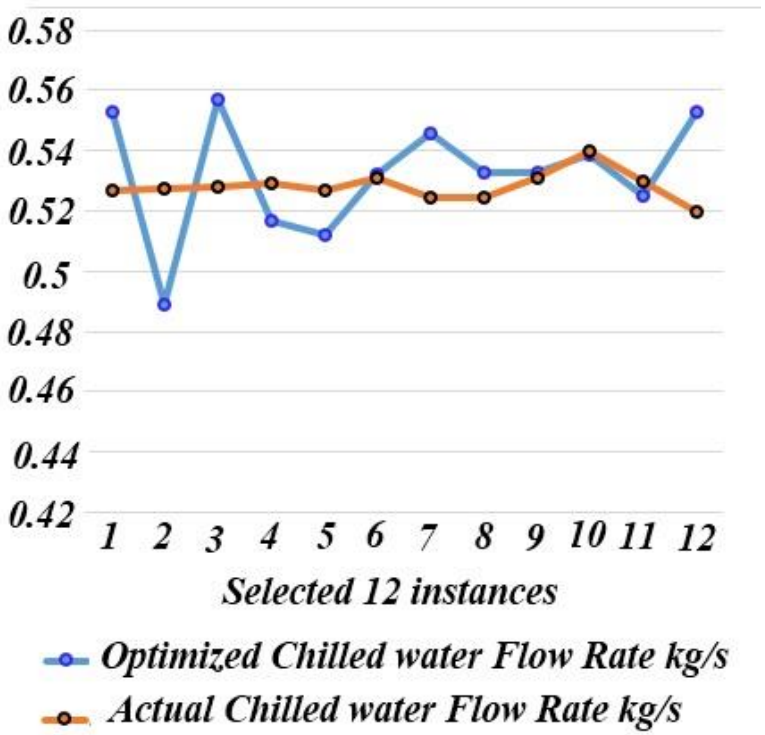

Figure 6-8. Optimized Vs Real chilled water flow rate settings kg/s

Figure 6-9 illustrates the comparison between the total energy consumption amount in actual condition and optimized condition. It is clear from the figure that the optimized condition requires lower amount of total energy than the actual condition in all incidents.

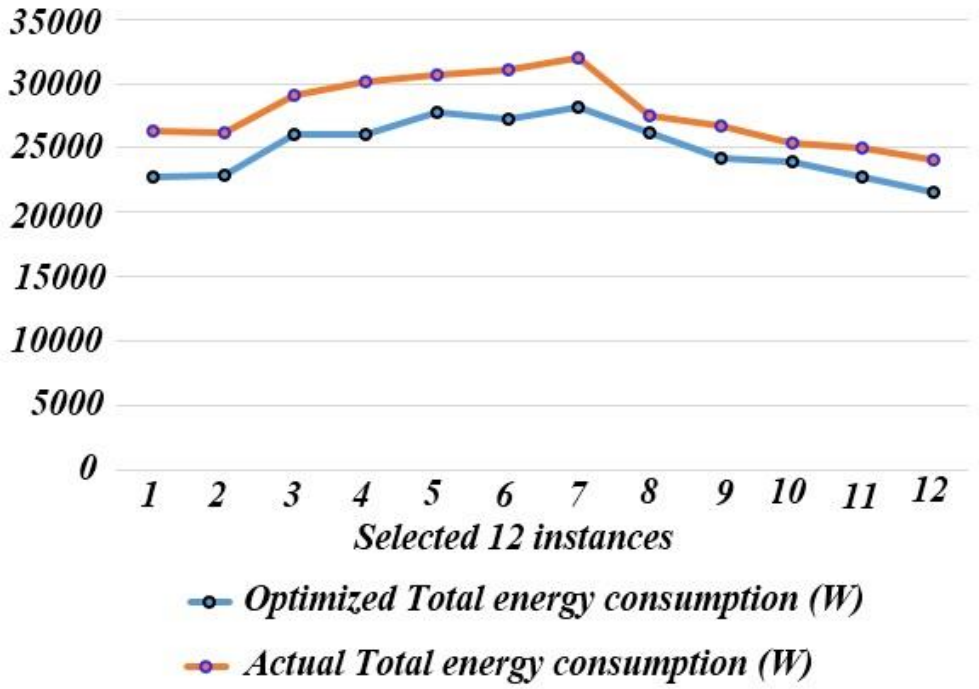

Figure 6-9. Optimized and Actual Total energy consumption variation

6.4 Summery

Multi objective genetic algorithm for vacuumed regenerator system was presented in this chapter. Optimization method was applied to the system by keeping heat and mass transfer relationships and total energy consumption as objectives of the optimization.

Heat and mass transfer of evaporator heat exchanger and condenser heat exchanger were considered as maximization problem and total energy consumption of the system was considered as minimization problem. Therefore, the system was considered as minimization problem by taking the inverse of heat and mass transfer rate of both evaporator and condenser. System controlling parameters (Hot water flow rate and temperature, chilled water flow rate and temperature, solution flow rate and initial vacuum pressure) were taken as deciding parameters for the optimization and upper and lower limits were introduced for the optimization. Heating capacity of the heater and cooling capacity of the chiller were considered as constraints.

MATLAB program was developed and multi objective genetic algorithm was conducted and pareto optimal solution was achieved. Considering the practical feasibility and economical factors, one solution was selected as optimum settings. Optimum settings of the system provided higher desorption rate, higher condensation rate. As a result higher LiBr concentration was achieved at the end.

Chapter 7 Conclusion and Recommendations

7.1 Conclusion

Liquid desiccant dehumidification system (LDDS) was recognized as one of the potential replacements for the conventional air conditioning systems. Improve the regeneration performance and modify the regeneration cycle such that to operate from a low temperature heat source are major challenges that was needed to be addressed. In this study, a new vacuumed chamber regenerator system was designed and tested, and a mathematical model was developed to optimize the operating settings to achieve highest performance.

The performance of the regeneration system relies on several design parameters like heat and mass transfer mechanism and driving force of evaporation and condensation processes, solution flow method through the heat exchanger, condenser tube arrangement, solution accumulation amount and vacuum rate of the pump and liquid desiccant properties. The system was designed to overcome issues related to previous systems and considering the above mentioned design criteria's. A vacuumed chamber was introduced into the system to reduce the saturation temperature of water. Hence low temperature heat source can be used for the evaporation process. The chamber was designed as a fully closed one to prevent the carry over effect of the desiccant solution. Vacuumed chamber was divided into two sections namely evaporator heat exchanger and condenser heat exchanger to separate the evaporation and condensation process. Water vapor releases and gathers in evaporator side and travels to condenser side, releases latent heat to the cooling water and then condenses. System was operated in very low temperature about 38^0C and achieved concentration increment more than 10% within 3 hours of operation. System was tested to identify the effect of design parameters and control parameters for different settings.

Different tests were carried out by varying hot water temperature and flow rate, chilled water temperature and flow rate, solution flow rate, initial solution concentration and initial vacuum level of the chamber. It was found that there was a significant effect from the vacuum level of the chamber for final concentration of the solution. Higher initial pressure inside the chamber not only increased the saturation temperature, it also reduced the mass transfer driving force for the desorption process. It was found that by changing the hot water flow rate by 1.3 m^3/hr and temperature by 5^0C, concentration of the final solution can be increased by more than 15%. Chilled water temperature and flow rate also have significant effects. As soon as the system started, inside pressure increased rapidly due to the evaporation of dissolved water. When the chilled water temperature was high and flow rate was low, water vapor was accumulated inside and pressure was risen and desorption rate was reduced. When the initial concentration of the solution is at a higher value, it was found difficult to further increase the concentration without a higher temperature heating source. A mathematical model was developed in order to study the system without carrying out many tests for different parameter conditions and analyzed the effect of those parameters in chapter 4 and 5.

Overall heat and mass transfer coefficient for evaporator heat exchanger was modeled by considering external convection over a tube bank and internal convection of a cylindrical tube. Heat transfer rate of the evaporator is a function of heat exchanger area, mean temperature difference, hot water mass flow rate, solution mass flow rate, solution density and solution heat capacity. Evaporator heat exchanger mass transfer Sherwood number is a function of two phases Reynolds number, Schmidt number, concentration gradient and heat flux. Heat transfer model and mass transfer model was validated within ±10% confidence interval. Condenser heat exchanger was modeled by considering external natural condensation over a tube bank and internal convection of a cylindrical tube. Heat transfer rate of the condenser is a function of chilled water flow rate, mean temperature difference and the number of rows of tubes. Convective heat transfer coefficient was

calculated by using Nusselt number relationship with Reynolds number, Prandlt number and friction factor. Heat transfer model and mass transfer model of the condenser were validated within ±10% confidence interval. This theoretical contribution can be equally applied to any kind of similar system by changing system dependent parameters.

Optimization for the developed model was presented in chapter 7 and best operating condition was found. Minimizing the total energy consumption and maximizing heat and mass transfer of evaporation and condensation processes were set as objectives. Fitness function was written as a minimization problem for the multi objective genetic algorithm optimization. Constraints were set based on lower and upper bound of the system controlling parameters and component capacities. The optimum settings had been found using MATLAB's genetic algorithm and a suitable operating setting was selected based on resource limitations and economic factors.

7.2 Recommendations for future research

There is a room for modifications to the current design and extend the proposed work. Some of these are identified and outlined below.

- Condenser used in the vacuum chamber was a horizontal tube condenser. Water vapor condensed on top of the tube surface and dropped down to the tube below and so on. When the liquid layer dropped further down the liquid film layer got thick and covered the tube. Thus, water vapor directly couldn't make contact with the tube and reduced the condensation effectiveness. A new design is proposed with inclined tubes. Instead of horizontal tubes, tubes can be arranged with a slight inclination. Condensed water flows on each tube to the edge instead of dropping down to the lower tube as shown in figure 7-1.

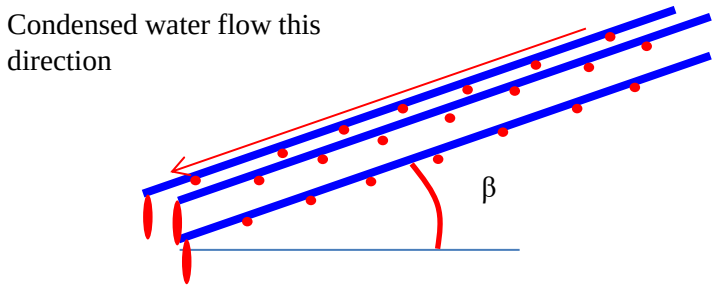

Figure 7-1. New condenser design for the Regenerator

- During the testing system hot water and chill water temperature couldn't maintain in a certain value. Chiller capacity and heater capacity was not enough to provide required cooling and heating load. A new heater and a chiller with a

large reservoir can be implemented with the system to prevent those temperature variations.

- Before system starts its cycle, the vacuum pressure should reach to the required level to have better performance. Present vacuum pump vacuum rate and power is not enough to reach a very low vacuum level. Therefore, high capacity vacuum pump can install with the system to achieve lower vacuum pressure.
- A proper control strategy can be introduced into the system. System runs without any proper controlling mechanism during the testing time period. Even though, the target values of control parameters cannot be controlled like maintaining constant flow rate, constant temperature, etc., a proper study needed to be conducted to understand how to control hot water temperature, hot water flow rate, chilled water temperature, chilled water flow rate and solution flow rate.
- System can be successfully implemented with renewable energy sources like solar thermal and waste heat. It was found that solution concentration can be increased more than 10% with very low heating temperature like 38 ^{0}C. So the next step is to adapt a low temperature heat source to the system. Therefore, this will be an interesting design and research to follow through.
- Even though the technical feasibility and performance of the new system were verified with small scale unit, the performance and the feasibility of the unit should be tested by implementing it to a real scale dehumidification cycle and it will be a good research area to follow.

References

1. Energy, B.S.R.o.W., *BP Statistical Review of World Energy* 1,2015.
2. Jos G.J. Olivier (PBL), G.J.-M.I.-J., Marilena Muntean (IES-JRC), Jeroen A.H.W. Peters (PBL), *Trend in global CO2 emissions*, P.a. JRC, Editor. 2015: PBL Netherlands Environmental Assessment Agency.
3. Pesaran, A.A. *A Review of Desiccant Dehumidification Technology*. in *Electric Dehumidification: Energy Efficient Humidity Control for Commercial and Institutional Buildings Conference*. June 2-3, 1993. New Orleans, Louisiana.
4. Lacourte, N.A., *Revision of Ashrae Standard 55 - Thermal Comfort Conditions Available for Review.* Ashrae Journal-American Society of Heating Refrigerating and Air-Conditioning Engineers, 1973. **15**(6): p. 59-59.
5. Mei, L. and Y.J. Dai, *A technical review on use of liquid-desiccant dehumidification for air-conditioning application.* Renewable and Sustainable Energy Reviews, 2008. **12**(3): p. 662-689.
6. Wang, X., et al., *A hybrid dehumidifier model for real-time performance monitoring, control and optimization in liquid desiccant dehumidification system.* Applied Energy, 2013. **111**: p. 449-455.
7. Factor, H.M. and G. Grossman, *A packed bed dehumidifier/regenerator for solar air conditioning with liquid desiccants.* Solar Energy, 1980. **24**(6): p. 541-550.
8. Jain, S., P.L. Dhar, and S.C. Kaushik, *Experimental studies on the dehumidifier and regenerator of a liquid desiccant cooling system.* Applied Thermal Engineering, 2000. **20**(3): p. 253-267.

9. Jain, S., P.L. Dhar, and S.C. Kaushik, *Evaluation of liquid dessicant based evaporative cooling cycles for typical hot and humid climates.* Heat Recovery Systems and CHP, 1994. **14**(6): p. 621-632.

10. Yin, Y., X. Zhang, and Z. Chen, *Experimental study on dehumidifier and regenerator of liquid desiccant cooling air conditioning system.* Building and Environment, 2007. **42**(7): p. 2505-2511.

11. *Heat and Mass Transfer in Packed Bed Liquid Desiccant Regenerators—An Experimental Investigation.* Journal of Solar Energy Engineering, 1999. **121**(3): p. 162-170.

12. Liu, X.H., Y. Jiang, and X.Q. Yi, *Effect of regeneration mode on the performance of liquid desiccant packed bed regenerator.* Renewable Energy, 2009. **34**(1): p. 209-216.

13. Yu, J., et al., *Study on performance of the ball packed-bed regenerator: experiments and simulation.* Applied Thermal Engineering, 2002. **22**(6): p. 641-651.

14. Krause, M., et al., *Absorberand Regenerator Models for Liquid Desiccant Air Conditioning Systems: Validation and Comparison Using Experimental Data*, in *Proceedings of ISES World Congress 2007 (Vol. I – Vol. V): Solar Energy and Human Settlement*, D.Y. Goswami and Y. Zhao, Editors. 2009, Springer Berlin Heidelberg: Berlin, Heidelberg. p. 770-774.

15. Ding, X., et al., *A hybrid condenser model for real-time applications in performance monitoring, control and optimization.* Energy Conversion and Management, 2009. **50**(6): p. 1513-1521.

16. Balamurugan, P. and A. Mani, *Heat and mass transfer studies on compact generator of R134a/DMF vapour absorption refrigeration system.* International Journal of Refrigeration, 2012. **35**(3): p. 506-517.

17. Suresh, M. and A. Mani, *Heat and mass transfer studies on a compact bubble absorber in R134a-DMF solution based vapour absorption refrigeration system.* International Journal of Refrigeration, 2013. **36**(3): p. 1004-1014.

18. Babakhani, D. and M. Soleymani, *Simplified analysis of heat and mass transfer model in liquid desiccant regeneration process.* Journal of the Taiwan Institute of Chemical Engineers, 2010. **41**(3): p. 259-267.

19. Fumo, N. and D.Y. Goswami, *Study of an aqueous lithium chloride desiccant system: air dehumidification and desiccant regeneration.* Solar Energy, 2002. **72**(4): p. 351-361.

20. Chen, M.M., *An Analytical Study of Laminar Film Condensation: Part 1—Flat Plates.* Journal of Heat Transfer, 1961. **83**(1): p. 48-54.

21. Tiwari, A., *Characterization of mass transfer by condensation on a horizontal plate*. 2011, Université Blaise Pascal - Clermont-Ferrand II.

22. Chen, M.M., *An Analytical Study of Laminar Film Condensation: Part 2—Single and Multiple Horizontal Tubes.* Journal of Heat Transfer, 1961. **83**(1): p. 55-60.

23. M. Saraireh, J.D.L.a.G.T., *Modeling of heat and mass transfer involving vapor condensation in the presence of non-condensable gases* in *Australasian fluid mechanics conference*. 2010: Auckland New Zealand

24. Abdullah, R., et al., *Condensation of steam and R113 on a bank of horizontal tubes in the presence of a noncondensing gas.* Experimental Thermal and Fluid Science, 1995. **10**(3): p. 298-306.

25. Elsarrag, E., *Performance study on a structured packed liquid desiccant regenerator.* Solar Energy, 2006. **80**(12): p. 1624-1631.

26. Tu, M., et al., *Simulation and analysis of a novel liquid desiccant air-conditioning system.* Applied Thermal Engineering, 2009. **29**(11–12): p. 2417-2425.

27. Jain, S. and P.K. Bansal, *Performance analysis of liquid desiccant dehumidification systems.* International Journal of Refrigeration, 2007. **30**(5): p. 861-872.

28. Wang, X., et al., *Optimization of Liquid Desiccant Regenerator with Multiobject Particle Swarm Optimization Algorithm.* Industrial & Engineering Chemistry Research, 2014. **53**(49): p. 19293-19303.

29. Kusiak, A., G. Xu, and F. Tang, *Optimization of an HVAC system with a strength multi-objective particle-swarm algorithm.* Energy, 2011. **36**(10): p. 5935-5943.

30. Kusiak, A. and M. Li, *Cooling output optimization of an air handling unit.* Applied Energy, 2010. **87**(3): p. 901-909.

31. Kusiak, A. and G. Xu, *Modeling and optimization of HVAC systems using a dynamic neural network.* Energy, 2012. **42**(1): p. 241-250.

32. Kusiak, A., M. Li, and F. Tang, *Modeling and optimization of HVAC energy consumption.* Applied Energy, 2010. **87**(10): p. 3092-3102.

33. Chambers, L.D., *Practical Handbook of Genetic Algorithms: Complex Coding Systems, Volume III*. 1999.

34. D.Seenivasan, V.S.a.P.S., *Optimization of Moisture condensation rate of Liquid Desiccant Dehumidifier through Genetic Algorithm.* International Journal of ChemTech Research, 2014-2015. **07-01**: p. 400-407.

35. R. Parameshwaran, R.K., S. Iniyan, Anand A. Samuel *Optimization of Energy Conservation Potential for VAV Air Conditioning System using Fuzzy based Genetic Algorithm* International Journal of Mechanical, Aerospace, Industrial, Mechatronic and Manufacturing Engineering, 2008. **2**(1).

36. Aly, A.A., *Optimization of Desiccant Absorption System Using a Genetic Algorithm* Journal of Software Engineering and Applications, 2011. **4**: p. 527-533

37. Ooka, R.L.a.R., *Multi-variable Optimization of HVAC System Using a Genetic Algorithm.* Energy and Power Engineering, February 28, 2014. **8**: p. 306-312

38. Rathakrishnan, E., *Elements of Heat Transfer*. 2012: CRC Press

39. Cengel, Y.A., *Heat Transfer: A Practical Approach 2nd Edition*. 2003: MC Graw Hill.

40. Beale, S., *Tube banks, single-phase heat transfer in*, in *International encyclopedia of heat and mass transfer*. 1997.

41. Kaita, Y., *Thermodynamic properties of lithium bromide–water solutions at high temperatures.* International Journal of Refrigeration, 2001. **24**(5): p. 374-390.

42. Kawamata, K., Y. Nagasaka, and A. Nagashima, *Measurements of the thermal conductivity of aqueous LiBr solutions at pressures up to 40 MPa.* International Journal of Thermophysics, 1988. **9**(3): p. 317-329.

43. Ding, X., et al., *Evaporator modeling – A hybrid approach.* Applied Energy, 2009. **86**(1): p. 81-88.

44. Potnis, S.V., T.G. Lenz, and E.H. Dunlop. *Measurement of water diffusivity in aqueous lithium bromide solution*. 1993. United States.

45. Lansing, F.L., *computer modeling of a single stage lithium bromide water absorption refrigeration unit*. DSN Engineering Section.

46. *Engineering data book 3*. Condensation on external surfaces. Wolverine Tube, Inc.

47. Warren M. Rohsenow, H.C., *Heat Mass and Momentum Transfer*. 1961.

48. Diwekar, U., *Introduction to Applied Optimization*, ed. D.W.H. Panos M. Pardalos. Vol. 80. 2003.

49. D. Seenivasan, V. Selladurai, and P. Senthil. Optimization of Liquid Desiccant Dehumidifier Performance Using Taguchi Method, Advances in Mechanical Engineering (Hindawi Publishing Corporation); 2014, p1

50. Wang, X., et al., Energy saving strategy development in liquid desiccant dehumidifier by genetic algorithm. Industrial Electronics and Applications (ICIEA), 2015.

51. Gaoming Ge, Davood Ghadiri Moghaddam, Ramin Namvar, Carey J. Simonson and Robert W. Besant. Analytical model based performance evaluation, sizing and coupling flow optimization of liquid desiccant run-around membrane energy exchanger systems, Energy and Buildings, 2013

52. Feuerecker, G. 1994. Entropieanalyse fuer Waermepumpensysteme: Methoden und Stoffdaten, Dissertation, Technischen Universitaet Muenchen.